UNIVERSITÉ de BRETAGNE OCCIDENTALE

U. E. R. DES SCIENCES DE LA MATIÈRE ET DE LA MER

THESE

PRÉSENTÉE POUR OBTENIR LE TITRE DE

Docteur de 3e Cycle

Spécialité : OCEANOGRAPHIE PHYSIQUE

PAR

A.S. UNNIKRISHNAN

NUMERICAL MODELING TECHNIQUES FOR THE STUDY OF HORIZONTAL CIRCULATION IN ESTUARIES APPLICATION TO THE GIRONDE

Soutenue le 4 Février 1985 devant la commission d'examen

Monsieur J.C. SALOMON	Professeur, Université de Bretagne Occidentale	*Président*
Messieurs G. PASCAL	Professeur, Université de Bretagne Occidentale	*Examinateurs*
P. CASTAING	Assistant, Université de Bordeaux I	
R. MAZE	Maître Assistant, Université de Bretagne Occidentale	
J.L. MAUVAIS	Chef du Département ELGMM, IFREMER, Brest	

UNIVERSITÉ de BRETAGNE OCCIDENTALE

U. E. R. DES SCIENCES DE LA MATIÈRE ET DE LA MER

THESE

PRÉSENTÉE POUR OBTENIR LE TITRE DE

Docteur de 3e Cycle

Spécialité : OCEANOGRAPHIE PHYSIQUE

PAR

A.S. UNNIKRISHNAN

NUMERICAL MODELING TECHNIQUES FOR THE STUDY OF HORIZONTAL CIRCULATION IN ESTUARIES APPLICATION TO THE GIRONDE

Soutenue le 4 Février 1985 devant la commission d'examen

Monsieur J.C. SALOMON	Professeur, Université de Bretagne Occidentale	*Président*
Messieurs G. PASCAL	Professeur, Université de Bretagne Occidentale	*Examinateurs*
P. CASTAING	Assistant, Université de Bordeaux I	
R. MAZE	Maître Assistant, Université de Bretagne Occidentale	
J.L. MAUVAIS	Chef du Département ELGMM, IFREMER, Brest	

ACKNOWLEDGEMENTS

I express my thanks to Prof. LE FLOCH who welcomed me to this laboratory and provided the necessary facilities.

I wish to express my deep sense of gratitude to Prof. J. C. SALOMON, who has been guiding me throughout the duration of three years of work.

I would like to thank Prof. G. PASCAL, Professor, Université de Bretagne Occidentale, Dr. J.L. MAUVAIS, Head of the department of ELGMM, IFREMER, Brest, Dr. R. MAZE, Maître Assistant, Université de Bretagne Occidentale and Dr. P. CASTAING, Assistant, Université de Bordeaux I who have given me the honour of participating in the committee of examiners of the thesis.

I express my thanks to the Port Autonome de Bordeaux for giving me an authorisation to consult the documents of the Laboratoire National d'Hydraulique about the Gironde estuary.

My sincere thanks are to all the collegues of the laboratory who have always encouraged me. In particular, I thank Dr. G. ROUGIER, Dr. V. MARIETTE, Dr. G. LANGLOIS and Mr. S. GHIRON, with whom I had useful discussions often.

The services made by Mr. P. DOARE and Mr. R. MARCHERON, IFREMER in preparing the diagrams are acknowledged.

Finally, I thank Miss Pascale MAZO, Who patiently typed the manuscript.

The financial assistance in the form of a fellowship awarded by the Ministry of External Affaires, Gov. of France under the Indo French cultural exchange programme is duly acknowledged.

CONTENTS

INTRODUCTION

Recent advances in fast computers have helped in developing numerical models for the study of estuarine and coastal dynamics. So far, different workers have made definitions of an estuary mainly based on salinity considerations. For example, following PRITCHARD (1965), an estuary may be defined as "a semi enclosed body of water having a free connection with the open sea within which sea water is mesurably diluted with fresh water derived from land drainage". In the case of european estuaries, which are caracterised by high tidal ranges, the tidal action extends well beyond the penetration of salinity. SALOMON (personal communications), gives a more appropriate definition for the limits of an estuary as follows : at the mouth, where a cross sectional line shows the influence of river by a slight decrease of salinity and at the head, where the periodic oscillations of water surface elevation disappear.

The necessity of learning estuarine dynamics is becoming increasingly important because of navigational purposes , sedimentological applications, pollution resulting from industrial discharges, thermal pollution due to the discharge of heat from nuclear power plants etc. The estuarine waters are highly nutrient rich and they are the spawning grounds for many fishes and the nursing grounds for many others. Hence any damage to the environment will cause subsequent effects on fish production.

The Gironde estuary (fig 1), situated at the southwestern part of France, near Bordeaux, has been an object of study since a number of years. This estuary is caracterised by a number of channels, longitudinal bars and islands. Historically, along the Gironde, there had been deposition of sediments in some regions and erosion in some other parts, where as certain regions have suffered alternate erosion and deposition. In order to learn the sedimentation problems, various workers have studied the circulation patterns based on the numerous observations available about the hydrology and currents. These measurements were carried out mainly by the Port Autonome de Bordeaux (P. A. B.), Institut Géologique du Bassin d'Aquitaine and the Electricité de France, besides the systematic data obtained from different tide gauges installed by P. A. B.

Recently, the E. D. F. has decided to choose the median channel at PK 52 of the estuary for thermal discharges from the nuclear power plant of Braud-et-Saint-Louis. This also has arisen a lot of interest among different

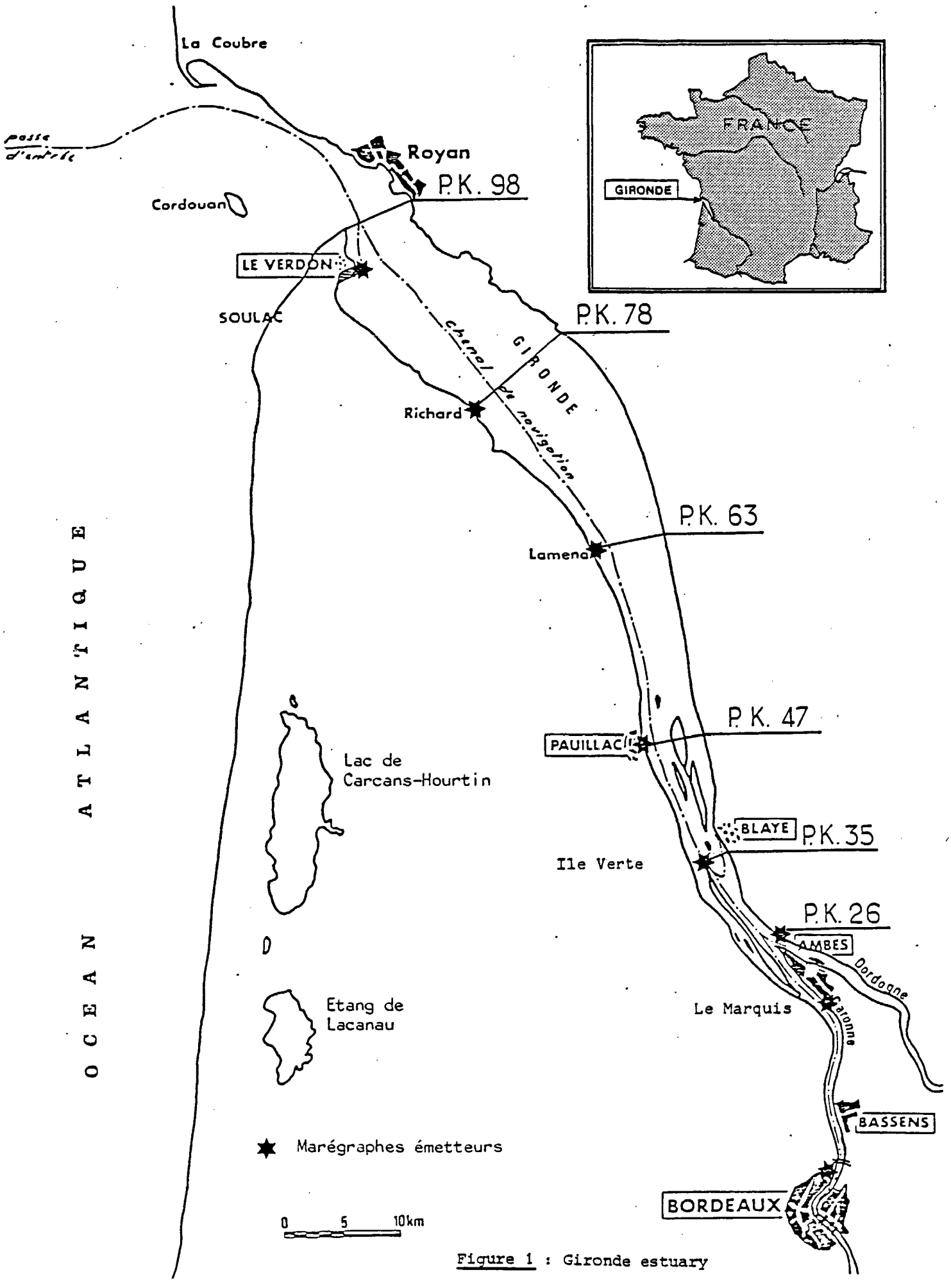

Figure 1 : Gironde estuary

workers in studying this estuary.

In this study, we attempt to develop numerical models to study the horizontal circulation in the Gironde. This involves the computation of depth averaged tidal currents and water surface elevations and to study the lateral variations of these physical parameters during a tidal period. The models used are two dimensional in the horizontal plane (x-y directions). In order to take into account of the geomorphological peculiarities of the estuary, such as the presence of channels and islands, we have used different numerical methods in modelling. The second objective of this work is to compare the relative advantages and disadvantages of the different techniques used.

CHAPTER I

DESCRIPTION OF THE GIRONDE ESTUARY

I. INTRODUCTION

The Gironde estuary is formed by the junction of two rivers, Dordogne and the Garonne. It is the largest of the French estuaries in area (450 km^2 during high tide). The rivers Dordogne and the Garonne drain from the Pyrènées and the Massif Central respectively. The total drainage basin (74000 km2) is the fourth largest in France, after the Loire, the Rhône, and the Seine.

II. GEOMORPHOLOGY

The Gironde is caracterised by a regular geometry with its breadth, mean depth and surface area decreasing exponentially towards the head. The distances are marked in kilometers as "point kilométrique" (P.K.) from the pointe de Grave towards the head. A detailled examination of the bathymetric chart of the Gironde reveals the following features.

1) Lower estuary

The lower estuary is caracterised by a typical two channel system with the navigation channel at the southern side and the Saintonge channel at the northern side (figure 2). The two channels are separated by regions of sand bars. The depth in the southern channel varies between 6 to 8 m. At PK 81, there is a break in its slope and downstream further, the depth increases. The Saintonge channel is wider and its depth is of the order of 3 to 5 m. From PK 80 onwards, its depth increases. Towards the mouth, the navigation channel merges with the northern channel where the depths attain upto 30 metres.

Between PK 91 and PK 78, there are a series of longitudinal bars situated in between the two principal channels. They are called "banc de Marguerites", "banc de Talais", "banc de Mets" and "banc de Goulée" in the order from PK 91 onwards towards the head. Besides, near PK 70 there is a submerged dike called "digue de Valeyrac".

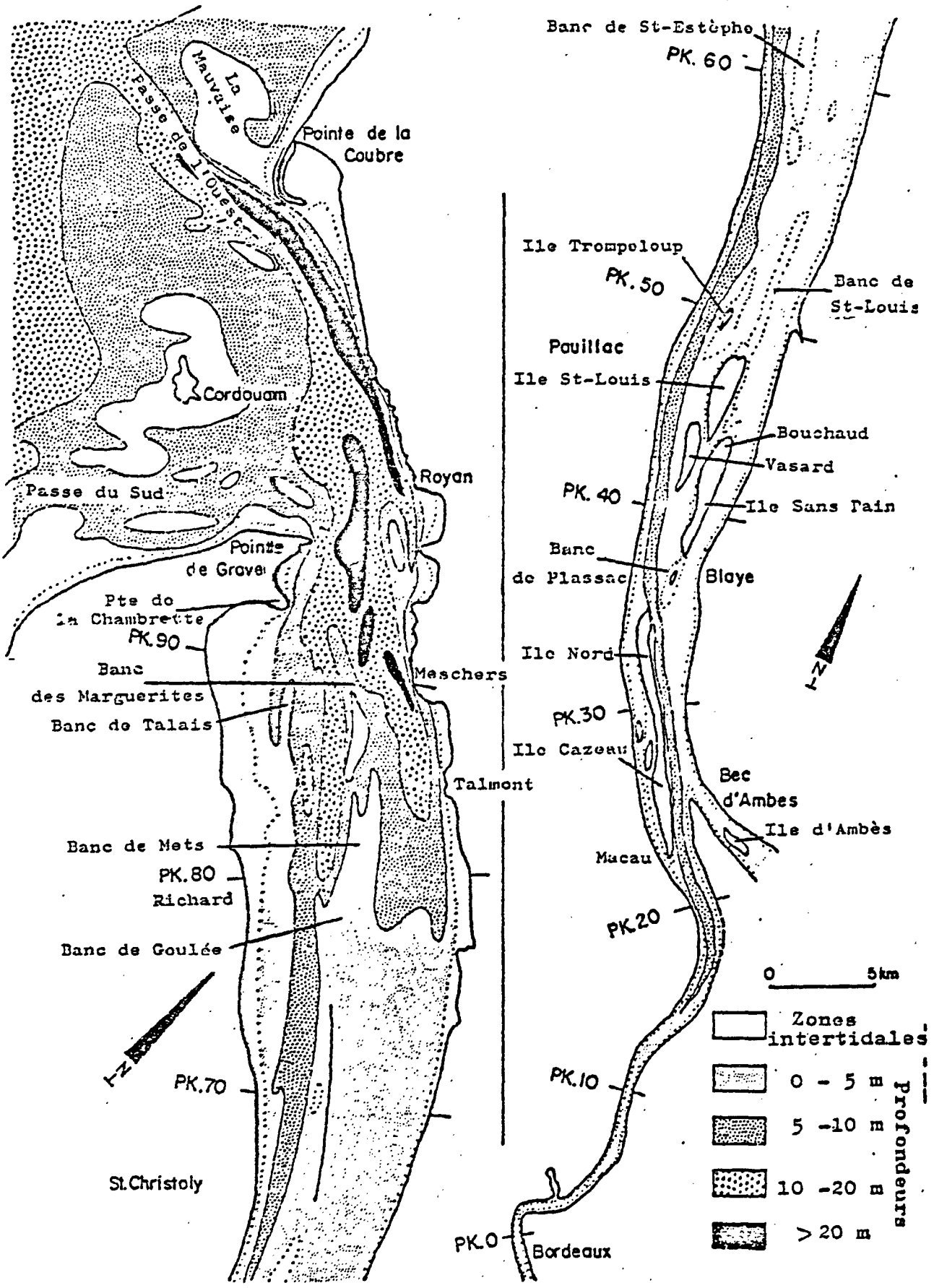

Figure 2 : Bathymetric charts of the estuary
a lower estuary b upper estuary
(in, TESSON GILET, 1981)

2) Upper estuary

The upper estuary is the region between Bec d'Ambes and St Christoly approximately. The geomorphological peculiarity of this region is the presence of numerous islands and longitudinal sand banks. Between Bec d'Ambes and Ile Verte, the principal channel is situated along and right side of a series of islands such as Ile Cazeau, Ile du Nord and Ile Verte. Downstream, up to St Christoly, the navigational channel continues along the southern side. Its depth is in between 7 to 10 m and breadth 400-800 m. The Blaye channel starting from PK 35 onwards towards the mouth is less wide and the depths are of the order of 5 m, with a maximum of 10 m at Blaye. Still further towards the mouth of the estuary, the northern channel is situated between the "banc de St Louis" and the north bank. Between Blaye and PK 50, there a series of islands namely, "Ile Sans Pain", "Ile Bouchaud", "Ile Patiras" and "Ile St Louis", situated in between the two principal channels. Downstream of PK 50, there are two main longitudinal sand banks, "banc de St Louis", between PK 50 and PK 55 approximately and "banc St Estephe" near PK 60, the former situated near the northern channel and the latter near the southern channel.

III. RIVER DISCHARGES

ALLEN (1972) gives the following figures for the river discharge rates of the Garonne and the Dordogne. These figures are calculated between 1961 and 1970.

The mean discharge rate of the Garonne is 444 m^3/s, with a maximum of 854 m^3/s in January and a minimum of 96 m^3/s in August. In the case of Dordogne, the mean value is 322 m^3/s with a maximum of 598 m^3/s in January and a minimum of 139 m^3/s in August.

Recent studies made by the P.A.B. (FERAL et al., 1982) show that the discharge rates are higher than those mentioned above.

It is estimated that the ratio of the tidal prism to the volume of water introduced by the rivers is more than 500 when the total discharge

rates are less than 500 m^3/s, where as in the case of exceptionally high river flow rates (7500 m^3/s), this ratio is of the order of 10 (CASTAING, 1981).

IV. TIDES AND TIDAL CURRENTS

Tides are semi diurnal in the Bay of Biscay (period of 12 hours and 25 minutes). Measurements by CAVANIE and HYACINTHE (1976) at a few stations near 200 m. isobath show that the tidal range varies between 1.50 to 2 m. during neap tide (coeff. 40 to 50), while during spring tide (coeff. 77 to 86) the range attains 3.50 m. Near the mouth of the Gironde, the tidal ranges are almost same at Cordouan and Coubre and is about 0.20 m. less than that of the Pointe de Grave (FICHOT, 1916). There is a tide gauge station at Cordouan (Fig. 1), through there are no stations near the north bank side. However, a few surface elevation measurements made by P.A.B. exist at Royan near the north bank side. A co tidal line passing near Cordouan (Fig. 15) indicates that the tidal wave comes from western direction before entering into the estuary.

The variations of surface elevations and currents inside the estuary will be discussed during the course of this dissertation. Here, it is only mentioned that the magnitudes of tidal currents at the surface are of the order of 1-2 m/sec, depending on the coefficient of tide and river flow rates.

CHAPTER II

DESCRIPTION OF THE NUMERICAL METHODS USED

This chapter deals with two aspects (I) a brief review of the different numerical methods existing for the calculation of tidal currents in the littoral zone and (II) a description of the various numerical techniques used in this work.

I. REVIEW OF LITERATURE

There exists various numerical techniques for computing tidal currents in thc estuarine and coastal zone. Here, we discuss mainly 2D models in the horizontal plane. One of the main problems facing a numerical modeller is in giving a good representation of the coastline. The classical method consists of a rectangular grid with the coastline approximated by a stair step boundary, and the equations being solved with a finite difference scheme. An example of this method is given by SALOMON (1976). The method will be discussed in detail later, in this chapter. This technique has the disadvantage of giving a poor representation of the coastline often resulting in poor values very near the coast.

In order to overcome this difficulty, certain workers have used the finite element method which uses meshes of variable dimensions usually triangular. The method described by CONNOR and WANG (1973) may be briefly summarised as follows. It consists of solution of boundary value problem with a function of piece wise continuous polynomials. The entair domain is discretised into a system of finite elements. The elements aire triangular in their method and the nodes are the vertices of the triangles. The values of the variables in the elements are assumed to be a linear function of the values at the nodes. The whole domain is treated by summation of the contributions of each element. However, finite element methods are found to be computationally expensive and need a lot of computer memory space. In the method of CONNOR and WANG, the authors point out that it needs 4·5 memory locations to describe each nodal point.

PEARSON and WINTER (1977) used a modified scheme in order to minimise the computational expenses of the finite element technique. A brief account of the method is as follows. The time dependent equations are written by a set of modal equations obtained by fourier decomposition, except for the

non linear terms which are treated by an iteration technique. The boundary value problem is then rephrased in terms of variational principles. The variational principle is then used together with a finite element method for the solution of the variables.

Another approach consists of an application of a hydraulic model, commonly referred to "link-node model". The method was utilised by KENNETH D. FEIGNER et.al (1970) for the San Fransisco delta systems. In this method, the grid network consists of polygons of variable dimensions whose centres of gravity are called junctions. Any two junctions are connected by a "channel element". The method consists of calculating velocities for the channel elements using the equation of momentum in the one dimensional form and the water surface elevations are computed at the junctions based on the flux of water entering and leaving a polygon. The method uses an explicit finite difference scheme. In 1978, LANGLEY R. MUIR used a similar principle with an implicit scheme for estuarine applications.

THACKER (1979), used a scheme called "Irregular grid finite difference scheme" for the forecast of storm surfaces. This method is similar to the finite element technique, as far as the grid net work is concerned, but the equations written in finite difference form. This scheme will be discussed in detail later, in this chapter.

II. APPLICATION OF A TWO DIMENSIONAL MODEL IN THE HORIZONTAL PLANE

Here, we apply a two dimensional model in the horizontal plane using a rectangular grid and the coastline represented by a stair step boundary. Hereafter, this model is referred to "stair step boundary model". for the sake of notation. The model was developed for the French estuaries by SALOMON (1976).

The model consists of equations of momentum and continuity integrated in the vertical plane, after being integrated over a very small interval of time, initially, in order to eliminate aleatory movements.

$$\frac{\partial U}{\partial t} + U\frac{\partial U}{\partial x} + V\frac{\partial U}{\partial y} - fV + g\frac{\partial \zeta}{\partial x} + \frac{gU\,(U^2 + V^2)^{\frac{1}{2}}}{C^2\,H} + \frac{\tau_{sx}}{\rho H} + \varepsilon\Delta U = 0 \qquad (1)$$

$$\frac{\partial V}{\partial t} + U\frac{\partial V}{\partial x} + V\frac{\partial V}{\partial y} + fU + g\frac{\partial \zeta}{\partial y} + \frac{gV\,(U^2 + V^2)^{\frac{1}{2}}}{C^2\,H} + \frac{\tau_{sy}}{\rho H} + \varepsilon\Delta V = 0 \qquad (2)$$

$$\frac{\partial \zeta}{\partial t} + \frac{\partial (HU)}{\partial x} + \frac{\partial (HV)}{\partial y} = 0 \qquad (3)$$

where

U and V	: the vertically integrated values of velocity components in the x and y directions, the integration being carried out between $-h$ to ζ
h	: depth of bottom
ζ	: water surface elevation
$H = h + \zeta$	: total depth of water
g	: acceleration due to gravity
f	: Coriolis parameter
C	: coefficient of Chezy
τ_{sx} , τ_{sy}	: wind stress components in the x and y directions
ε	: coefficient of pseudo viscosity
ΔU, ΔV	: Laplacians of velocities U and V.

x and y are the cartesian coordinates in the horizontal plane and t is the time.

Equations (1) and (2) are the equationsof momentum in the x and y directions and (3), the equation of continuity. The terms $\varepsilon \Delta U$ and $\varepsilon \Delta V$ are the terms of pseudo viscosity, introduced in the model by SALOMON, in order to dissipate small wave length energy.

The bottom friction is parameterised in terms of the coefficient of Chezy, by the following relation based on the hypothesis of PRANDTL. The coefficient of Chezy is a function of the total height of water column.

$$C = 7.83 \text{ Log } (0.37 \, H/_{z_o}) \qquad (4)$$

where z_o is the thickness of rugosity.

The wind stress components in the x and y directions are given as follows.

$$\tau_{sx} = \rho_a C_D \, (u_x - U) \sqrt{(u_x - U)^2 + (u_y - V)^2} \qquad (5)$$

$$\tau_{sy} = \rho_a C_D \, (u_y - V) \sqrt{(u_x - U)^2 + (u_y - V)^2} \qquad (6)$$

where

ρ : density of air

C_D : drag coefficient

u_x, u_y : wind velocities in the x and y directions.

1) Numerical Resolution

The model uses an implicit in alternate direction scheme. This numerical scheme was introduced by PEACEMAN and RACHFORD in meteorology. The principle of the method is as follows.

In the computational grid, U, V and ζ are calculated at different points as shewn in figure 3.

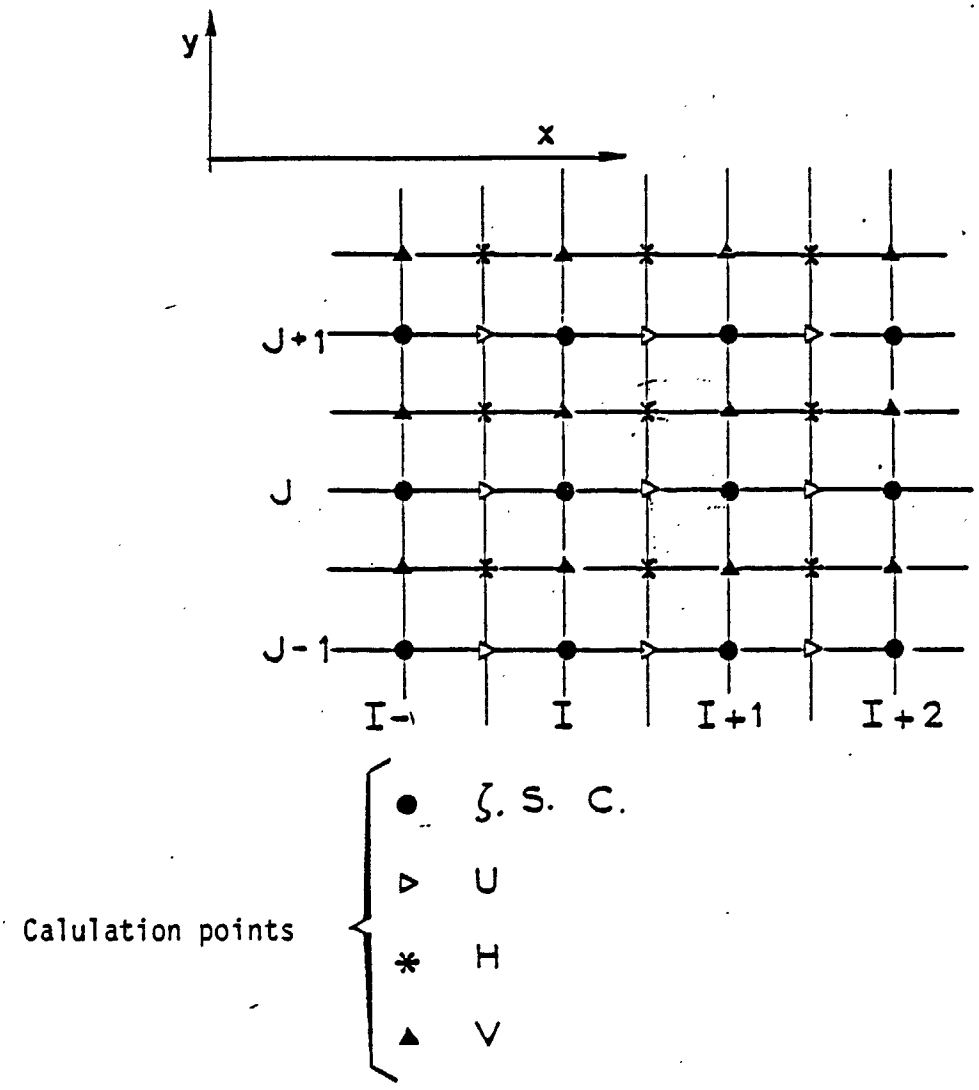

Figure 3 : Calculation points for different variables on the grid

The computation procedure may be described briefly as follows. For the first half time interval, the equation of momentum in the x direction and the equation of continuity are solved for each row of the matrix. The variables situated at the row concerned are treated implicitly, while the variables situated at the adjacent rows are solved explicitly. For the next half time interval, the momentum equation in the y direction and the equation of continuity are solved for each column of the matrix in a similar manner. The equations (1) to (3) can be written in finite difference form and may be expressed as tridiagonal matrices. Finally, the solution is made by an inversion of matrix.

2) Stability

LEENDERTSE (1971) showed that the scheme is unconditionally stable, when the equations are linearised. When non linear terms are included, the stability is governed by the following relation.

$$\Delta t < \frac{2g\ (\Delta x)^2}{C^2\ HU} \qquad (7)$$

3) Conservation

The system is conservative for a constant topography. In the case of variations in depths, an oscillation of small wave length was observed in the case of the Seine (SALOMON, 1980). This is overcome by the introduction of the pseudo viscosity as discussed earlier.

4) Application

In the present work, the model is applied to the Gironde estuary in the following manner. The entair domain consists of a matrix of 93*20 grid points. Each of the rivers, namely, Dordogne and the Garonne is represented by a one dimensional model and they are connected to the 2D model. This method was utilised by SALOMON in the case of the Loire. The 1D models for the Dordogne and the Garonne consist of 94 and 74 grid points respectively. In the 1D models, Δx is the same as in the 2D model and Δy is varies according to the breadth of the section concerned.

In the Gironde, the reference point of depths i.e, the lowest low water mark of Nivellement General de la France (N. G. F.) varies irregularly from the Pointe de Grave towards the head of the estuary. The lowest low water mark at the Pointe de Grave is used as a reference

point and the depths are corrected accordingly so as to bring all the depths of the domain to a horizontal plane. The grid spacing is 960 metres and the time step used is 180 seconds. The value of the coefficient of viscosity chosen is 850 and it is the same troughout the domain.

5) Open boundary conditions

The seaward boundary conditions are given in terms of water surface elevations. This is done supposing that the tidal wave enters in the form of an arc of a circle, with the amplitude varying as a sinusoidal function and the phase determined by the distance from the centre of the arc The amplitudes are defined based on the tide gauge data at Cordouan. It is true that this method of defining the open boundary conditions needs more precision. Limitations lie in the fact that the tidal variations near the seaward boundary are known only at one point, namely Cordouan. At the river sides, the open boundary conditions are given in terms of the river discharge rates.

III. LINK NODE MODEL

The second type of model used in the present study is a hydraulic model, commonly referred to as link node model. This type of model is originally designed to describe the flow in open channels, where the flow is mainly one directional. We have chosen the method described by FEIGNER, which is briefly described in page 9, for the application of the Gironde estuary. The model is one dimensional. By laying a grid network of polygons of variable sizes, two dimensional aspects of the flow can be represented.

1) Model equations

The model consists of momentum equation in one dimensional form applied to the channel elements and the equation of continuity to the junctions.

The momentum equation in one dimensional form may be expressed as :

$$\frac{\partial U}{\partial t} = -U\frac{\partial U}{\partial x} - k|U|U - g\frac{\partial \zeta}{\partial x} \qquad (8)$$

where

U : velocity along the channel element

K : coefficient of friction

ζ : water surface elevation

the direction x is taken positive towards the head of the estuary.

The equation of continuity is written as :

$$\frac{\partial \zeta}{\partial t} = - \frac{1}{b} \frac{\partial}{\partial x} (UA) \qquad (9)$$

It is to be noted that in applying this hydraulic model to the case an estuary, the following assumptions are made.

(i) The wind and Coriolis forces are negligible.

(ii) The parameters like velocity, depth and area of cross section are constant for a channel element.

(iii) A channel element is a straight line.

(iV) The cross sectional area is uniform along a channel.

(V) The tidal wave length is at least twice the channel depth.

(Vi) Acceleration normal to the direction of the channel element is neglected.

Since velocity is constant for a channel element, advection term cannot be evaluated directly. FEIGNER computed the advection term indirectly using the continuity equation by a method proposed by LAI (1966).

Expanding (9) and rearranging the terms,

$$\frac{\partial U}{\partial x} = \frac{-b}{A} \frac{\partial \zeta}{\partial t} - \frac{U}{A} \frac{\partial A}{\partial x} \qquad (10)$$

where

b : mean channel width

A : area of cross section of the channel element.

2) Method of Resolution

The equations (8) can be written in finite difference form as follows :

$$\frac{\Delta U_i}{\Delta t} = -U_i \frac{\Delta U_i}{x_i} - k\, U_i |U_i| - g \frac{\Delta \zeta}{x_i} \qquad (11)$$

where i indicates the index of the channel element.
The equation of continuity (9) becomes :

$$\frac{\Delta \zeta_n}{\Delta t} = \frac{\Sigma\, Q_n}{A_n} \qquad (12)$$

where n is the index of the junction and ΣQ_n is the algebraic sum of the flux of water entering and leaving a polygon and A_n is the surface area of a polygon.

3) Computation procedure

It involves the following stages :

(i) Velocities are calculated for the channel elements at time $t+\Delta t/2$ using the momentum equation based on the initial conditions at time t. The initial conditions are the velocities, cross sectional areas and water surface elevations.

(ii) Flux of water through each side of a polygon is calculated at $t+\Delta t/2$ using the velocities obtained above and the cross sectional areas at t.

(iii) The water surface elevations are computed at $t+\Delta t/2$ based on the continuity equation using the flux obtained in the second stage.

(iV) The cross sectional areas are calculated at $t+\Delta t/2$ using the water surface elevations computed in the third stage.

(V) The velocities are computed at $t+\Delta t$ utilising the cross sectional areas and water surface elevations at $t+\Delta t/_2$

The procedure is continued for the following time steps.

4) Stability

The explicit nature of calculation makes a constraint on the time step given by the following relation.

$$x_i > (\alpha_i \pm U_i)\ \Delta t \qquad (13)$$

where

x_i : the length of a channel

α_i : the velocity of the tidal wave in the channel element.

For shallow water, $\alpha_i = \sqrt{gh}$, where h is the depth of a channel element.

5) Evaluation of the coefficient of friction

The coefficient of friction is evaluated using a quadratic law based on Mannings equation. It is given as follows :

$$K = \frac{gn^2}{2.208\ R^{\frac{4}{3}}} \qquad (14)$$

where

n : Manning's roughness coefficient

R : hydraulic radius

$R = \zeta + h$, where h is the depth.

6) Application of the link node model to the Gironde

GAUDETTE (Rapport Intern, 1980) adapted the algorithm of FEIGNER and we have applied the model to the Gironde estuary. In the application of the Gironde, the model domain extends from plateau de Cordouan at the seaward side and upto Pessac in the Dordogne river and the Réole in the Garonne.

In the case of the Gironde, the calculation of the advection term by the above mentioned method gave numerical instabilities. Accordingly, we have omitted the advection term for the simulations.

7) Construction of the grid

The composition of the grid is made in such a way as to take into account the islands , natural channels, longitudinal sand banks etc. The channel elements are oriented in such a manner as to minimise the variations of depth along them.

Let us see how a polygon is constructed (figure 4).

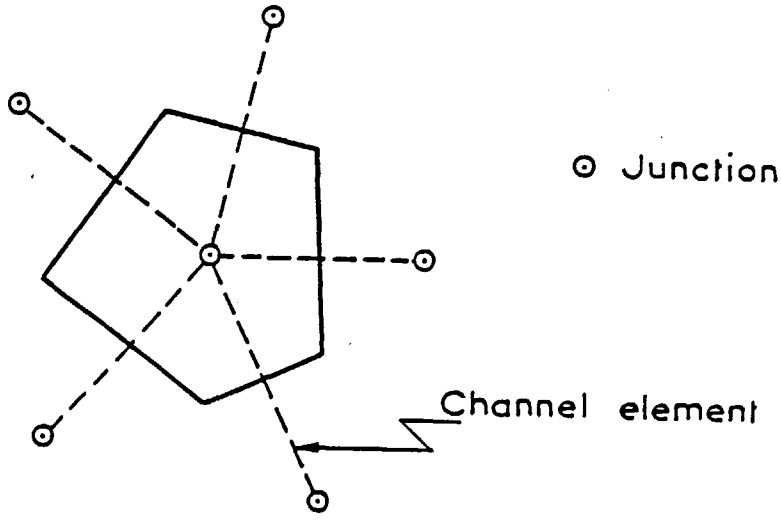

Figure 4 : A typical polygon in the grid

A junction is situated at the centre of gravity of the polygon. The distance between any two junctions corresponds to the length of a channel element. The side of a polygon is the width of the channel element concerned.

The whole network consists of 407 channel elements and 241 junctions. The channel length varies from 900 to 7000 metres, with typical values between 2000 to 3000 metres. The channel widths have variations between 120 to 6000 metres, lower values occuring in the rivers. A typical channel width is of the

order of 2000 to 2500 metres. The time step used for simulation is 60 seconds.

To calibrate the model, the coefficient of Manning used are in between .04 to .02, with lower values assigned to the channel elements situated near to the head of the estuary.

7) Open boundary conditions

The seaward boundary conditions are given in terms of variations of water surface elevation. This is done in a similar way as in the case of the stair step boundary model, as discussed in page 14.

The open boundary conditions at the river sides are given in terms of river discharge rates.

8) Tidal flats

The model takes into account of the tidal flats which get exposed above the water surface elevation during low tide. Consider the situation in which the surface elevation at a junction becomes inferior to the depth of an adjacent junction. In that case, the polygon containing the former junction will be removed from the calculations until the surface elevation in it attains sufficient height. It means that the flux of water through all sides of the removed polygon is zero. Hence, the temporary disappearance of a few polygons makes the calculations done on a redefined grid.

Moreover, when the depth of water of any channel element becomes inferior to a "critical value", the equations for the velocities are no longer utilised and they are replaced by the following equations.

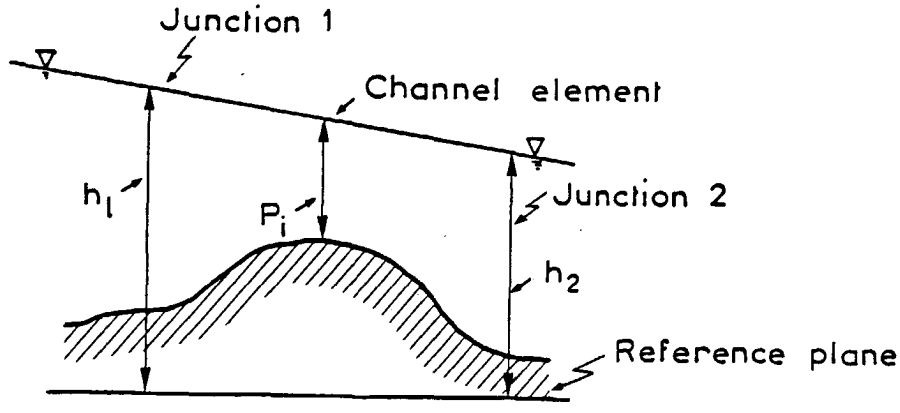

Figure 5 : Situations in which depth of a channel element becomes inferior to a critical value

In figure 5, if P_i < HLIM,

$$Q = K' P_i \sqrt{h_1 - h_2} \cdot b_i \qquad (17)$$

where

Q : flux of water in m3/s.

P_i : depth of the channel element.

h_1, h_2 : are the surface elevations at the first and second junctions respectively.

HLIM : critical value of depth.

Velocity can be calculated from (17) as follows :

$$U = K' \sqrt{h_1 - h_2} \qquad (18)$$

where

$$K' = \frac{(2,208)^{1/2} \cdot (HLIM)^{2/3}}{n_i \cdot (x_i)^{1/2}}$$

IV. IRREGULAR GRID FINITE DIFFERENCE MODEL FOR ESTUARINE APPLICATIONS

This part of the work consists of developing a numerical model for estuarine and coastal applications using irregular grid finite difference scheme. The purpose is to adopt a technique which could give a better representation of the coastline and islands. This attempt is particularly relevant in the case of the Gironde, which is caracterised by complex geomorphological features.

1) Origin

Irregular grid finite difference scheme was introduced for oceanic problems by THACKER (1976) for the simulations of shallow water oscillations,

where the equations were linearised. Later, in 1979, he developed a full fledged model, with non linear terms included, for the forecast of storm surges. In this work, we try to develop a 2D model in the horizontal plane for the computation of tidal currents in estuaries.

2) Principle

The principle of the irregular grid finite difference scheme may be summarised as follows. The slope of a curved surface may be approximated by the slope of a triangular plane passing through points as shown in figure 6.

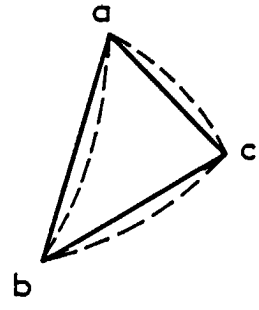

Figure 6 : Approximation of a curved surface by a triangular plane

The partial derivative of the surface is approximated by the slope of the plane passing through the surface. The domain of interest can be divided into a number of triangular elements.

Inside the domain, each vertex of a triangle is surrounded by six triangles, where as at the boundary by three, four or five. The vertices of the triangles are taken as grid points. The partial derivative at a grid point is calculated by a weighted average of the values obtained from adjacent triangles. The weighting factor depends on the area of the triangle. The formulas used are as follows. (THACKER, 1979)

$$\frac{\partial f}{\partial x} = \sum_{i=1}^{N} f_i \, (Y_{i+1} - Y_{i-1} / \delta \tag{19}$$

$$\frac{\partial f}{\partial y} = -\sum_{i=1}^{N} f_i \, (x_{i+1} - x_{i-1} / \delta \tag{20}$$

where f is any variable U, V or ζ

and

$$\delta = \sum_{i=1}^{N} x_i \, (Y_{i+1} - Y_{i-1})$$

i is the index of the grid point and N varies from 3 to 6.

3) Model equations

The above mentioned principle of approximating the partial derivatives is used in developing a numerical model in the present study. Model equations are the equations of momentum in the x and y directions and the equation of continuity. The equations are in the vertically integrated form.

$$\frac{\partial U}{\partial t} + U\frac{\partial U}{\partial x} + V\frac{\partial U}{\partial y} - fV + g\frac{\partial \zeta}{\partial x} + \frac{gU\,(U^2 + V^2)^{\frac{1}{2}}}{C^2 H.} = 0 \tag{21}$$

$$\frac{\partial V}{\partial t} + U\frac{\partial V}{\partial x} + V\frac{\partial V}{\partial y} + fU + g\frac{\partial \zeta}{\partial y} + \frac{gV\,(U^2 + V^2)^{\frac{1}{2}}}{C^2 H} = 0 \tag{22}$$

$$\frac{\partial \zeta}{\partial t} + \frac{\partial (HU)}{\partial x} + \frac{\partial (HV)}{\partial y} = 0 \tag{23}$$

where the symbols have the same meaning as in the stair step boundary model (see page 10).

The model contains advection terms and the Coriolis term. It is to be noted that in the present scheme, there is no direct method for approximating the second derivatives. Accordingly, we have not introduced the viscosity term in the momentum equations.

4) Numerical resolution

The model uses a leap frog time scheme. The equations (21) to (23) can be written in finite difference scheme as follows.

$$\frac{U_i^{n+\frac{1}{2}} - U_i^{n-\frac{1}{2}}}{\Delta t} + U_i^{n+\frac{1}{2}} \left(\frac{\partial U}{\partial x}\right)_i^{n-\frac{1}{2}} + V_i^{n-\frac{1}{2}} \left(\frac{\partial U}{\partial y}\right)_i^{n-\frac{1}{2}} - fV_i^{n+\frac{1}{2}} + g\left(\frac{\partial \zeta}{\partial x}\right)_i^{n} + \frac{gU_i^{n+\frac{1}{2}} \left(U_i^{2\,n-\frac{1}{2}} + V_i^{2\,n-\frac{1}{2}}\right)^{\frac{1}{2}}}{C^2 H_i} = 0 \qquad (24)$$

$$\frac{V_i^{n+\frac{1}{2}} - V_i^{n-\frac{1}{2}}}{\Delta t} + U_i^{n-\frac{1}{2}} \left(\frac{\partial V}{\partial x}\right)_i^{n-\frac{1}{2}} + V_i^{n+\frac{1}{2}} \left(\frac{\partial V}{\partial y}\right)_i^{n-\frac{1}{2}} + fU_i^{n+\frac{1}{2}} + g\left(\frac{\partial \zeta}{\partial y}\right)_i^{n} + \frac{gV_i^{n+\frac{1}{2}} \left(U_i^{2\,n-\frac{1}{2}} + V_i^{2\,n-\frac{1}{2}}\right)^{\frac{1}{2}}}{C^2 H_i} = 0 \qquad (25)$$

$$\frac{\zeta_i^{n+1} - \zeta_i^{n}}{\Delta t} + \frac{\partial}{\partial x} (HU)_i^{n} + \frac{\partial}{\partial y} (HV)_i^{n} = 0 \qquad (26)$$

where i is the index of the triangle and n corresponds to the time step.

5) Stability and Convergence

THACKER (1978 a,b) determined the stability and convergence conditions of the scheme as follows. The stability is governed by a term called courant number given as :

$$\gamma = \frac{(gh)^{1/2} \cdot \Delta t}{\Delta x} \qquad (27)$$

The condition for the scheme to be stable is that γ should be less than 1 .

By the application of Green's theorem on an irregular grid, it is proved that the numerical scheme is convergent as long as there is no flow across the boundaries.

6) Sensibility of the scheme

It is to be noted that the formulas for partial derivatives depend on the spatial distribution of grid points. Hence, for a highly irregular grid the system may be unstable. Sunderman (1966) introduced a factor called numerical viscosity, which is given as follows.

$$f(x) = \alpha f + \frac{1-\alpha}{N} \sum_{i=1}^{N} f_i \qquad (28)$$

Where $0 \leq \alpha \leq 1$ and f is any variable U, V or ζ. The summation is done over the values of the variable at the neighbouring grid points multiplied by α.

7) Application in the Gironde

The extent of model domain and grid resolution is the same as the stair step boundary model. The whole domain consists of 1330 triangles (fig 8) In the estuarine region isoceles triangles of equal dimensions are used with $\Delta x = \Delta y = 960$ metres. In the region of Ile Verte, triangles of smaller size are used. Inside the rivers, the grid is very irregular, with Δx same as in the estuarine region and Δy varying according to the breadth of the section concerned. In fact, the grid can be made more irregular than

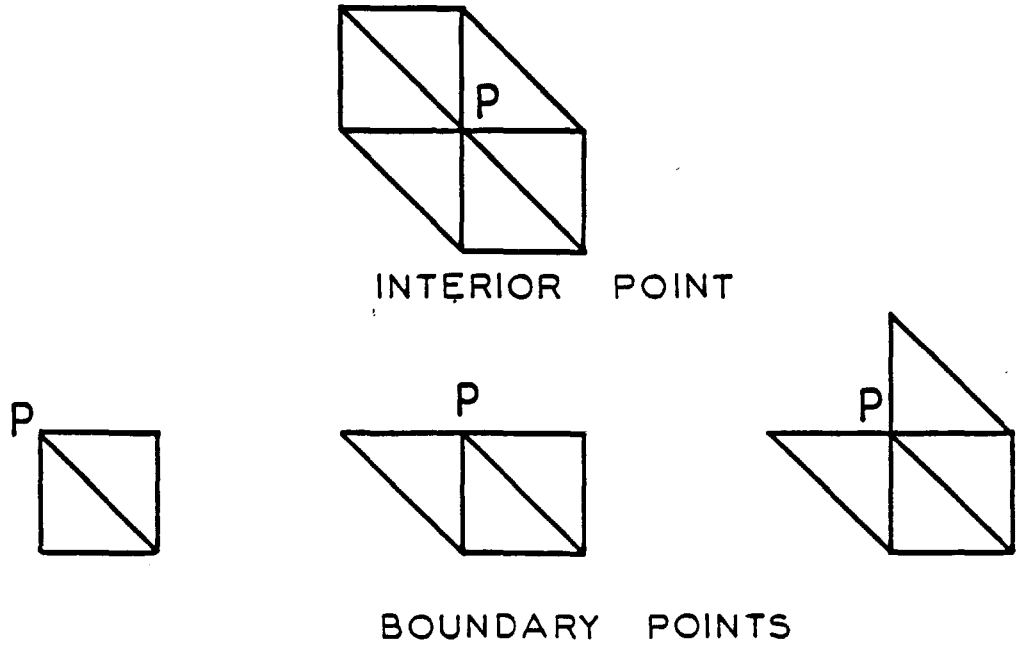

Figure 7 : Types of triangles used for the application of the Gironde

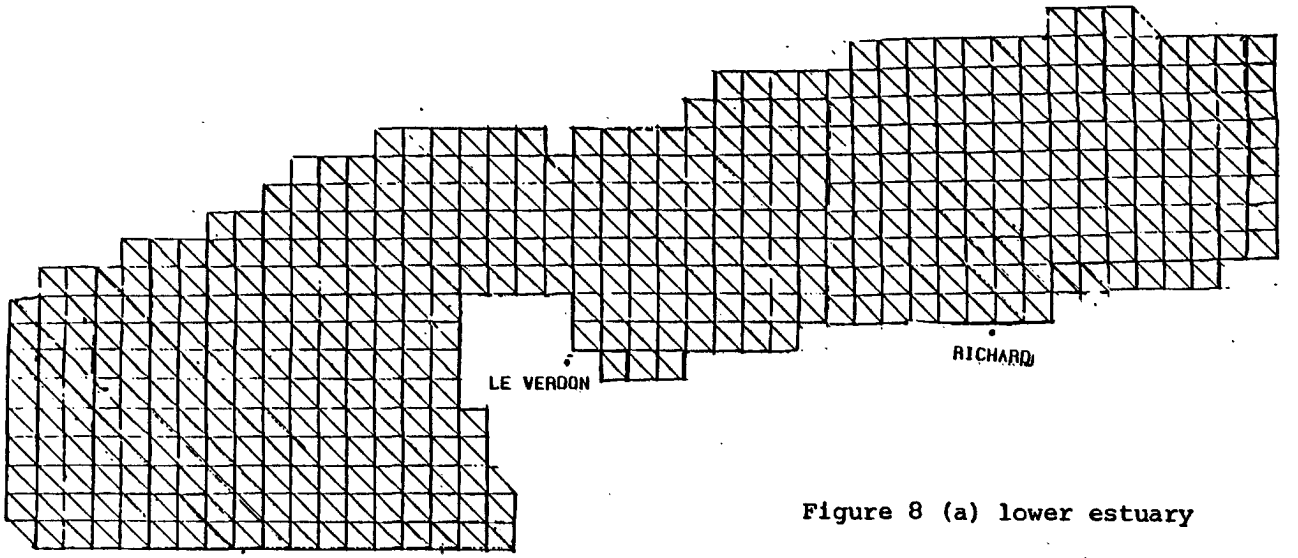

Figure 8 (a) lower estuary

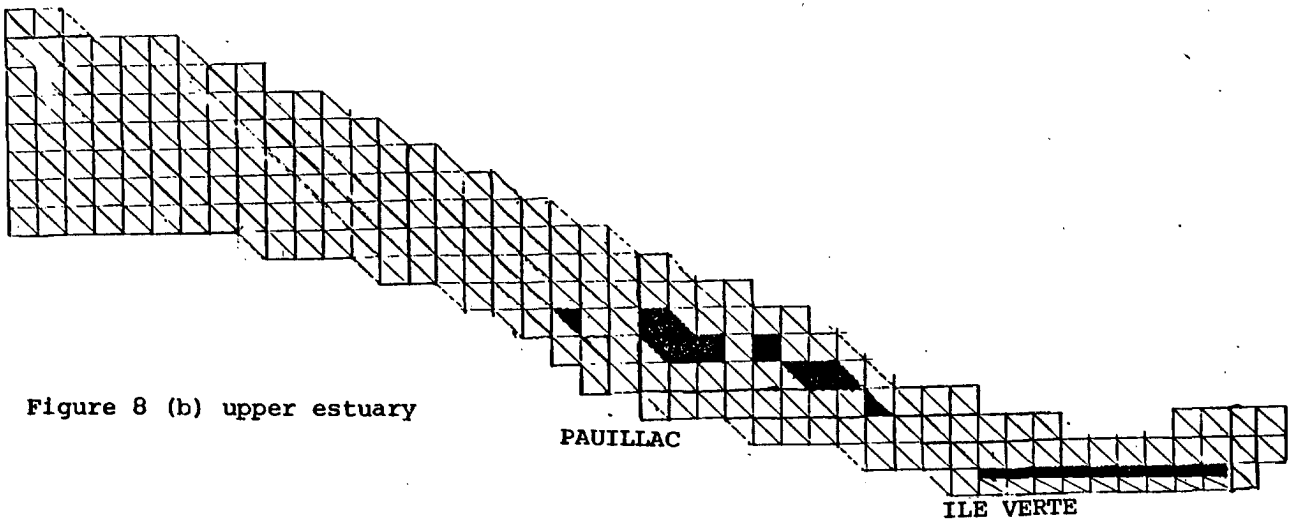

Figure 8 (b) upper estuary

Figure 8 : Irregular grid used for the application of Gironde

(The shaded areas represent the islands)

the present one. Using bigger triangles near the seaward side, where the depths are high, is useful in increasing the time step. In the present application, the grid spacing is taken constant and it is equal to that of the stair step boundary model. This permits to compare the performance of the two models more closely. However, in the upper estuary, the triangles are oriented in such a way as to represent the coastline and the islands in a better way. In the lower estuary, such a procedure is not necessary, mainly because of the regular geometry of the region.

Initial conditions are given as follows. The water surface elevations are defined to be equal to the mean tide and velocities to be zero. The model is run for more than two tidal periods, before the utilisation of the results. The time step chosen is 30 seconds. This corresponds to about one third of the maximum allowed time step (formula 27). In the present application, a time step much less than the maximum allowed value is found to give a better solution. The value of α used is equal to 0.99. For the region of islands, the value of α taken is 0.97.

All the variables U, V and ζ are calculated at the same point i.e., at the vertices of the triangles. Each grid point is given only one index, ascending from the open boundary towards the head. For each grid point, a table of values of neighbouring grid points is stored and recalled at each time step. The neighbouring points are arranged in a counter clockwise sense. The partial derivatives are calculated according to the formulas (19) to (20). The equations (24) to (26) can be solved for $n + \frac{1}{2}$ time step, by knowing the variables at $n - \frac{1}{2}$ and n time steps.

8) Open boundary conditions

The open boundary conditions at the seaward side as well as river ends are given as in the case of the stair step boundary model, as discussed in page 14.

9) Lateral boundary conditions

Lateral boundary condition states that the flow across a closed boundary is zero. For those points situated on the closed boundary, the velocity variables are projected on to a line parallel to the boundary so as to guarentee this condition.

CHAPTER III

CIRCULATION IN THE GIRONDE

Introduction

This chapter deals with a brief review of the circulation studies in the Gironde and discussion of numerical simulation results obtained from the models applied during the course of this work. Here, the emphasis is made on studying the lateral variations of different physical parameters and the circulation in the region of islands. Attempt has been made to compare the simulated results to the observed data.

The circulation in the Gironde is relatively well known, thanks to numerous observed data available from various cruises. These cruises have been conducted by the following organisations.

(i) Port Autonome de Bordeaux (PAB)
(ii) Institut Géologique du Bassin d'Acquitaine (IGBA)
(iii) Electricité de France (Laboratoire National d'Hydraulique)

Based on these data, various workers have studied the different aspects of tidal propagation and circulation in the estuary. Their important conclusions will be discussed during the course of this chapter. Numerical modelling studies were made by DE GRANDPRE and DU PENHOAT (1978). They developed a two dimensional model in the x-z plane to study the vertical circulation in the Gironde.

In the present work, the horizontal circulation in the Gironde is studied. The different physical parameters discussed are water surface elevation and currents. The current chapter consists of two parts, namely, Part I dealing with the water surface elevation and Part II circulation.

PART I - WATER SURFACE ELEVATION

I. INTRODUCTION

The characteristics of the propagation of the tidal wave in the Gironde estuary are relatively well understood. This is made possible mainly due to the availability of data from different tide gauges installed at different places (fig 1). It is to be noted that all the tide gauges, except the one at PK 26, are placed near the south bank side. This limits the knowledge of tidal propagation to the navigation channel, where as the phenomenon is less understood in the other channels. However, surface elevation data in the north bank side is available from a few cruises, which are mentioned above. SIMMON (1979) made a prediction of different harmonic constants of tide at different points along the abscisse of the estuary by harmonic analysis method and other methods.

II. CALIBRATION

The three models used in the present study are calibrated using the tide gauge data. The curves of gemetrical positions of high tide and low tide dressed by DE GRANDPRE and DU PENHOAT (1976) have also been used for this purpose. The calibration procedure consists of adjusting the coefficients of friction at various points in the domain in such a way that the differences between computed and observed surface elevations are minimum. The models are calibrated from Pointe de Grave towards the head.

III. LONGITUDINAL VARIATIONS

In the Gironde, as the tidal wave advances towards the head of the estuary, the following modifications are observed. Fig 9 (a) indicates the geometric positions of high tide and low tide along the abscisse of the estuary. It is seen that modifications in tidal range depend on the coefficient of tide. For a given coefficient of tide, when the river discharges are high, the positions of the curves get elevated in the upper estuary. In all cases, the shape of the sinusoidal curve, representing the variations of water surface elevation with time, gets gradually deformed towards the head of the estuary. A few tide gauges curves (fig 9 (b)) indicate the nature of the variations of surface elevations with time along the abscisse of the estuary. The duration of ebb increases from the Pointe de Grave towards the head.

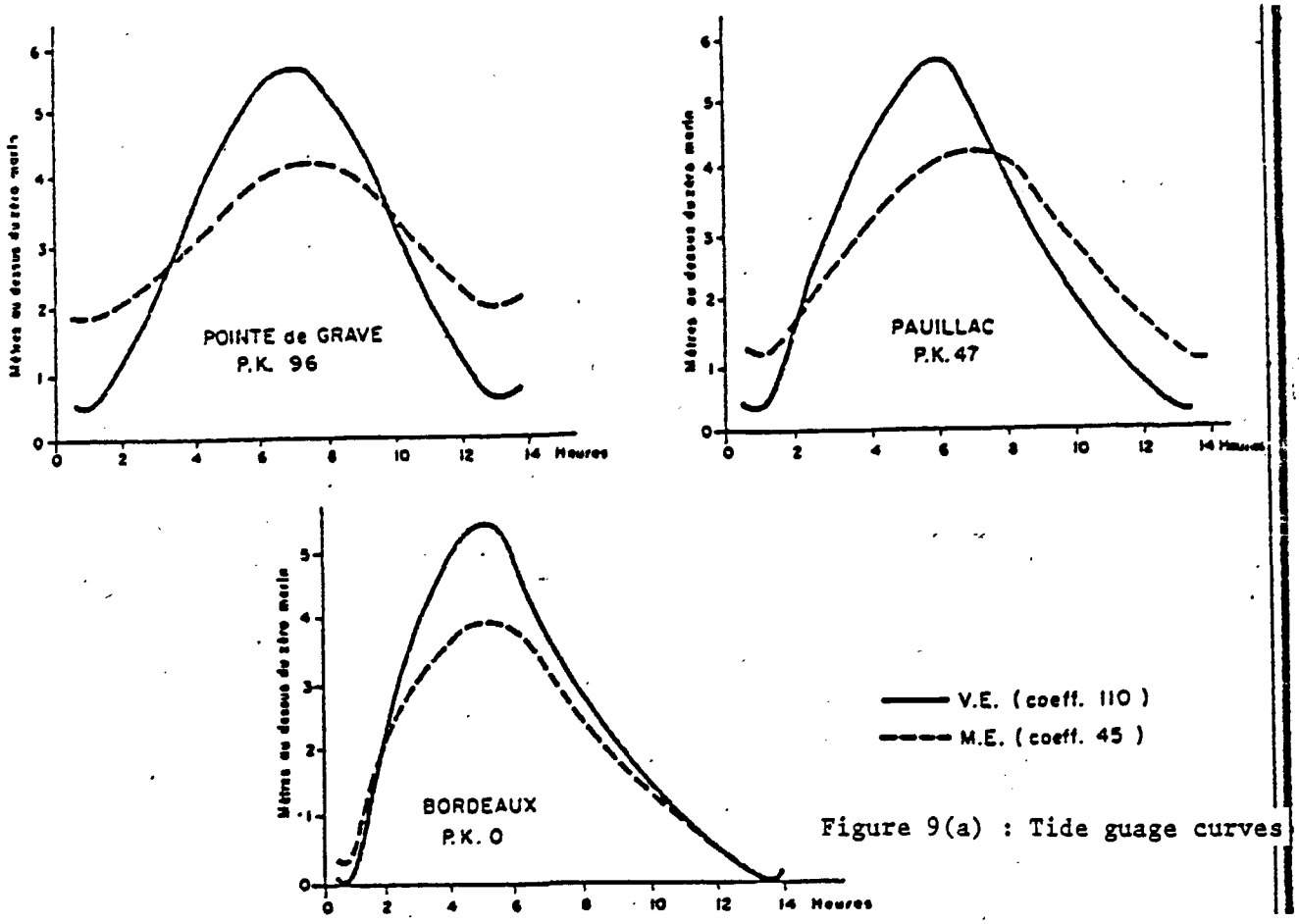

Figure 9(a) : Tide guage curves

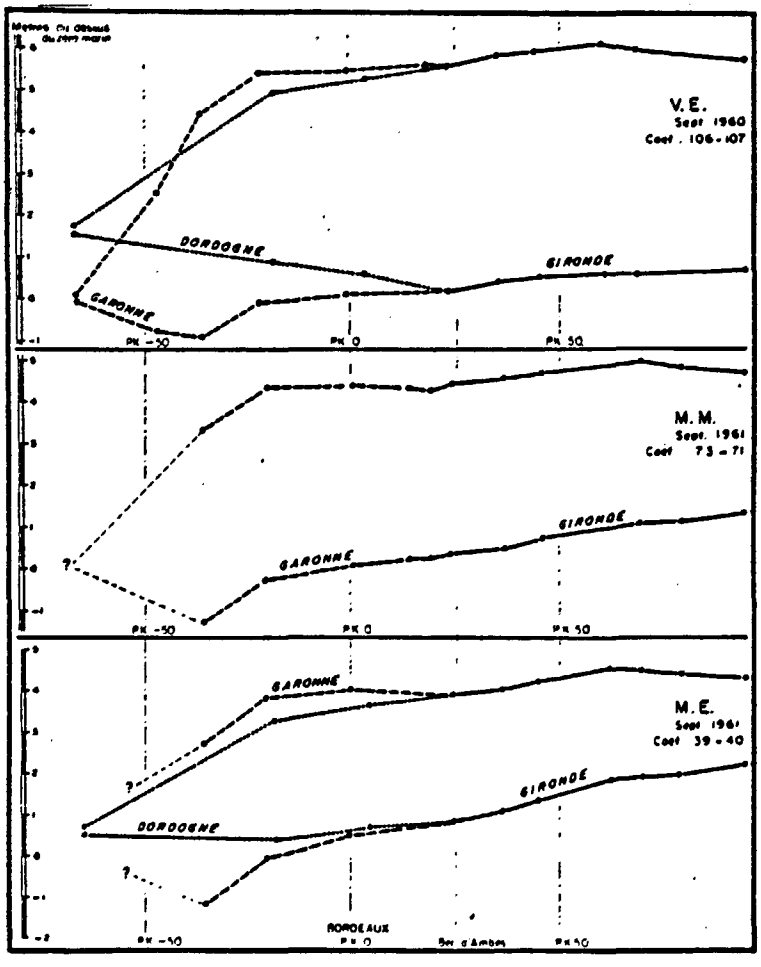

Fig 9(b) : Geometrical positions of high tide and low tide in the Gironde

(After ALLEN, 1972 ; in CASTAING, 1981)

Simulation results

A simulation of tide of 6 July 1983 is made with the link node model and irregular grid finite difference model each (River flow rates equal to 187 m^3/s). This corresponds to a coefficient of tide 52 in the morning and 56 in the evening. The models are run for a coefficient of tide 52. It is to be noted that the coefficient of tide does not evolve with time in the models. The results are presented in fig 10-14. In general, there is a good agreement between computed and observed water surface elevations. However, there is a phase difference between the two, which increases towards the head.

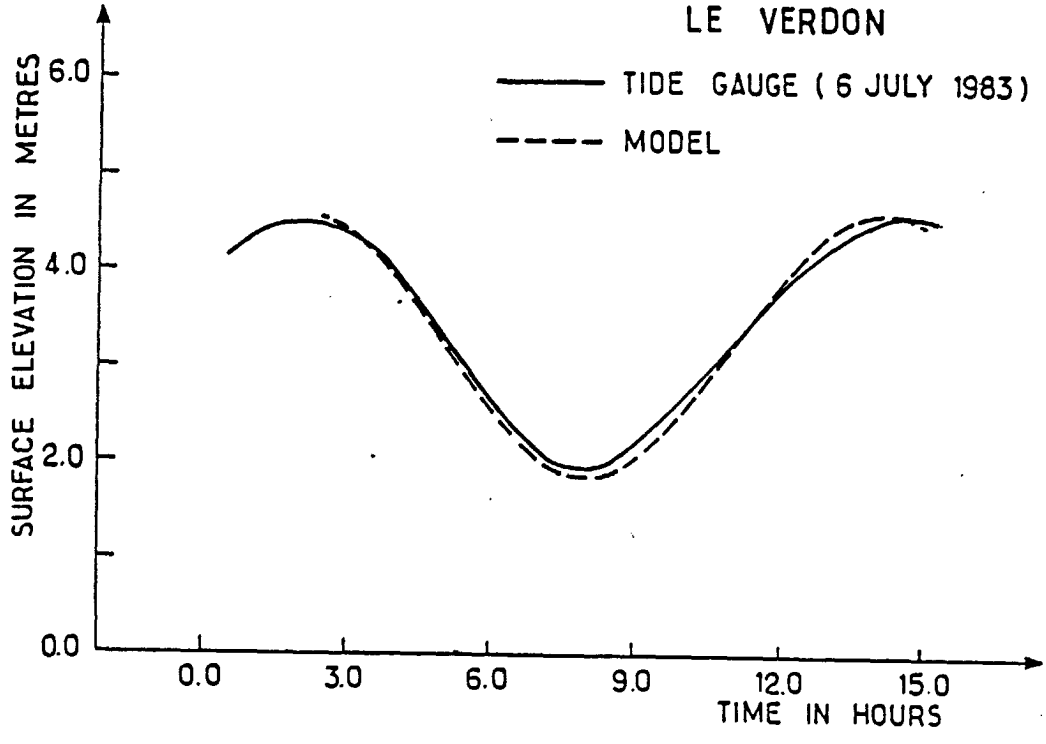

Figure 10 : Comparisons between observed and computed (link node model) water surface elevations

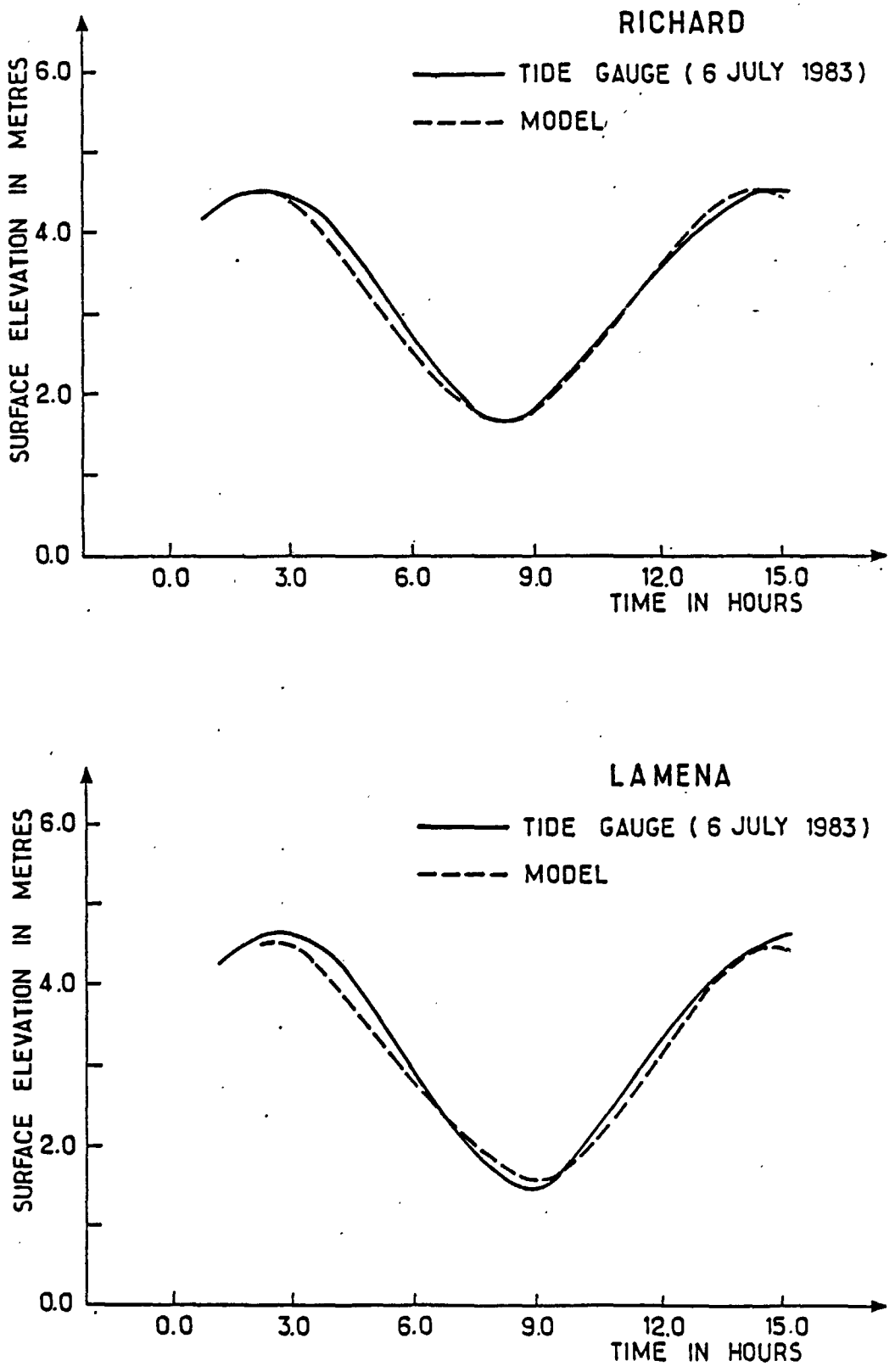

Figure 11 : Comparison between observed and computed (link node model) water surface elevations

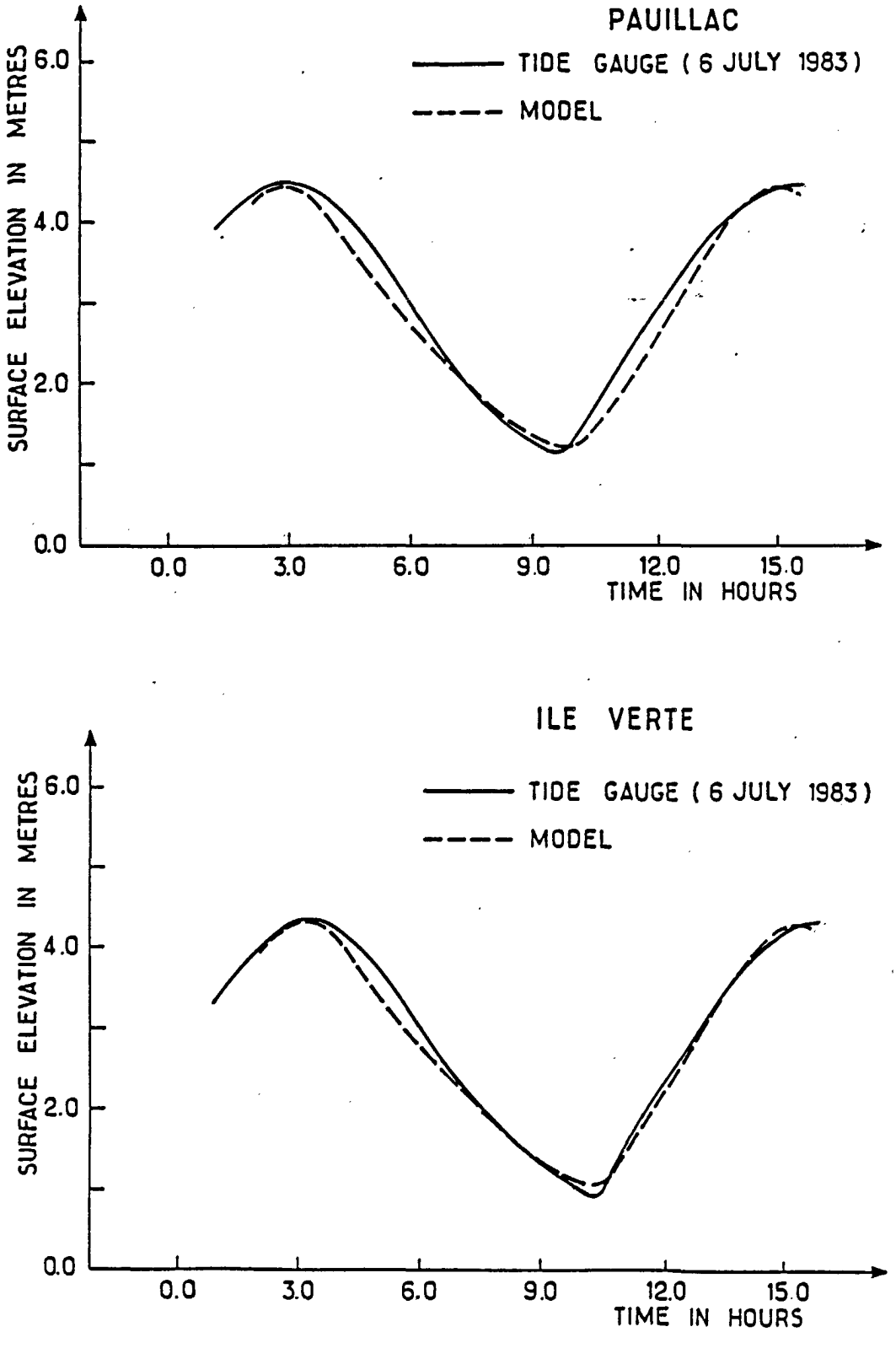

Figure 12 :Comparison between observed and computed (link node model) water surface elevations

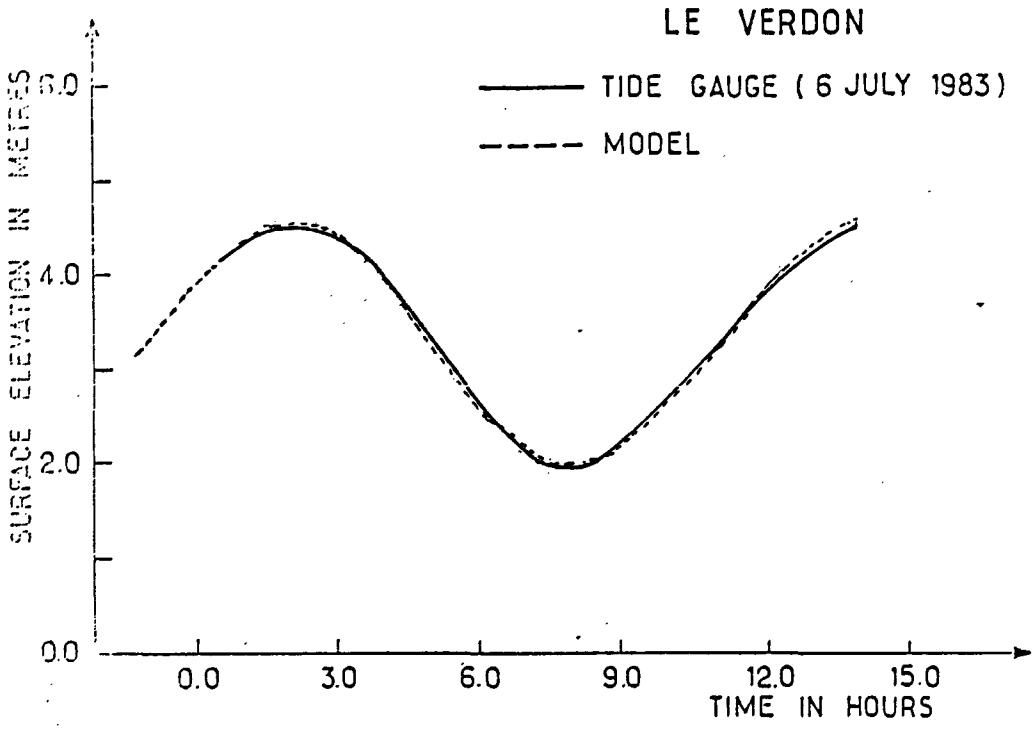

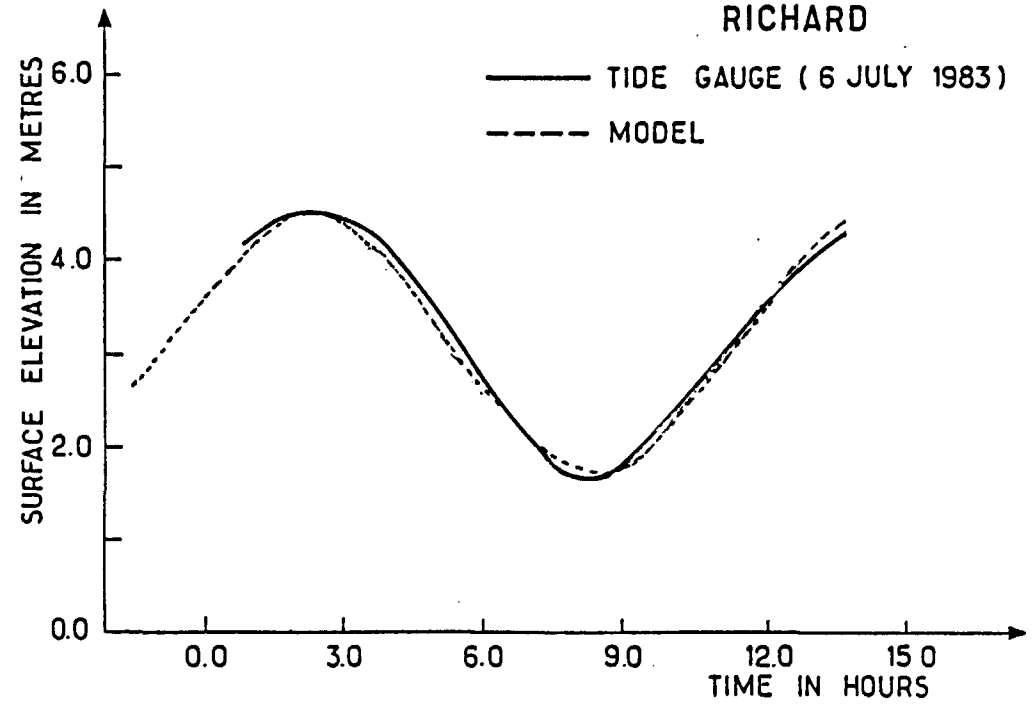

Figure 13 : Comparison between observed and computed (irregular grid model) water surface elevations.

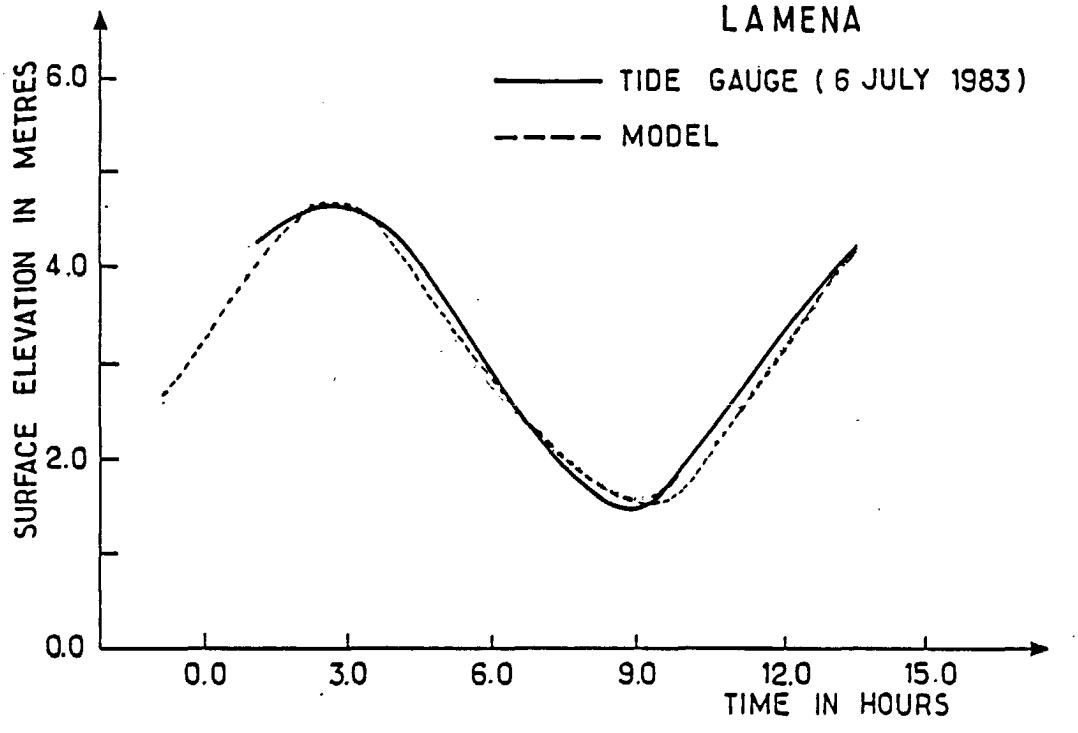

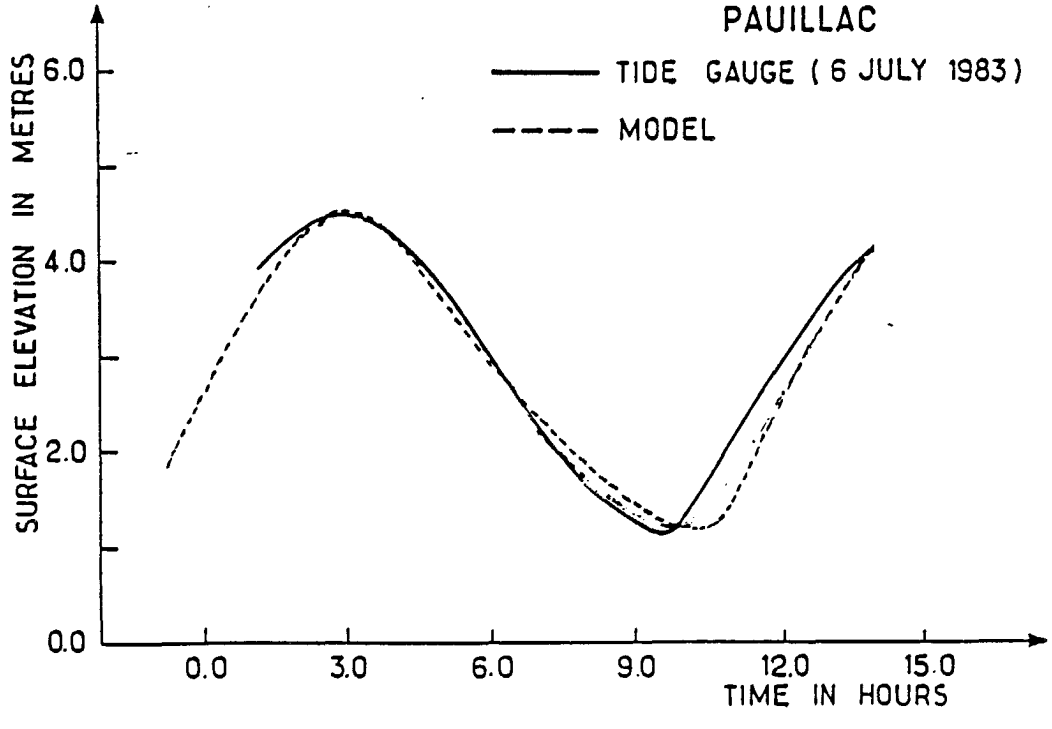

Figure 14 : Comparison between observed and computed (irregular grid finite difference model) water surface elevations

IV. LATERAL VARIATIONS

The transversal variations of tidal propagation are mainly due to the depth variations across the section. The lateral differences also occur due to meandering effects, presence of islands, sand banks etc. In fact, these small lateral differences in phase speed of tidal wave generate transversal currents.

In shallow water, the tide propagates with a velocity, which is approximately equal to $\sqrt{gh}$ (in the absence of friction), where h is the depth. Thus in deep channels, the tide propagates fast (further if friction is taken into account, the deeper regions are subjected to less bottom friction than shallow regions). The tidal wave propagates with lateral variations due to the presence of islands, sand banks etc.

Since the data from tide gauges is available only at the southern bank side, comparison of transversal differences of surface elevation between two bank sides is not always possible. In a study of lateral differences in tidal propagation, TESSON GILET (1981) compared the observed surface elevation data with calculations done by the author herself by an interpolation of tide gauge data. The results showed much difference between the observed and computed values. The calculations seem to be susceptible to errors and the results are not reliable.

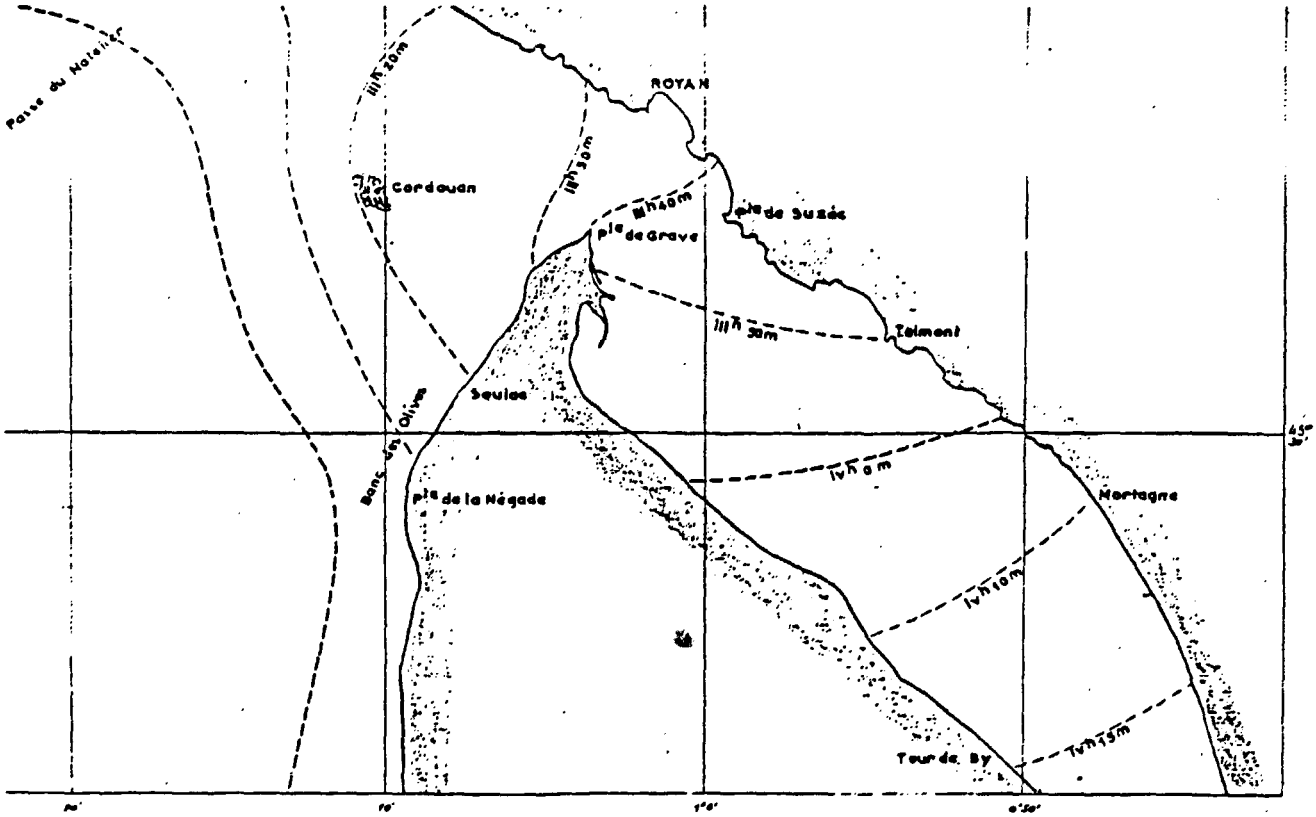

Figure 14 : Co tidal lines in lower estuary

Fig 15 represents the cotidal lines for lower estuary. It can be seen that the tide propagates in advance in the Saintonge channel. From Mortagne (PK 74), onwards the phase differences between two banks are absent. At Pauillac, the observations (ALLEN, 1972) show that the tidal wave propagates faster in the navigation channel.

Simulation results

Stair step boundary model results presented in fig. 16 to 18 show that at Richard, Valeyrac and St. Christoly, the phase differences between the two bank sides is more along the southern side and these differences increase gradually towards the head. It is to be noted that the comparison is made along the y direction of the model domain,

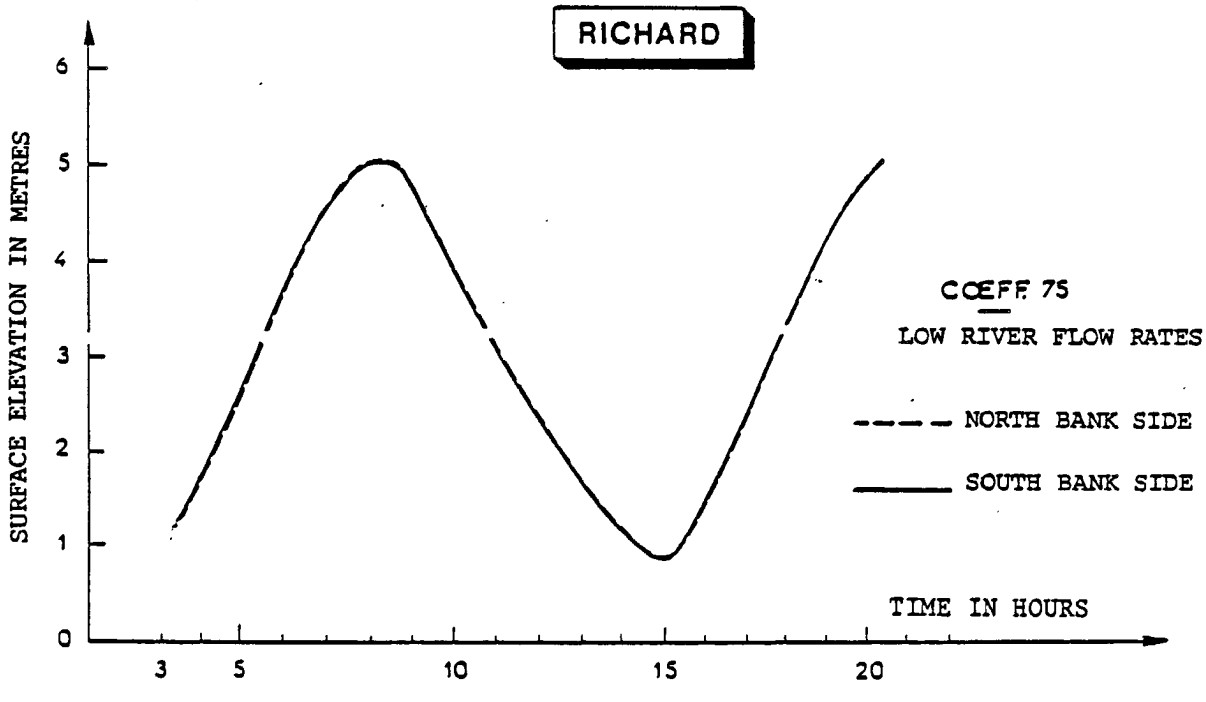

Figure 16 : Comparison of surface elevations between two bank sides of the estuary - stair step boundary model

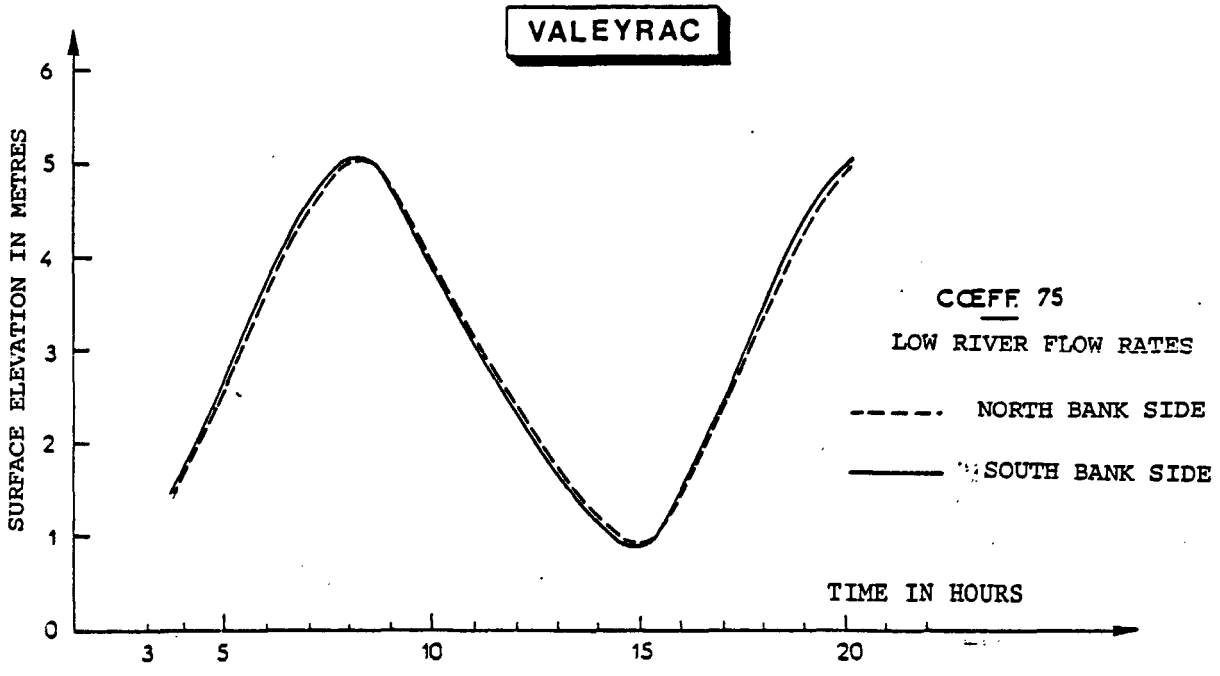

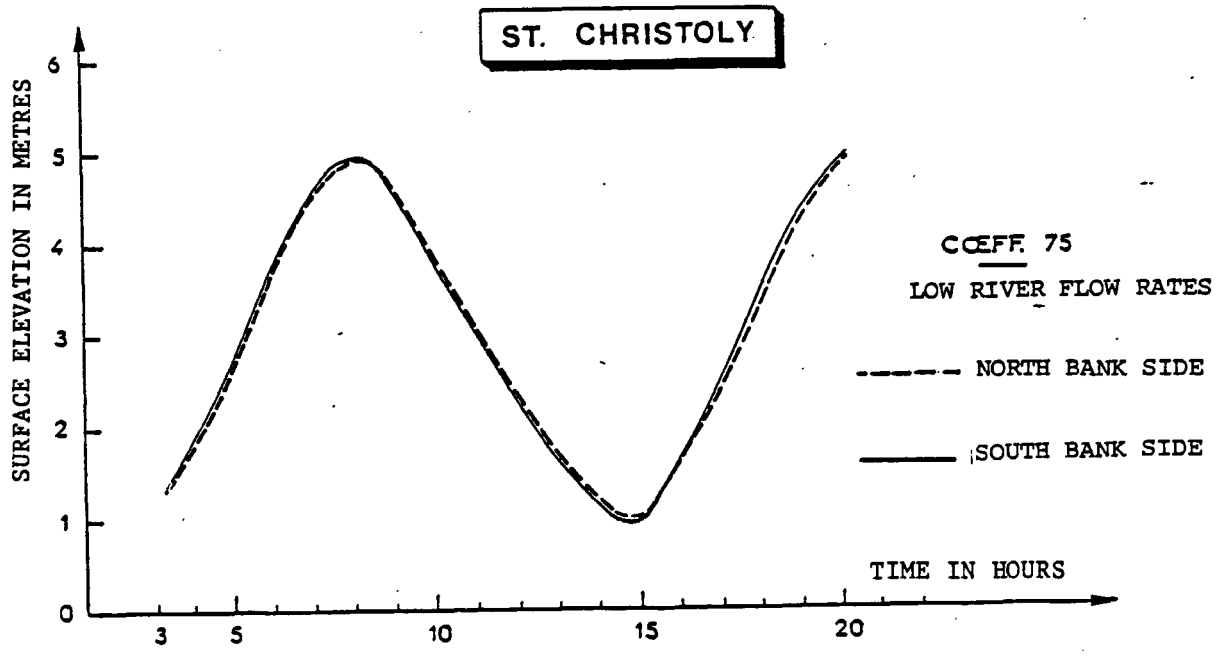

Figure 17 : Comparison of surface elevations between two bank sides of the estuary - stair step boundary model

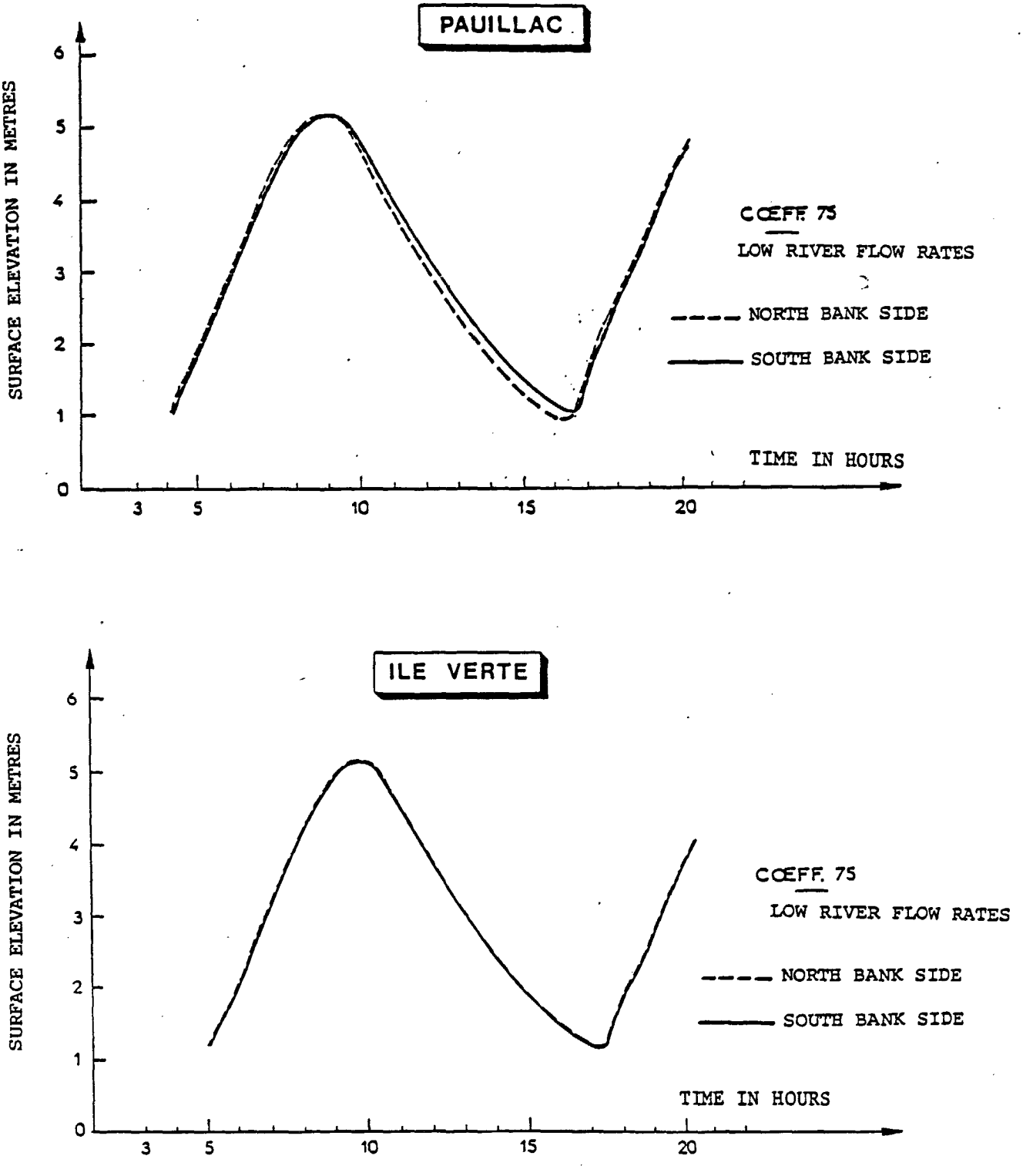

Figure 18 : Comparison of surface elevations between two bank sides of the estuary (stair step boundary model) .

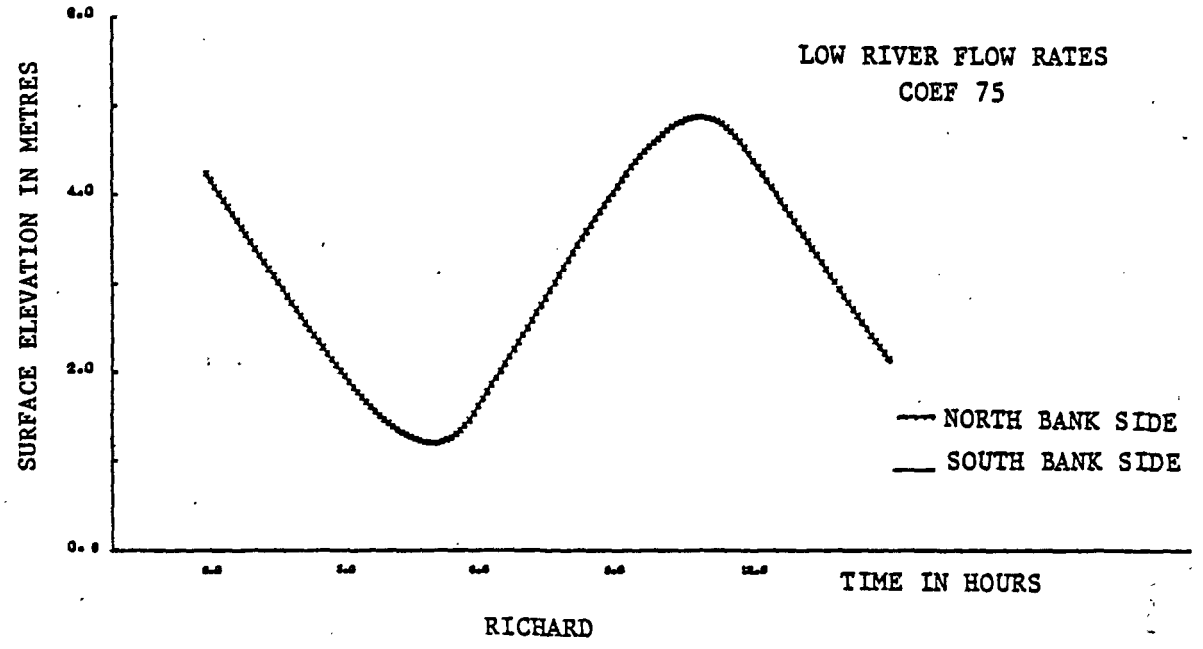

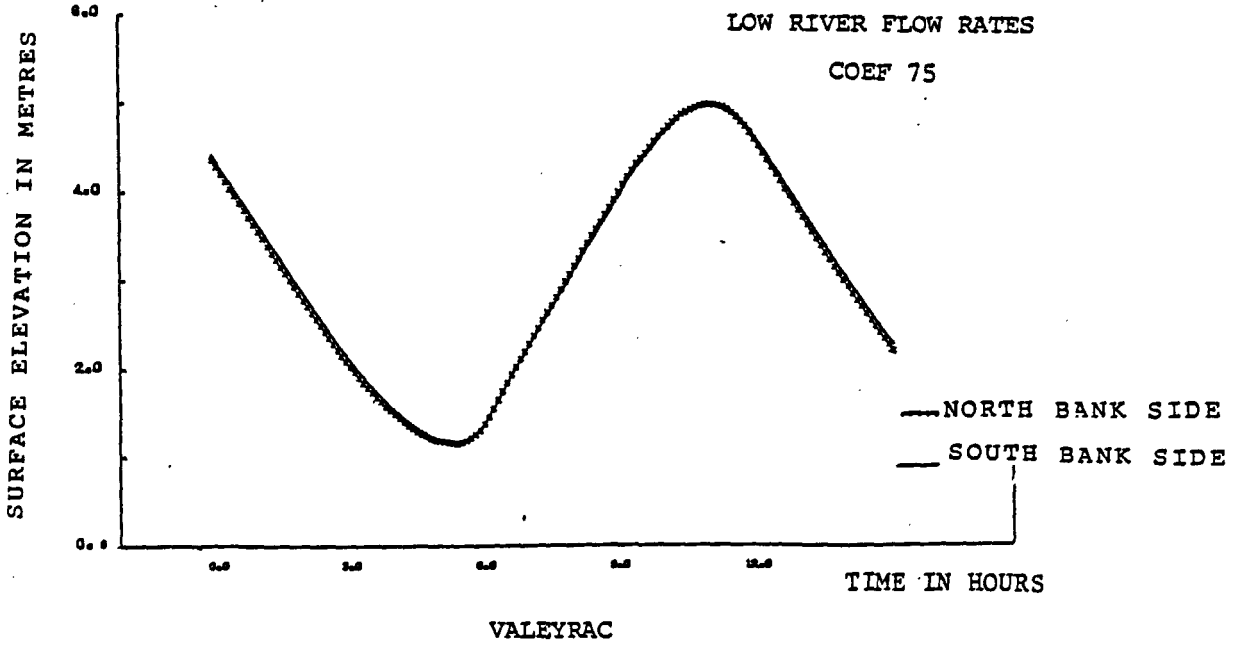

Figure 19 : Comparison of surface elevations between two bank sides of the estuary - irregular grid model

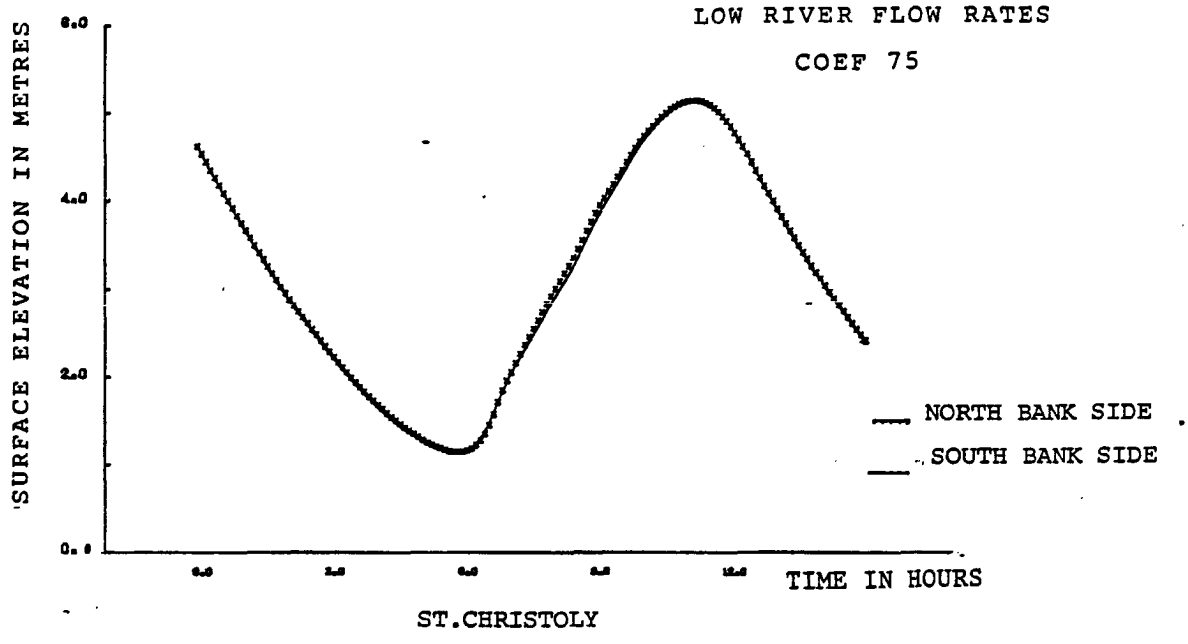

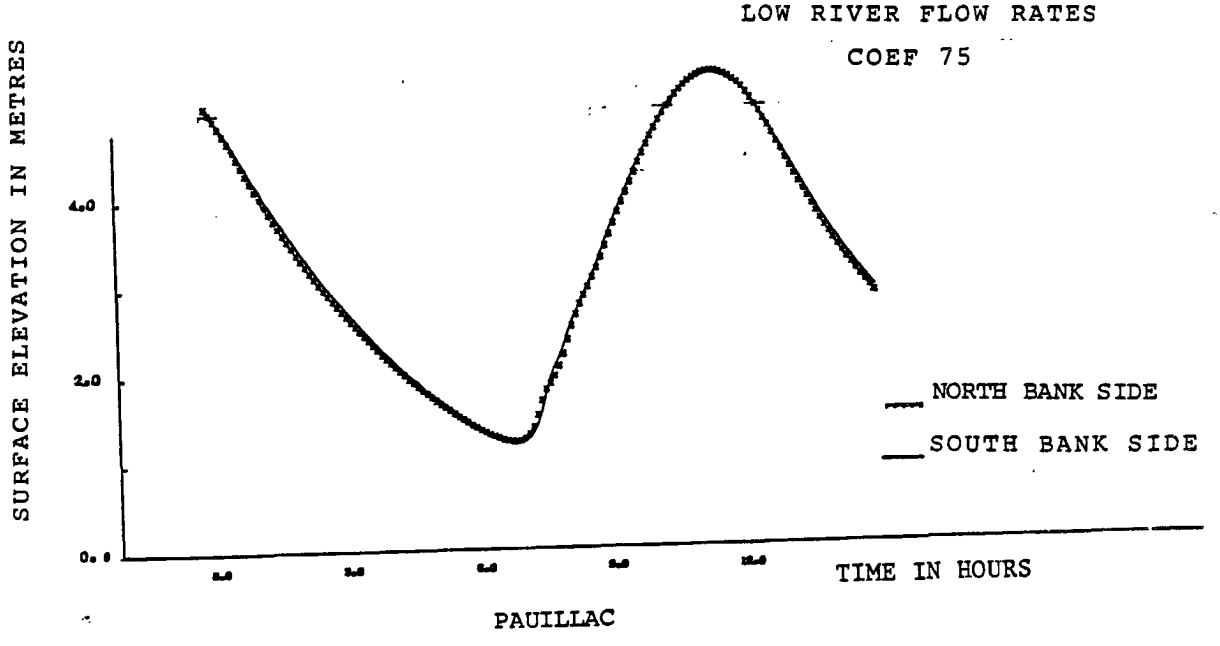

Figure 20 : Comparison of surface elevations between two bank sides of the estuary - irregular grid model

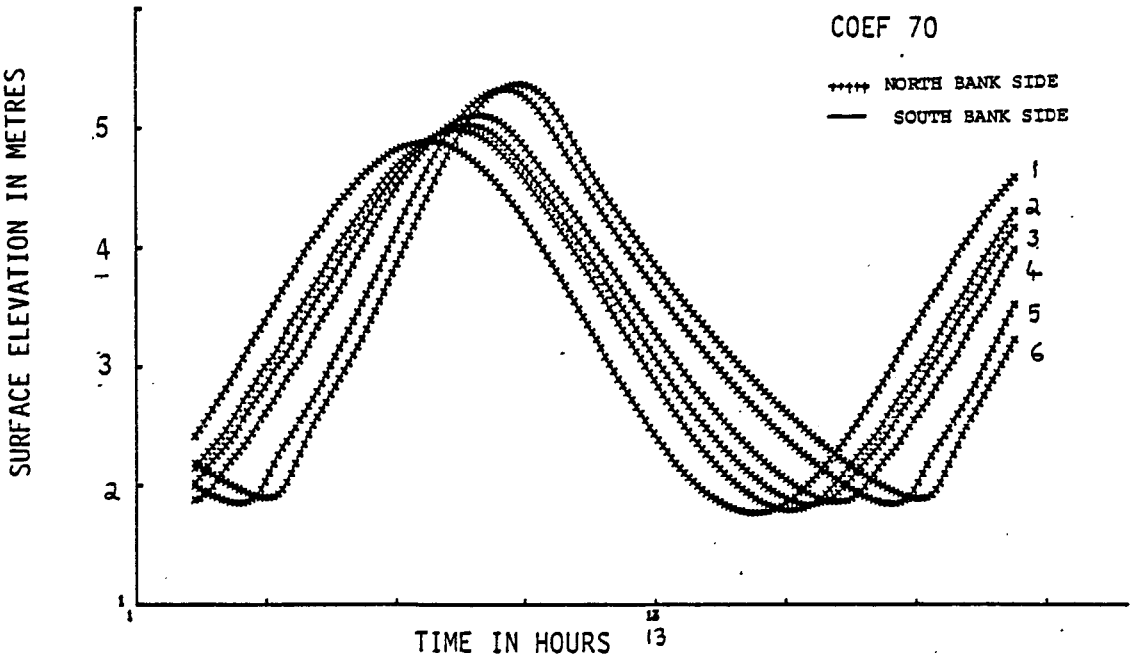

Figure 21(a) : Comparison of surface elevations between two bank sides of the estuary (link node model)

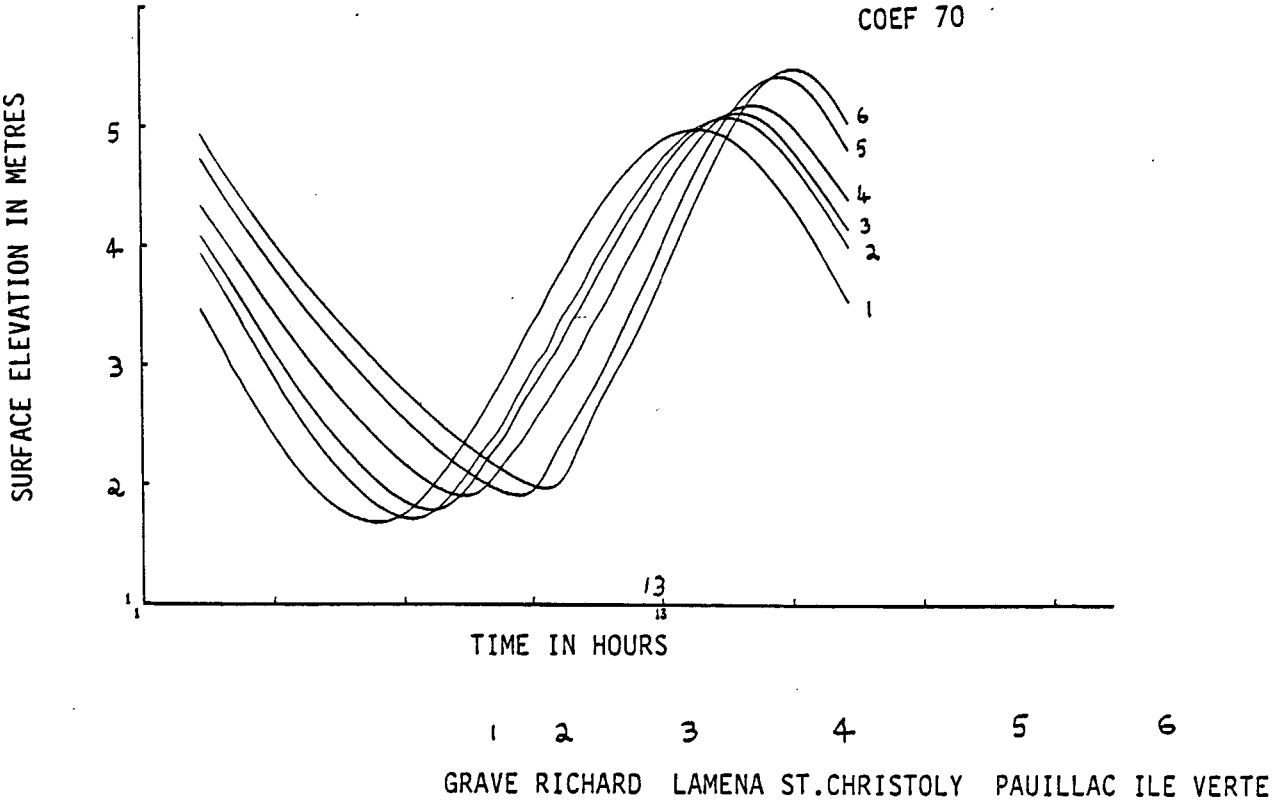

Figure 21(b), : Surface elevations along the axis of the estuary during high river discharges (link node model)

It means that in the region of regular geometry of the estuary, the tidal wave accelerates in the deeper region i.e., along the navigation channel, which is situated near the south bank side. Co tidal lines (fig. 15) indicate that the tidal wave enters into the estuary with a slight advance along the north bank side and the phase differences between the two bank sides are absent from Mortagne onwards. Upstream, from the middle region of the estuary, there is no data regarding the tidal variations along the north bank side. At Pauillac, the simulated curve of surface elevations indicates that the tidal wave is in advance along the north bank side. It is to be noted that along the lateral section considered for comparison at Pauillac, the distance travelled by the tidal wave is less at the north bank side than at the southern side. However, observations (page 36) show that the tidal wave moves faster in the navigation channel at Pauillac. Upstream, at Ile Verte, the lateral differences in phase speed between two bank sides are absent, as the width of the estuary reduces considerably towards the head.

A comparison of surface elevations between two bank sides is made using irregular grid finite difference model, (fig. 19-20). The lateral difference are less significant in these results so as to make comparisons between the two bank sides.

Fig. 21 (a) indicates that small lateral variations in surface elevation are practically absent in the link node model. This explains the fact that this type of model cannot fully describe two dimensional aspects of the flow.

Fig. 21 (b) represents the surface elevation curves as a function of time along the abscisse of the Gironde during high river flow rates (1300 m^3/s). For those points in the upper estuary, these curves get shifted upwards compared to fig. 21 (a), though there is not much change in tidal ranges.

PART II - CIRCULATION

I. INTRODUCTION

The French estuaries such as the Seine, Loire and the Gironde are caracterised by high tidal ranges. In these estuaries, the dynamics is controlled by the action of tide. The currents produced by density gradients, which are observed in the estuaries of certain other continents, for example, Vellar estuary (India), are negligible. In fact, in the case of the Gironde, DU PENHOAT and SALOMON (1979) proved that the effect of introducing a density gradient in their 2D model in the vertical plane (X-Z) made little influence on the current patterns. In the present study, the models do not take into account of the density gradient currents.

Since the Gironde is a hypersynchronous estuary (ALLEN and SALOMON, 1983), in general, the intensities of currents increase from the mouth towards the head. Variations of velocities in different lateral sections are determined by the topographical variations. Generally, maximum currents are observed in deep regions. Modifications in circulation patterns are caused due to meandering effects, presence of islands, sand banks etc.

II. BRIEF REVIEW OF CIRCULATION STUDIES IN THE GIRONDE

Various workers have described the circulation patterns in the Gironde. Here, only a few of them will be mentioned. ALLEN (1972) deduced the circulation patterns in the estuary based on the data between 1965 and 1972. He described the main features of longitudinal and lateral variations of currents. Some of his conclusions may be summarised as follows. At PK 93 and PK 89 maximum flood currents are observed in the Saintonge channel. However, at PK 89, the bottom flood currents are found to be maximum in the navigation channel. This is explained due to the curvature of the Pointe de Grave which directs the flood currents towards the northern channel. Further upstream, upto Pauillac (PK 47) both flood and ebb currents are found to be maximum in the navigation channel. Between PK 41 to PK 35, the ebb currents are of same intensity in navigation and Blaye channel, during spring tide and mean river flow rates. In the same region, during the same conditions, flood currents are found to be stronger in the navigation channel at PK 35.

TESSON GILET (1981) made a study of lateral variations of velocity maximum along a few lateral sections. These informations are synthesised for a coefficient of tide equal to 80 and slightly above. The river discharge rates are 1000-1500 $m^3 sec^{-1}$. At PK 89, intensity maximum of flood currents occur in the Saintonge channel, where as ebb is stronger in navigation channel. At PK 71, the lateral variations are less with slightly higher values found in navigation channel. Along this lateral section, surface ebb currents are stronger towards the right of the dike of Valeyrac, which is due to the presence of the dike. At PK 52, during flood, the velocities are found to be maximum in the median channel, whereas the ebb currents have their maximum intensities in the navigation channel . Accordingly, median channel is referred to flood channel at PK 52.

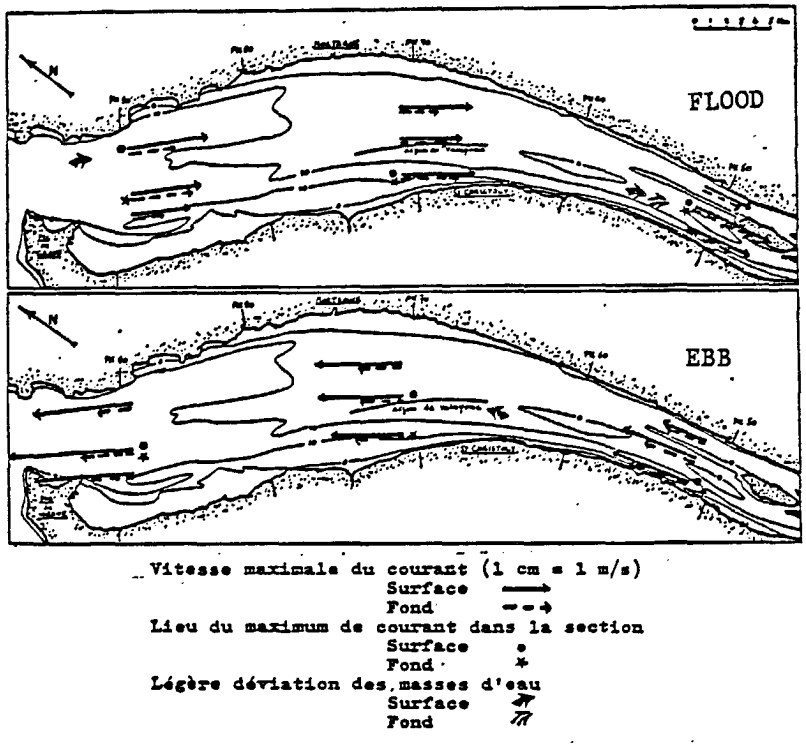

Figure 22 : Observed velocity maximum along a few lateral sections of the Gironde (After TESSON GILET,1981)

CASTAING (1981) gave much additional informations to ALLEN's work on circulation. This includes a study of the influence of river discharges on currents. Fig 23 gives an example indicating that the intensities of surface currents during ebb are considerably increased, when discharges are high. However, at the bottom, there is not much change in the magnitude of currents.

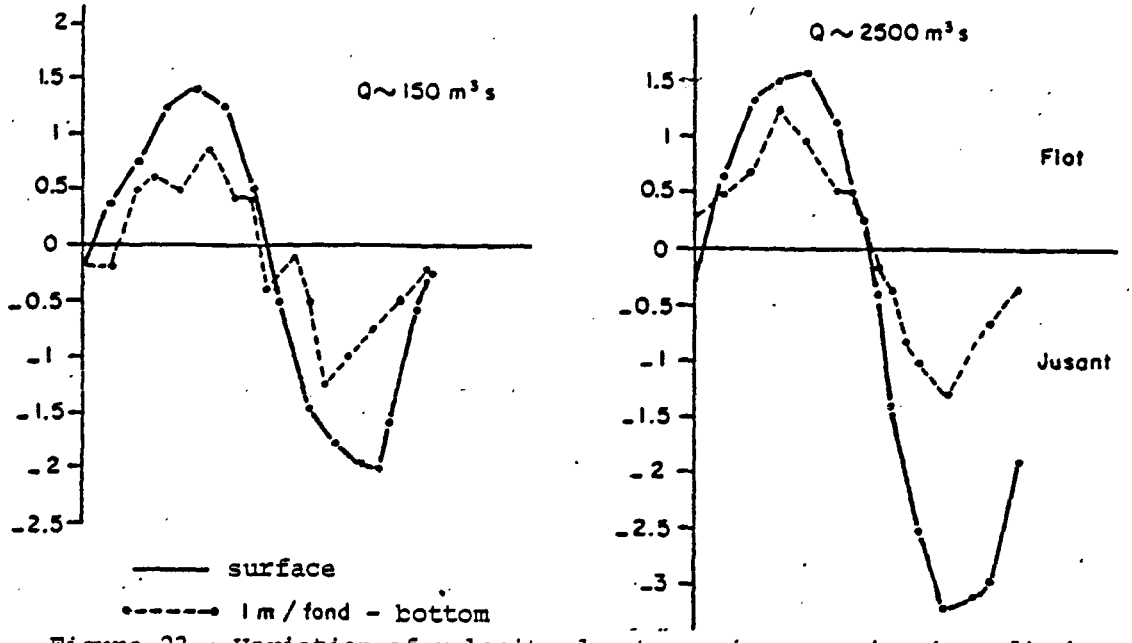

Figure 23 : Variation of velocity due to an increase in river discharges in the navigation channel at PK 89 (After CASTAING, 1981)

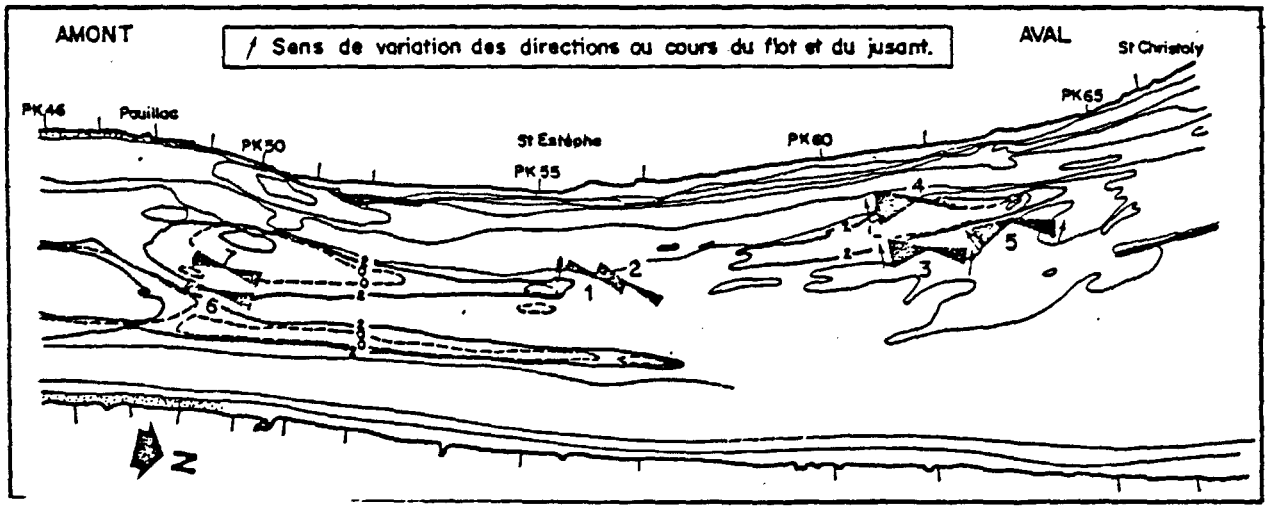

Figure 24 : Hydrological exchanges between different channels (After CREMER, 1975)

CREMER (1975) and CASTAING (1981) studied the significance of transverse currents in certain regions of the estuary (Fig 24). For example, near PK 49, the currents are parallel to the axis of median channel. Near PK 56, the ebb currents tend to move towards the north bank side. At stations 3 and 4 (PK 62), the currents are found to be parallel to the sand bank in the beginning of flood and later become more inclined, where as at station 5, flood currents are parallel to the bank.

Laboratoire National d'Hydraulique (L.N.H.) made various studies on the circulation and hydrology of the Gironde. Besides numerous in situ measurements, these studies include mathematical modelling and hydraulic modelling. Two of the hydraulic models developed are (Rapport n° 32 - 1975 and n° 17 - 1971 : personal communications) the one developed for the region between Pointe de Grave and St. Christoly and the other for the region between St. Christoly and Bec d'Ambes. Based on tidal variations and salinity (at the seaward side) at the left hand side of the boundary and river discharge rates at the right hand side, the current pattern in the domain was simulated. The results are presented in the form of instantaneous current vector diagrams for every one hour during a tidal period together with a few comparisons with observed currents at the surface. A few of these results will be discussed later in this chapter in relation to a comparison with simulation results obtained during the present study.

The current measurements made by L.N.H. give a few additional details to the circulation in the estuary described above. The surface current charts for the lower estuary show the predominance of flood in the northern channel between Pointe de Grave and Talmont (PK 85). However, ebb currents are found to be slightly more intense in the navigation channel than those in the northern channel in this region. Near Lamena, at PK 64, a few measurements across the section show that flood currents are stronger towards the north bank side, where as during ebb, currents are of maximum intensities in the navigation channel in that section. The current measurements also show the presence of an eddy between PK 67 and PK 65 during the slack from ebb to flood.

In the upper estuary, observed data across a few lateral sections reveals the following features.

(i) At PK 54, there is a sharp gradient of axial velocities across the navigation channel during flood and ebb, with higher values found towards the south bank side.
(ii) At PK 50, high intensities of currents are observed very near the south bank side.
(iii) At PK 38, the surface currents have almost same magnitudes in the navigation channel and the Blaye channel, with slightly higher values found in the former than in the latter during flood and vice versa, during ebb.

The hydraulic model simulations show a relatively good agreement between simulated currents and observed currents. In the model of St. Christoly, at Grave, flood starts five hours before high tide and lasts until two hours

after high tide. Three transient eddies are present in the current field. They are found near PK 92, PK 83 and PK 66. Sufficient observed data is not available to verify this point, except for the one present at PK 66

The hydraulic model developed for the region of islands shows the following aspects. Flood currents start at four hours before high tide and continue upto the hour of high tide at Pauillac. Slack of flood occurs one hour after the high tide at Pauillac. The duration of ebb is in between one hour after high tide at Pauillac and four hours before high tide. The slack of ebb is produced slightly in advance than in nature.

III. DISCUSSION OF SIMULATION RESULTS

Numerical experiments are done with the stair step boundary model and the irregular grid finite difference model for a coefficient of tide 75 and low river discharge rates (183 m^3/s for both the Dordogne and Garonne combined). The results are presented in Appendix I - III. A simulation of tide of coefficient 70 and for the same discharge rates, as mentioned above, is made with the link node model. The computed currents are presented at every one hour.

1) Stair step boundary model

The general features of circulation may be described as follows (Appendix I) . In the lower estuary, the currents flow parallel to the coast with intensities decreasing from the centre towards either coast. This pattern continues upto PK 60. Between PK 85 - 90, the ebb currents are found to be intense in Saintonge channel. During slack, a few transient eddies are present in the current field, a prominent one being observed between Valeyrac and St. Christoly. Their lifetime is about one hour. During the transition from ebb to flood, the eddies are clockwise and vice versa. These transient eddies get dissipated due to bottom friction and viscosity.

Between PK 60 and PK 50, flood currents are very small in intensities near both the bank sides, though navigation channel has high depths in this region. This is probably due to the fact that the navigation channel is situated very near the coast in this region and any possible poor representation of the coast can affect the computed values of currents. During ebb, the currents are equally intense in this channel as those found at the central region. This confirms the fact that navigation channel is an ebb channel in this zone.

In the region of islands, the notable features are as follows. Between Pauillac and the island of Philippe, flood currents are strong near the north bank side. Upstream, between PK 41 and PK 35, flood is more predominant in the navigation channel. In the Blaye channel, along the same longitudinal distance, both flood and ebb currents are found to be less in magnitude than those of navigation channel. During ebb, all along the upper estuary, maximum intensities of currents in different lateral sections are found in the navigation channel

2) Irregular grid finite difference model

The computed currents are shown in appendix II . It is to be recalled that this model has the same topography and open boundary conditions as the stair step boundary model. Accordingly, the discussion of the results is made in comparison with those obtained in the previous model.

The current field in the region between the Pointe de Grave and seaward boundary is different from the one obtained from the stair step boundary model. Considering the fact that the calibration is done from the Pointe de Grave towards the head of the estuary, this aspect is not discussed here.

In the lower estuary, the computed currents are very much similar and comparable to those values obtained from the previous model. In the different lateral sections, the velocity gradients are less marked and currents near the coast are less feeble than those found in the previous model. A transient eddy is present at the same location as the previous model, i.e., between Valeyrac and St. Christoly. In this model, the eddy dissipation is only by bottom friction, viscosity being absent.

In the upper estuary, the grid configuration near the coast is different from the previous model. Between Pauillac and St. Christoly, the ebb currents are represented in a better way than the previous model. Again, lateral differences are less visible in this region. At PK 50, ebb is the strongest in the navigation channel between the island of Trompeloup and left bank side in that section. It is recalled that in the stair step boundary model, high intensities in ebb are observed in the passage between the islands of Trompeloup and Philippe. Considering the high depths of the navigation channel in this region, the results obtained from this model seem to be more reliable.

In this model, lateral differences in the computed parameters are less present compared to the stair step boundary model. This may be attributed to the effect of the procedure of smoothing (equation 28). For the present

simulations, a small value of the smoothing factor of the order of 0.01 (corresponds to $\alpha = 0.99$ in the equation 28) is found to be necessary to guarantee numerical stability. This procedure does not have much physical significance and it is found to be necessary because of the difficulties in introducing the viscosity term in the model.

In the region of islands, the computed currents are not much precise. It may be necessary to choose smaller triangles than those used to improve this point. The circulation in this region, based on this model, is not included in the discussions.

3) Link node model

The computed currents are shown in (Appendix III), the simulation being made for a coefficient of tide 70 and low discharge rates (189 m^3/s for both the Dordogne and Garonne combined). As discussed earlier in page 42, in this model the tidal wave propagates without any significant phase difference in the lateral. Moreover, since the centrifugal force is absent, the phenomenon caused by meandering cannot be reproduced by this model. Lateral and longitudinal variations in velocities are determined uniquely by the depth variations.

A few of the salient features can be mentioned as follows. Near PK 90, both flood and ebb currents are found to be of maximum intensity in the Saintonge channel : upstream, maximum currents are observed in the navigation channel in the lower estuary. In the upper estuary, between PK 35 to PK 45, the currents in Blaye channel are slightly more intense than those values found in navigation channel. This is in accordance with the observations (page, 43) and a significant improvement from the other two models.

Small transversal currents are present at certain regions and during certain stages of tidal propagation. These currents are present due to the grid configuration. Their significance lies in the fact that they are present only during slack. These transversal currents are, probably, comparable to the presence of transient eddies in a 2D model. To indicate a few examples, during ebb, feeble lateral currents flow downward from the bank of Plessac at PK 35 towards the navigation channel. In the lower estuary, between PK 80 and PK 85, lateral currents towards the north bank side are present. Downstream, near Verdon, feeble currents flow towards the southern side. During flood, the direction of transverse currents is opposite to those of ebb.

4) Trajectories

The simulated current field can be used to compute the trajectory of a water particle at different points in the domain. This allows to determine two lagrangian parameters, namely, the displacement made by a water particle and the residual displacement during one tidal period. The former parameter will be discussed here and the latter during the V chapter. The calculation is done as follows.

$$x\ (t) = \int_0^t U(x,t)\ dt + x_0$$

where x_0 is the starting point, U, the velocity and x is the co-ordinate of the point of arrival.

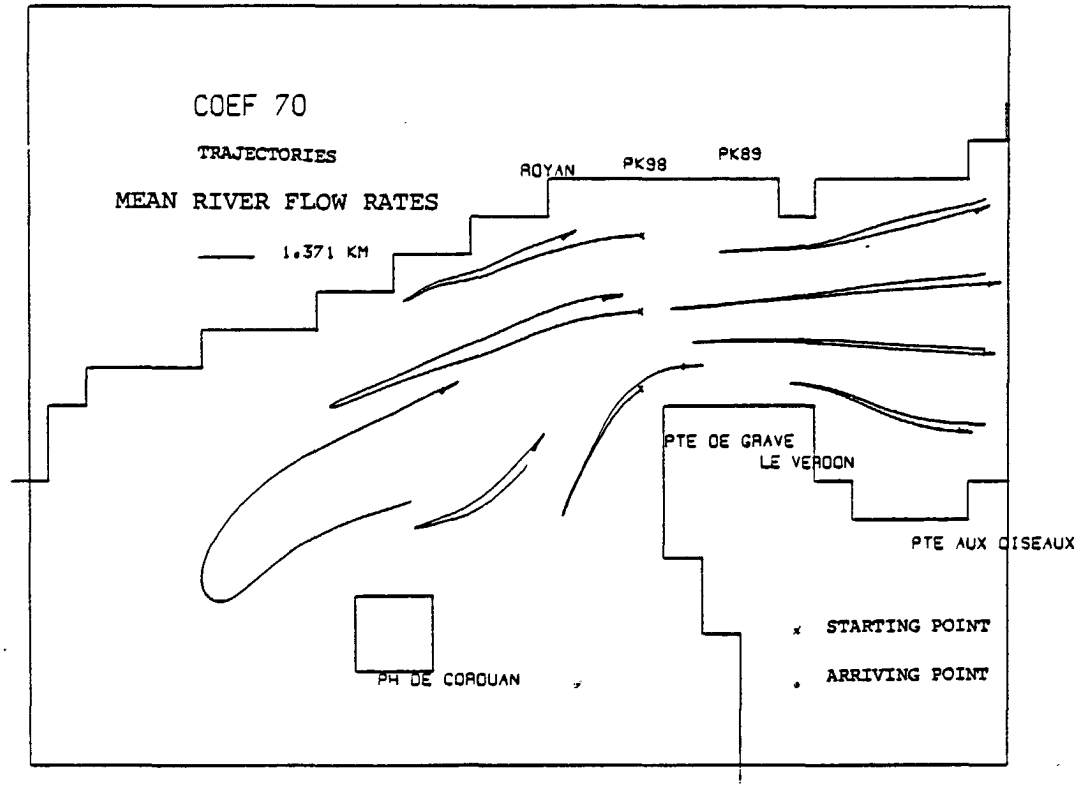

Figure 25 : Computed trajectories of water particles at a few points in the lower estuary (stair step boundary model).

The calculation is done using the stair step boundary model, the integration being carried out over an interval of time equal to 6 minutes. A few examples of results are presented in fig 25 to 27. In figure 25, consider two particles of water starting at PK 85, one travelling through the navigation channel and the second through the Saintonge channel. It can be seen that the displacement of the particle is more in the northern channel. This shows the predominance of flood and ebb near the north bank side in this region.

Upstream, between PK 78 and PK 62, during flood as well as ebb, displacements are maximum for the trajectroies of particles near the centre (fig. 26). In this region, velocities are the strongest at the centre with intensities decreasing towards either coast, as may be observed in current vector diagrams.

A few trajectories drawn for upper estuary are shown in figure 27. Let us consider the particles starting at PK 54 and PK 52 travelling downstream. It is seen that the displacements are maximum for those passing through the centre and the navigation channel. During ebb, the displacement is maximum in the navigation channel, showing the importance of this channel in this region in canalysing ebb currents.

Between Bec d'Ambes and Pauillac, the computed trajectories have displacements slightly higher in the navigation channel than in the Blaye channel.

A few trajectories are drawn from the current field obtained from a simulation made for high river flow rates (1300 m^3/s). In the upper estuary (fig 27), the displacements of water particles are maximum in the navigation channel. Moreover, these increases in displacements are more pronounced during ebb.

A few informations about the observed trajectories are available in the form of displacements obtained by the release of drifting poles. These give the displacements along a column of water. CASTAING (1981) computed a few trajectories based on the observed residual currents using a method proposed by SIMMONS (1966). These results are supplemented wirh a few data obtained from the release of drifting poles and are presented in figure 28. The trajectories are outside the model domain or very near to the seaward boundary so as to make comparisons with the computed trajectories. Also, a few release

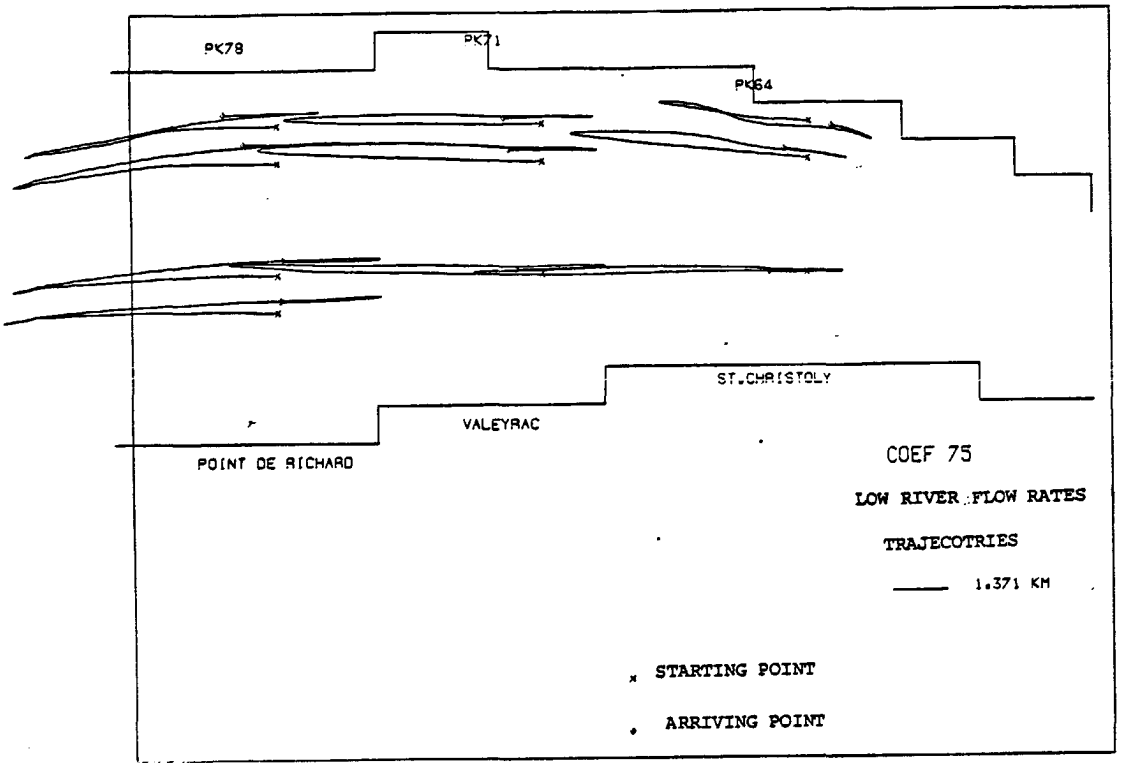

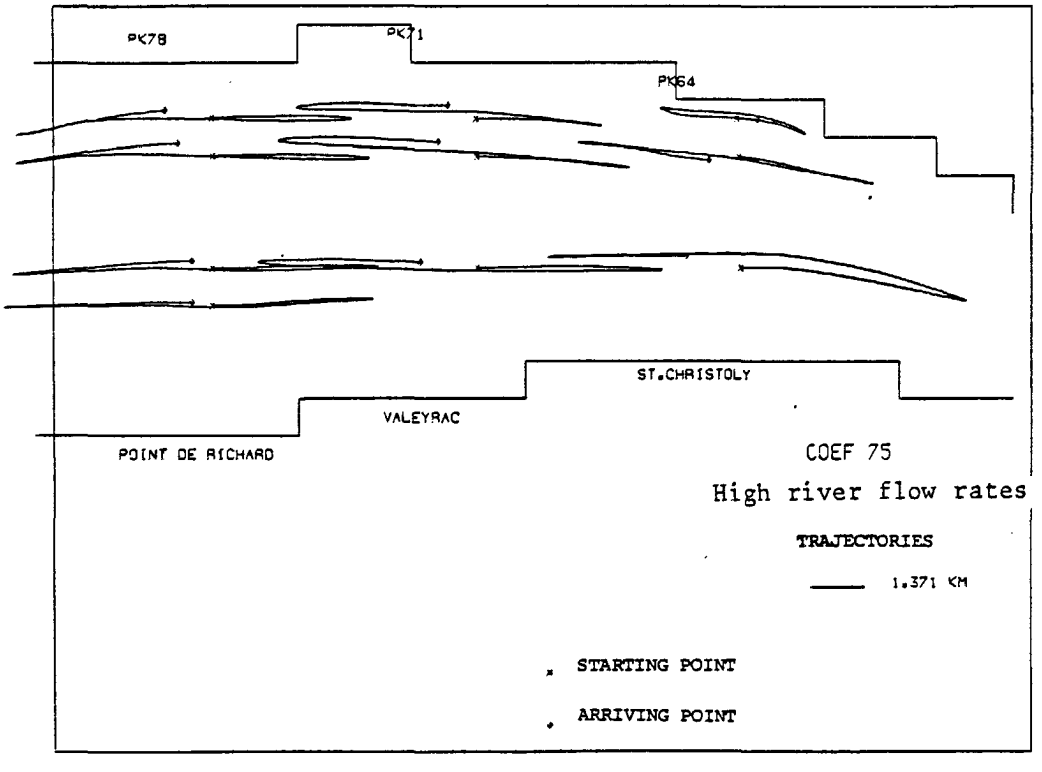

Figure 26 : Computed trajectories of water particles at a few points in the middle part of the Gironde

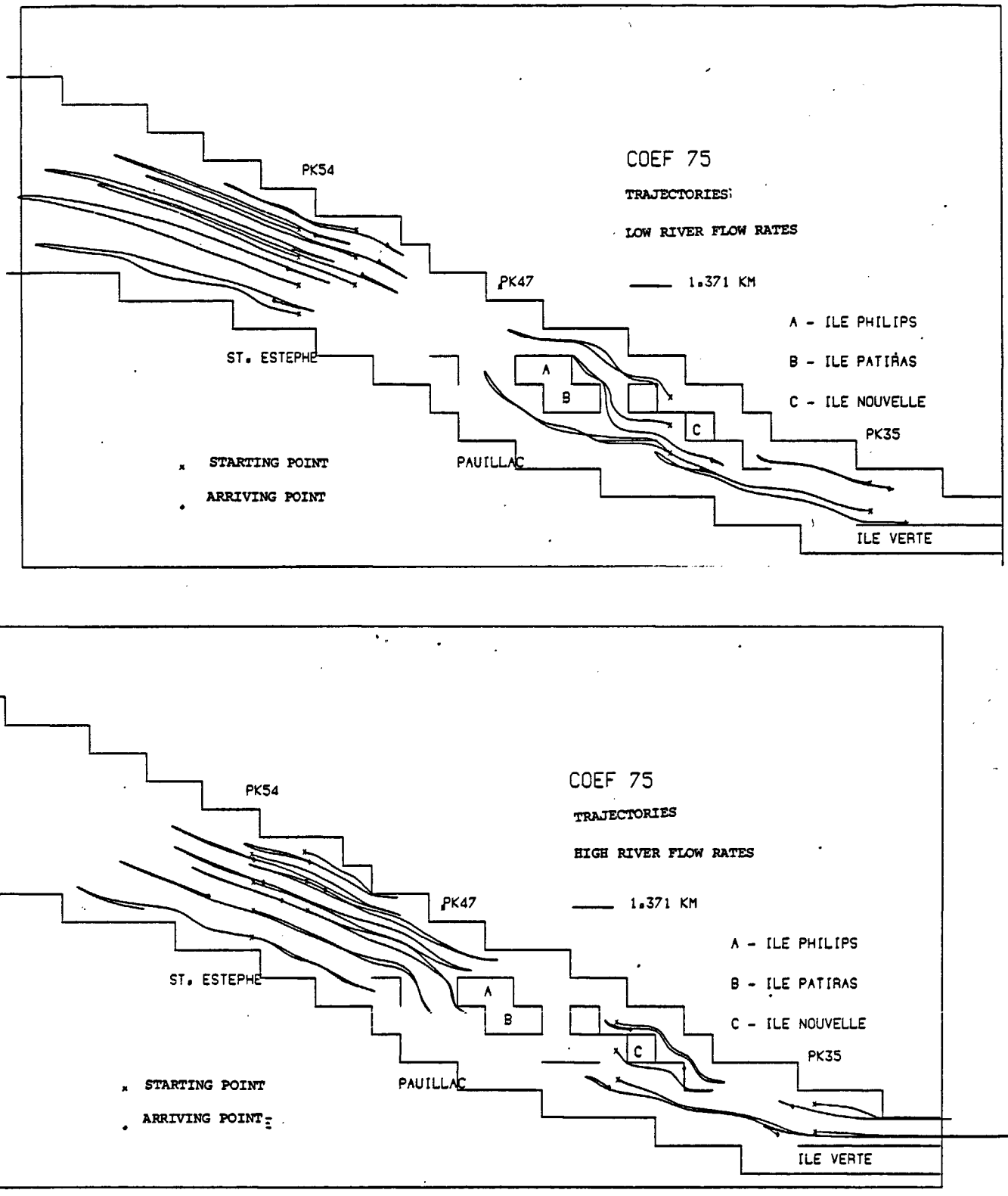

Figure 27 : Computed trajectories in the upper estuary

of drifting poles were made by Laboratoire Municipal de Bordeaux in 1962 and 1970 in the region of Bordeaux. For the estuarine region, much data is not available for comparing with the computed trajectories from the stair step boundary model.

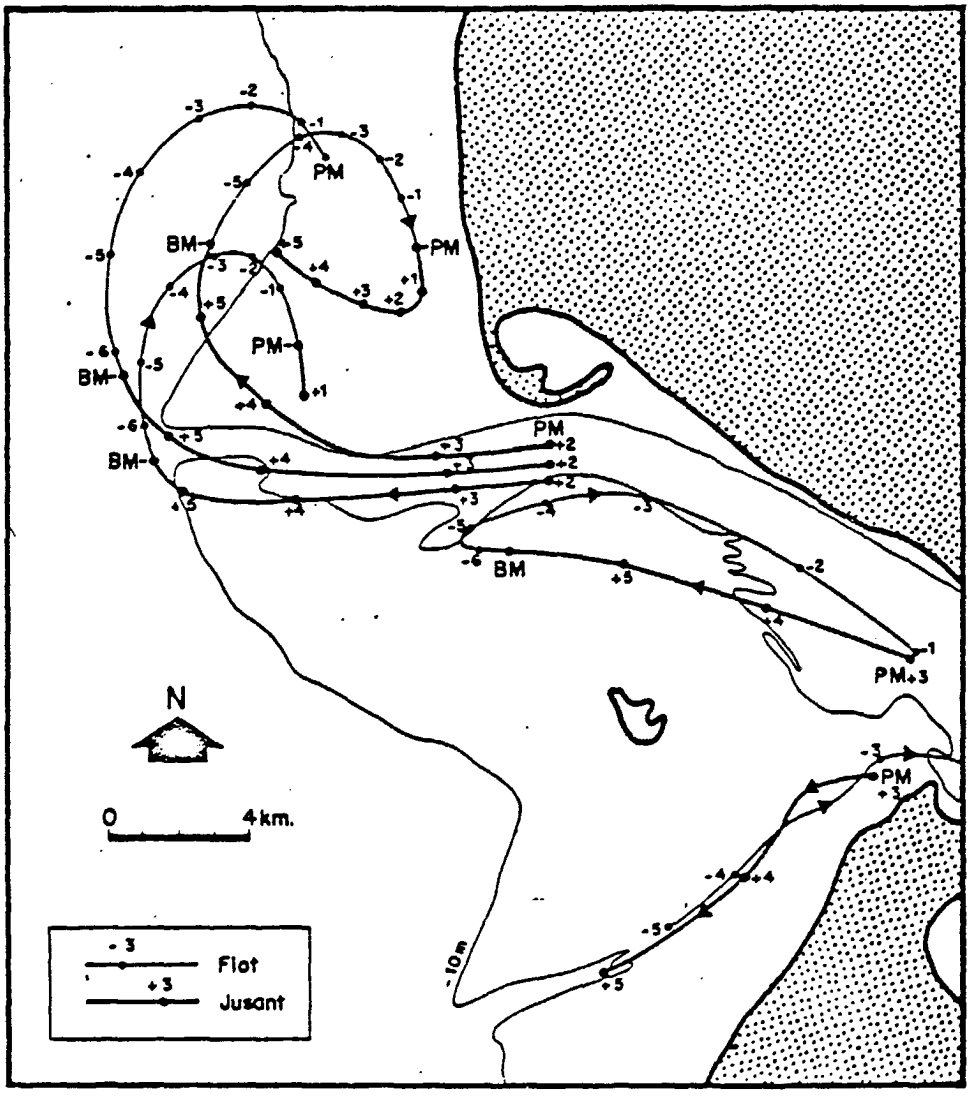

Figure 28 : Trajectories of currents during spring tide (after CASTAING, 1981).

COMPARISONS WITH OBSERVATIONS

The simulation results obtained from the different numerical models are compared with the measurements and simulation results obtained from the hydraulic models developed by the L.N.H. (page 46). The comparisons show that the 2 D models reproduce well the hours at which slack occurs and the presence

of transient eddies during slack. In the hydraulic model of St. Christoly, the transient eddies are located in the principal channel. In the case of numerical models, the width of the estuary is found to determine the size of eddies. The link node model also reproduces well the hour of slack.

A few of the differences found with reference to the L.N.H. results may be mentioned as follows. In the case of stair step boundary model, the computed values of currents near the south bank side between PK 50 - 60 are found to be very small, in spite of the presence of the principal channel. This is explained (page 47) due to the representation of the coast by a stair step boundary in this region. The current measurements in the navigation channel at PK 50 by L.N.H. (Rapport n° 17) show that the magnitude of surface currents are of the order of 2 m/sec, during spring tide. Upstream, at PK 38, the computed currents in the Blaye channel are found to have less magnitudes than those in the navigation channel, in the case of both the 2D models. Observations show that the magnitudes of currents in these two channels are comparable. This aspect is reproduced only in the case of the link node model. This illustrates that the flexibility of the link node model is useful in describing the circulation around the islands.

The computed currents obtained from the different models are compared with observations at a few points in the estuary. The measured currents (MOYES, 1975), exist at the surface, mid depths and bottom. During the period of measurements, the river discharge rates were 600 m^3/sec. for both the rivers together. Figure 29, gives observed values at a few stations. The depth averaged currents obtained from different models are compared with these observed currents at mid depths (see figure 29).
30

It can be seen that the stair step boundary model is giving the maximum precision. The irregular grid model is also sufficiently precise in the comparisons. The link node model results show that the magnitudes of computed currents are less than those of observed. In this model, for a given polygon, the flux of water occurs through various sides of the polygon, whose dimensions are not the same. So the velocities obtained may not be compared with observed velocities.

Fig. 30 31 shows observed currents at two stations near the south bank side of PK 86. The first station is situated at zero metre isobath and the

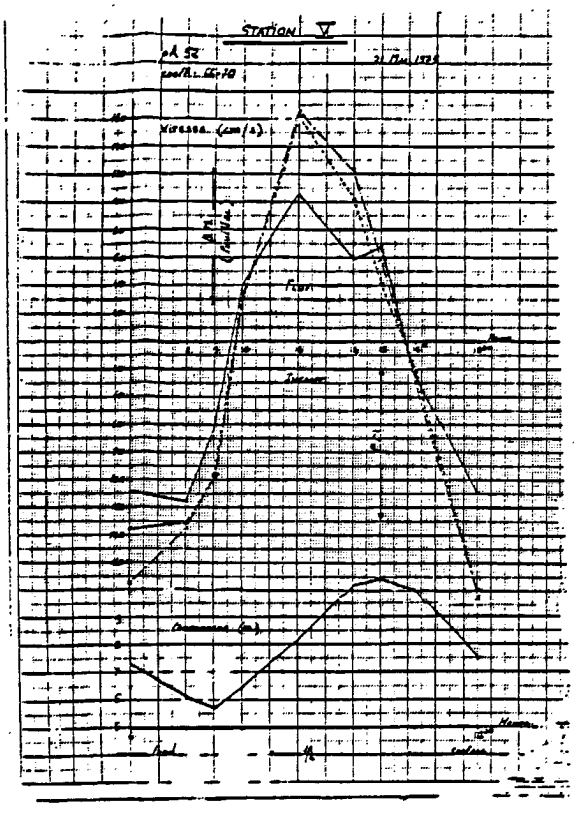

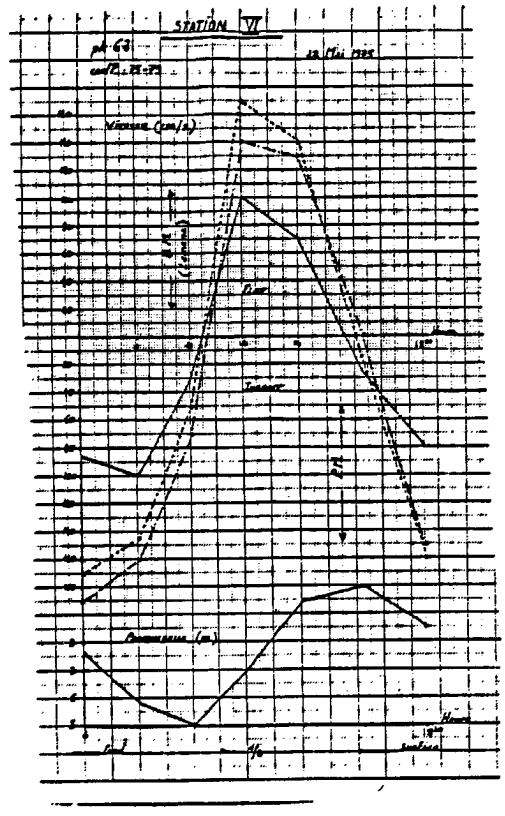

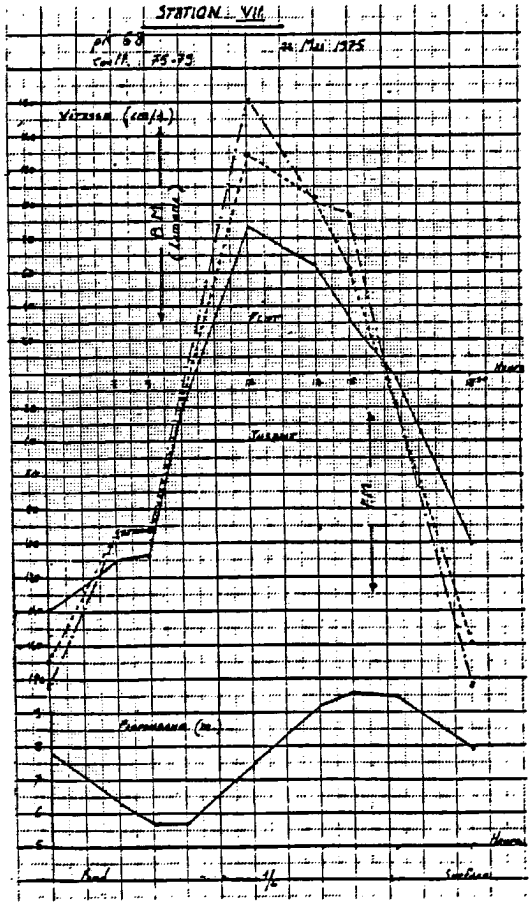

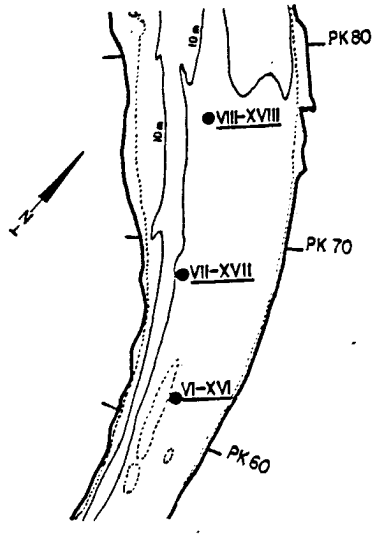

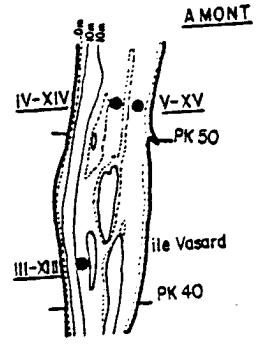

Figure 29 : Observed currents at a few stations

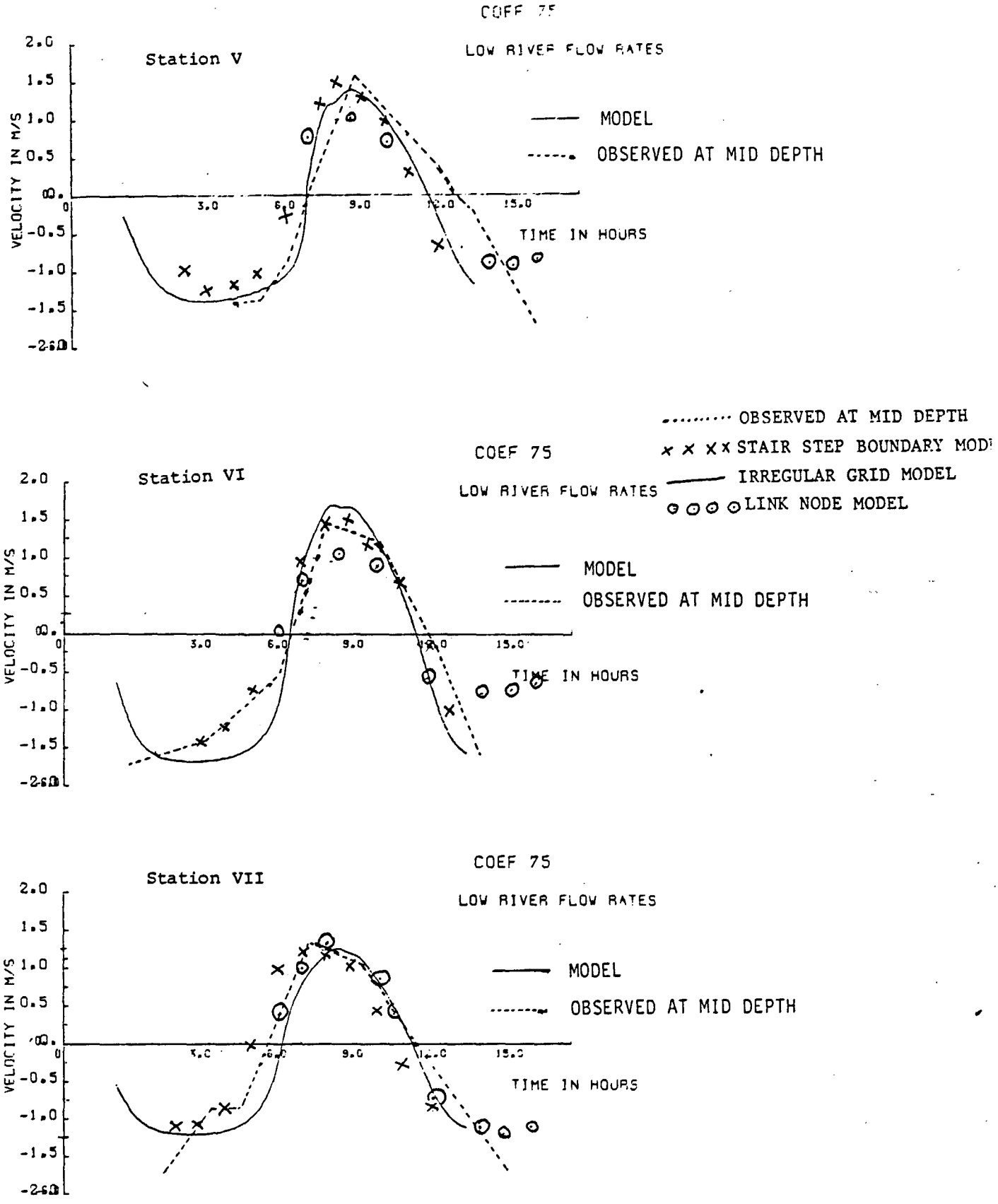

Figure 30 : Comparison between depth averaged currents(irregular grid model) and observed currents at mid depths.

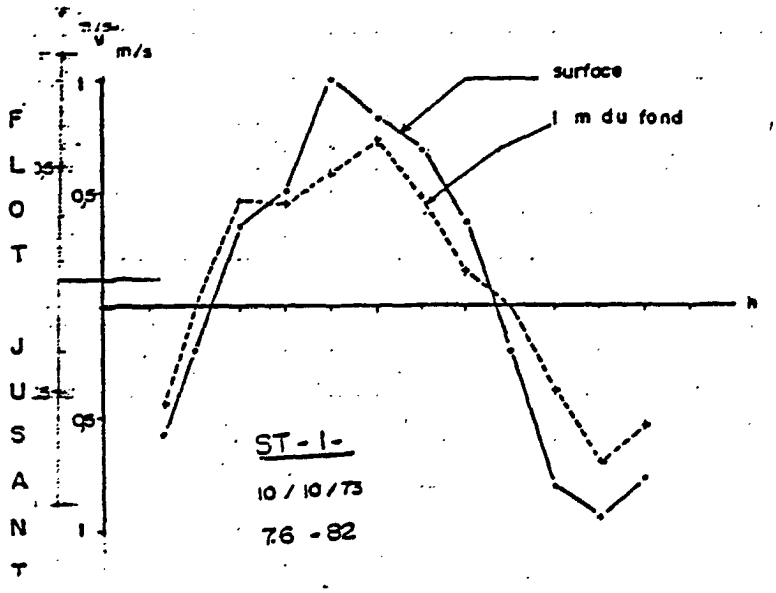

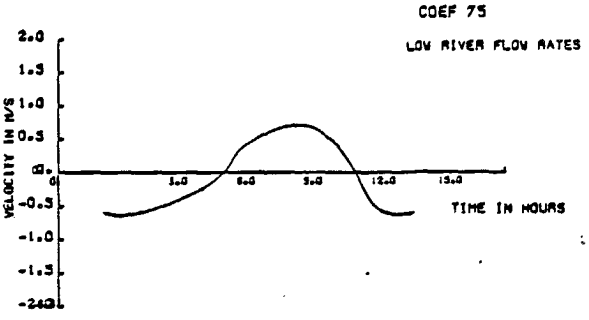

(b) Computed (irregular grid model)

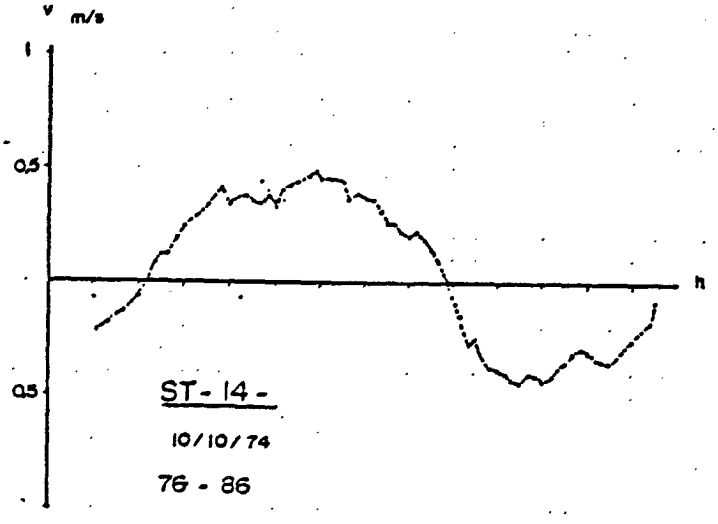

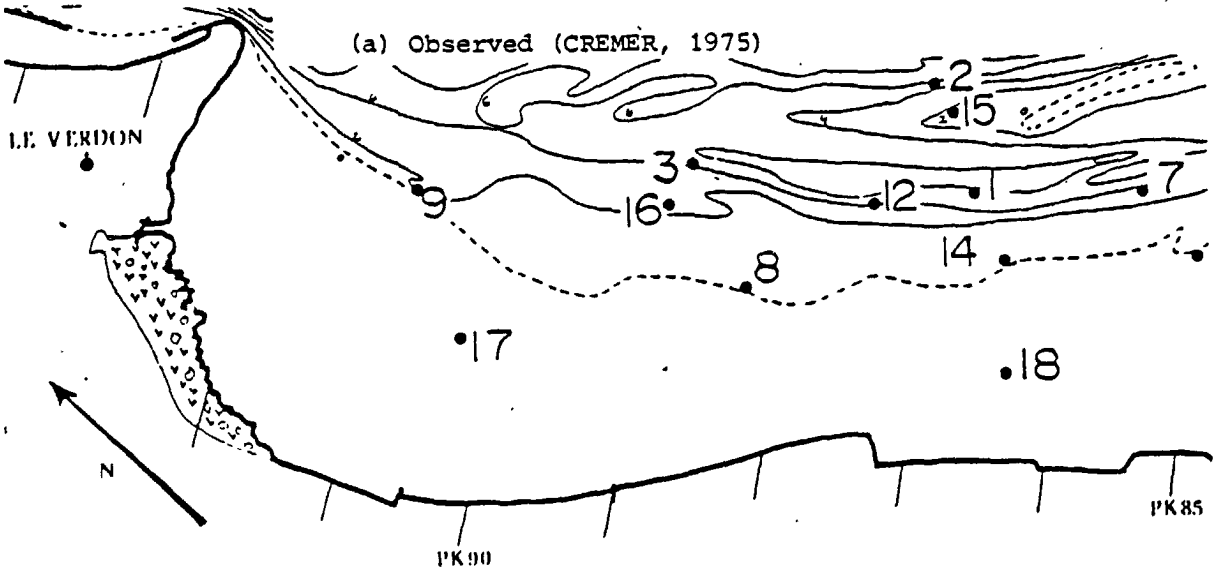

Figure 31 : Observed and computed currents near the south bank side at PK 86

second one at 4 metre isobath. The computed values of depth averaged currents at these points by the irregular grid model are compared with observed values. It can be seen from the current vector diagrams that the currents computed by the stair step boundary model are less than the observed values near the south bank side at PK 86.

CONCLUSION

The lateral and longitudinal variations in intensities of currents occur due to the topographical pecularities. A few comparisons made with the different models show relatively good agreement between observed and computed values of currents. A better precision is achieved near the bank sides in this irregular grid model than in the stair step boundary model.

Computations of trajectories of water particles by the stair step boundary model have helped in identifying clearly the ebb channels in the estuary, namely, the navigation channel in the upper estuary and Saintonge channel in the lower estuary. The trajectories are found to be useful in studying the effects of river discharges on circulation.

A few limitations lie in the fact that the sand banks and the dike of Valeyrac are not represented in the models. In the case of link node model, these shortcomings are partiallly overcome by the orientation of the grid network so as to represent these topographical features. It is found that circulation in the region of islands is well described by this model.

APPENDIX I

Instantaneous current vector diagrams

(Stair step boundary model)

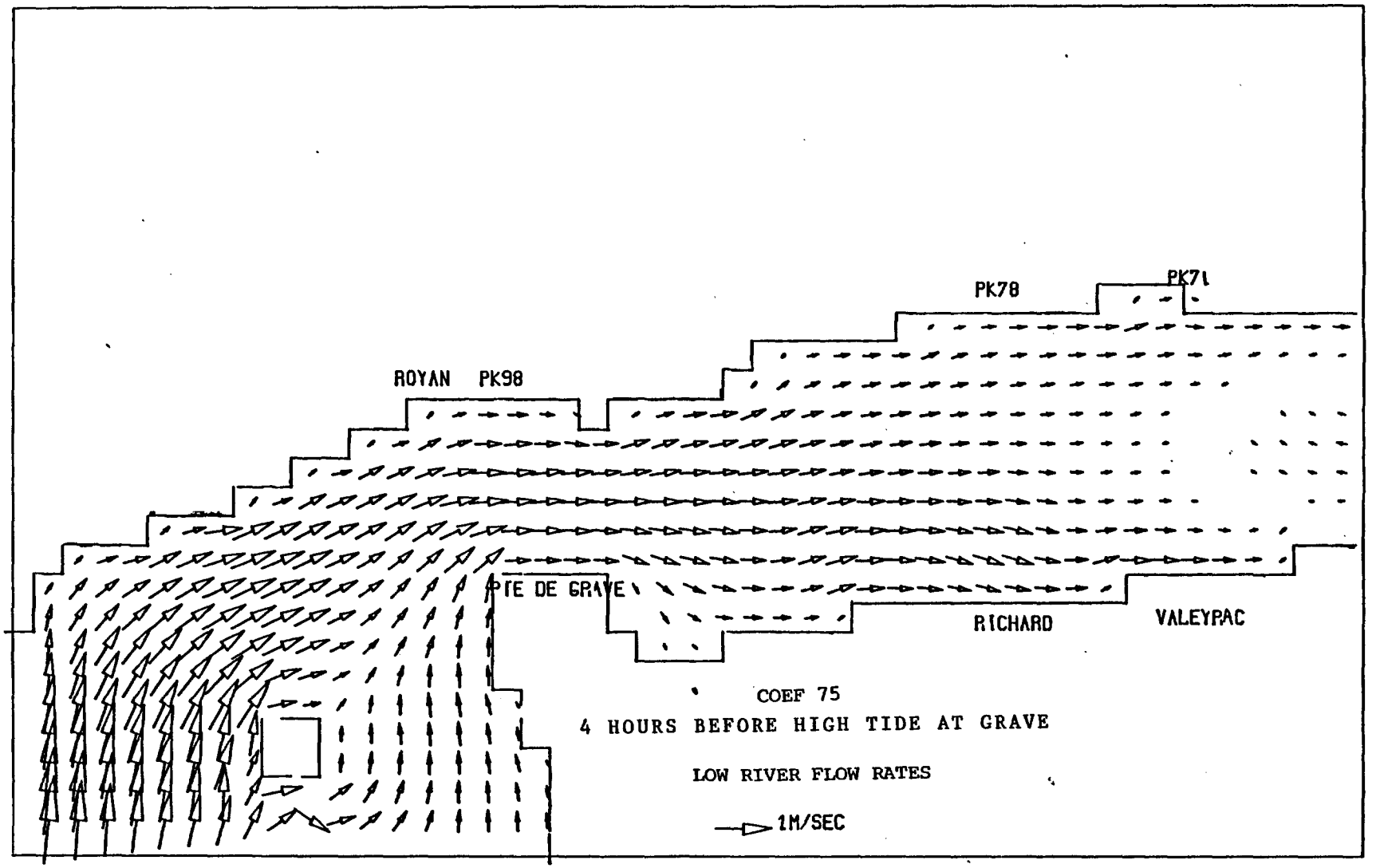
PK78
PK71
ROYAN PK98
PTE DE GRAVE
RICHARD
VALEYPAC
COEF 75
4 HOURS BEFORE HIGH TIDE AT GRAVE
LOW RIVER FLOW RATES
1M/SEC

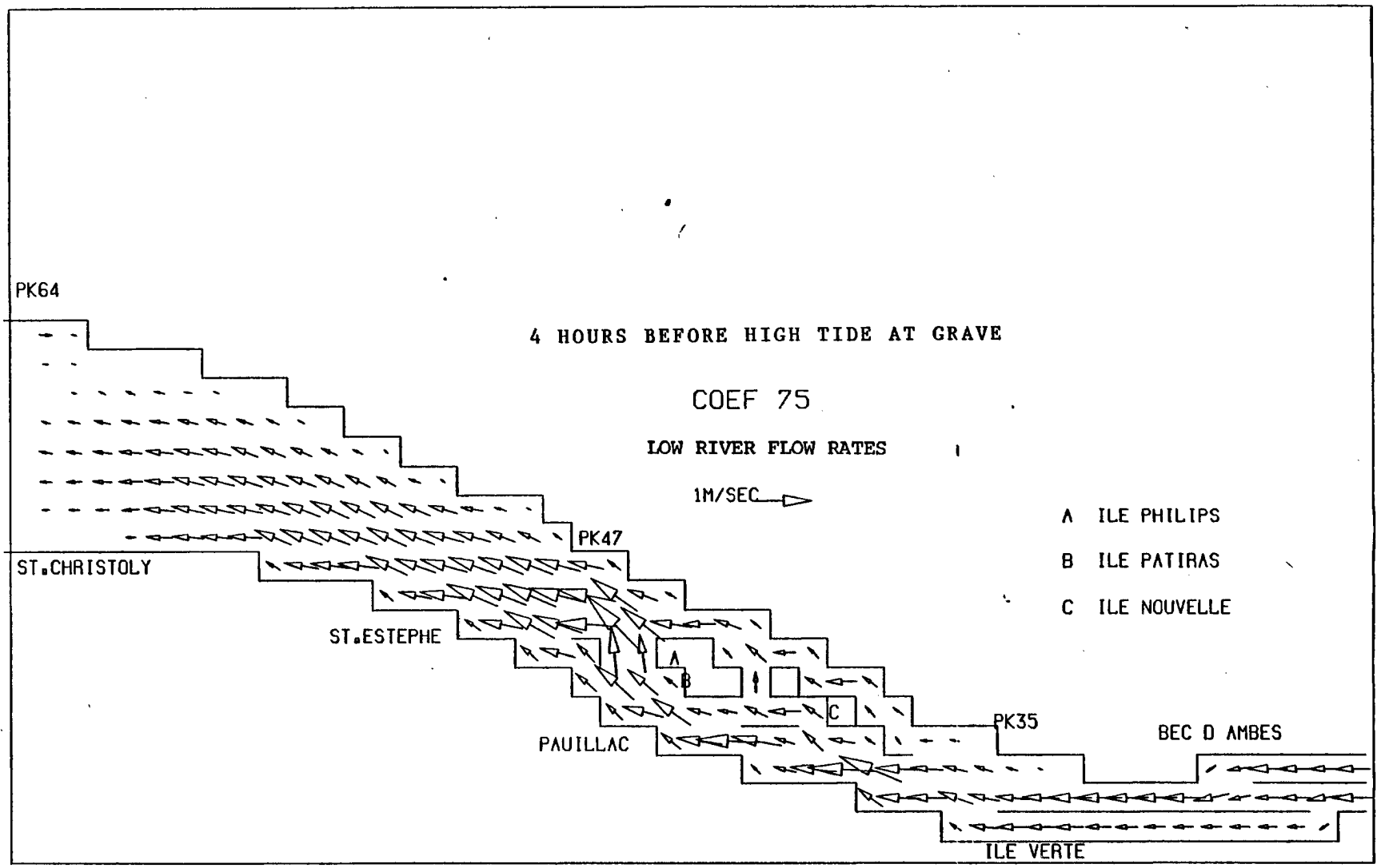
PK64
4 HOURS BEFORE HIGH TIDE AT GRAVE
COEF 75
LOW RIVER FLOW RATES
1M/SEC
A ILE PHILIPS
B ILE PATIRAS
C ILE NOUVELLE
PK47
ST.CHRISTOLY
ST.ESTEPHE
A
B
C
PK35
BEC D AMBES
PAUILLAC
ILE VERTE

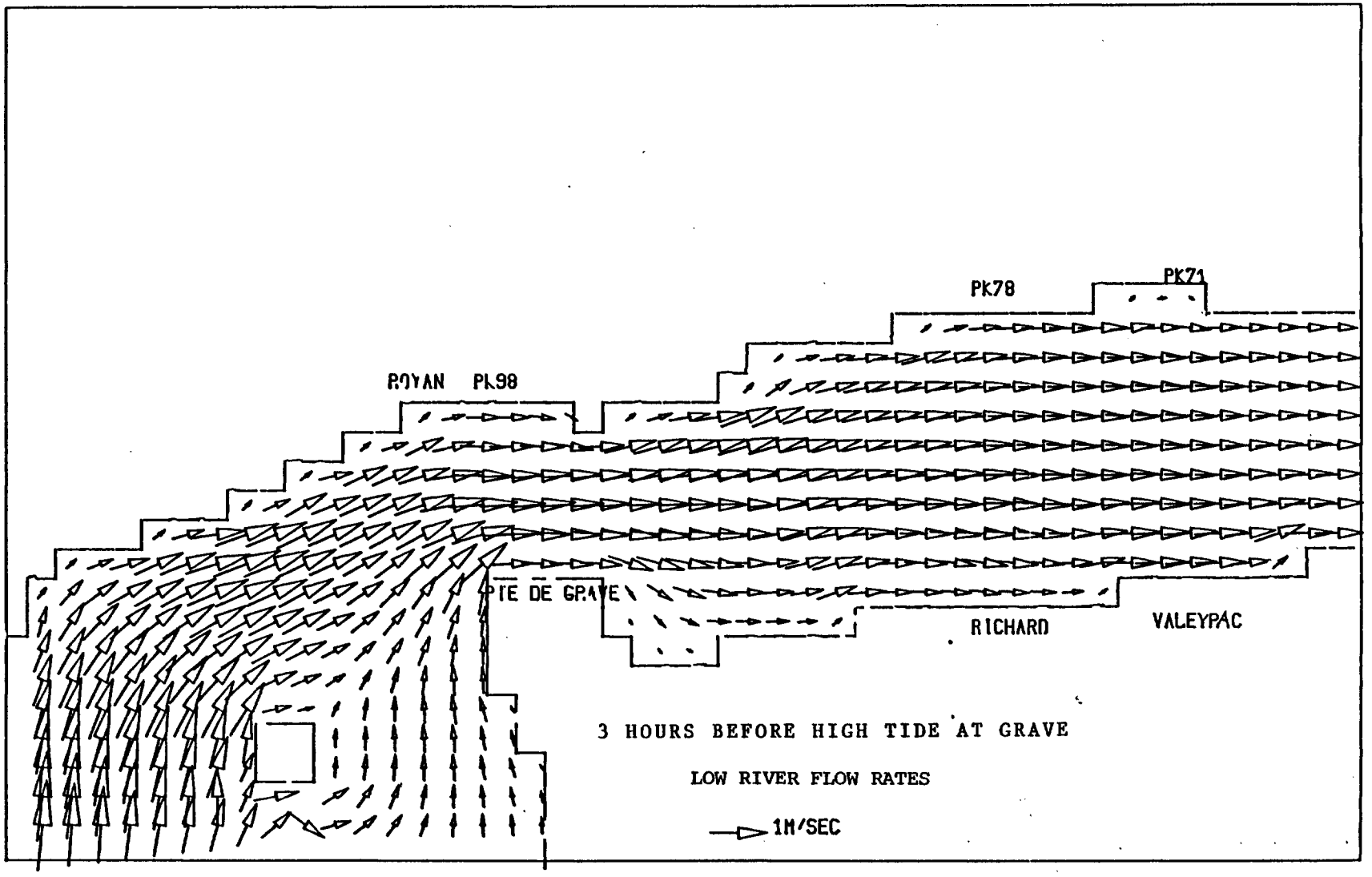
PK78
PK71
ROYAN PK98
PTE DE GRAVE
RICHARD
VALEYPAC
3 HOURS BEFORE HIGH TIDE AT GRAVE
LOW RIVER FLOW RATES
1M/SEC

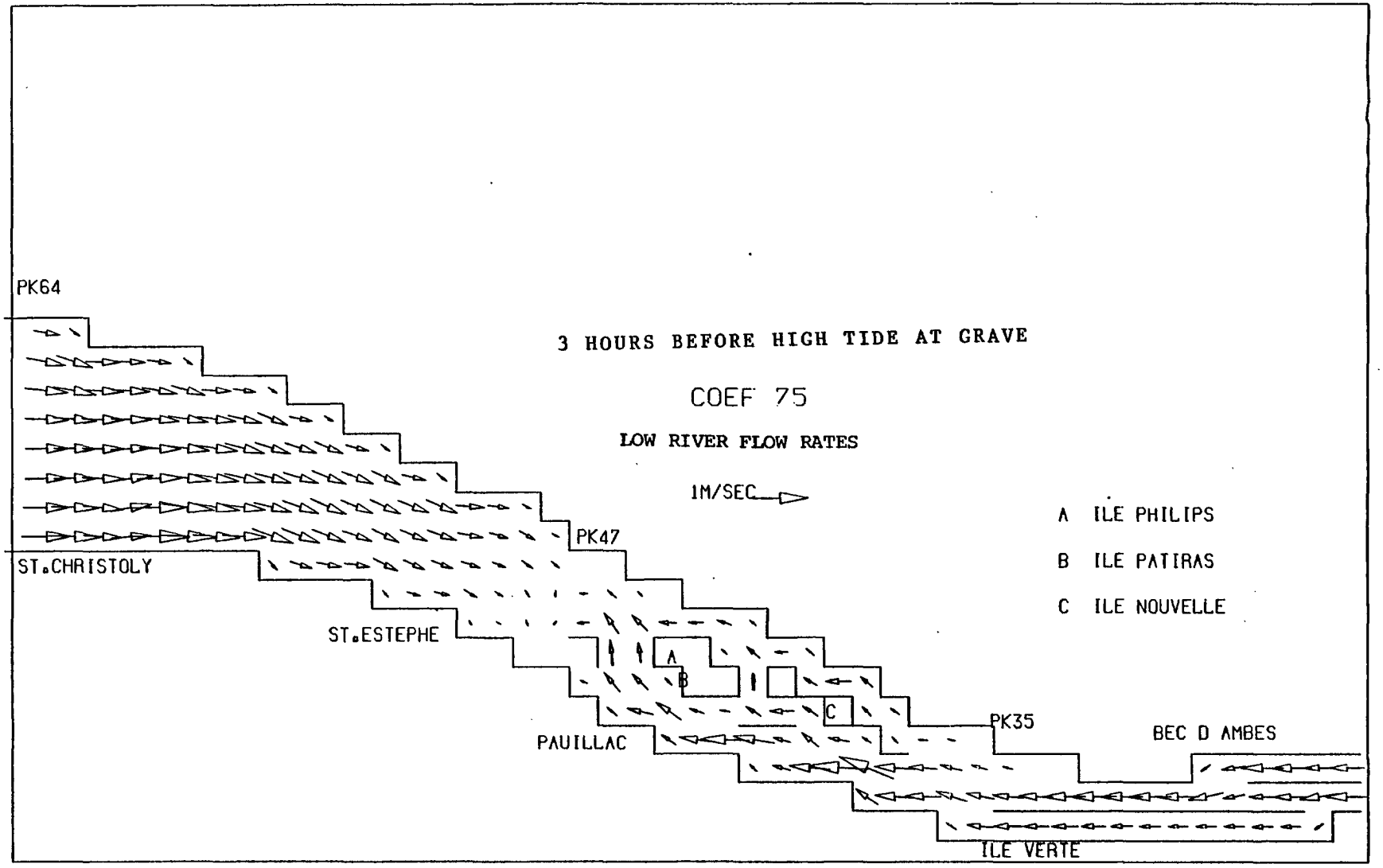
PK64
3 HOURS BEFORE HIGH TIDE AT GRAVE
COEF 75
LOW RIVER FLOW RATES
1M/SEC
A ILE PHILIPS
B ILE PATIRAS
C ILE NOUVELLE
PK47
ST.CHRISTOLY
ST.ESTEPHE
A
B
C
PK35
PAUILLAC
BEC D AMBES
ILE VERTE

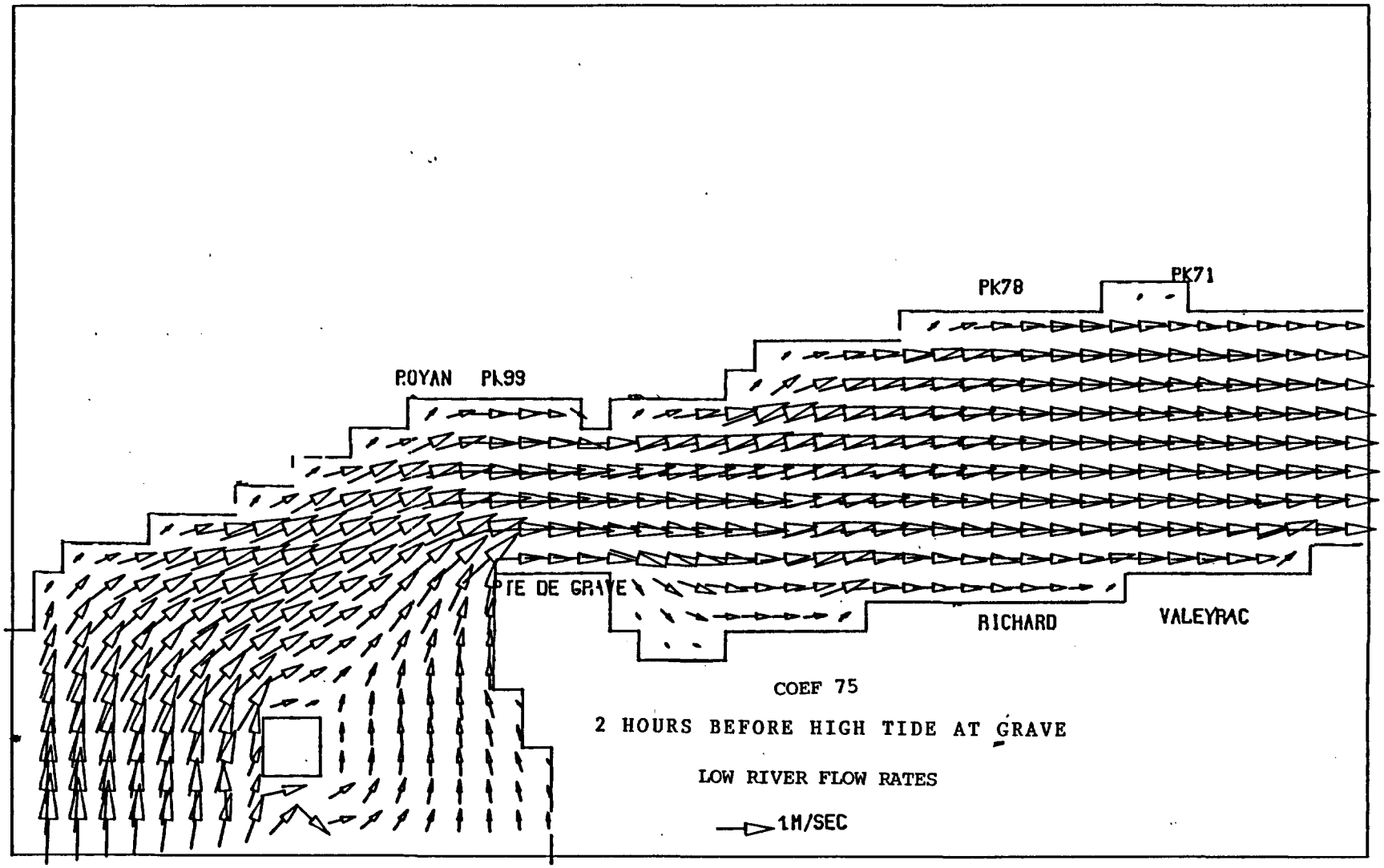
PK78
PK71
POYAN PK99
TE DE GRAVE
RICHARD
VALEYRAC
COEF 75
2 HOURS BEFORE HIGH TIDE AT GRAVE
LOW RIVER FLOW RATES
1M/SEC

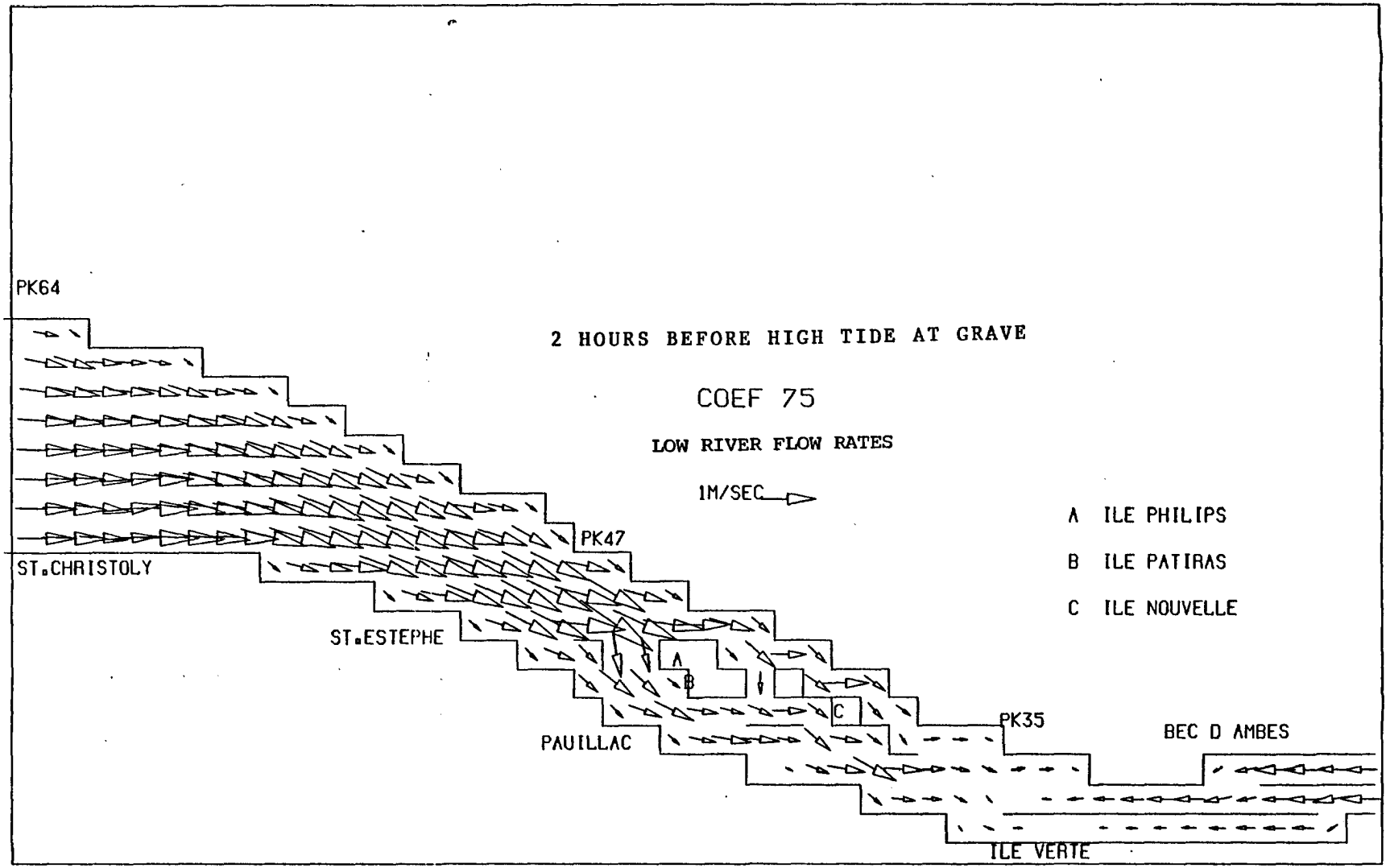
PK64
2 HOURS BEFORE HIGH TIDE AT GRAVE
COEF 75
LOW RIVER FLOW RATES
1M/SEC
A ILE PHILIPS
B ILE PATIRAS
C ILE NOUVELLE
PK47
ST.CHRISTOLY
ST.ESTEPHE
A
B
C
PK35
BEC D AMBES
PAUILLAC
ILE VERTE

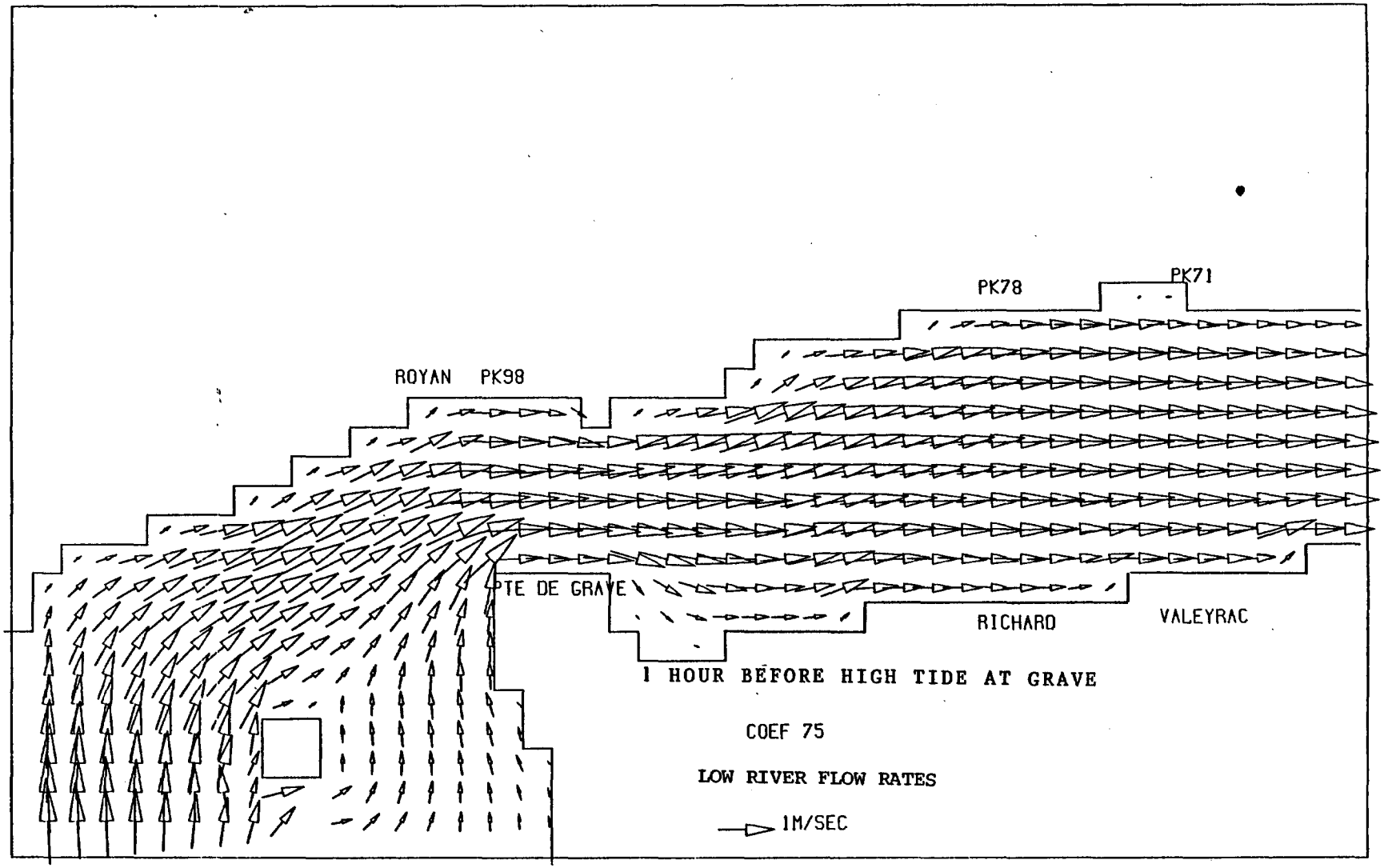
PK78
PK71
ROYAN PK98
PTE DE GRAVE
RICHARD
VALEYRAC
1 HOUR BEFORE HIGH TIDE AT GRAVE
COEF 75
LOW RIVER FLOW RATES
1M/SEC

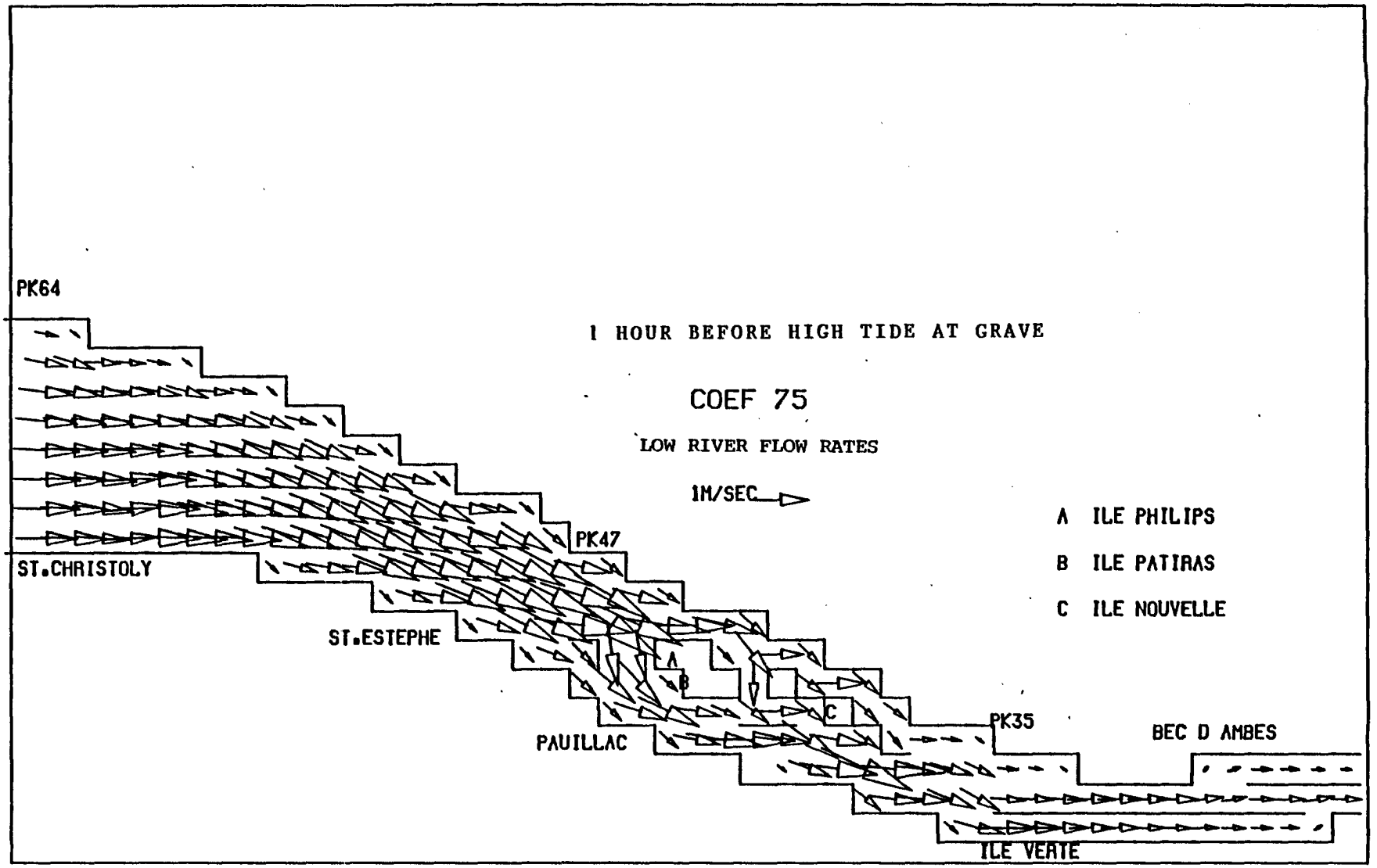
PK64
1 HOUR BEFORE HIGH TIDE AT GRAVE
COEF 75
LOW RIVER FLOW RATES
1M/SEC
A ILE PHILIPS
B ILE PATIRAS
C ILE NOUVELLE
PK47
ST.CHRISTOLY
ST.ESTEPHE
A
B
C
PK35
BEC D AMBES
PAUILLAC
ILE VERTE

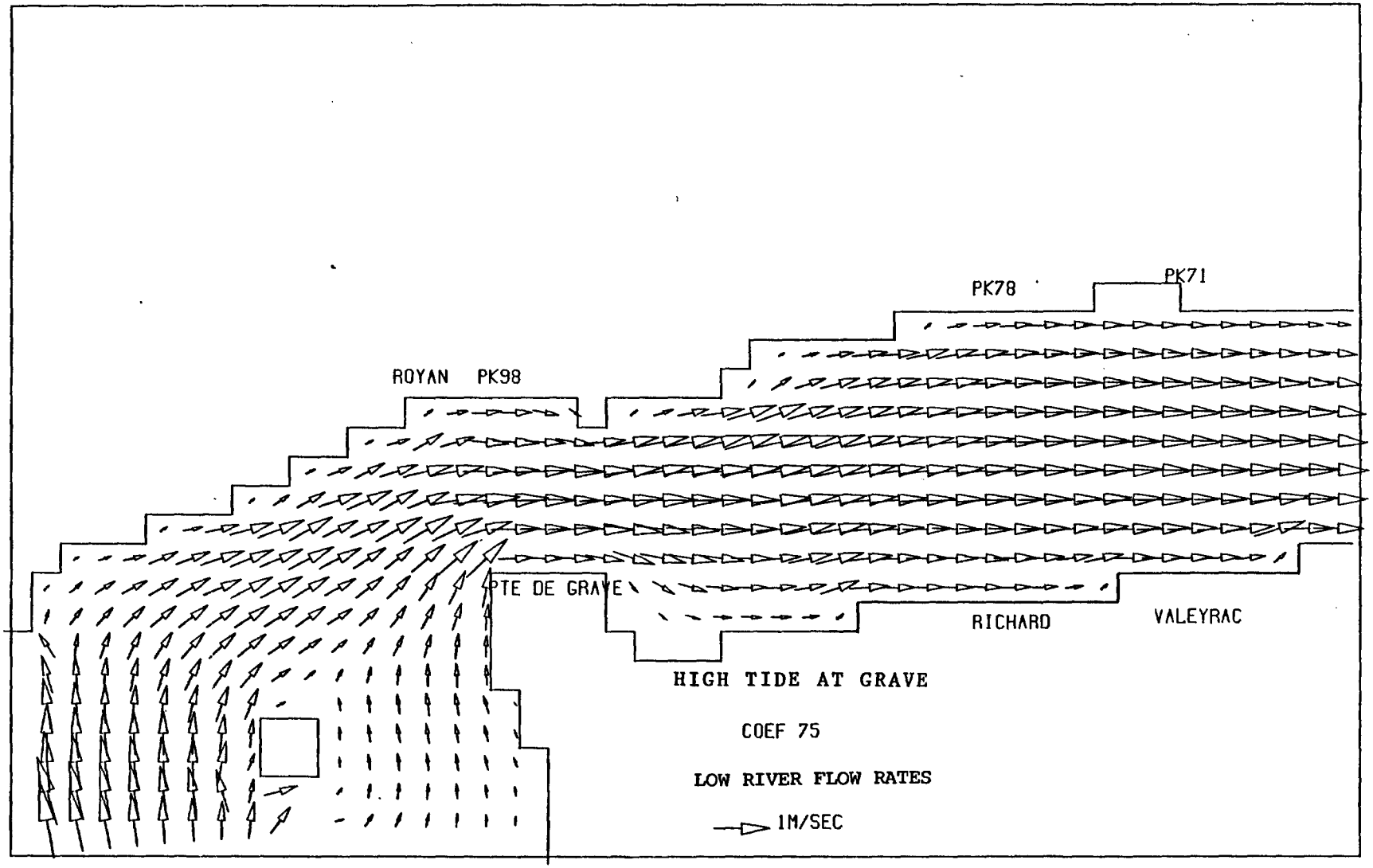
PK78
PK71
ROYAN PK98
PTE DE GRAVE
RICHARD
VALEYRAC
HIGH TIDE AT GRAVE
COEF 75
LOW RIVER FLOW RATES
1M/SEC

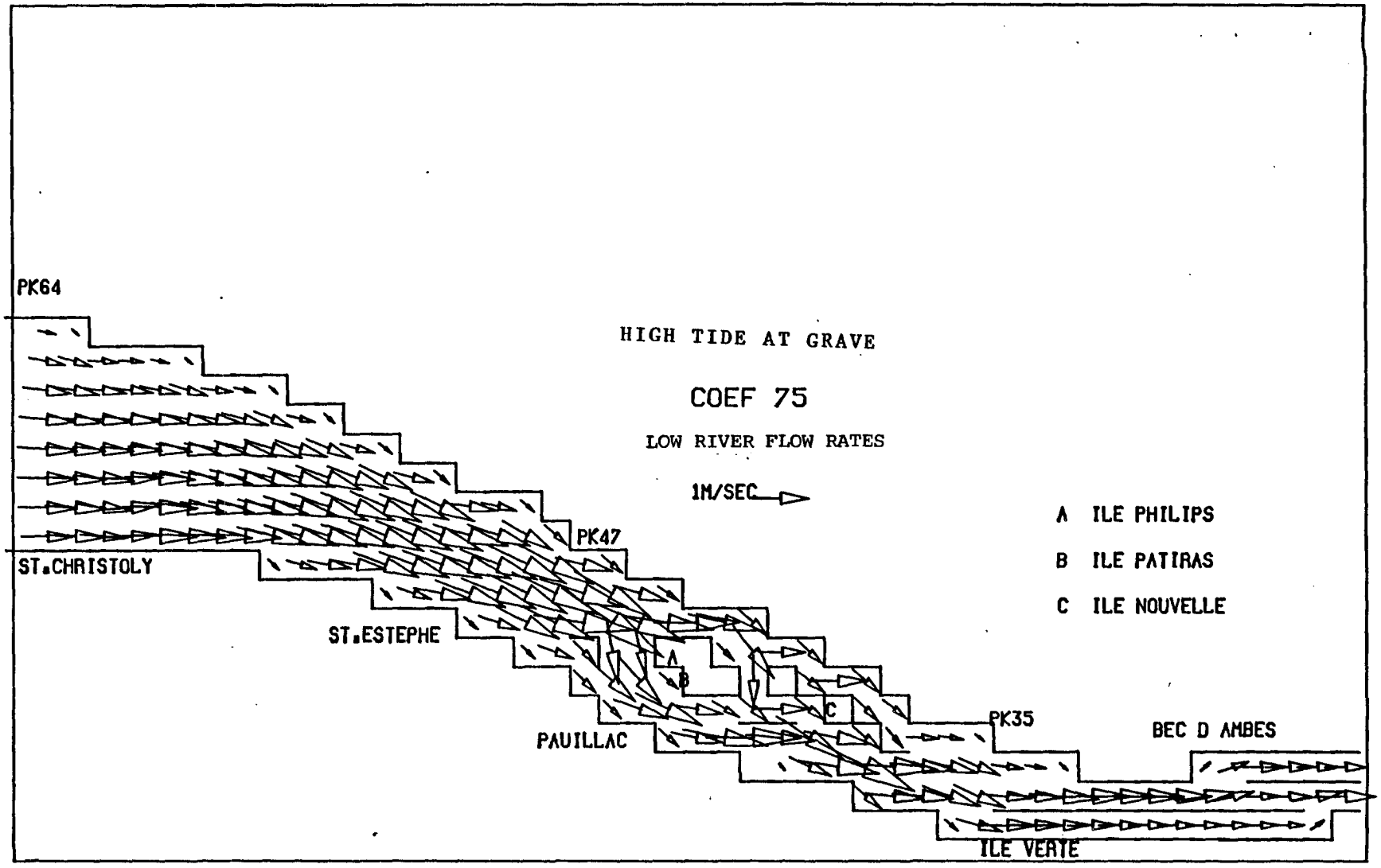
PK64
HIGH TIDE AT GRAVE
COEF 75
LOW RIVER FLOW RATES
1M/SEC
A ILE PHILIPS
B ILE PATIRAS
C ILE NOUVELLE
PK47
ST.CHRISTOLY
ST.ESTEPHE
A
B
C
PK35
PAUILLAC
BEC D AMBES
ILE VERTE

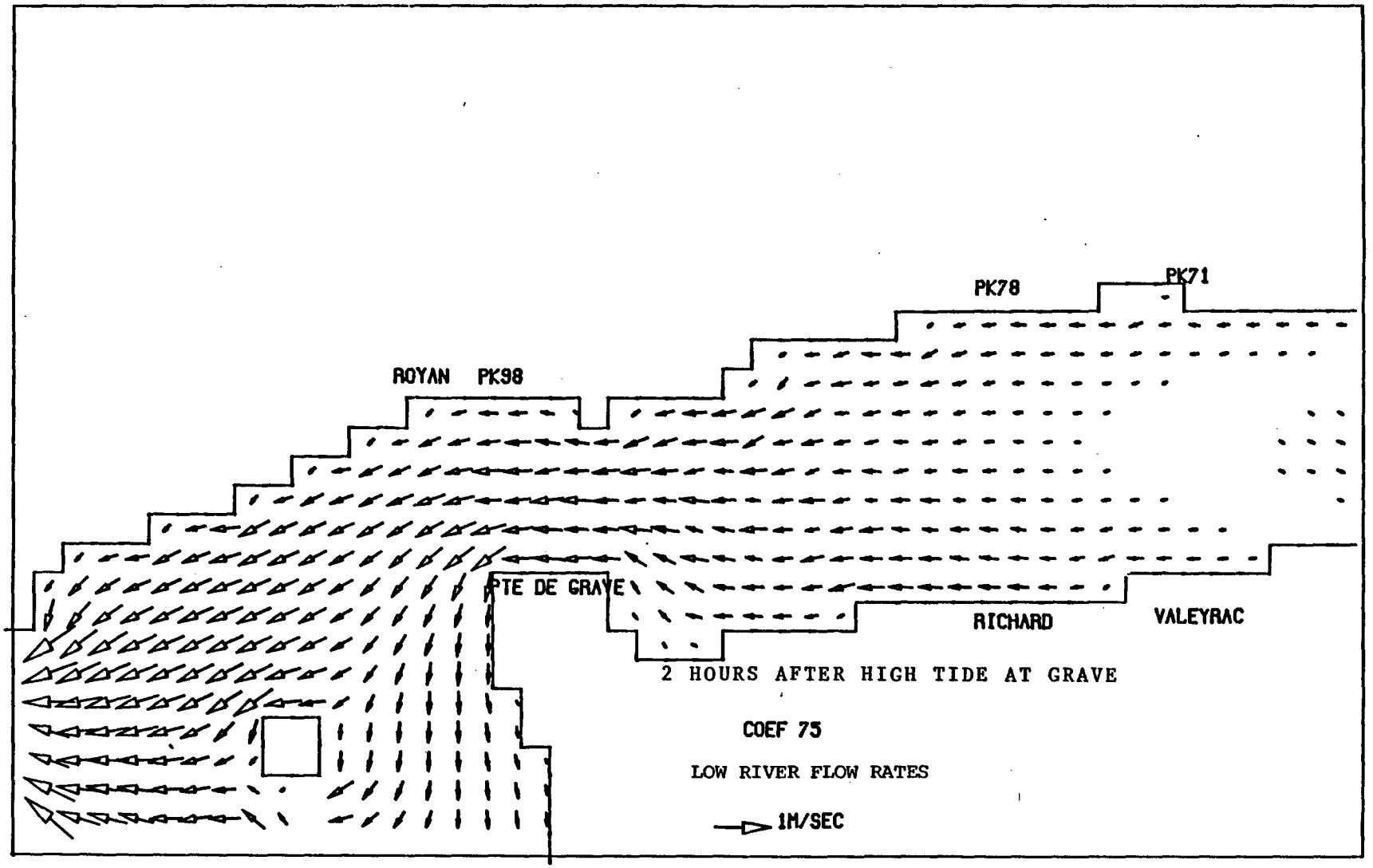
PK78
PK71
ROYAN PK98
PTE DE GRAVE
RICHARD
VALEYRAC
2 HOURS AFTER HIGH TIDE AT GRAVE
COEF 75
LOW RIVER FLOW RATES
1M/SEC

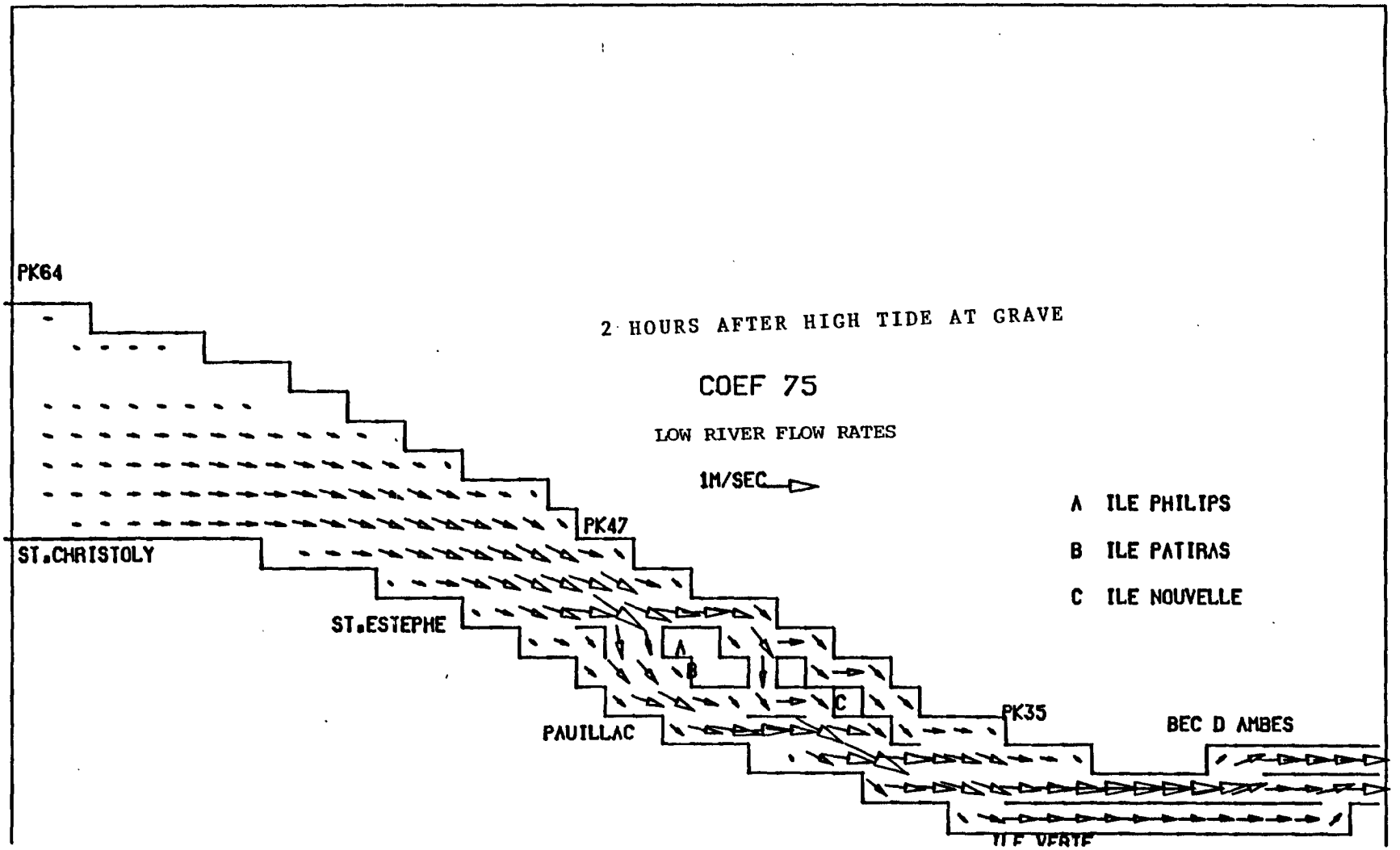
PK64
2 HOURS AFTER HIGH TIDE AT GRAVE
COEF 75
LOW RIVER FLOW RATES
1M/SEC
A ILE PHILIPS
B ILE PATIRAS
C ILE NOUVELLE
PK47
ST.CHRISTOLY
ST.ESTEPHE
A
B
C
PK35
PAUILLAC
BEC D AMBES

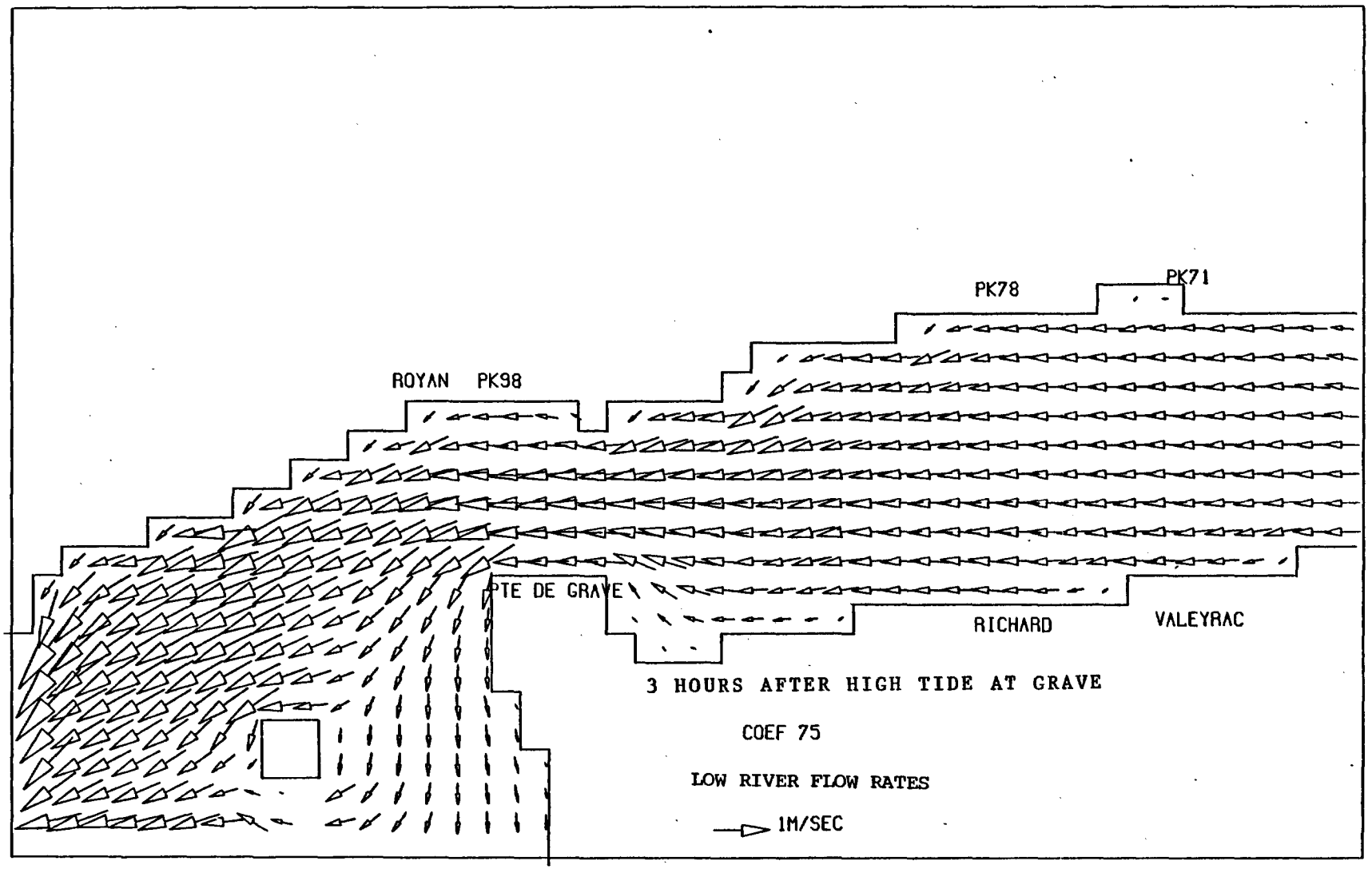
PK78
PK71
ROYAN PK98
PTE DE GRAVE
RICHARD
VALEYRAC
3 HOURS AFTER HIGH TIDE AT GRAVE
COEF 75
LOW RIVER FLOW RATES
1M/SEC

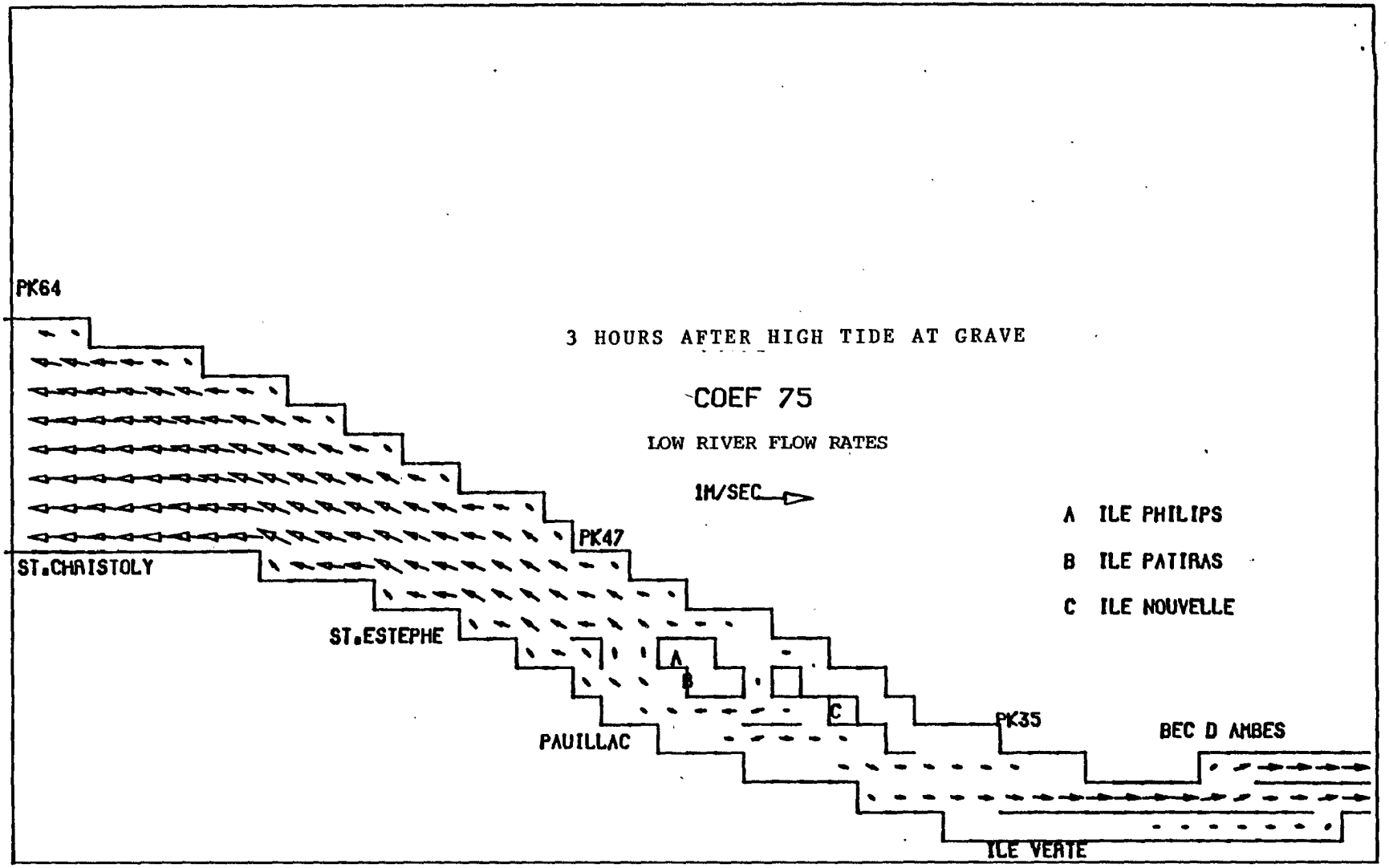
PK64
3 HOURS AFTER HIGH TIDE AT GRAVE
COEF 75
LOW RIVER FLOW RATES
1M/SEC
A ILE PHILIPS
B ILE PATIRAS
C ILE NOUVELLE
PK47
ST.CHRISTOLY
ST.ESTEPHE
A
B
C
PK35
PAUILLAC
BEC D AMBES
ILE VERTE

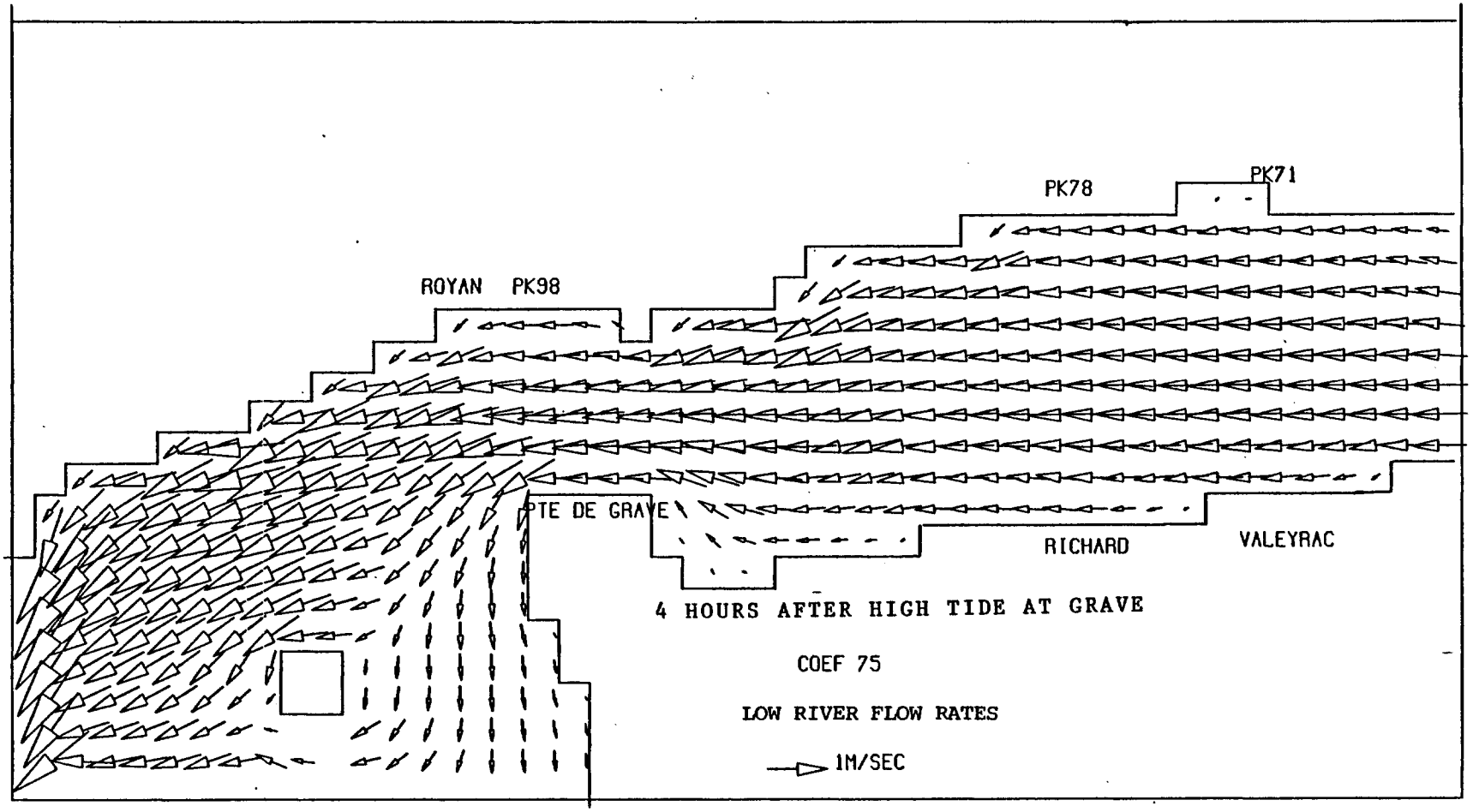
PK78
PK71
ROYAN PK98
PTE DE GRAVE
RICHARD
VALEYRAC
4 HOURS AFTER HIGH TIDE AT GRAVE
COEF 75
LOW RIVER FLOW RATES
1M/SEC

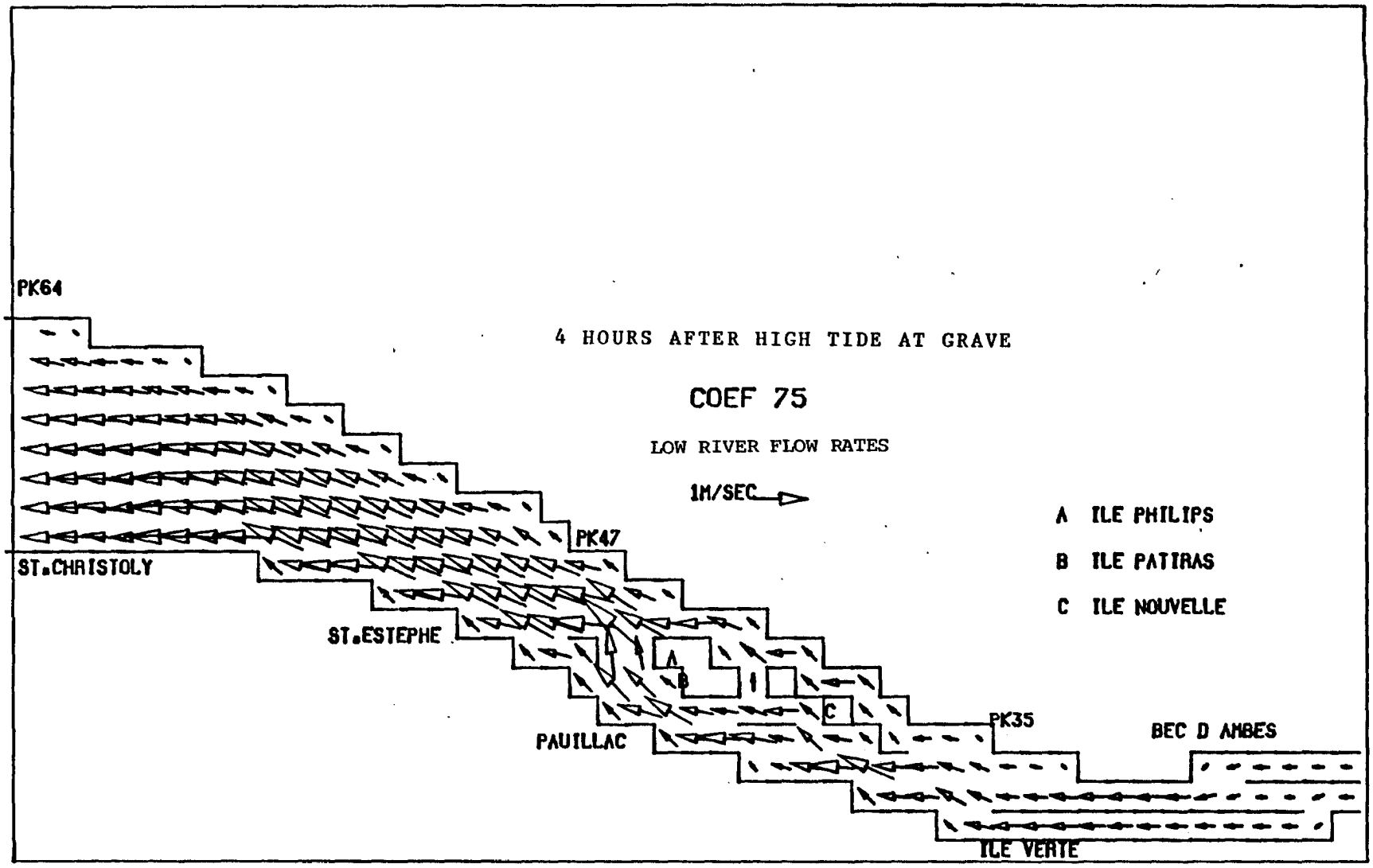
PK64
4 HOURS AFTER HIGH TIDE AT GRAVE
COEF 75
LOW RIVER FLOW RATES
1M/SEC
A ILE PHILIPS
B ILE PATIRAS
C ILE NOUVELLE
PK47
ST.CHRISTOLY
ST.ESTEPHE
A
B
C
PK35
BEC D AMBES
PAUILLAC
ILE VERTE

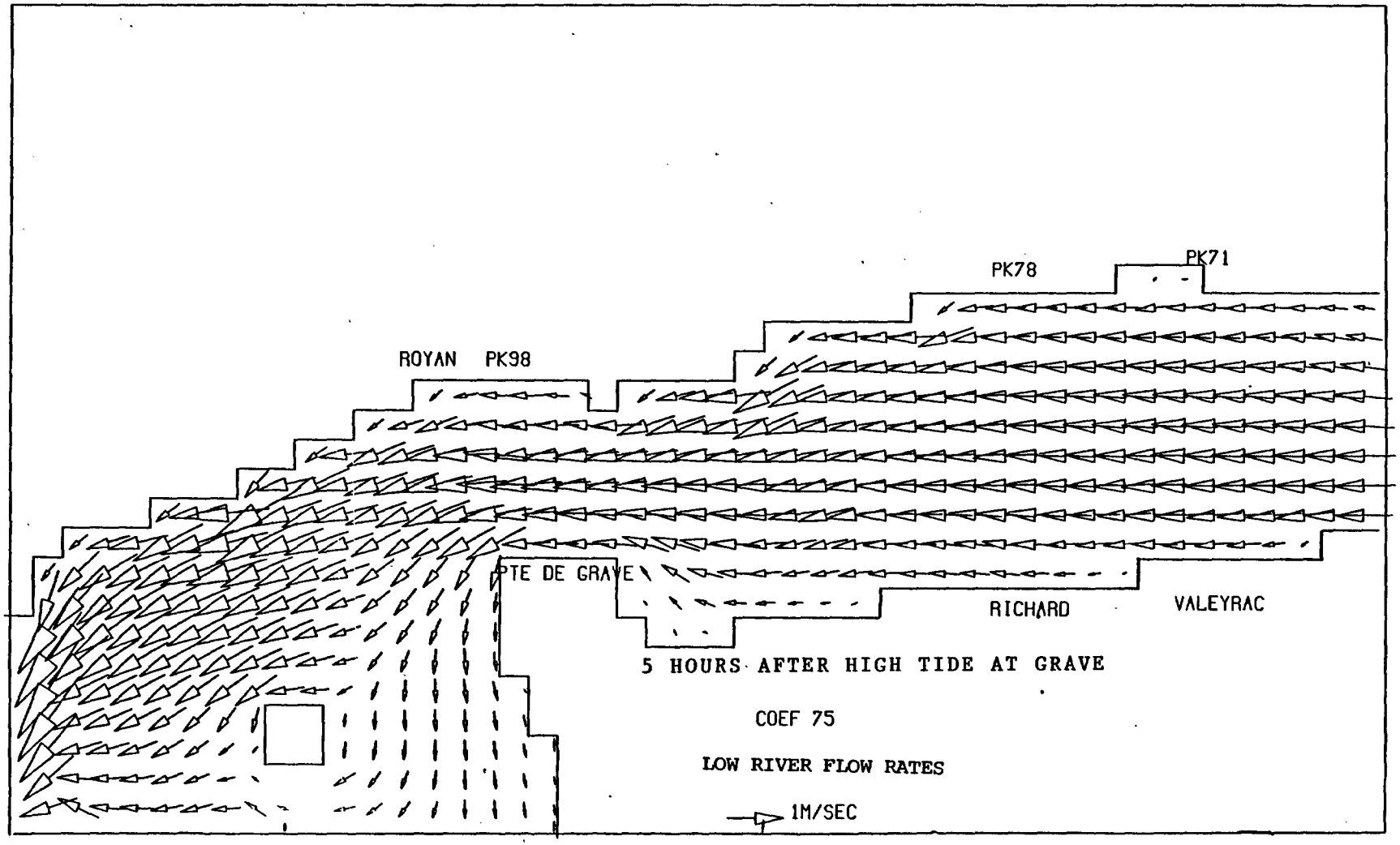
PK78
PK71
ROYAN PK98
PTE DE GRAVE
RICHARD
VALEYRAC
5 HOURS AFTER HIGH TIDE AT GRAVE
COEF 75
LOW RIVER FLOW RATES
1M/SEC

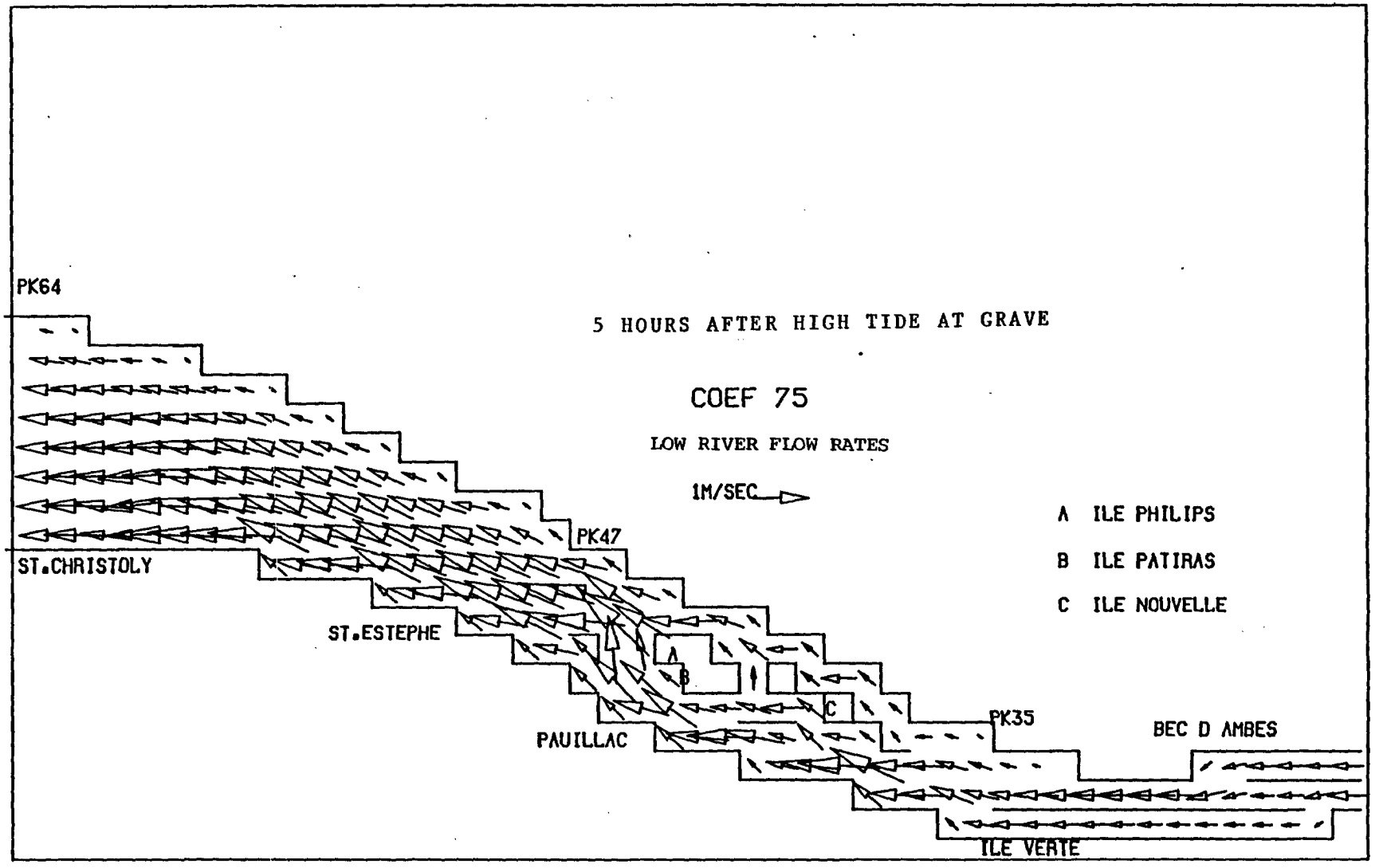
PK64
5 HOURS AFTER HIGH TIDE AT GRAVE
COEF 75
LOW RIVER FLOW RATES
1M/SEC
A ILE PHILIPS
B ILE PATIRAS
C ILE NOUVELLE
PK47
ST.CHRISTOLY
ST.ESTEPHE
A
B
C
PK35
PAUILLAC
BEC D AMBES
ILE VERTE

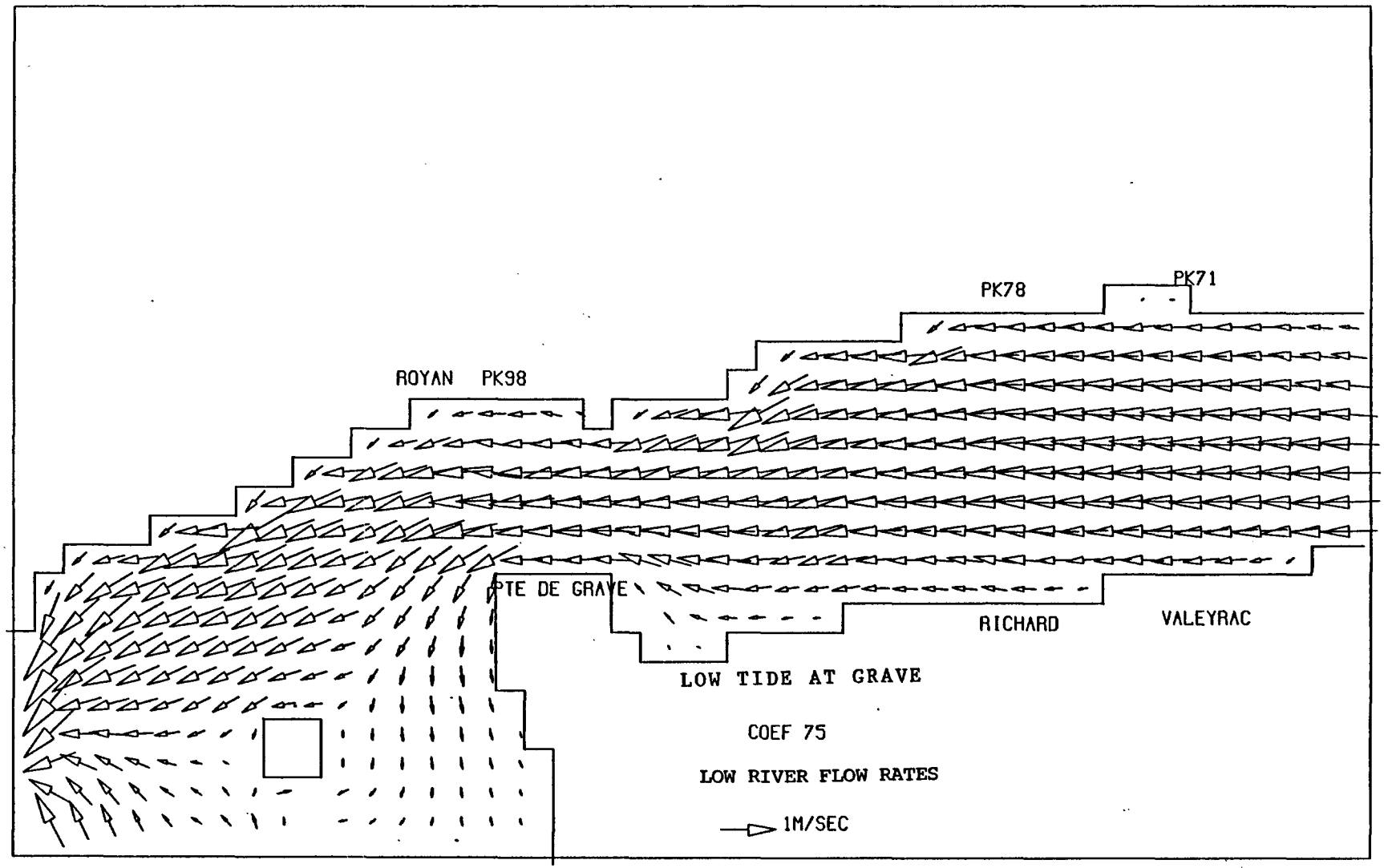
PK78
PK71
ROYAN PK98
PTE DE GRAVE
RICHARD
VALEYRAC
LOW TIDE AT GRAVE
COEF 75
LOW RIVER FLOW RATES
1M/SEC

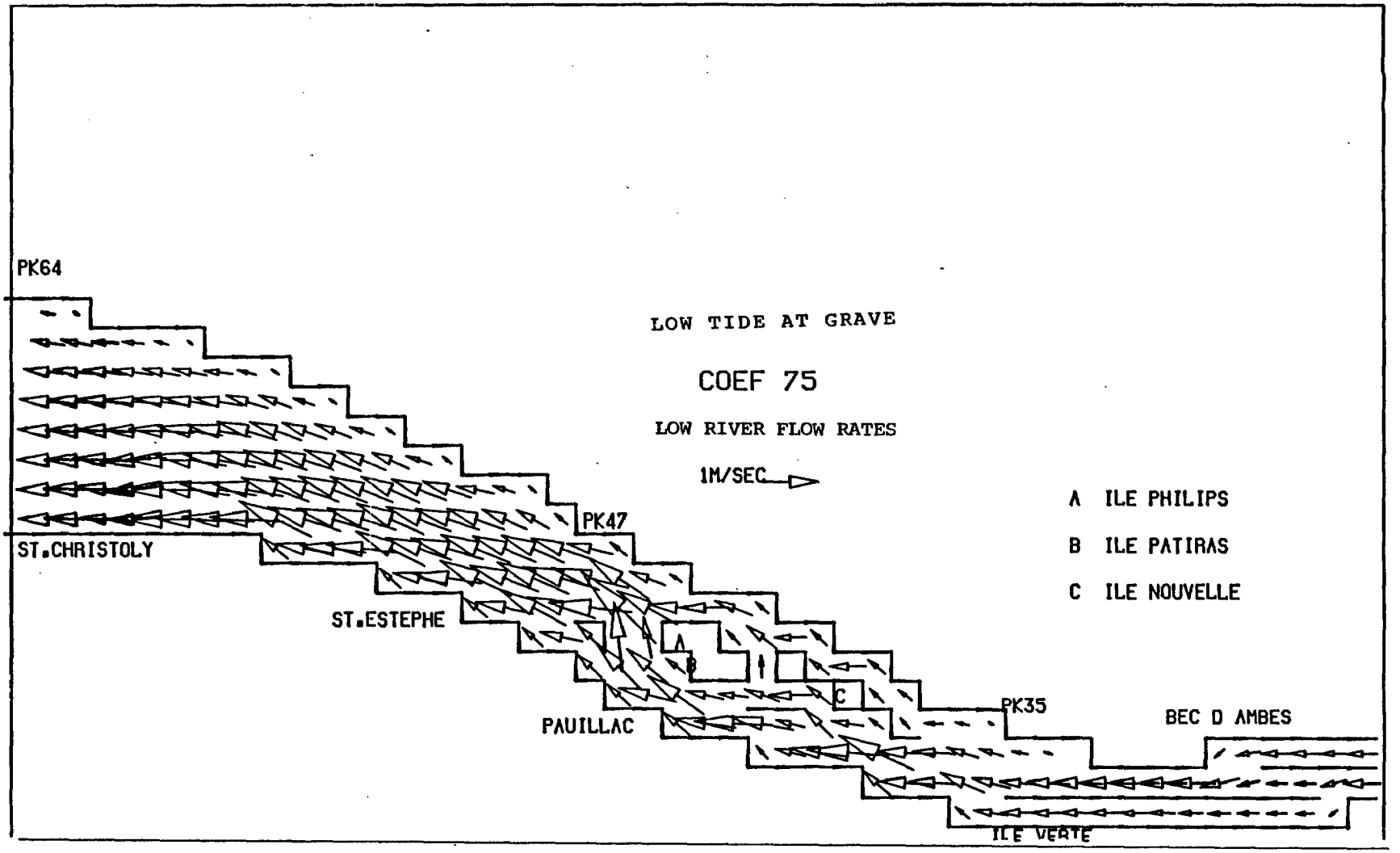
PK64
LOW TIDE AT GRAVE
COEF 75
LOW RIVER FLOW RATES
1M/SEC
A ILE PHILIPS
B ILE PATIRAS
C ILE NOUVELLE
PK47
ST.CHRISTOLY
ST.ESTEPHE
A
B
C
PK35
BEC D AMBES
PAUILLAC
ILE VERTE

APPENDIX II

Instantaneous current vector diagrams

(Irregular grid finite difference model)

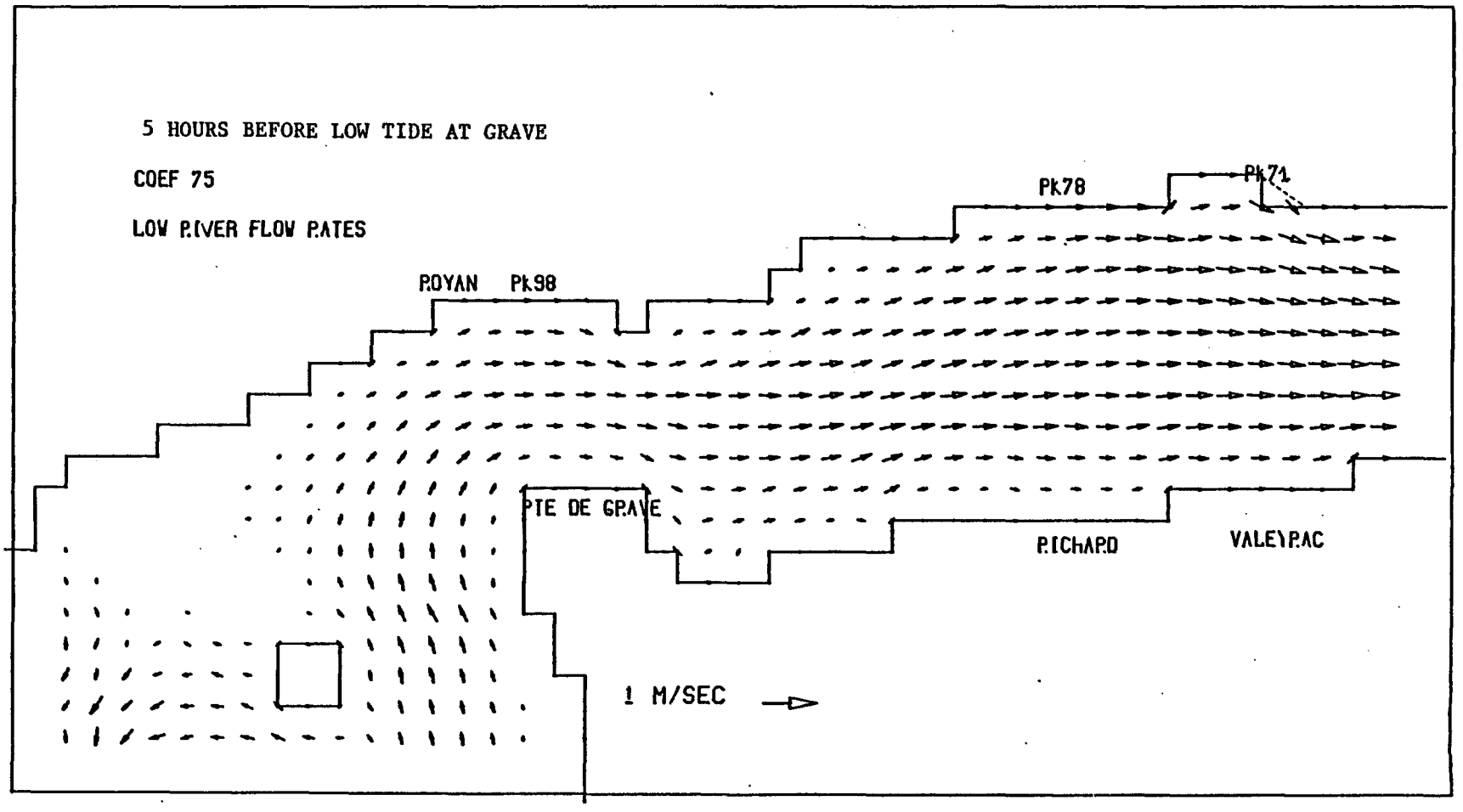
5 HOURS BEFORE LOW TIDE AT GRAVE
COEF 75
LOW RIVER FLOW RATES
Pk78
Pk71
ROYAN Pk98
PTE DE GRAVE
PICHAPO
VALEYRAC
1 M/SEC

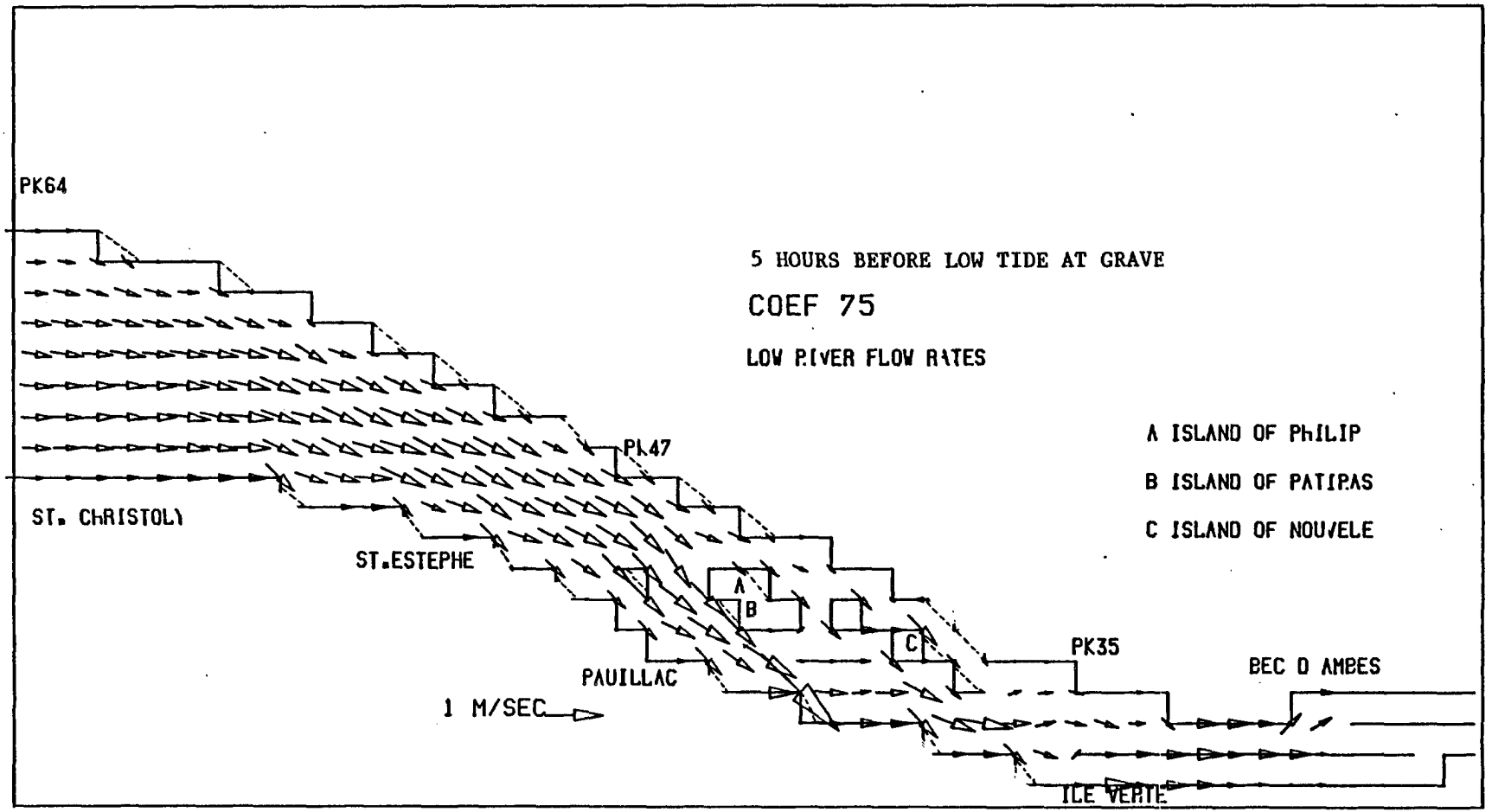
PK64
5 HOURS BEFORE LOW TIDE AT GRAVE
COEF 75
LOW RIVER FLOW RATES
A ISLAND OF PHILIP
B ISLAND OF PATIPAS
C ISLAND OF NOUVELE
PK47
ST. CHRISTOLY
ST.ESTEPHE
A
B
C
PK35
BEC D AMBES
PAUILLAC
1 M/SEC
ILE VERTE

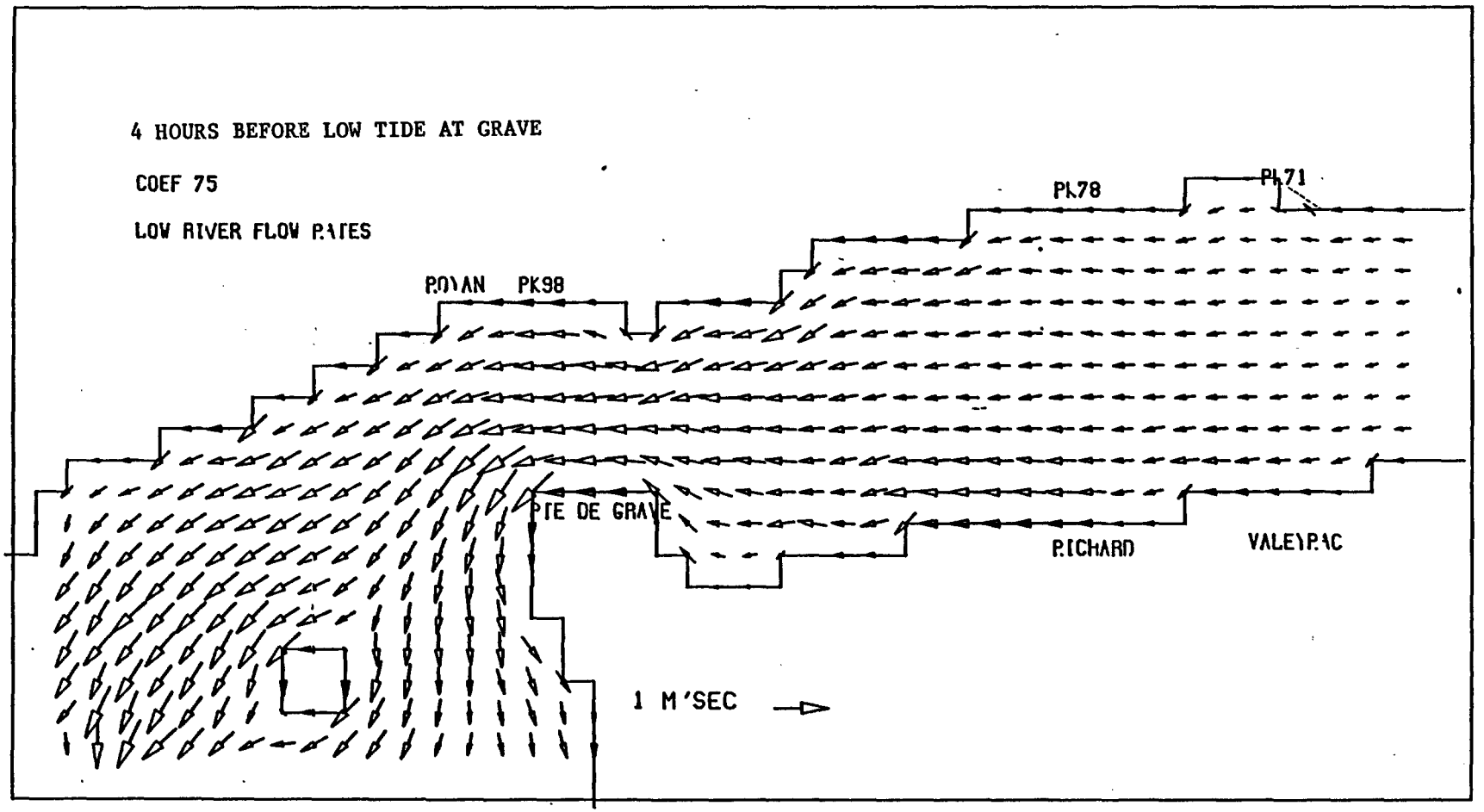
4 HOURS BEFORE LOW TIDE AT GRAVE
COEF 75
LOW RIVER FLOW RATES
PK78
PK71
POYAN
PK98
PTE DE GRAVE
PICHARD
VALEYRAC
1 M'SEC

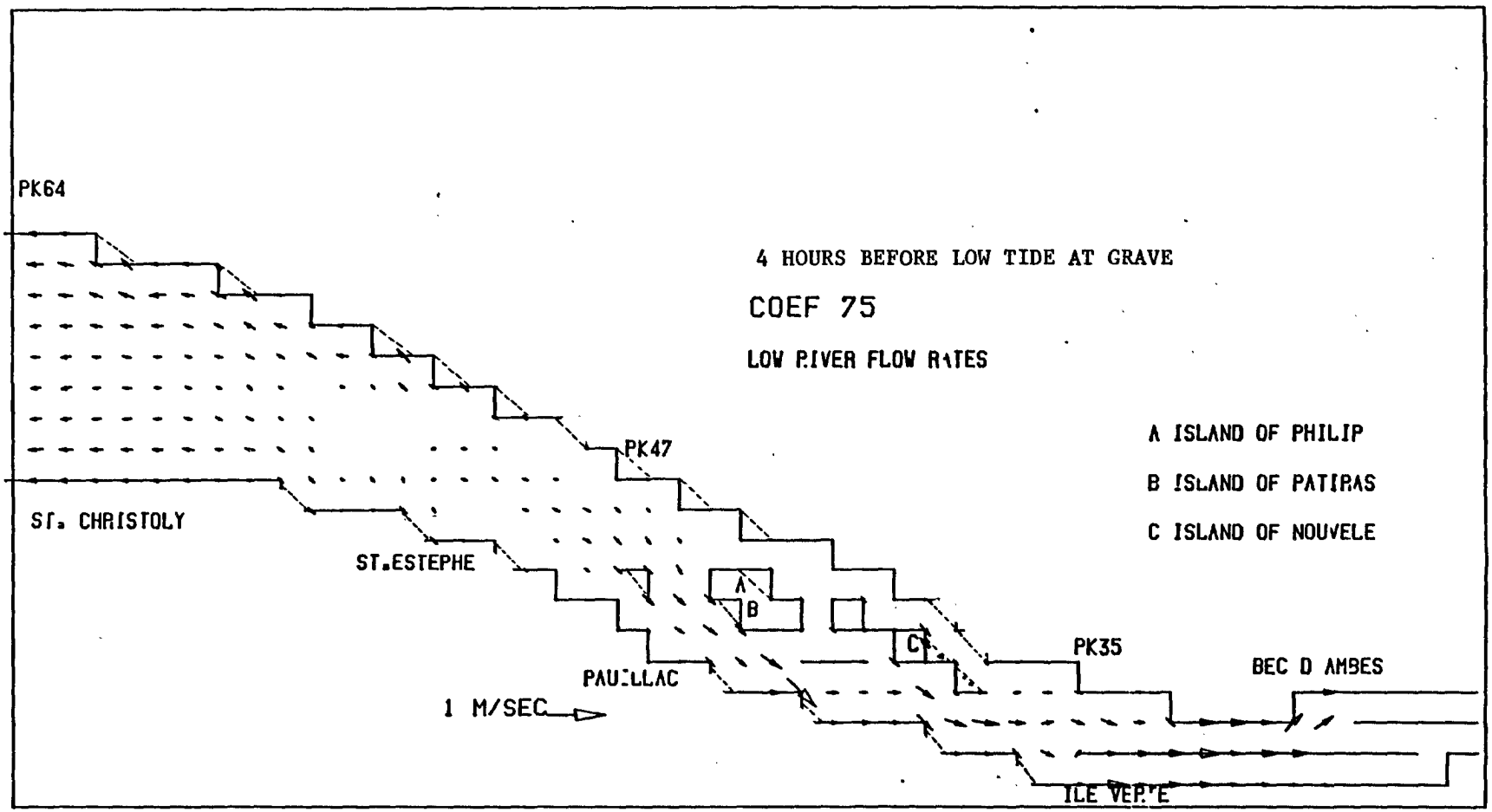
PK64
4 HOURS BEFORE LOW TIDE AT GRAVE
COEF 75
LOW RIVER FLOW RATES
A ISLAND OF PHILIP
B ISLAND OF PATIRAS
C ISLAND OF NOUVELE
PK47
ST. CHRISTOLY
ST.ESTEPHE
A
B
C
PK35
BEC D AMBES
PAULLAC
1 M/SEC
ILE VERTE

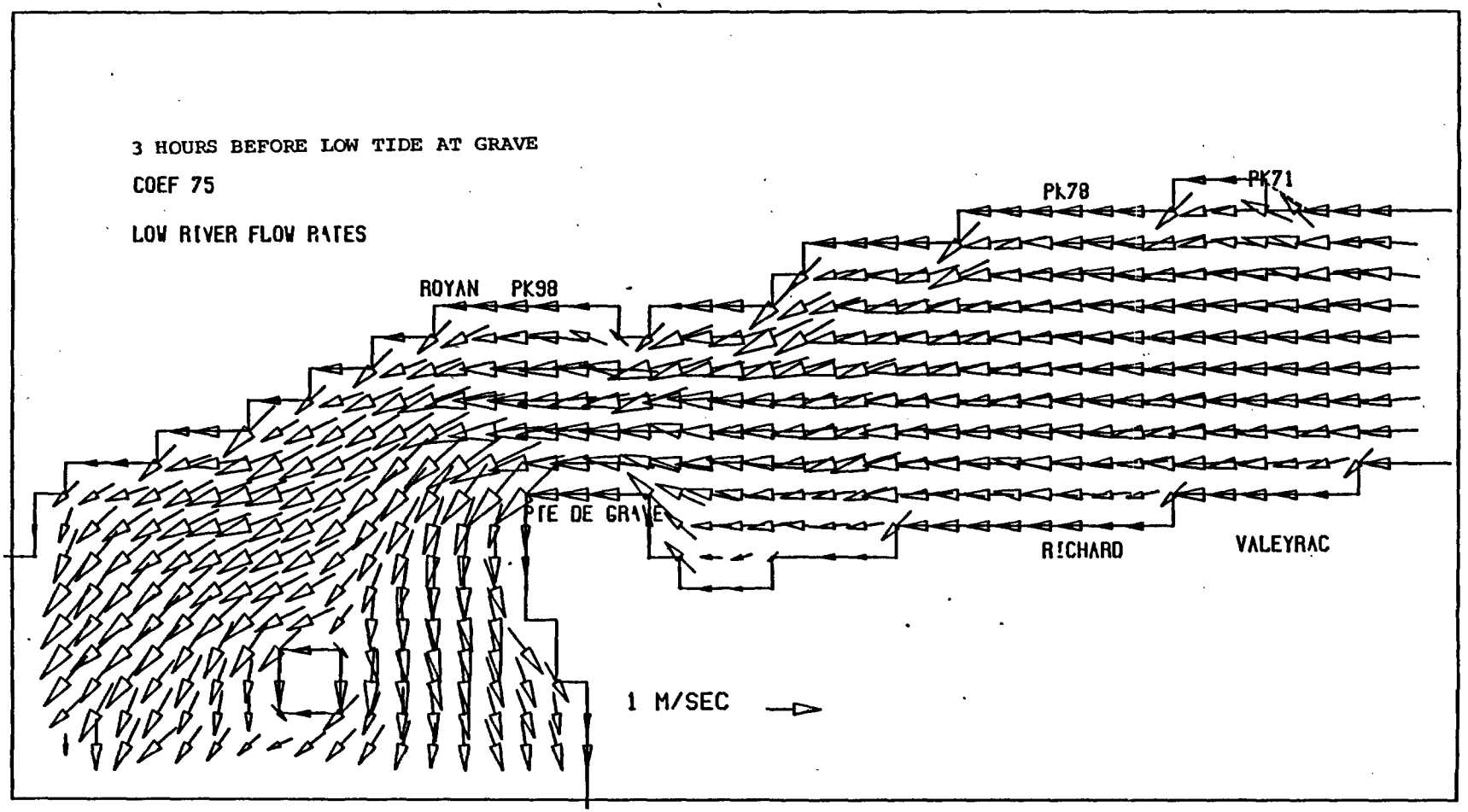
3 HOURS BEFORE LOW TIDE AT GRAVE
COEF 75
LOW RIVER FLOW RATES
ROYAN
PK98
PK78
PK71
PTE DE GRAVE
RICHARD
VALEYRAC
1 M/SEC

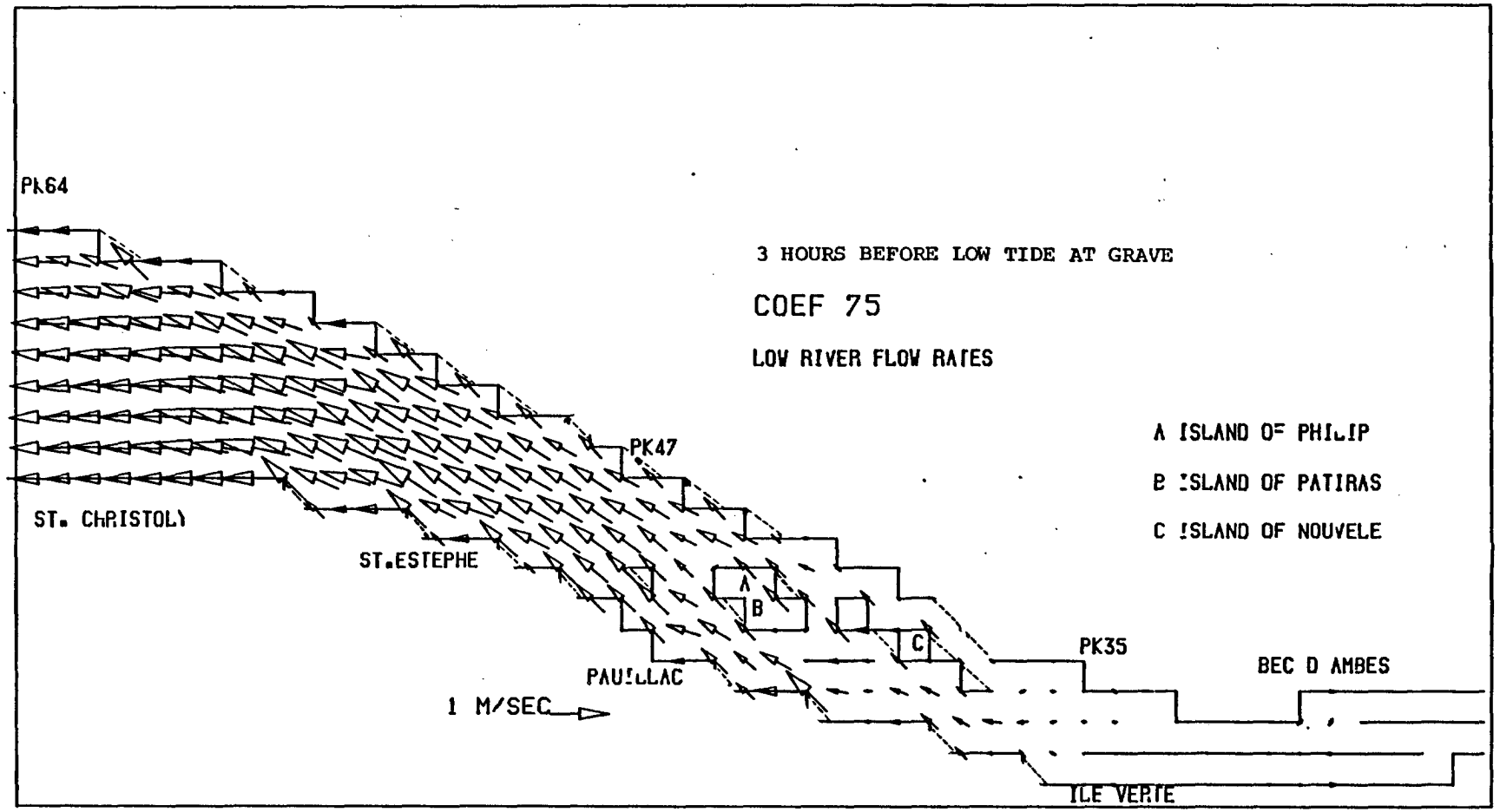
PK64
3 HOURS BEFORE LOW TIDE AT GRAVE
COEF 75
LOW RIVER FLOW RATES
A ISLAND OF PHILIP
B ISLAND OF PATIRAS
C ISLAND OF NOUVELE
PK47
ST. CHRISTOLY
ST.ESTEPHE
B
C
PK35
BEC D AMBES
PAULLAC
1 M/SEC
ILE VERTE

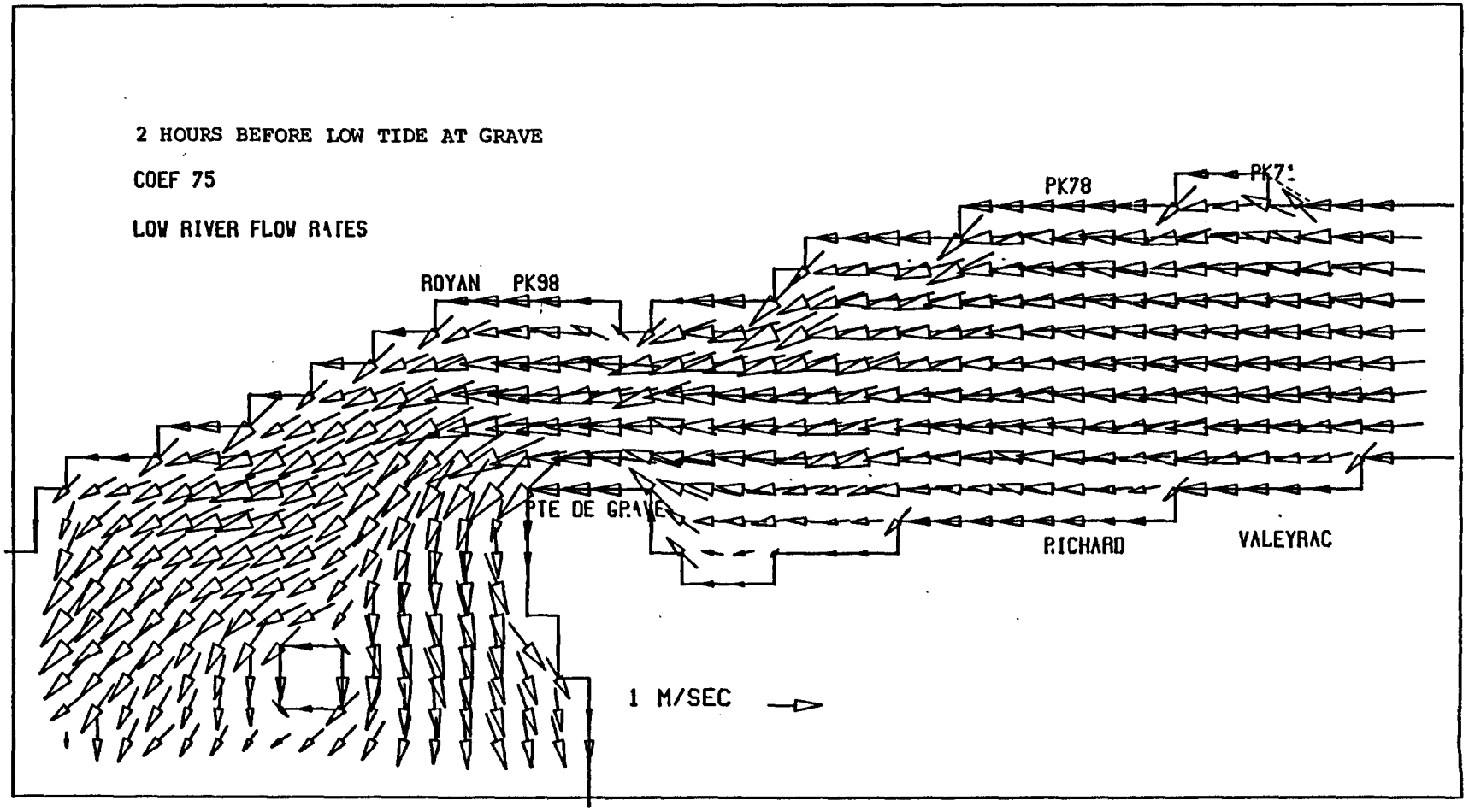
2 HOURS BEFORE LOW TIDE AT GRAVE
COEF 75
LOW RIVER FLOW RATES
ROYAN
PK98
PK78
PK7
PTE DE GRAVE
RICHARD
VALEYRAC
1 M/SEC

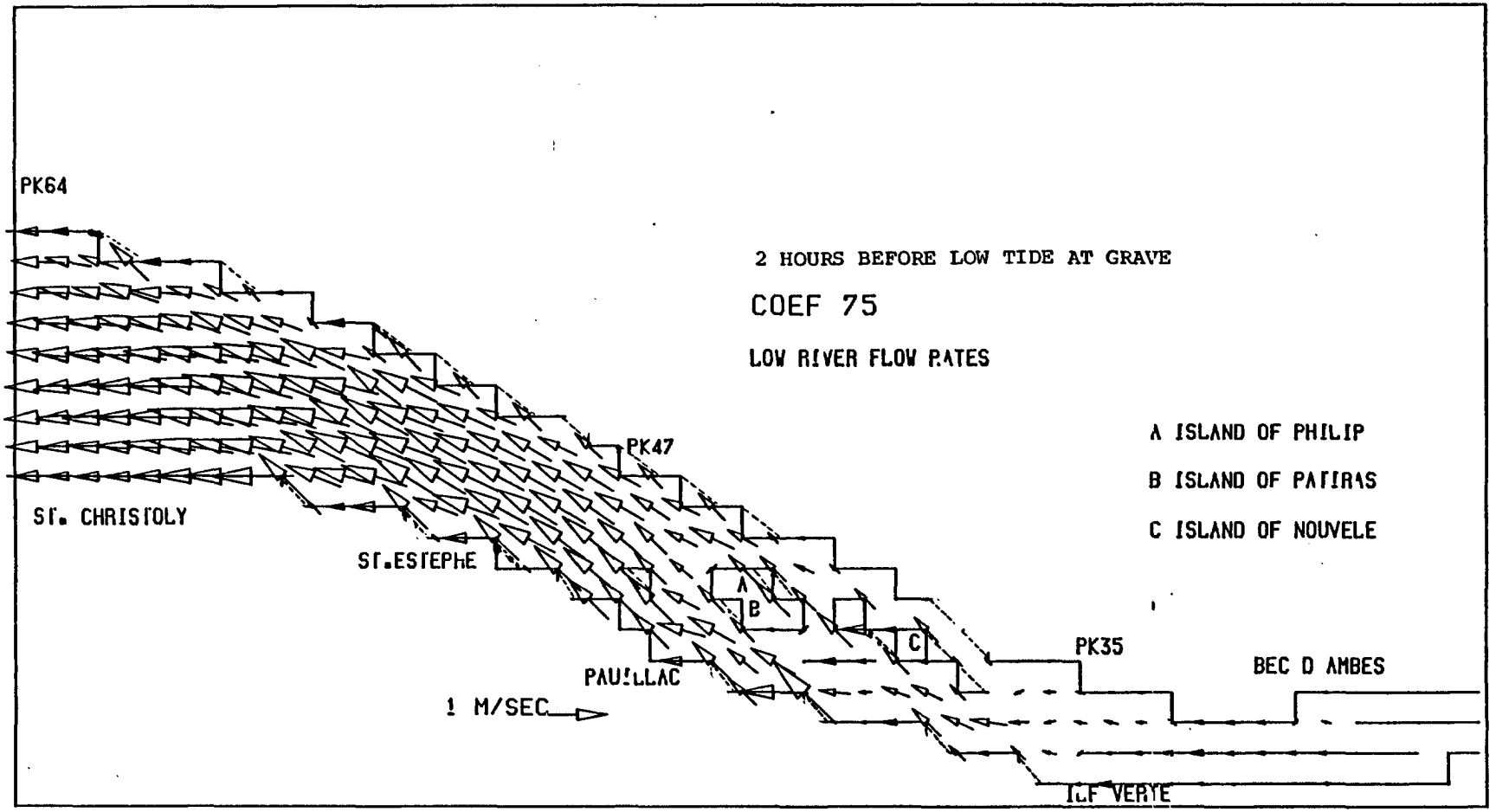
PK64
2 HOURS BEFORE LOW TIDE AT GRAVE
COEF 75
LOW RIVER FLOW RATES
A ISLAND OF PHILIP
B ISLAND OF PATIRAS
C ISLAND OF NOUVELE
PK47
ST. CHRISTOLY
ST.ESTEPHE
A
B
C
PK35
BEC D AMBES
PAULLAC
1 M/SEC
ILE VERTE

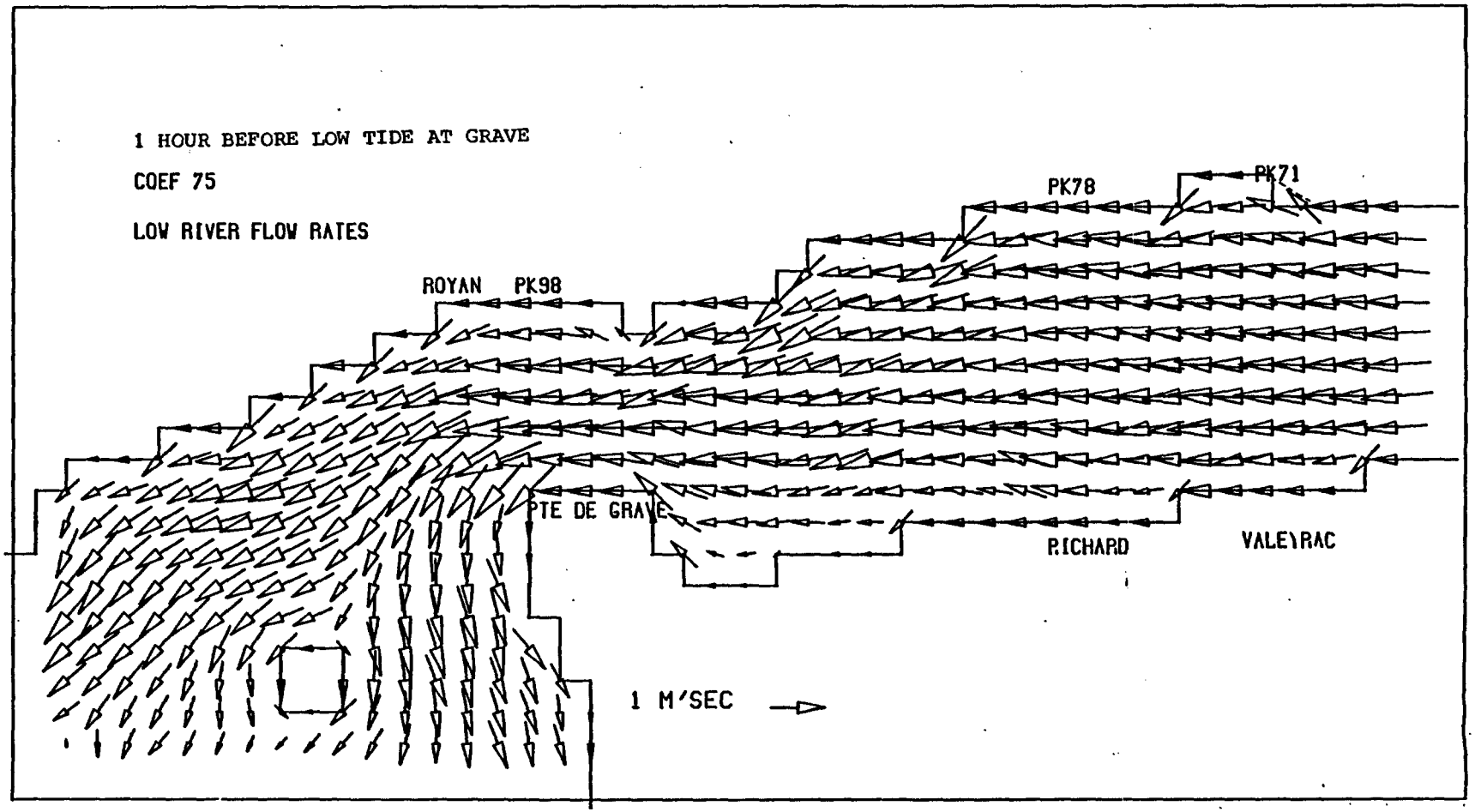
1 HOUR BEFORE LOW TIDE AT GRAVE
COEF 75
LOW RIVER FLOW RATES
PK78
PK71
ROYAN PK98
PTE DE GRAVE
P.ICHARD
VALEYRAC
1 M/SEC

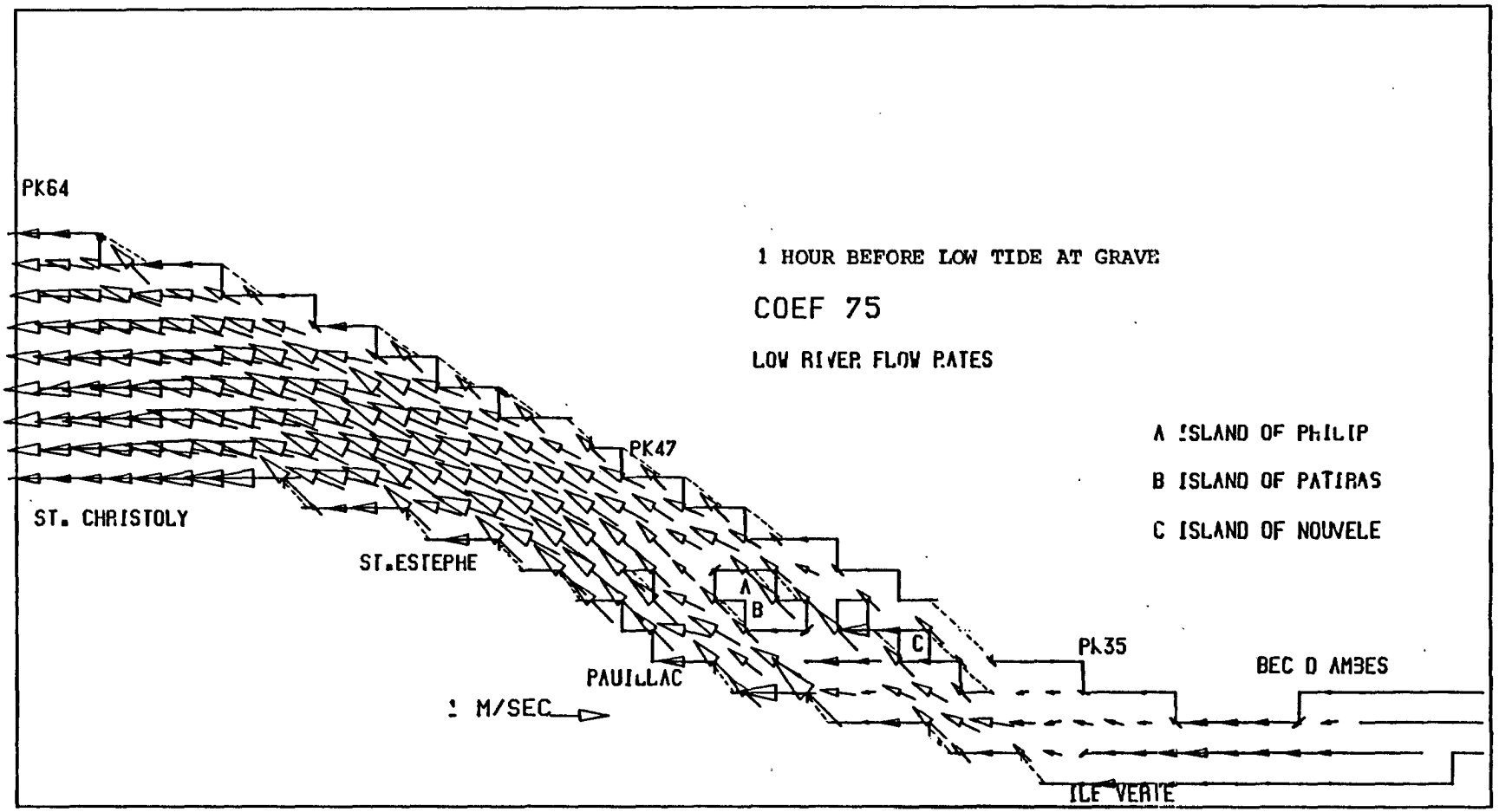
PK64
1 HOUR BEFORE LOW TIDE AT GRAVE
COEF 75
LOW RIVER FLOW RATES
A ISLAND OF PHILIP
B ISLAND OF PATIRAS
C ISLAND OF NOUVELE
PK47
ST. CHRISTOLY
ST.ESTEPHE
A
B
C
PK35
BEC D AMBES
PAUILLAC
1 M/SEC
ILE VERTE

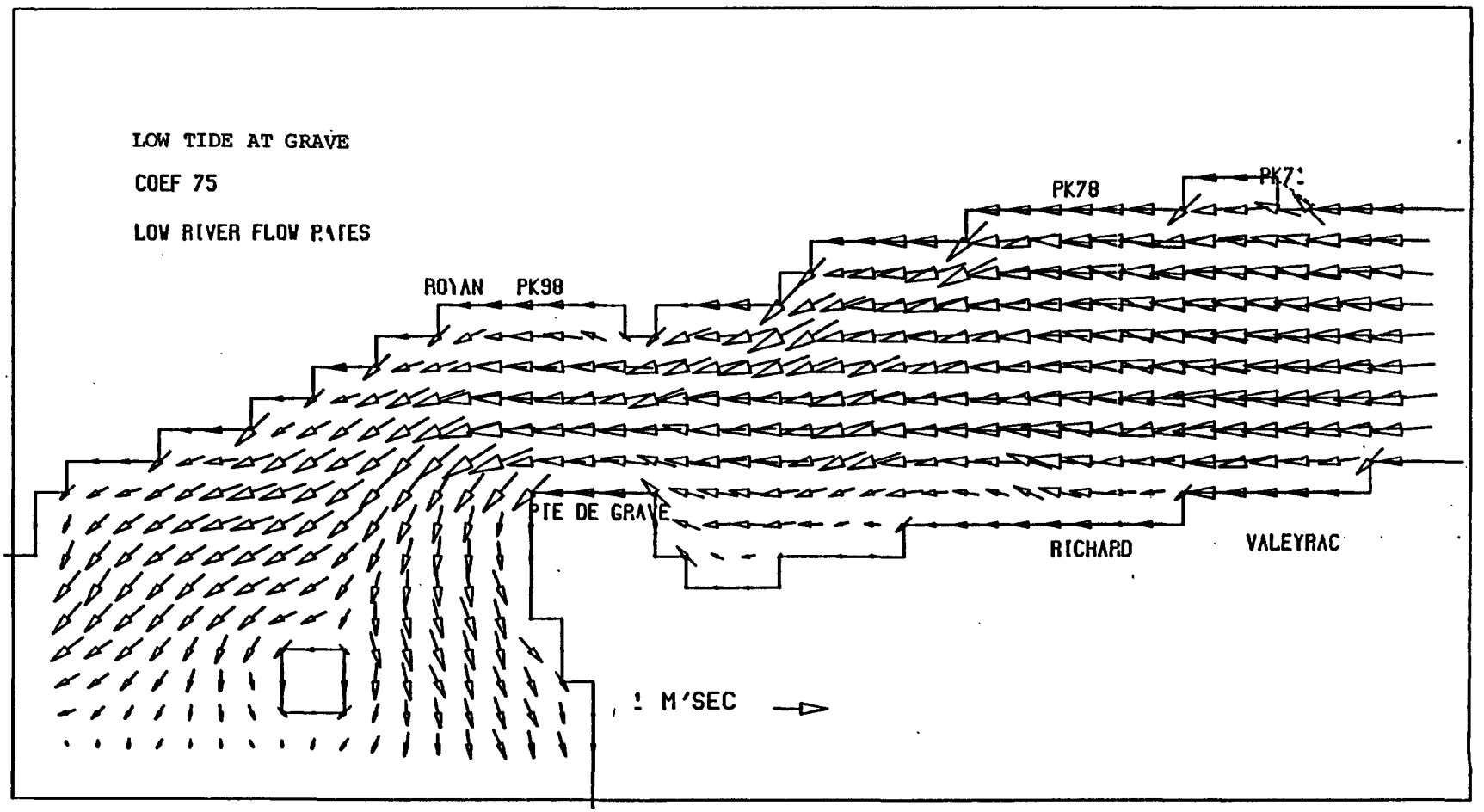
LOW TIDE AT GRAVE
COEF 75
LOW RIVER FLOW RATES
ROYAN PK98
PK78
PK7:
PTE DE GRAVE
RICHARD
VALEYRAC
1 M/SEC

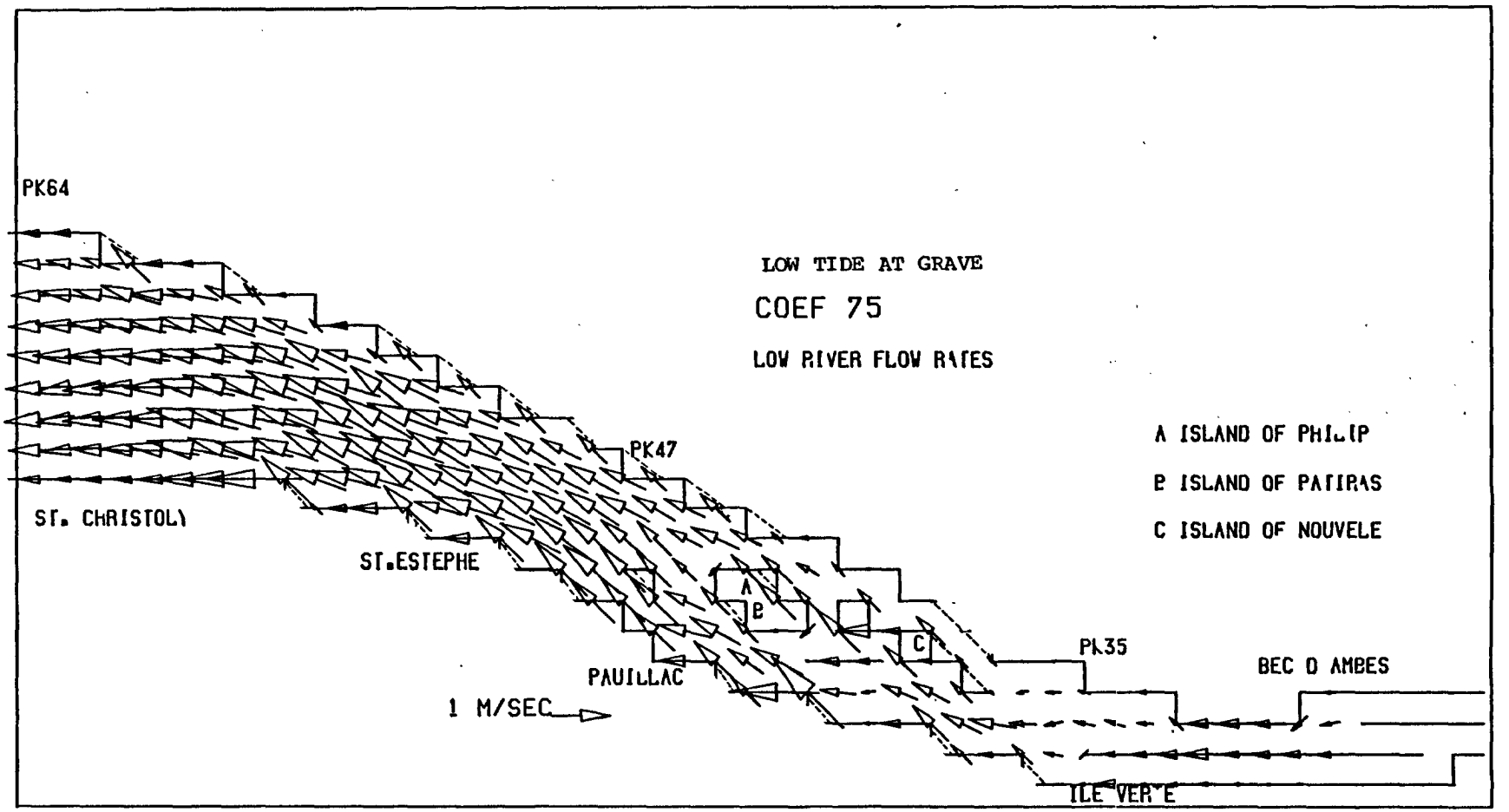
PK64
LOW TIDE AT GRAVE
COEF 75
LOW RIVER FLOW RATES
A ISLAND OF PHILIP
B ISLAND OF PATIRAS
C ISLAND OF NOUVELE
PK47
ST. CHRISTOLY
ST.ESTEPHE
A
B
C
PK35
BEC D AMBES
PAUILLAC
1 M/SEC
ILE VERTE

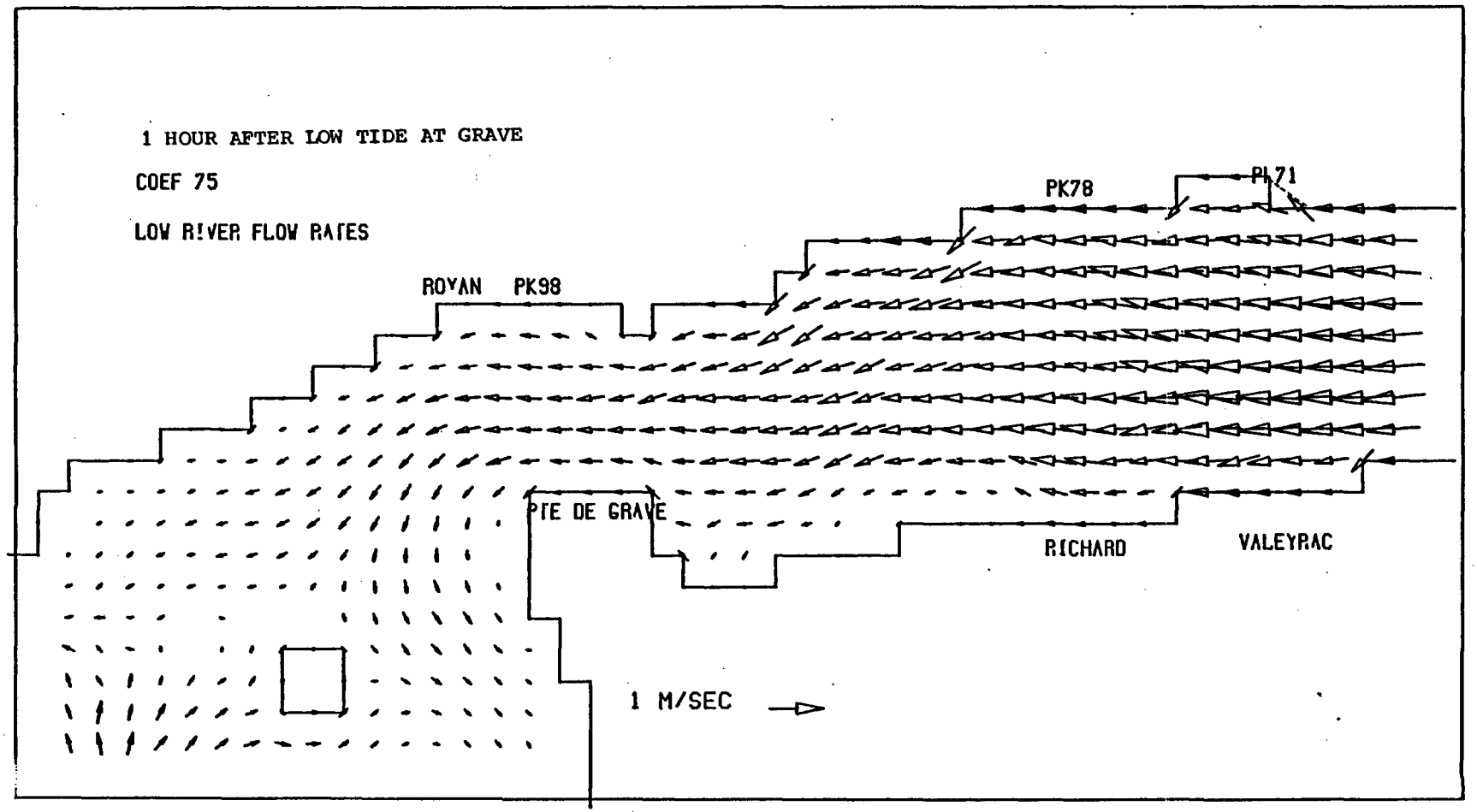
1 HOUR AFTER LOW TIDE AT GRAVE
COEF 75
LOW RIVER FLOW RATES
ROYAN PK98
PK78
PK71
PTE DE GRAVE
RICHARD
VALEYRAC
1 M/SEC

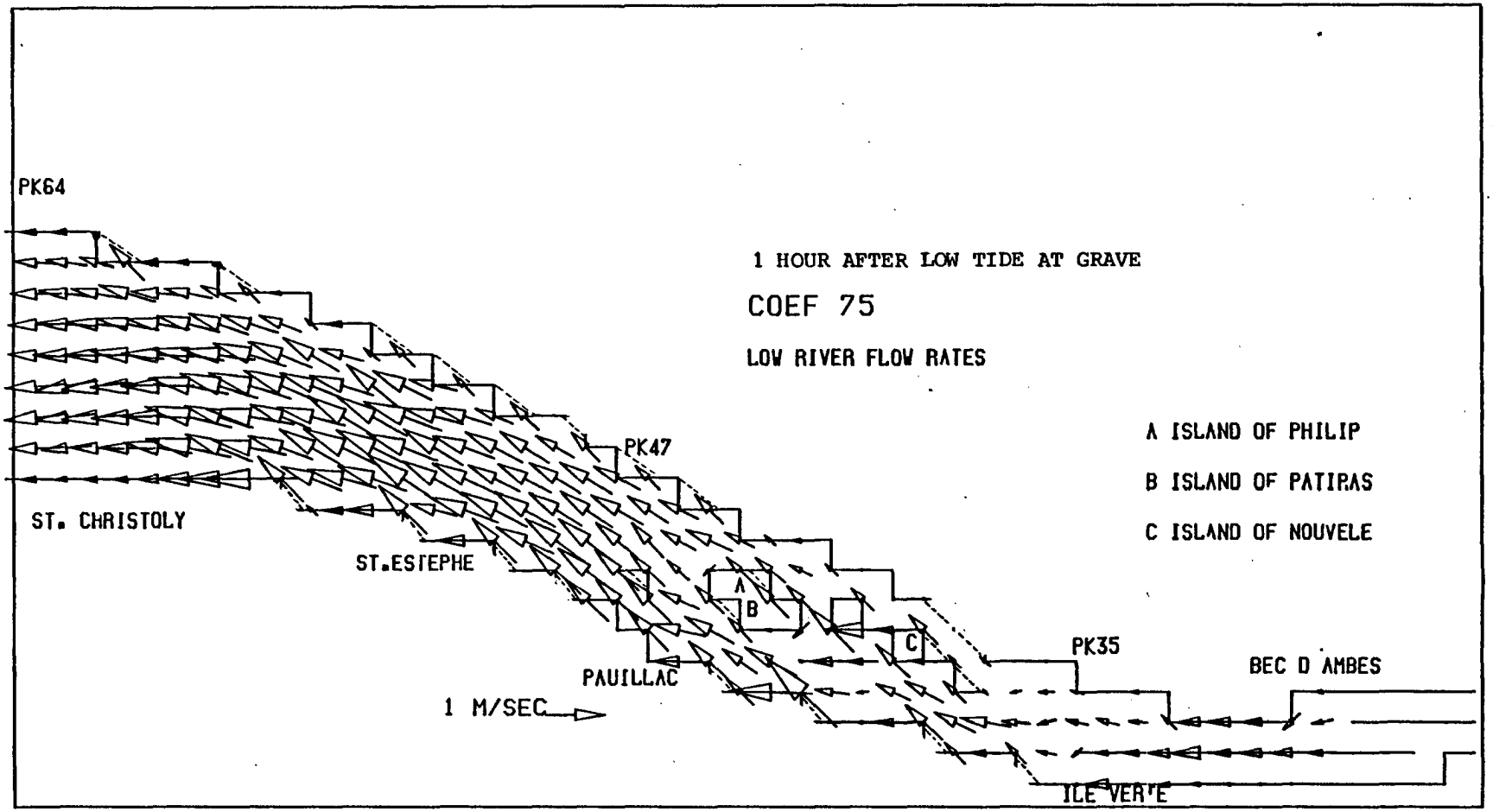
PK64
1 HOUR AFTER LOW TIDE AT GRAVE
COEF 75
LOW RIVER FLOW RATES
A ISLAND OF PHILIP
B ISLAND OF PATIRAS
C ISLAND OF NOUVELE
PK47
ST. CHRISTOLY
ST.ESTEPHE
A
B
C
PK35
BEC D AMBES
PAUILLAC
1 M/SEC
ILE VERTE

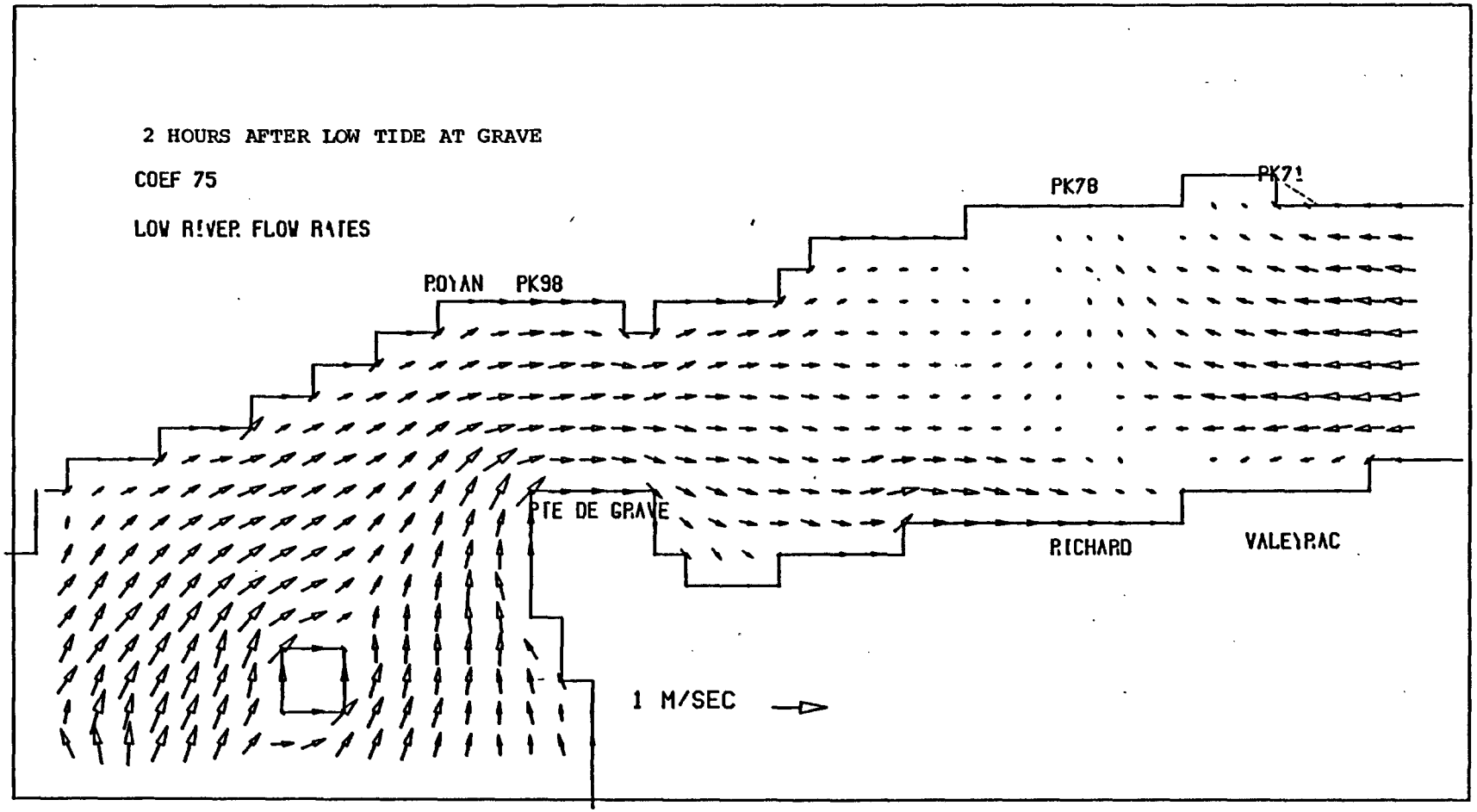
2 HOURS AFTER LOW TIDE AT GRAVE
COEF 75
LOW RIVER FLOW RATES
POYAN PK98
PK78
PK71
PTE DE GRAVE
RICHARD
VALEYRAC
1 M/SEC

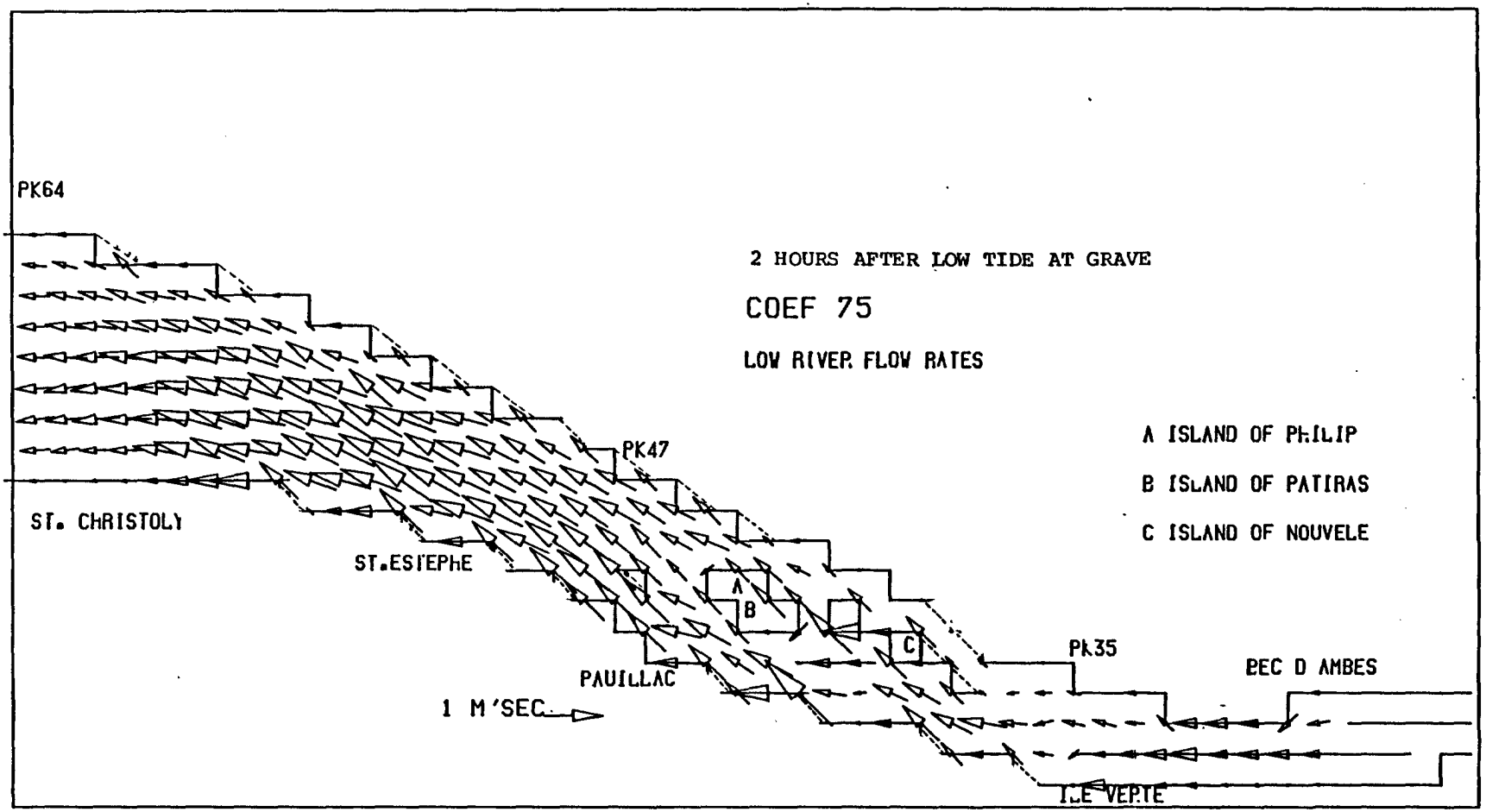
PK64
2 HOURS AFTER LOW TIDE AT GRAVE
COEF 75
LOW RIVER FLOW RATES
A ISLAND OF PHILIP
B ISLAND OF PATIRAS
C ISLAND OF NOUVELE
PK47
ST. CHRISTOLY
ST.ESTEPHE
A
B
C
PK35
PAUILLAC
BEC D AMBES
1 M'SEC
I.E VERTE

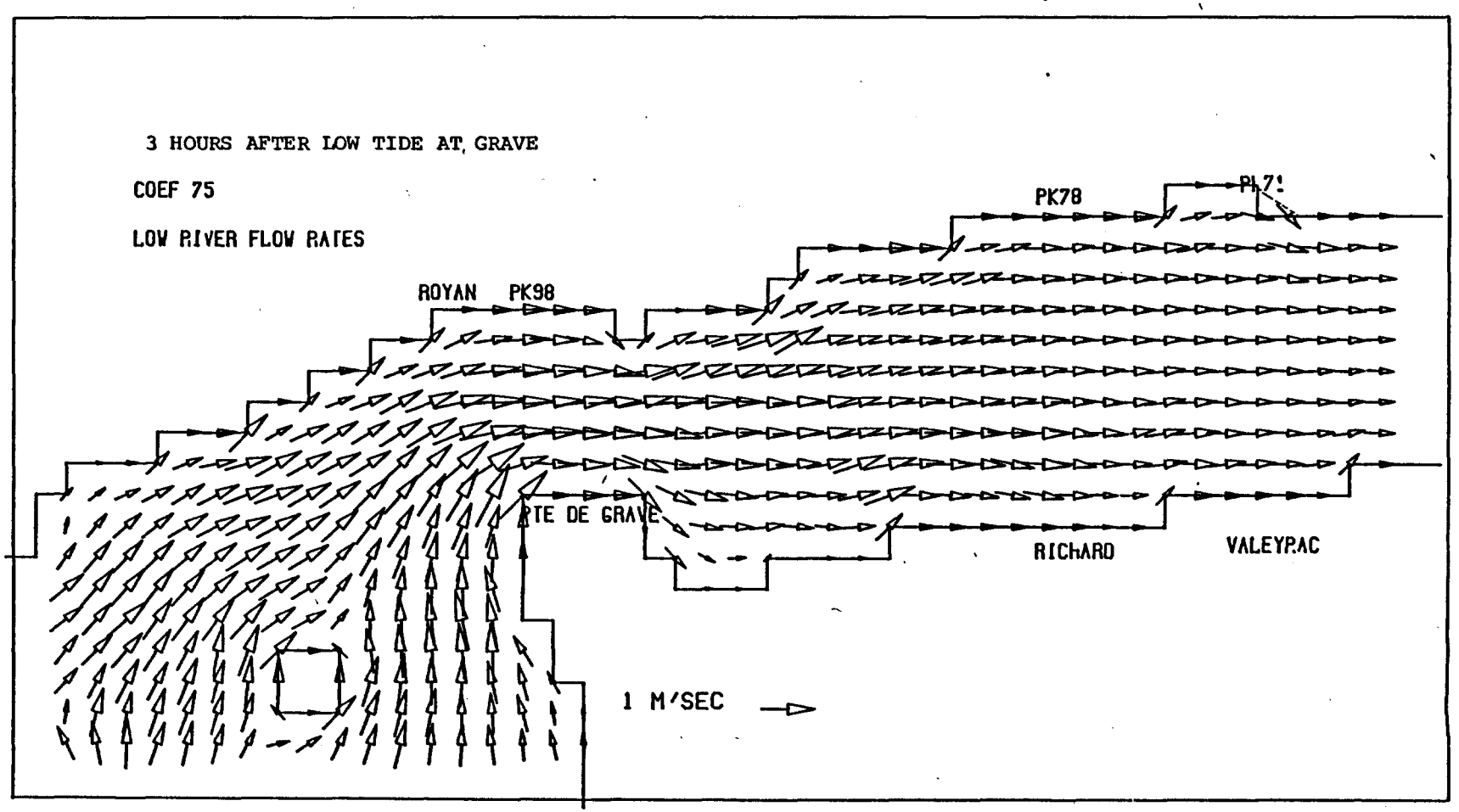
3 HOURS AFTER LOW TIDE AT GRAVE
COEF 75
LOW RIVER FLOW RATES
ROYAN
PK98
PK78
PK7?
PTE DE GRAVE
RICHARD
VALEYPAC
1 M/SEC

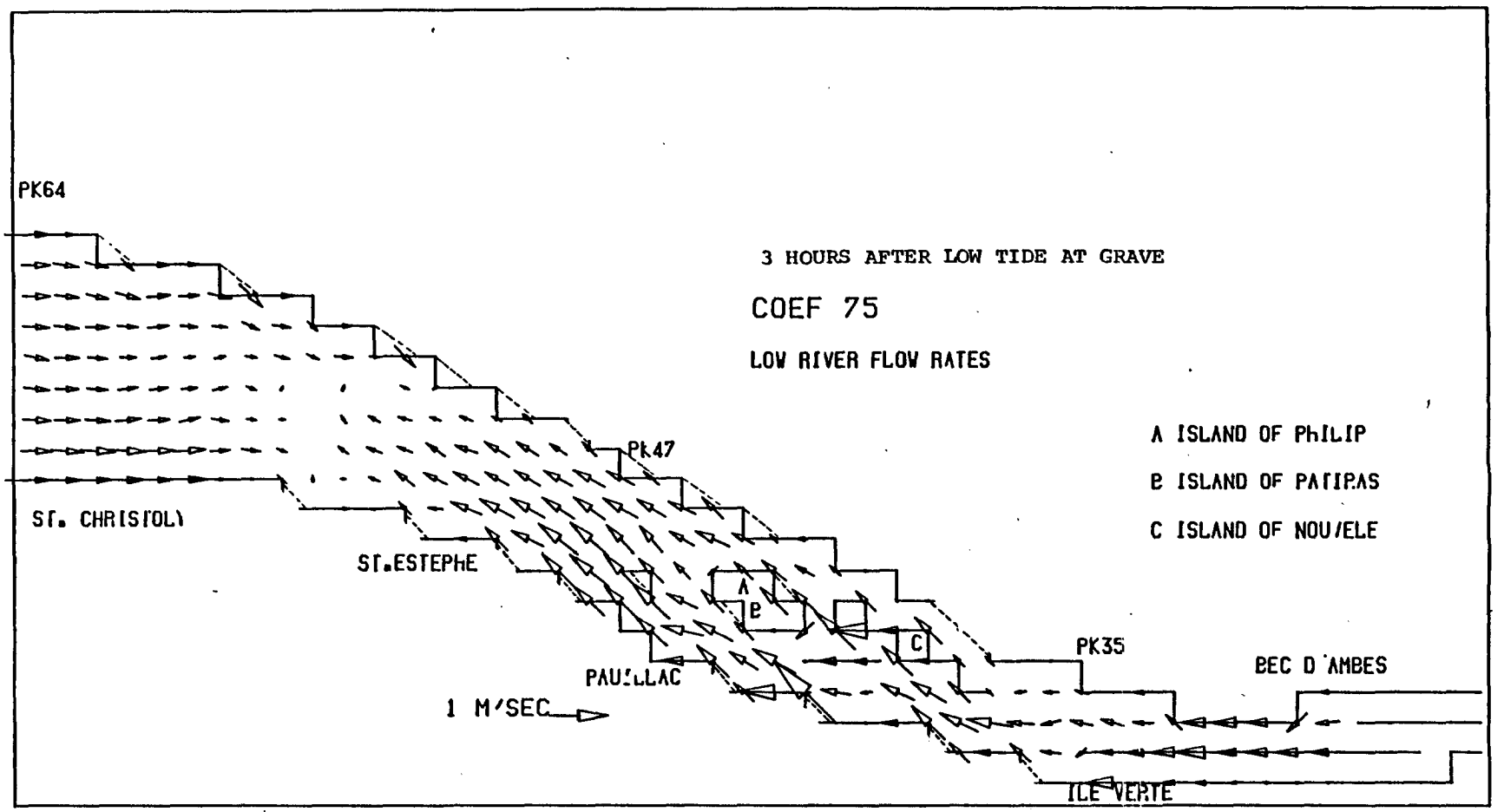
PK64
3 HOURS AFTER LOW TIDE AT GRAVE
COEF 75
LOW RIVER FLOW RATES
A ISLAND OF PHILIP
B ISLAND OF PATIPAS
C ISLAND OF NOUVELE
Pk47
St. CHRISTOLY
St.ESTEPHE
A
B
C
PK35
BEC D'AMBES
PAULLAC
1 M/SEC
ILE VERTE

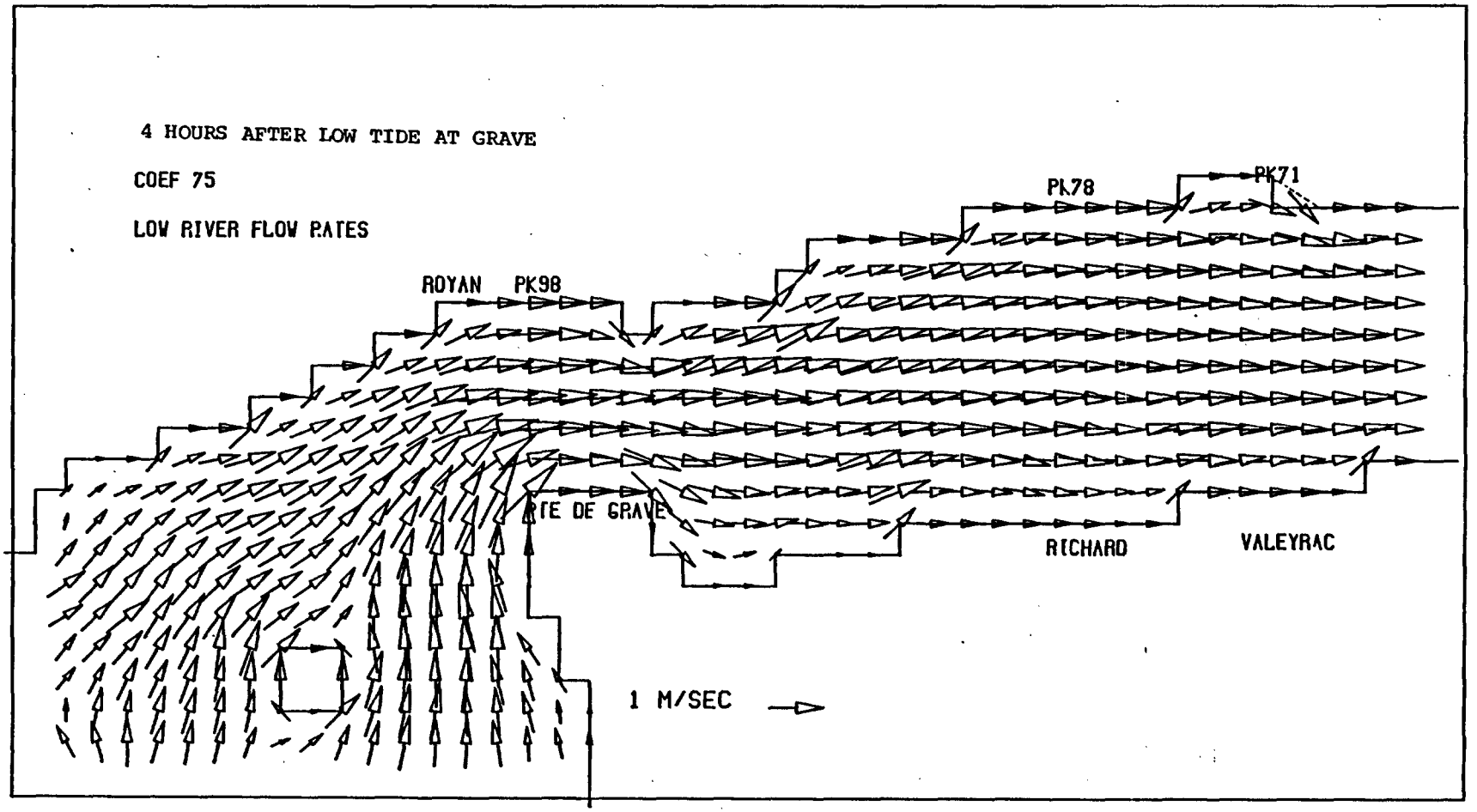
4 HOURS AFTER LOW TIDE AT GRAVE
COEF 75
LOW RIVER FLOW RATES
ROYAN
PK98
PK78
PK71
TE DE GRAVE
RICHARD
VALEYRAC
1 M/SEC

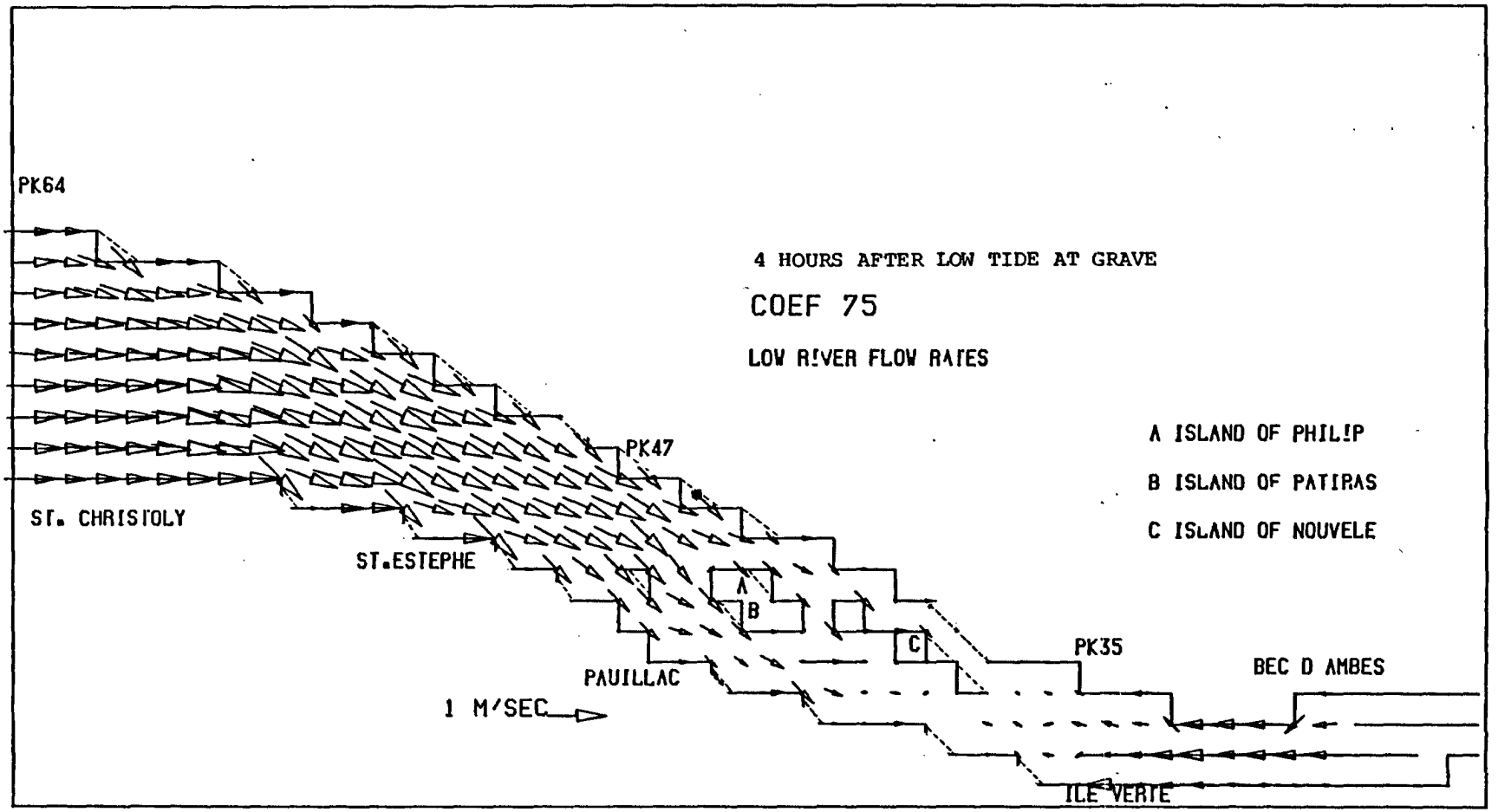
PK64
4 HOURS AFTER LOW TIDE AT GRAVE
COEF 75
LOW RIVER FLOW RATES
A ISLAND OF PHILIP
B ISLAND OF PATIRAS
C ISLAND OF NOUVELE
PK47
ST. CHRISTOLY
ST.ESTEPHE
A
B
C
PK35
BEC D AMBES
PAUILLAC
1 M/SEC
ILE VERTE

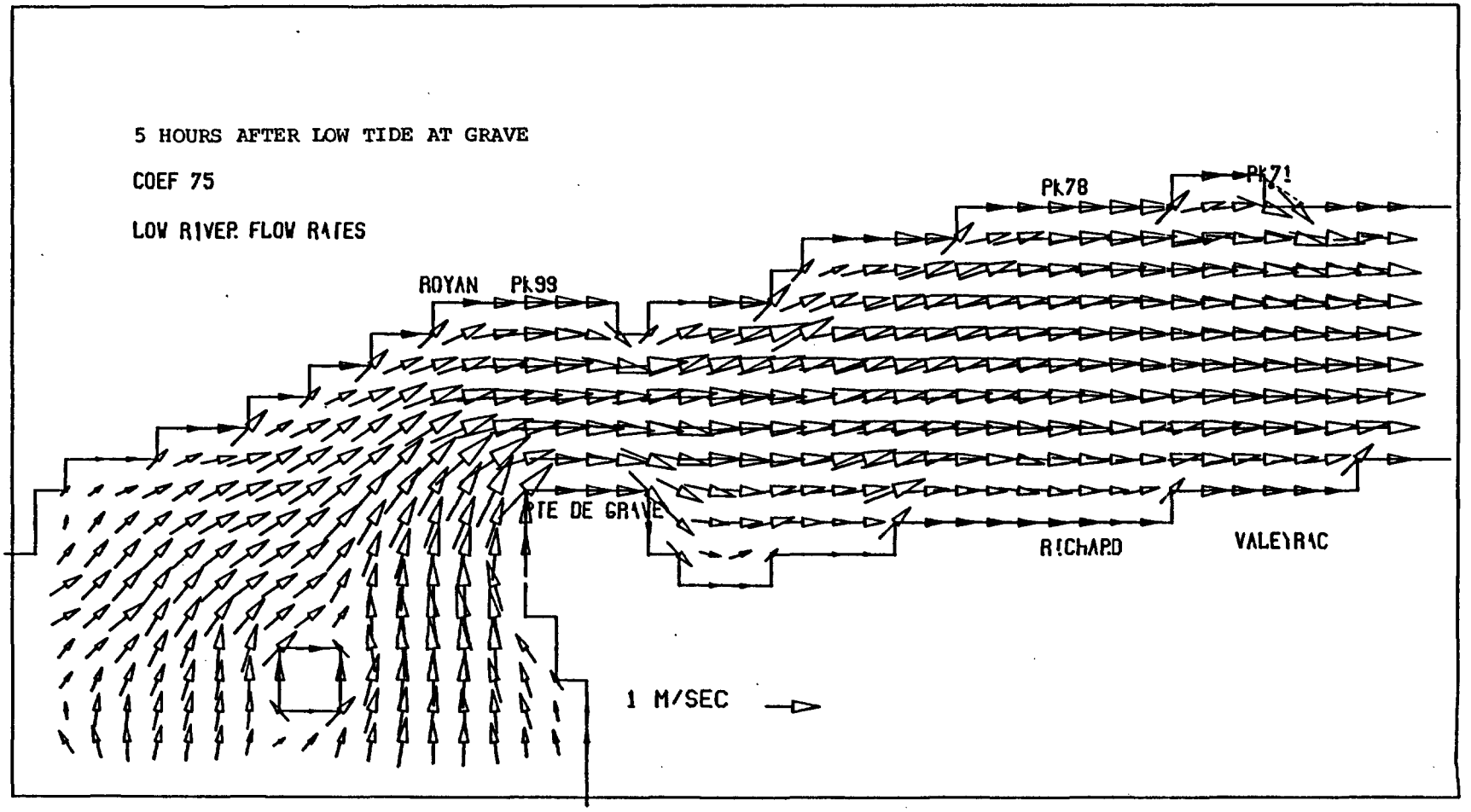
5 HOURS AFTER LOW TIDE AT GRAVE
COEF 75
LOW RIVER FLOW RATES
ROYAN
Pk99
Pk78
Pk71
RICHARD
VALEYRAC
1 M/SEC

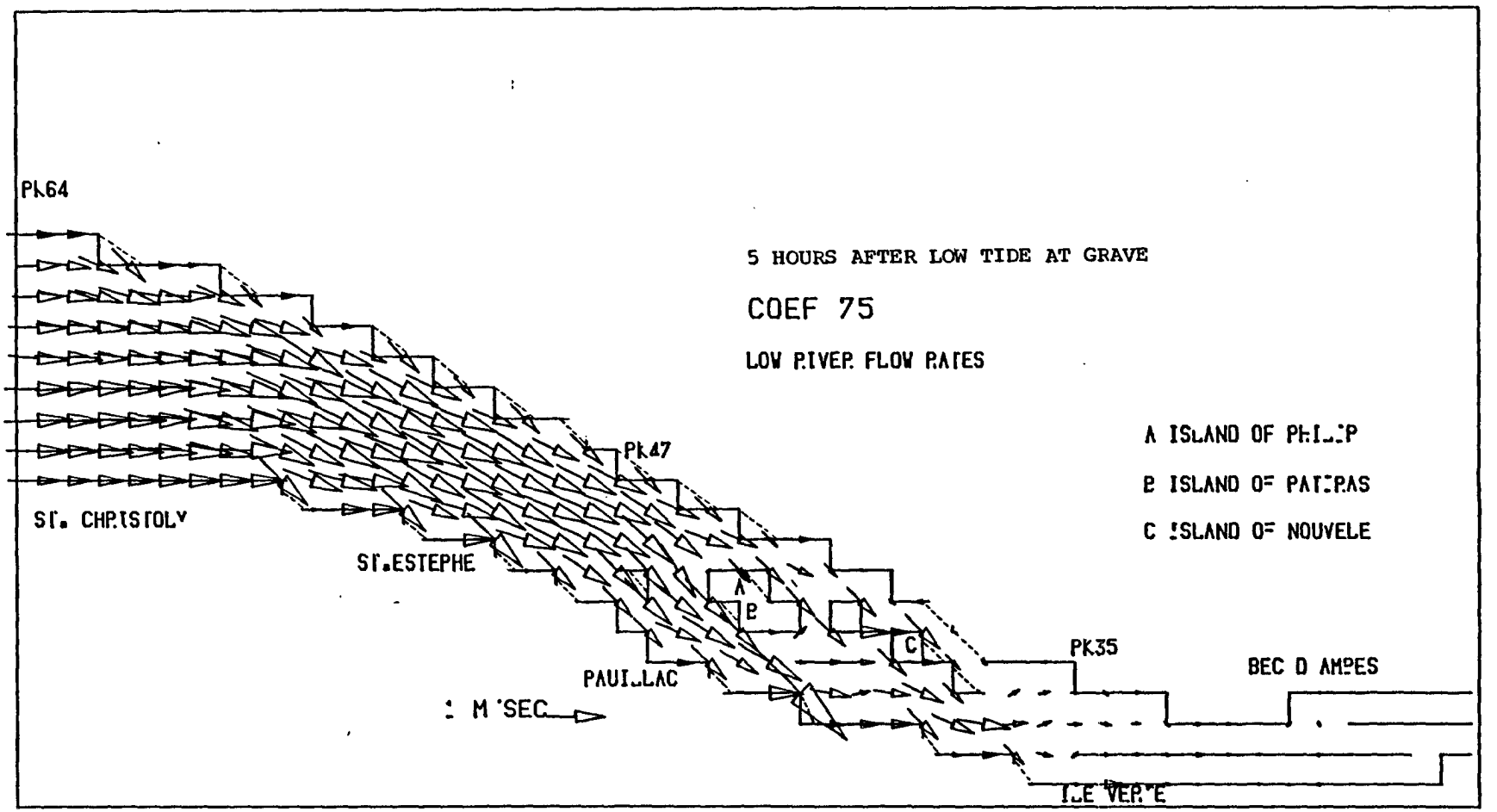
PK64
5 HOURS AFTER LOW TIDE AT GRAVE
COEF 75
LOW RIVER FLOW RATES
A ISLAND OF PHILIP
B ISLAND OF PATIPAS
C ISLAND OF NOUVELE
PK47
ST. CHRISTOLY
ST.ESTEPHE
A
B
C
PK35
BEC D AMPES
PAUILLAC
: M 'SEC
ILE VERTE

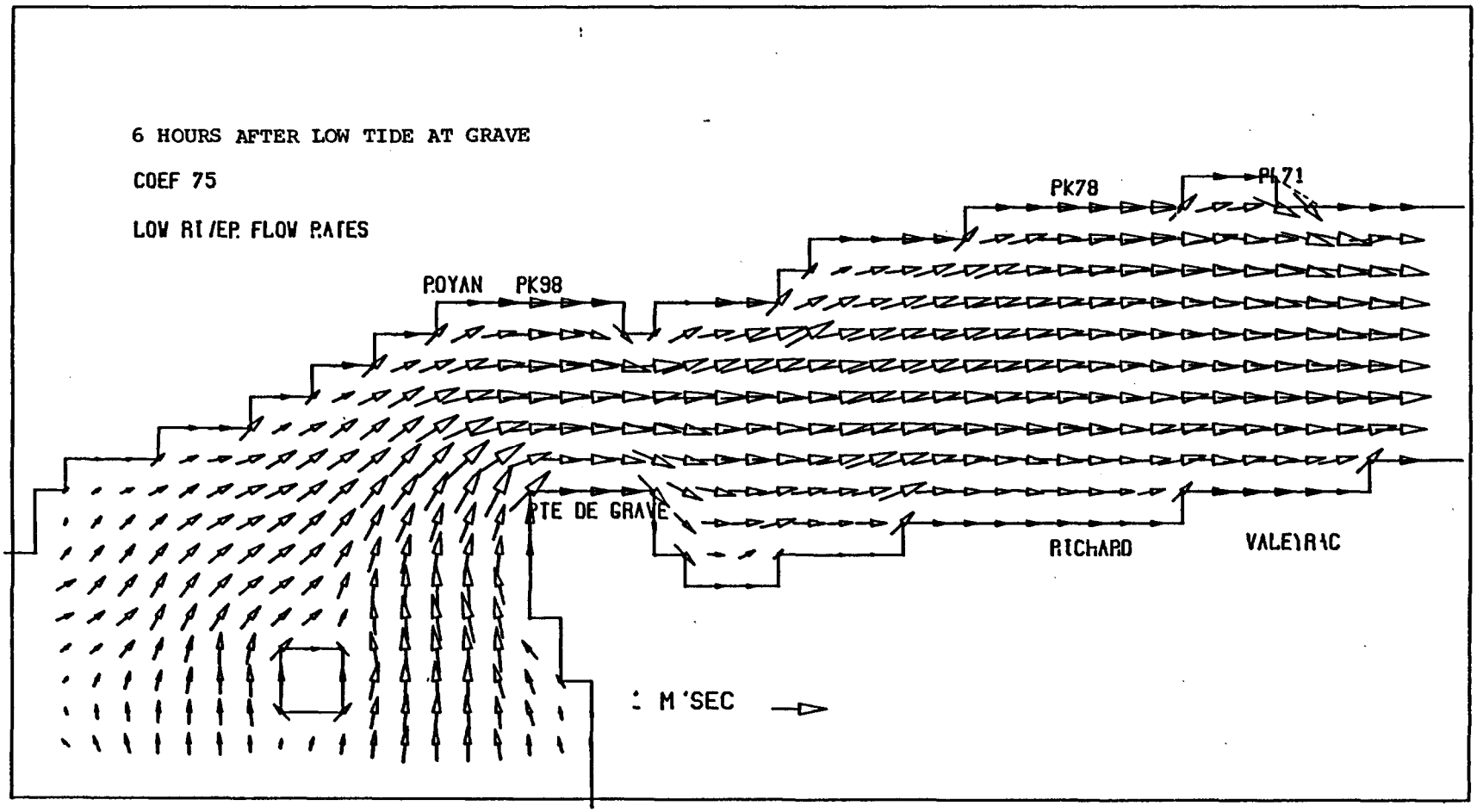
6 HOURS AFTER LOW TIDE AT GRAVE
COEF 75
LOW RIVER FLOW RATES
POYAN
PK98
PK78
PK71
PTE DE GRAVE
RICHARD
VALEYRAC
: M/SEC

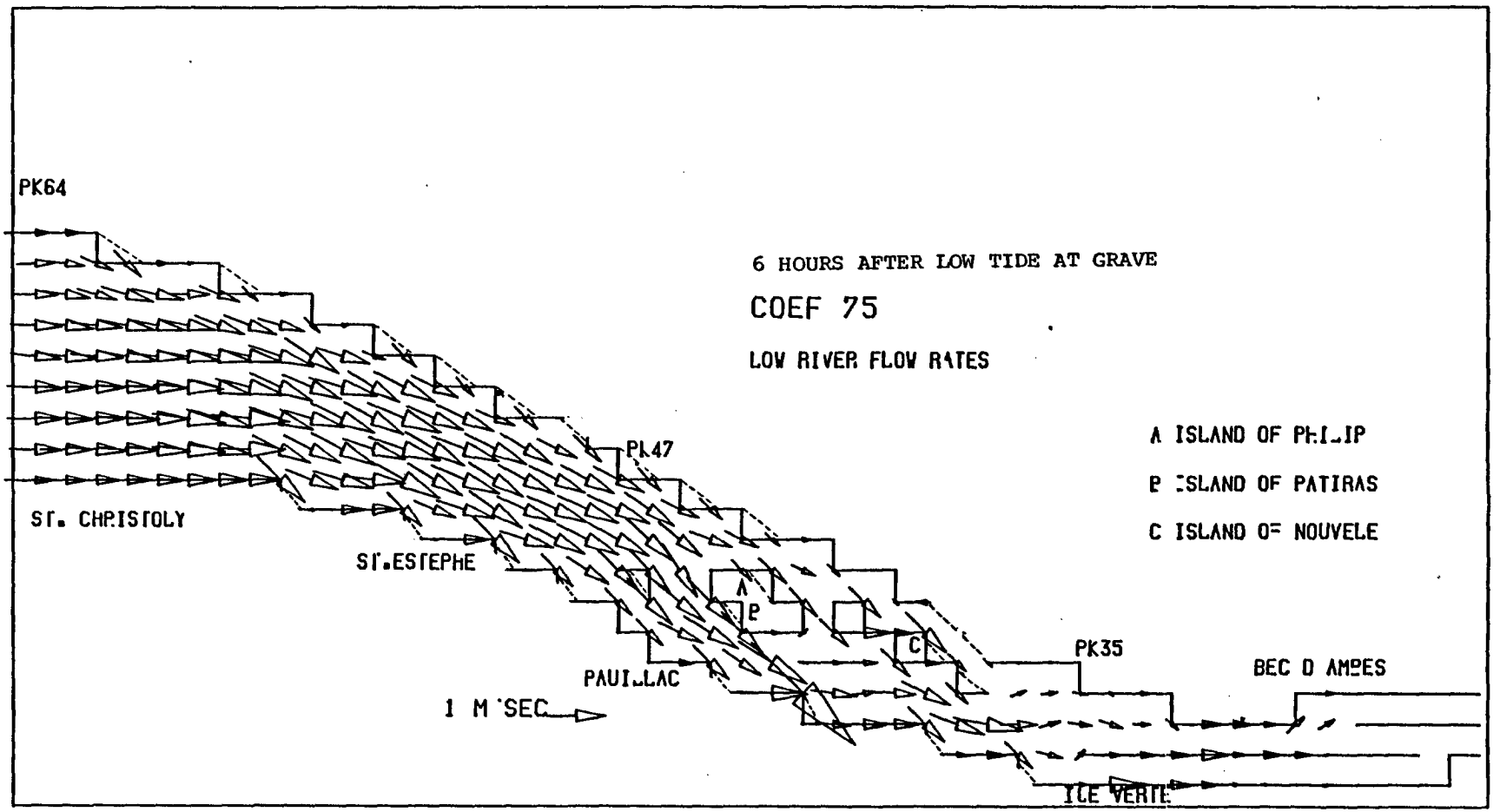
PK64
6 HOURS AFTER LOW TIDE AT GRAVE
COEF 75
LOW RIVER FLOW RATES
A ISLAND OF PHILIP
B ISLAND OF PATIRAS
C ISLAND OF NOUVELE
PK47
ST. CHRISTOLY
ST.ESTEPHE
A
B
C
PK35
BEC D AMBES
PAULLAC
1 M/SEC
ILE VERTE

APPENDIX III

Instantaneous current vector diagrams

(Link node model)

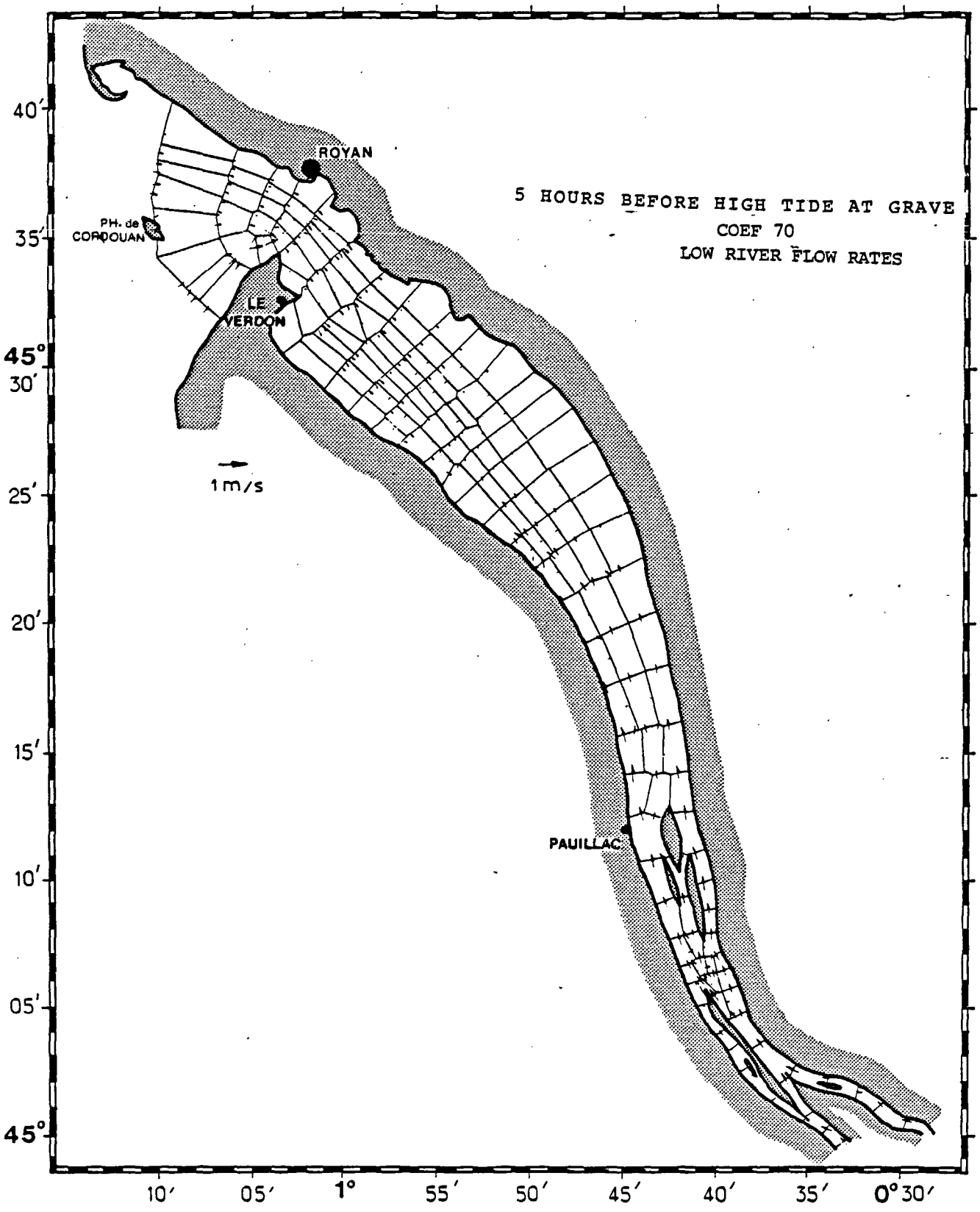
5 HOURS BEFORE HIGH TIDE AT GRAVE
COEF 70
LOW RIVER FLOW RATES
ROYAN
PH. de CORDOUAN
LE VERDON
PAUILLAC
1 m/s
40′
35′
45° 30′
25′
20′
15′
10′
05′
45°
10′
05′
1°
55′
50′
45′
40′
35′
0° 30′

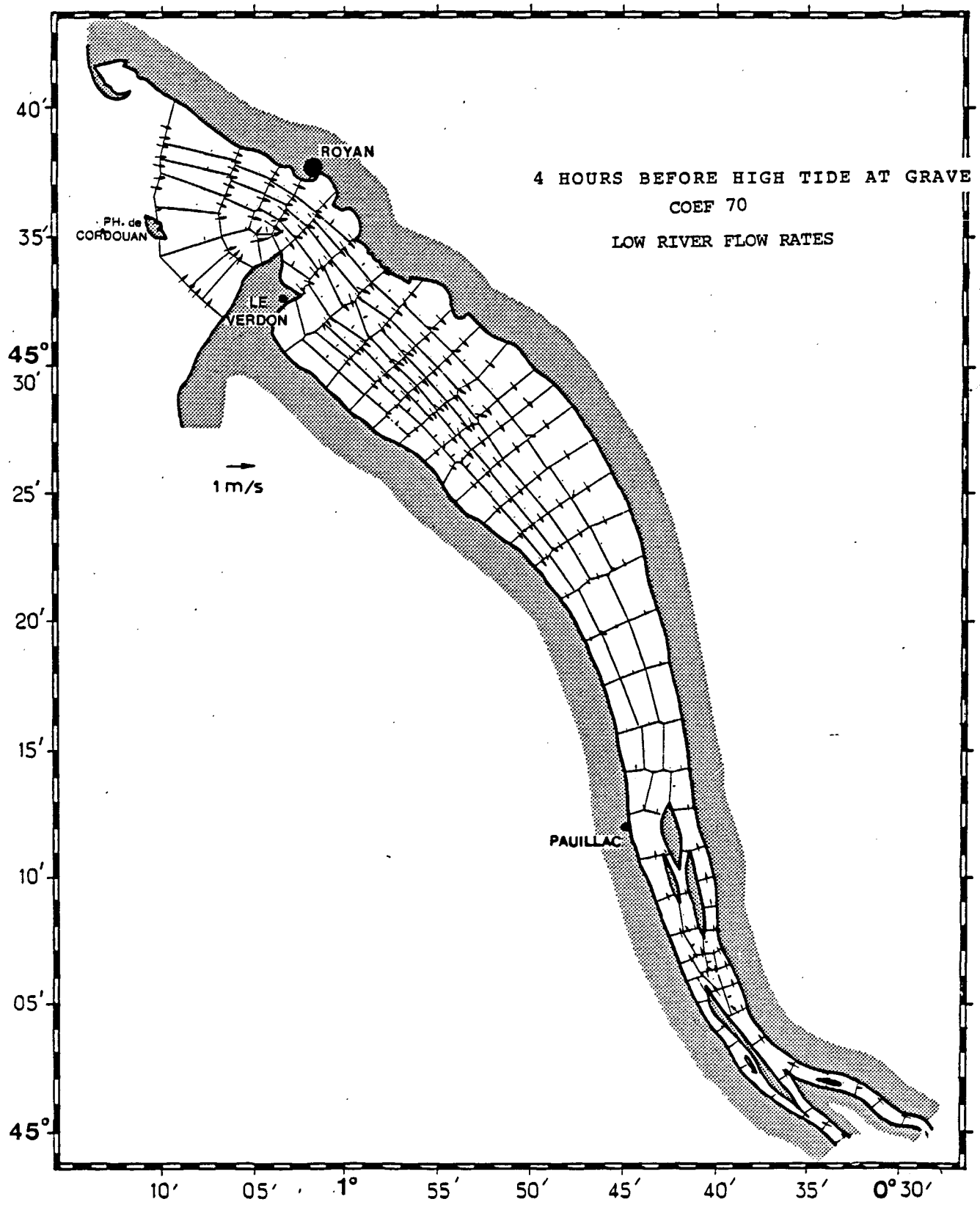
4 HOURS BEFORE HIGH TIDE AT GRAVE
COEF 70
LOW RIVER FLOW RATES
ROYAN
PH. de CORDOUAN
LE VERDON
PAUILLAC
1 m/s
40'
35'
45° 30'
25'
20'
15'
10'
05'
45°
10'
05'
1°
55'
50'
45'
40'
35'
0° 30'

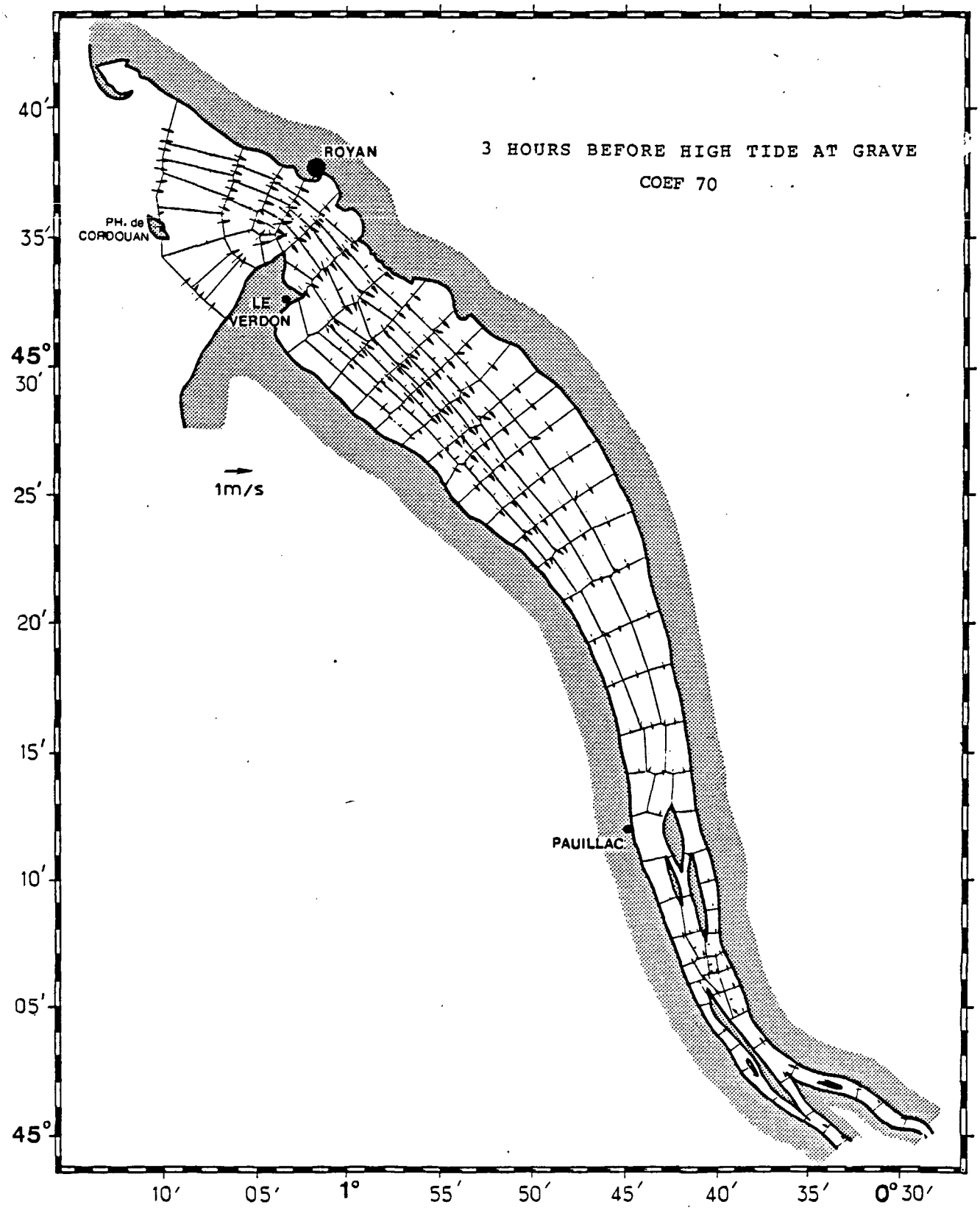
3 HOURS BEFORE HIGH TIDE AT GRAVE
COEF 70
ROYAN
PH. de CORDOUAN
LE VERDON
PAUILLAC
1m/s
40′
35′
45°
30′
25′
20′
15′
10′
05′
45°
10′
05′
1°
55′
50′
45′
40′
35′
0°30′

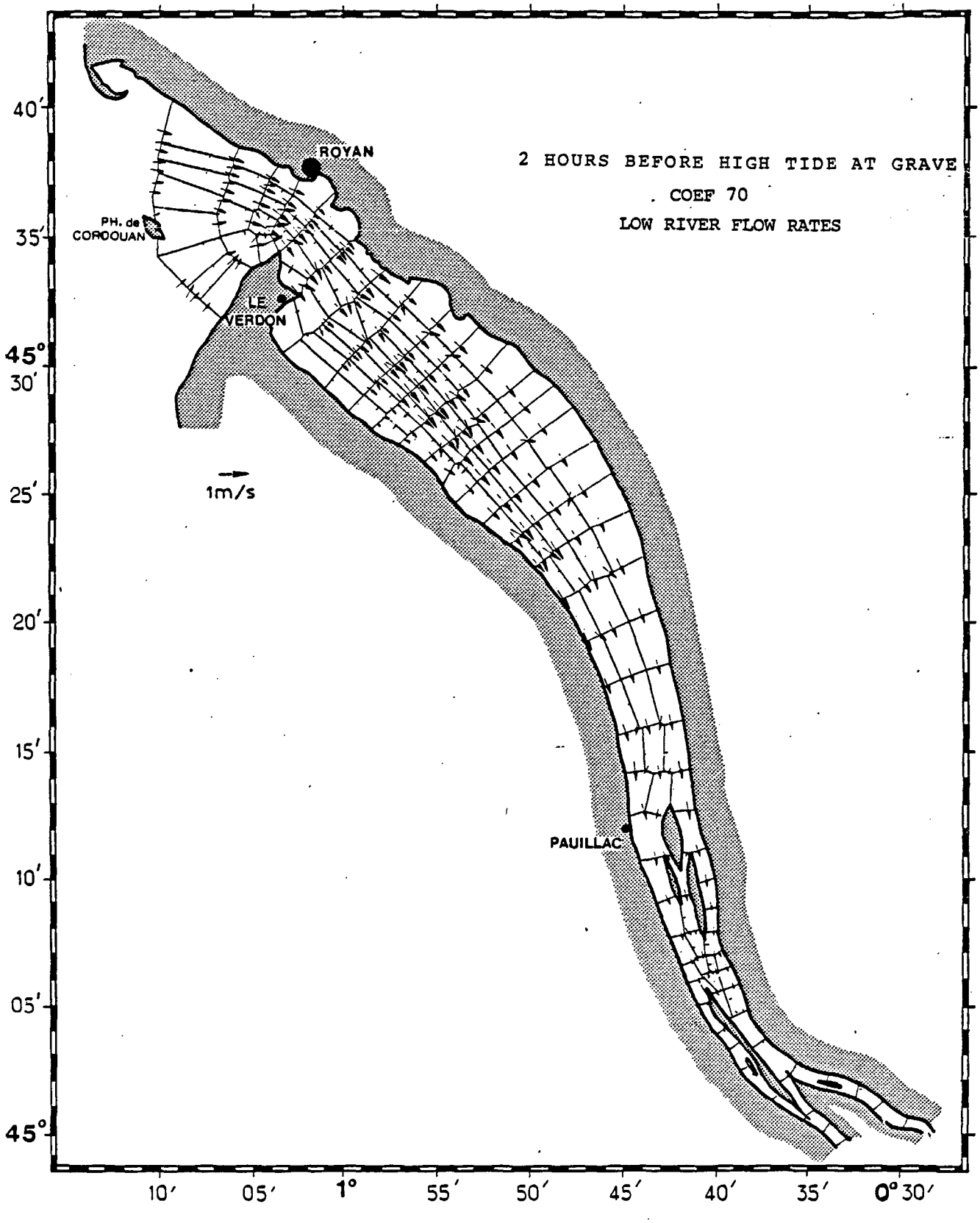
2 HOURS BEFORE HIGH TIDE AT GRAVE
. COEF 70
LOW RIVER FLOW RATES
ROYAN
PH. de CORDOUAN
LE VERDON
PAUILLAC
1m/s
40′
35′
45° 30′
25′
20′
15′
10′
05′
45°
10′
05′
1°
55′
50′
45′
40′
35′
0° 30′

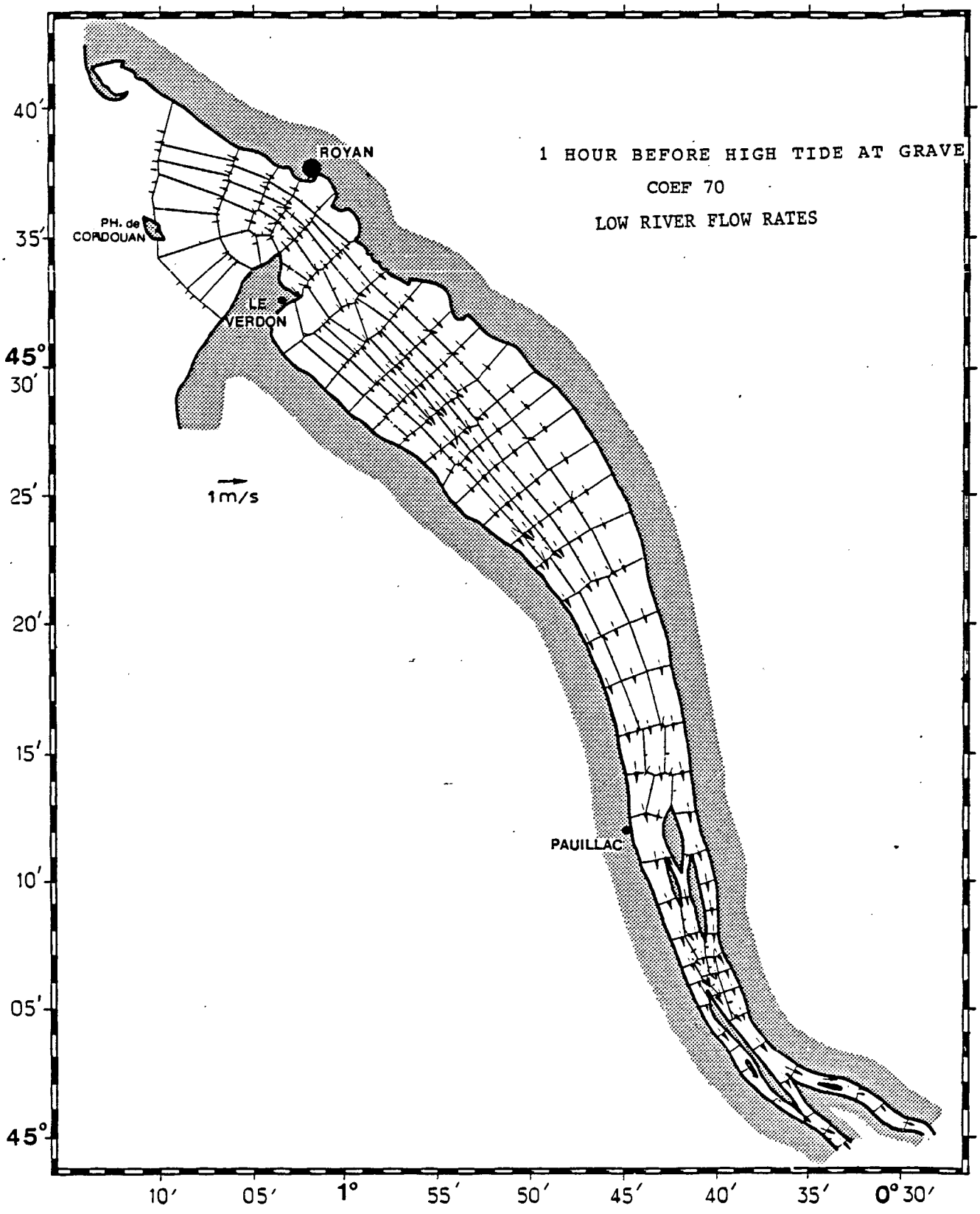
1 HOUR BEFORE HIGH TIDE AT GRAVE
COEF 70
LOW RIVER FLOW RATES
ROYAN
PH. de CORDOUAN
LE VERDON
PAUILLAC
1m/s
40′
35′
45° 30′
25′
20′
15′
10′
05′
45°
10′
05′
1°
55′
50′
45′
40′
35′
0° 30′

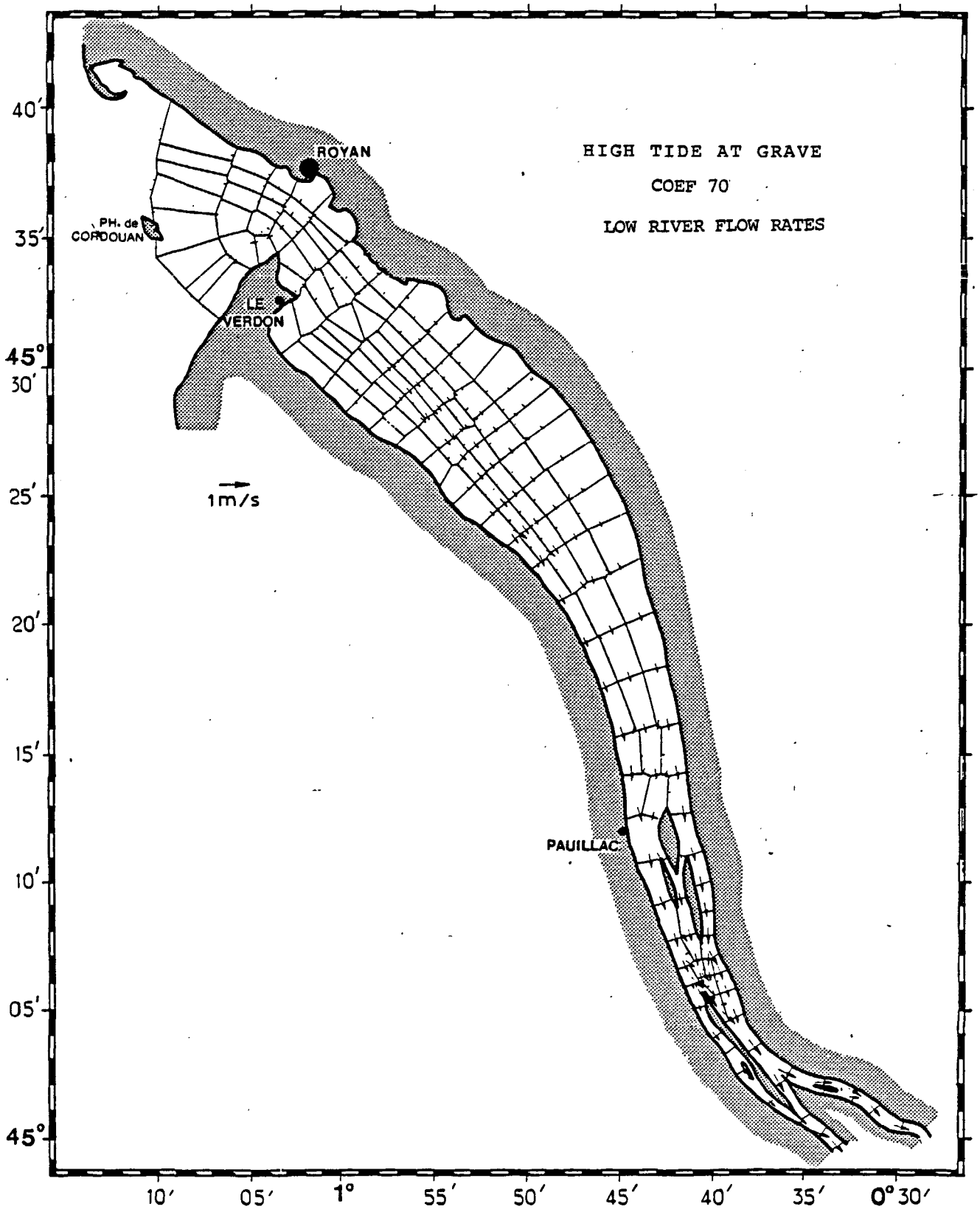
HIGH TIDE AT GRAVE
COEF 70
LOW RIVER FLOW RATES
ROYAN
PH. de CORDOUAN
LE VERDON
PAUILLAC
1m/s
40′
35′
45°
30′
25′
20′
15′
10′
05′
45°
10′
05′
1°
55′
50′
45′
40′
35′
0°30′

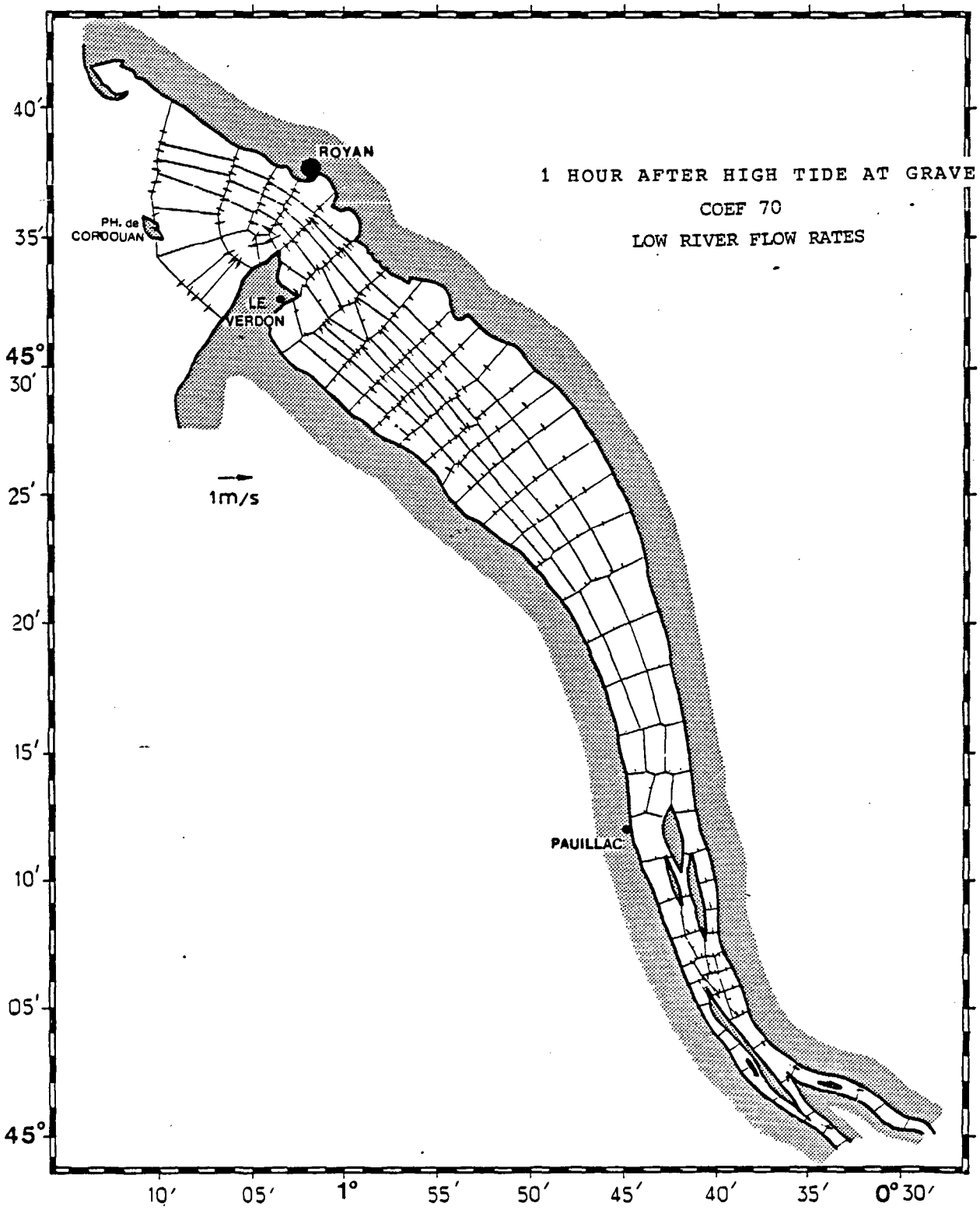
1 HOUR AFTER HIGH TIDE AT GRAVE
COEF 70
LOW RIVER FLOW RATES
ROYAN
PH. de CORDOUAN
LE VERDON
PAUILLAC
1m/s
40′
35′
45° 30′
25′
20′
15′
10′
05′
45°
10′
05′
1°
55′
50′
45′
40′
35′
0° 30′

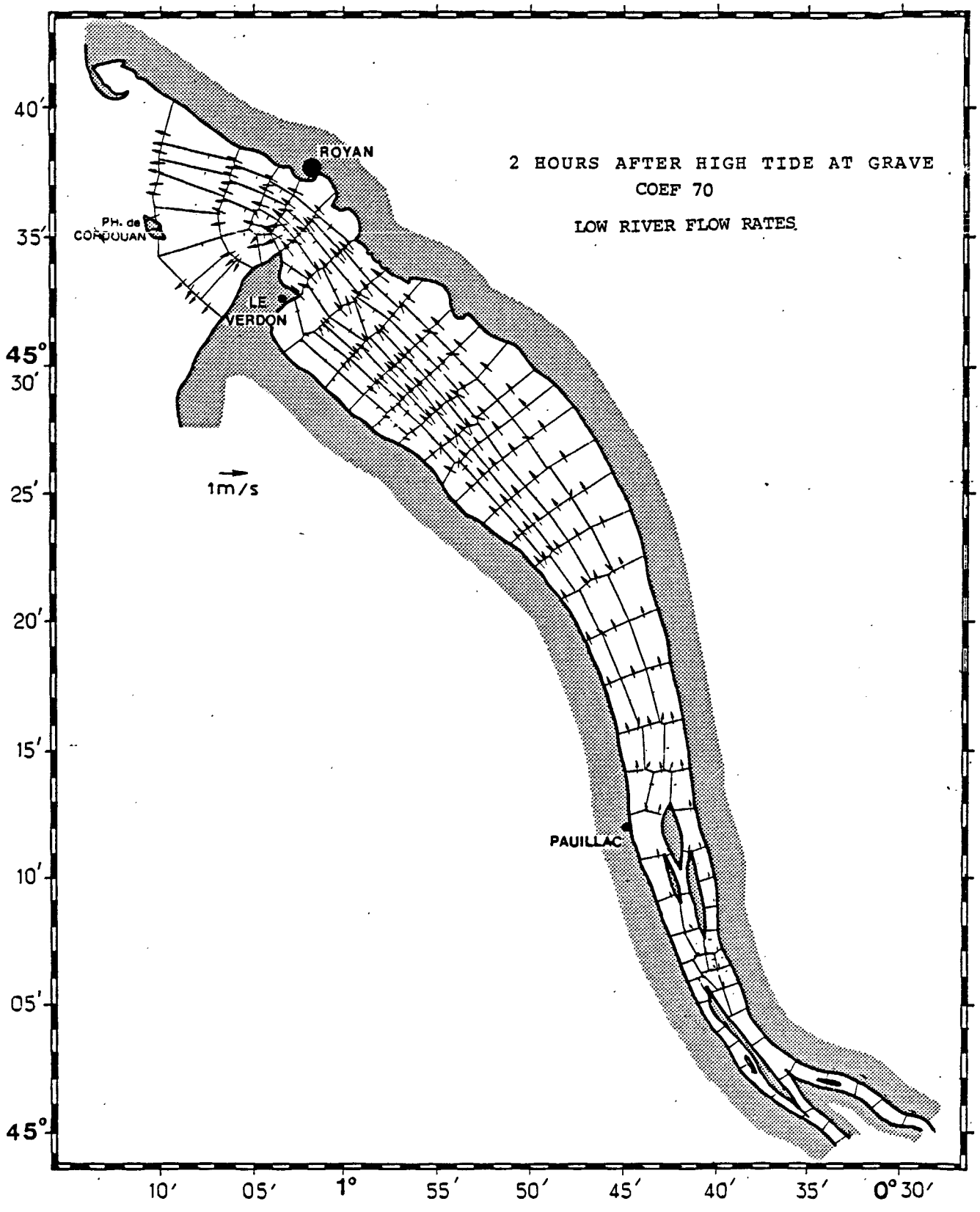
2 HOURS AFTER HIGH TIDE AT GRAVE
COEF 70
LOW RIVER FLOW RATES
ROYAN
PH. de
COR
LE
VERDON
PAUILLAC
1m/s
40′
35′
45°
30′
25′
20′
15′
10′
05′
45°
10′
05′
1°
55′
50′
45′
40′
35′
0°30′

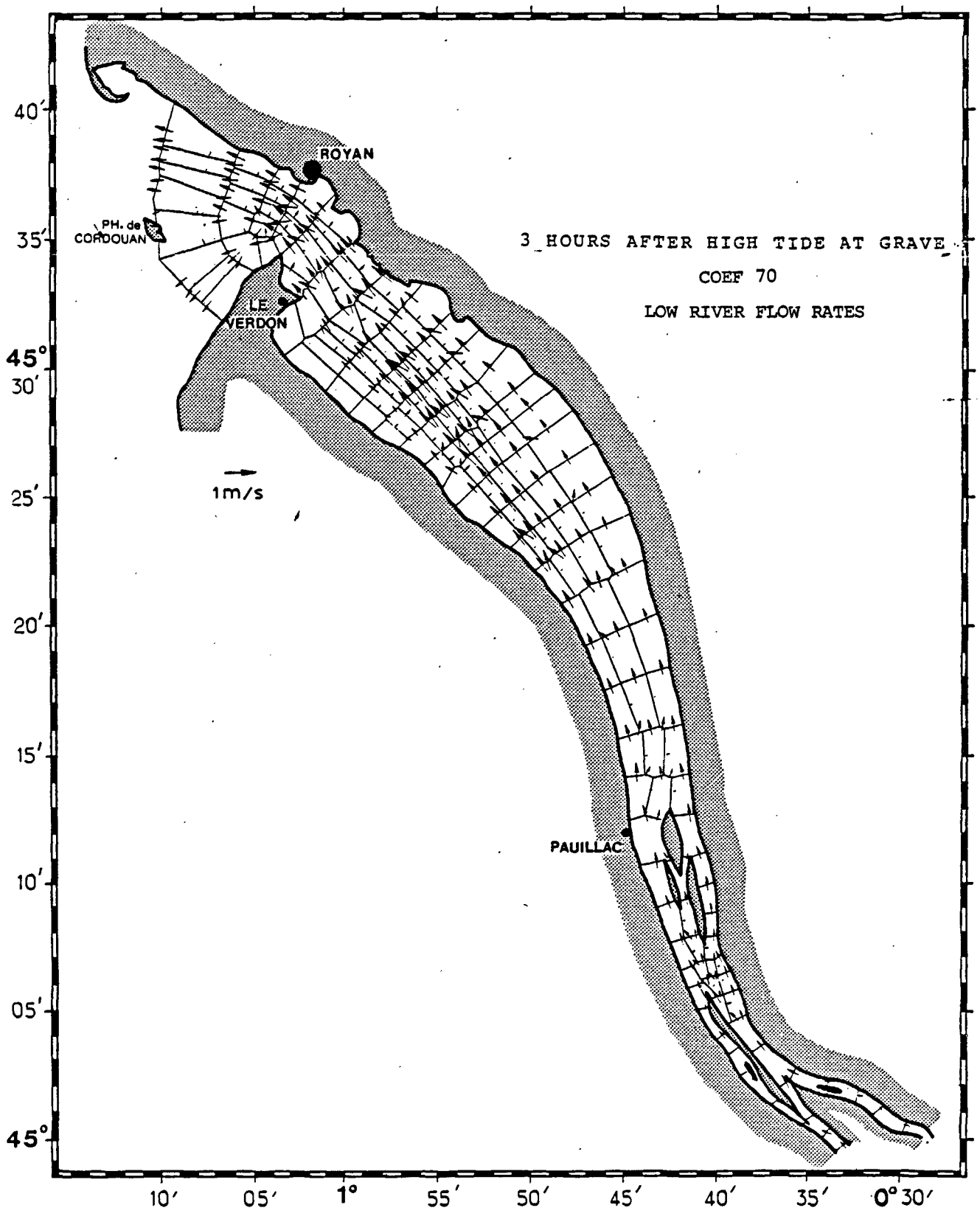
3 HOURS AFTER HIGH TIDE AT GRAVE
COEF 70
LOW RIVER FLOW RATES
ROYAN
PH. de CORDOUAN
LE VERDON
PAUILLAC
1m/s
40'
35'
45° 30'
25'
20'
15'
10'
05'
45°
10'
05'
1°
55'
50'
45'
40'
35'
0° 30'

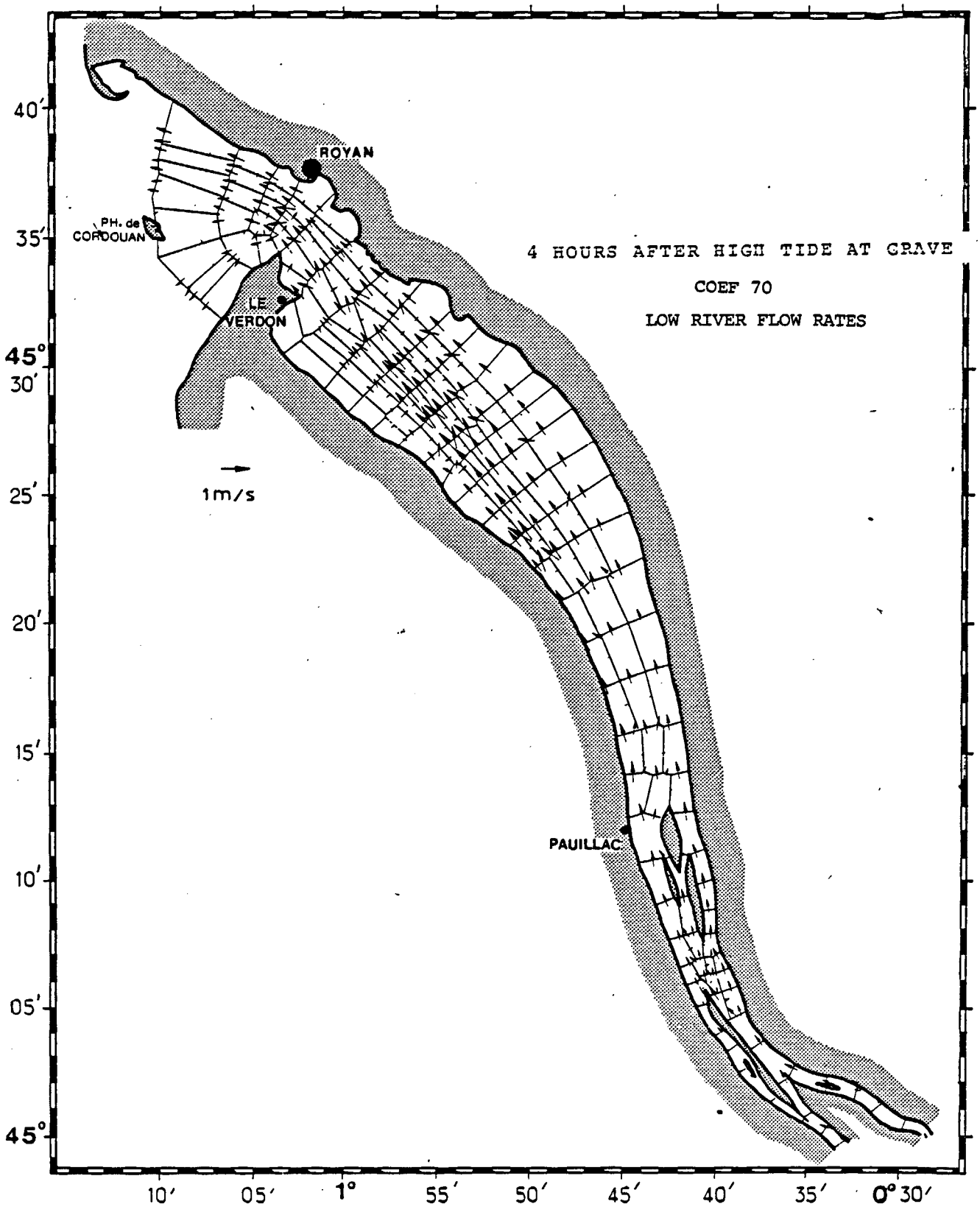
4 HOURS AFTER HIGH TIDE AT GRAVE
COEF 70
LOW RIVER FLOW RATES
ROYAN
PH. de CORDOUAN
LE VERDON
PAUILLAC
1m/s
40'
35'
45° 30'
25'
20'
15'
10'
05'
45°
10'
05'
1°
55'
50'
45'
40'
35'
0° 30'

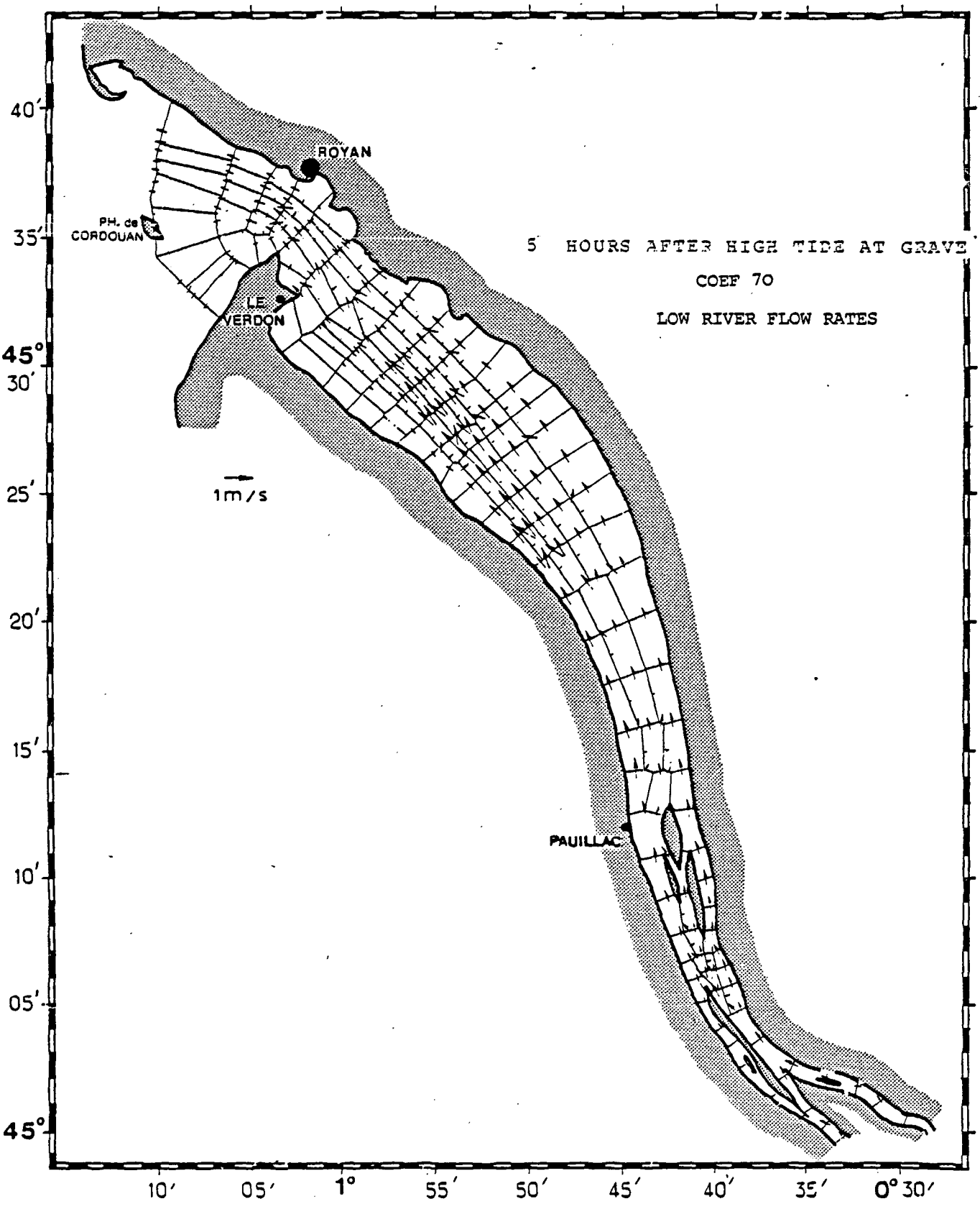
5 HOURS AFTER HIGH TIDE AT GRAVE
COEF 70
LOW RIVER FLOW RATES
ROYAN
PH. de CORDOUAN
LE VERDON
PAUILLAC
1m/s
40'
35'
45° 30'
25'
20'
15'
10'
05'
45°
10'
05'
1°
55'
50'
45'
40'
35'
0° 30'

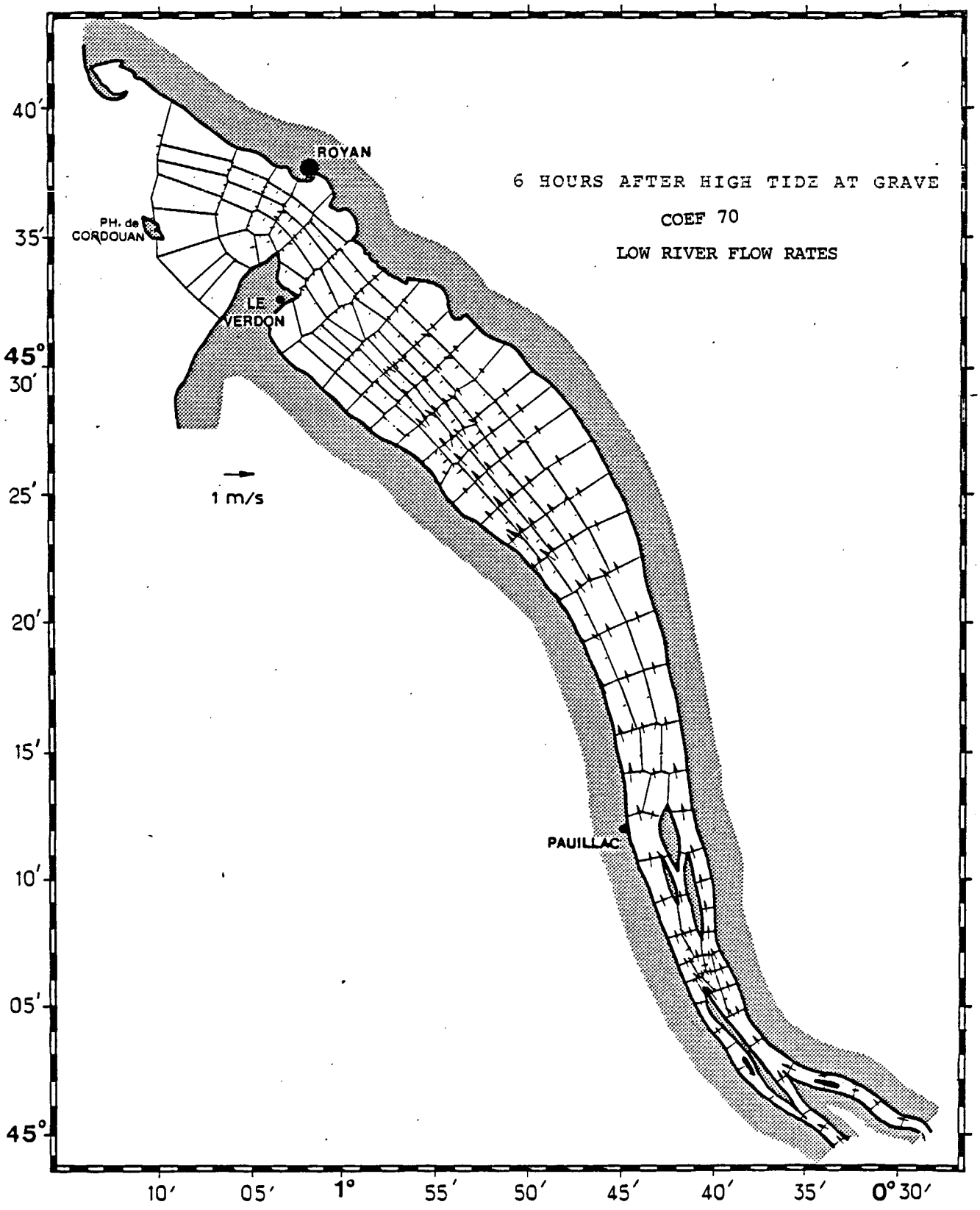
6 HOURS AFTER HIGH TIDE AT GRAVE
COEF 70
LOW RIVER FLOW RATES
ROYAN
PH. de CORDOUAN
LE VERDON
PAUILLAC
1 m/s
40'
35'
45° 30'
25'
20'
15'
10'
05'
45°
10'
05'
1°
55'
50'
45'
40'
35'
0° 30'

CHAPTER IV

RESIDUAL CIRCULATION IN THE GIRONDE

I. INTRODUCTION

This chapter deals with the study of residual circulation in the Gironde during one tidal period. Such a study finds application in sedimentological problems and also to determine the behavior of pollutants. This aspect becomes relevant in view of the proposed outfall location for thermal discharges at PK 52 in the median channel from the nuclear power plant of Braud-et-Saint-Louis. Knowledge of residual currents during a tidal period helps in determining the role of different channels in canalysing the flood and ebb currents.

II. RESIDUAL CIRCULATION STUDIES IN THE GIRONDE

The work of BONNEFILLE (1971) and ALLEN (1972) has provided a good knowledge of residual circulation in the Gironde estuary. Some of their important conclusions may be summarised as follows.

1) Low river discharge rates

Fig 32 shows that the residual currents in the surface are always directed towards the mouth of the estuary. Lateral variations are less visible. The bottom residual currents flow towards the head upto nearly PK 50, with higher intensities found in navigation channel, except at PK 72 and PK 54. At PK 72, the residual currents at the bottom are stronger towards the northern side of the dike of Valeyrac and at PK 54, intensity maximum in the section occurs in the median channel.

2) High river discharge rates

The pattern of residual circulation in the surface is similar to the above mentioned case. The lateral differences in intensities can be noted as follows. At PK 72, high values are found in navigation channel, at PK 78, the transversal differences are less and at PK 89, high intensities occur near the north bank side. In the bottom, the currents in navigation channel are directed towards the head upto PK 55 approximately. Near the north bank side, the informations show a residual bottom flow towards the mouth.

TESSON GILET (1981) computed the residual currents in the estuary based on the current measurements available using the method of planimetry.

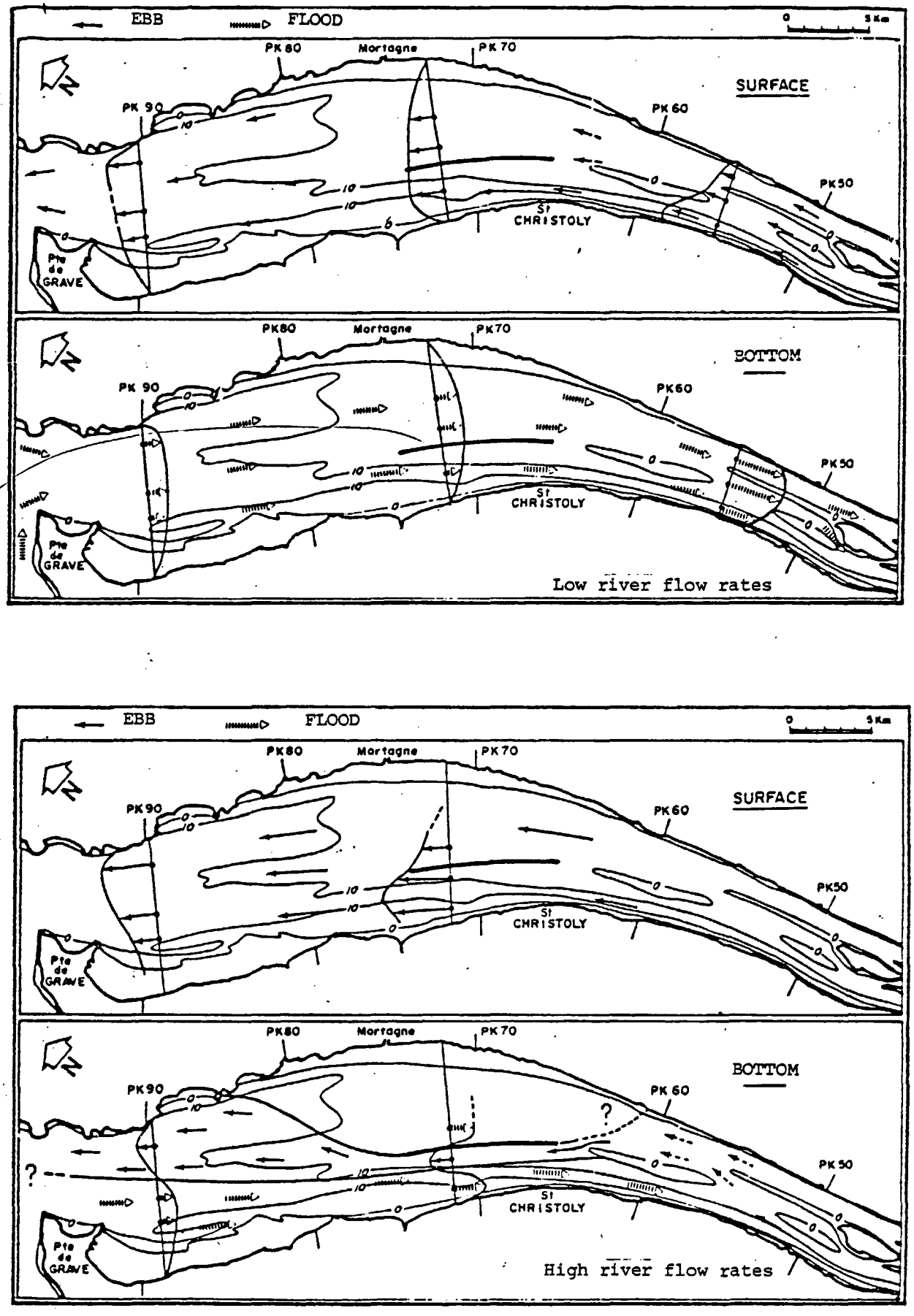

Figure 32 : Observed residual currents at the surface and bottom during average tidal coefficients (After ALLEN, 1972)

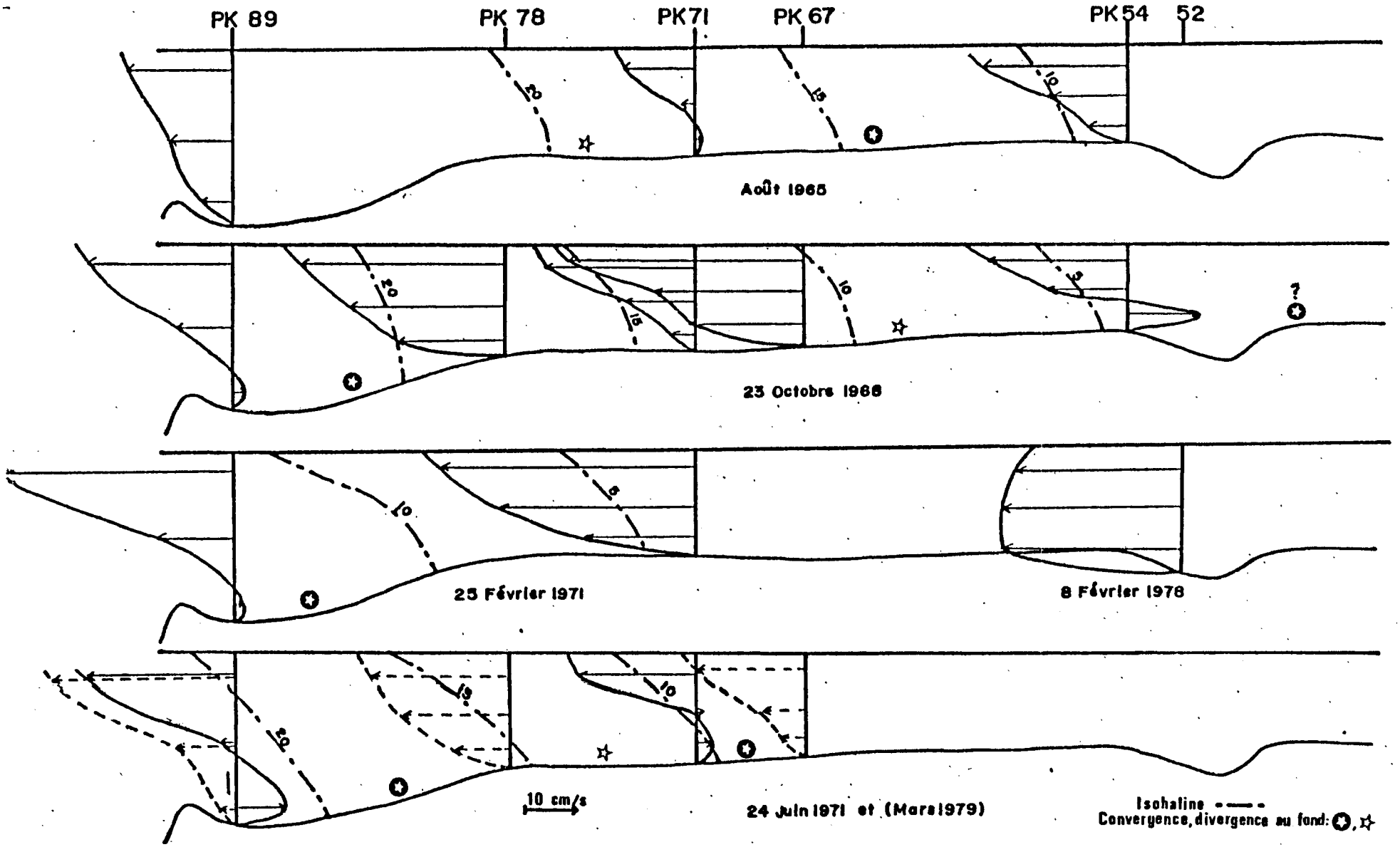

Figure 33 : Residual currents at different depths in the navigation channel (After TESSON GILET, 1981)

The results, show in figure 33, show that the intensities are of the order of 10-50 cm/sec. in the navigation channel, the magnitudes varying with seasons. The position of the nodal point gets displaced depending on river discharge rates. Along the navigation channel of the estuary, the maximum intensities are found at PK 71 and PK 89.

III. DEPTH AVERAGED RESIDUAL PARAMETERS

A few numerical experiments have been conducted with the different models used. These involves the computation of Eulerian residual currents, Eulerian residual transport velocities and the lagrangian residual displacements of a water particle at different points in the domain. The former two parameters are calculated as follows.

$$u_r = \frac{1}{T}\int_0^T u\,dt \quad ; \quad v_r = \frac{1}{T}\int_0^T v\,dt$$

$$u_t = \frac{\int_0^T u(\zeta + h)\,dt}{\int_0^T (\zeta + h)\,dt} \quad ; \quad v_t = \frac{\int_0^T v(\zeta + h)\,dt}{\int_0^T (\zeta + h)\,dt}$$

where, u_r and v_r are the x and y components of depth averaged residual current vector and u_t and v_t are the corresponding components of the depth averaged transport velocity vector.

The lagrangian residual displacements are evaluated from the computed trajectories of water particles, as discussed in the previous Chapter.

It is true that the depth averaged Eulerian residual parameters are only mathematical entities and their physical significance is not much clear. SALOMON (1976) reported that the study of Eulerian residual parameters coupled with the lagrangian residual parameters are complimentary in the study of estuarine dynamics.

1) Stair step boundary model

The principal features observed in the computed field of residual currents can be summarised as follows (refer, fig 34 to 37). Mean river flow rates correspond to a discharge rate of 700 $m^3 sec^{-1}$.

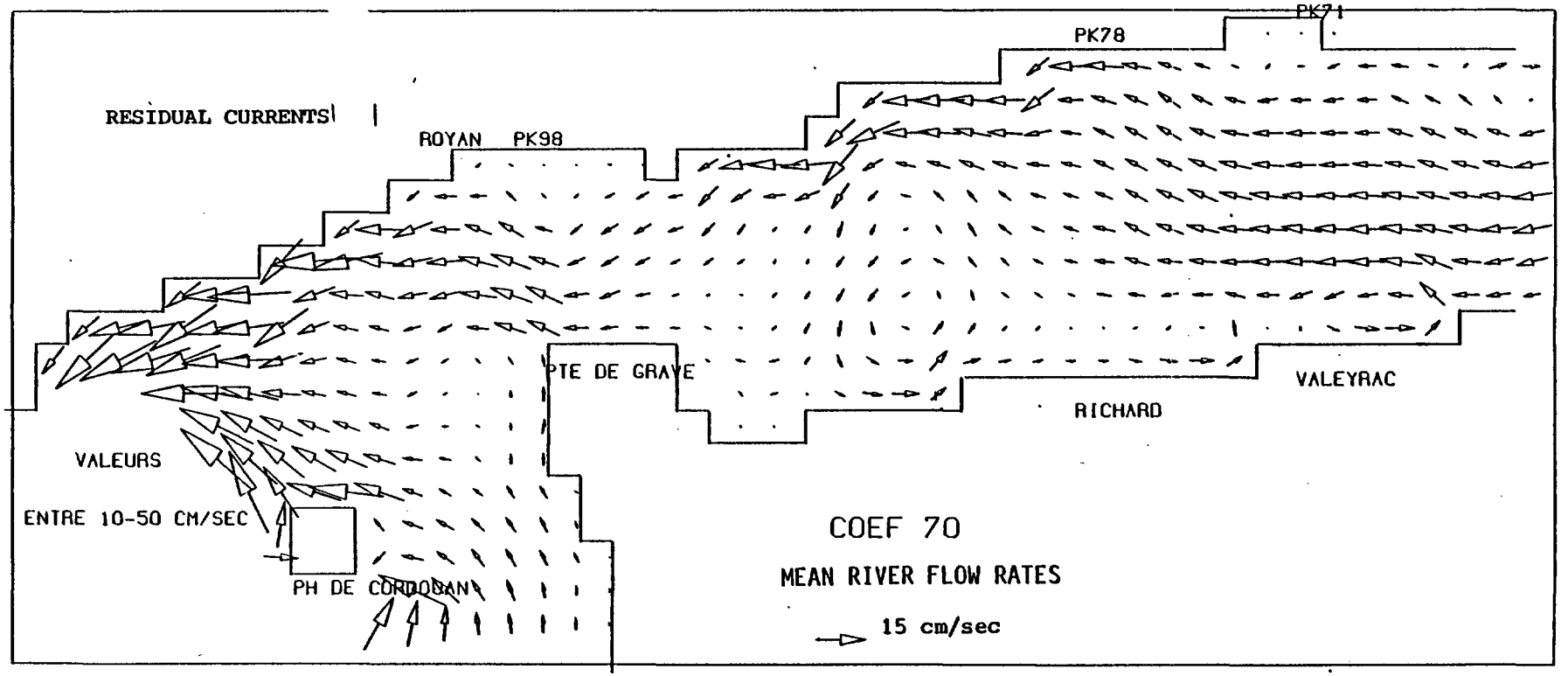

Figure 34 : Depth averaged residual currents (stair step boundary model) during mean river flow rates

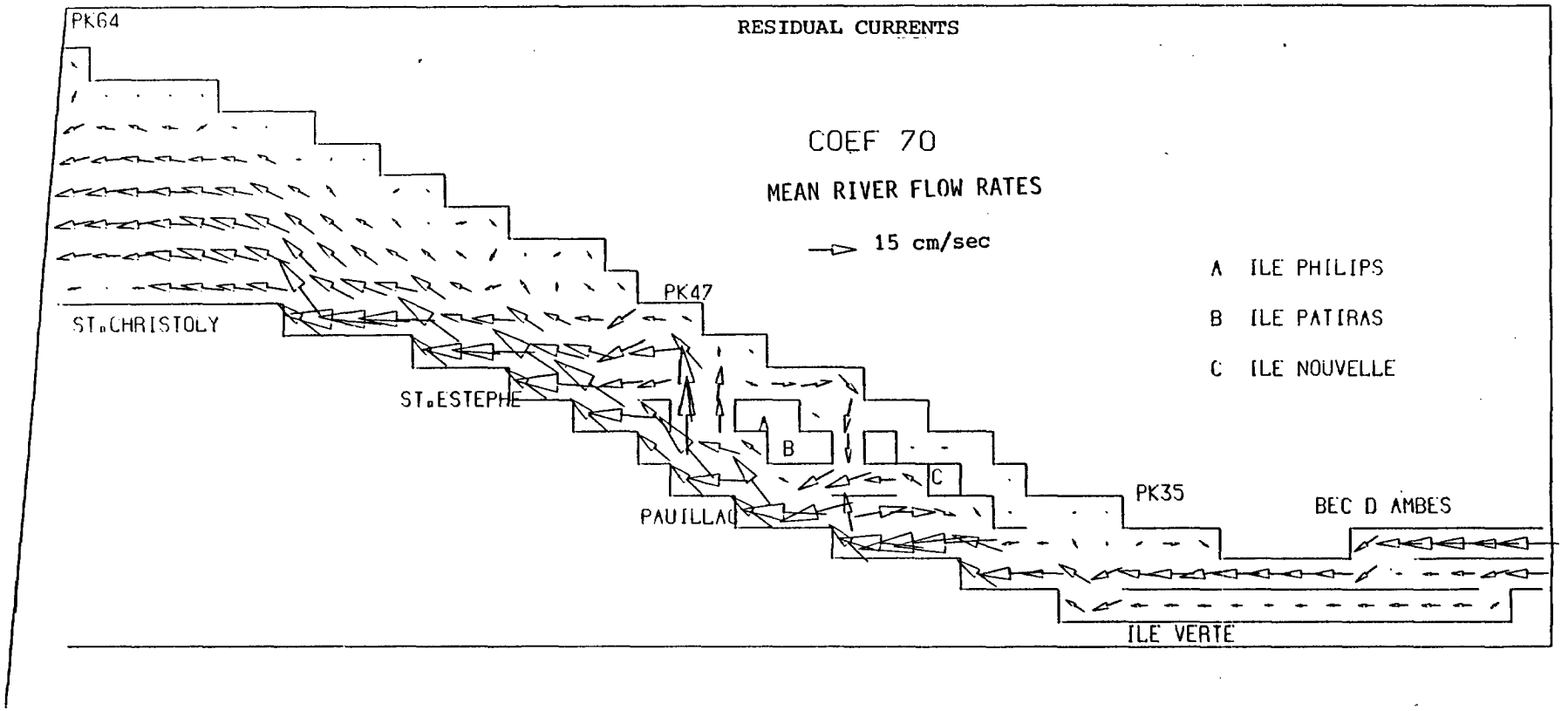

Figure 35 : Depth averaged residual currents (stair step boundary model) during mean river flow rates

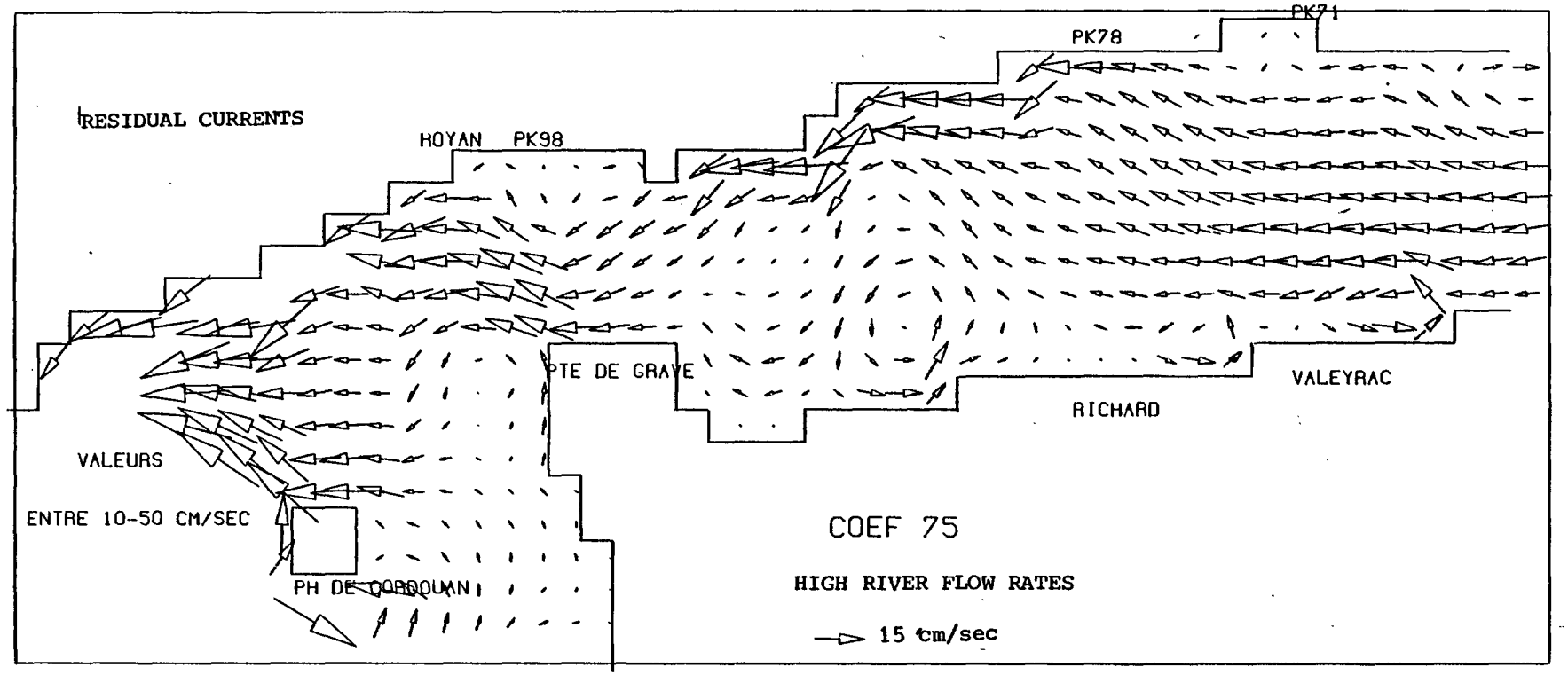

Figure 36 : Depth averaged residual currents (stair step boundary model) during high river flow rates

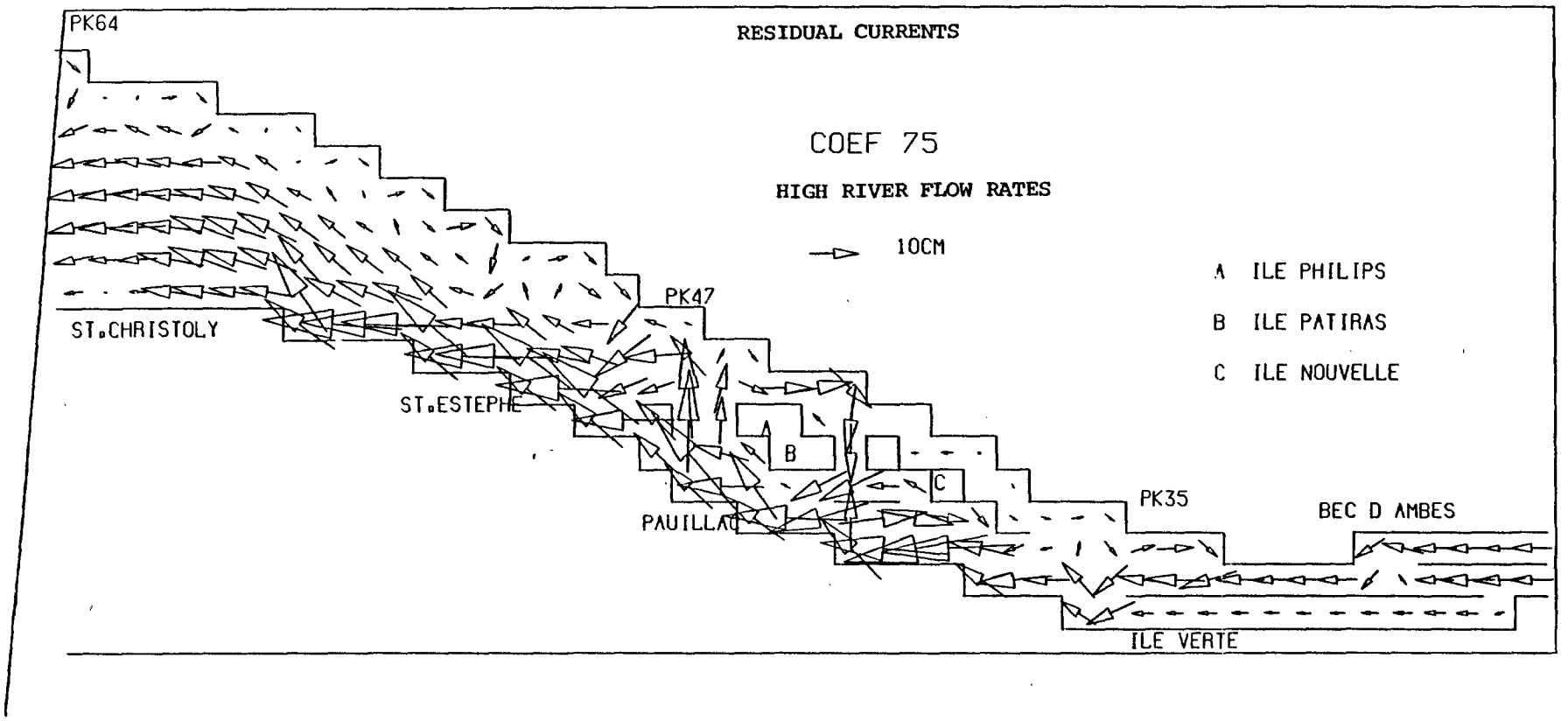

Figure 37 : Depth averaged residual currents (stair step boundary model) during high river flow rates

In the upper estuary, intense residual currents occur in the navigation channel. Between PK 35 to PK 41, residual currents are practically absent in Blaye channel. Around the islands of Philippe and Patiras a residual eddy is present. The eddy is in the clockwise direction. It can be seen in the instantaneous current vector diagrams that (Appendix I), at Pauillac, ebb currents are strong in between the islands of Trompeloup and Philippe, where as flood is more predominant near the north bank side. Hence these differences found during ebb and flood can produce a residual circulation around the islands. Downstream, between Pauillac and St. Estèphe, the residual currents are intense in navigation channel. In the corresponding region, the currents are very feeble at the right bank side. These values are considerably less than the observed values (fig 32) at PK 54. It means that the residual flow is concentrated along the principal channel in this region. Downstream, from PK 60 upto St. Christoly, lateral differences in the residual current field are less marked.

In the lower estuary, between St. Christoly and Richard, the residual currents flow parallel to the coast, with high values observed in the navigation channel. Downstream from Richard, a transition occurs from the navigation channel to the Saintonge channel with residual currents tending to flow from the former to the latter. Also, residual currents become intense along the north bank side. Near PK 85, a residual eddy is present. The residual eddy is situated just downstream of sudden change of residual circulation from the navigation channel towards the northern channel. In this region, the presence of bank of Vivian along the south bank side and the deep Saintonge channel along the north bank side make sharp gradients of depth in lateral sections. This depth gradient is mainly responsible for the formation of the residual eddy.

From PK 87 onwards, the residual flow is downward and the currents get evacuated to the sea along the south bank side at the Pointe de Grave. Outside the mouth of the estuary, the residual currents are strong in the passage of navigation near the northern side. The residual circulation outside the mouth of the estuary is sensible to the seaward boundary conditions and this aspect is not discussed here.

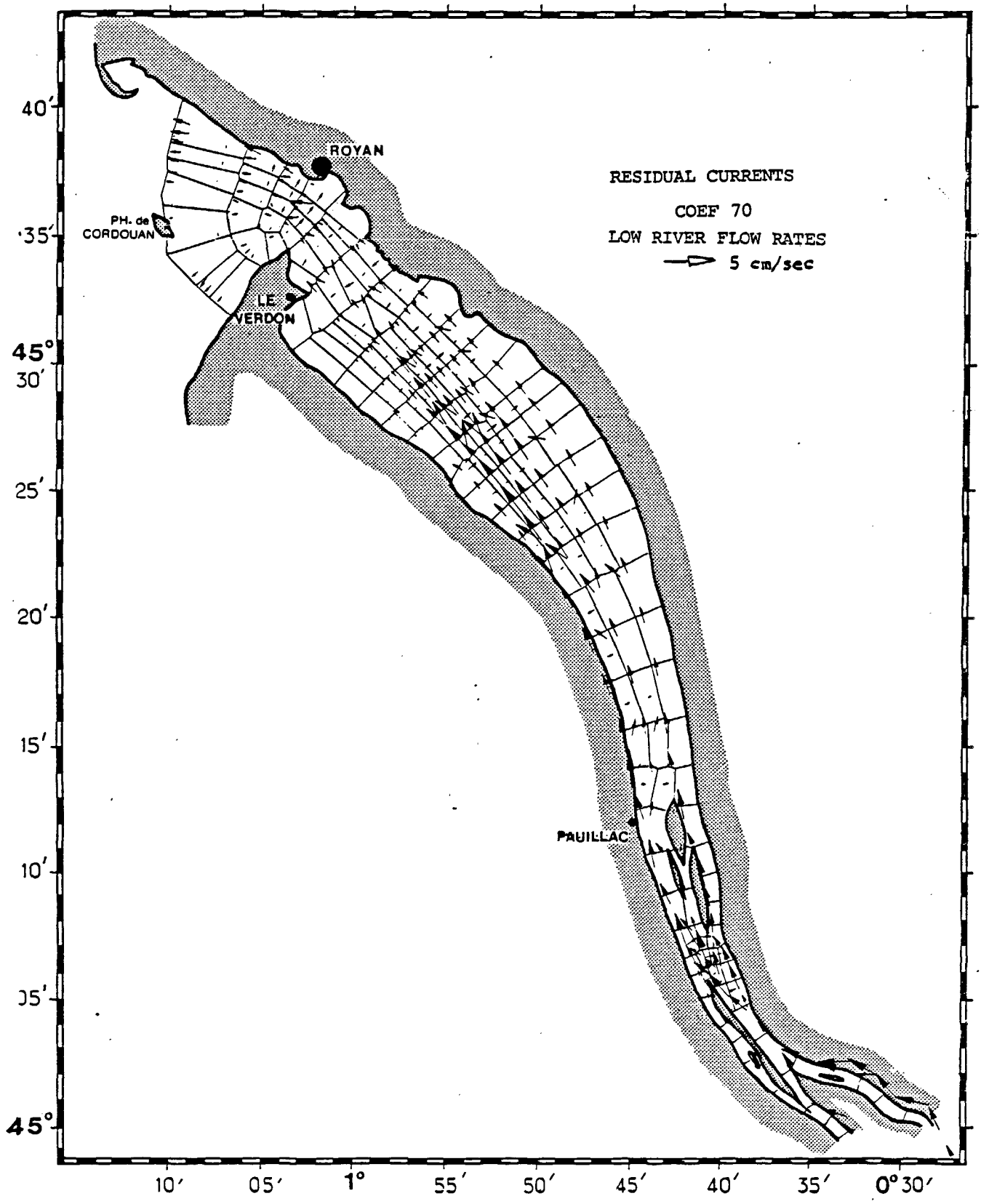

Figure 38 : Depth averaged residual currents (link node model) during low river flow rates

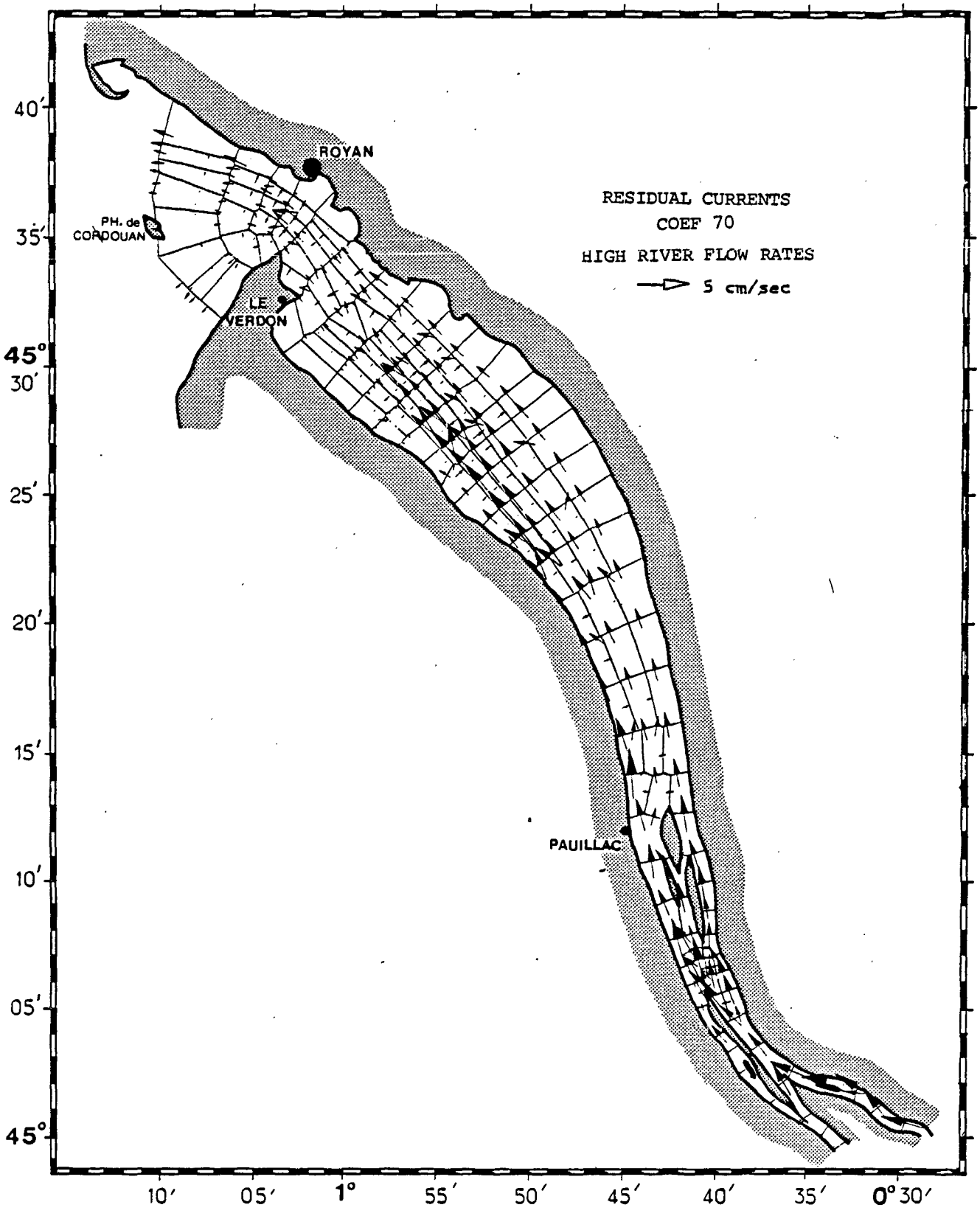

Figure 39 : Depth averaged residual currents (link node model) during high river flow rates

Fig 36 to 37 represent the residual currents computed for high river discharge rates (1300 m^3/s). The phenomena observed are quite similar to the case of low river flow rates. In this case, the magnitudes of residual currents are higher and the residual eddies are more pronounced than in the previous case. The high intensities are particularly marked in the regions which canalyse ebb, namely the navigation channel in the upper estuary and the Saintonge channel between PK 80 - 92. When the discharges are high, between PK 75 - 80, the residual currents at the south bank side are directed towards the mouth. In the case of low river discharges feeble residual currents directed towards the head are found at the south bank side of this region.

2) Link node model

Eulerian residual currents are computed as in the case of stair step boundary model. Here, the integration over a tidal period is made of one dimensional current vectors. The computations involve both the cases of low river discharges (183 $m3/s$) and high river discharges (1300 m^3/s). The results are presented in figures 38 to 39.

In the upper estuary, residual currents are found to be maximum in the navigation channel. Between PK 35 to PK 41, the magnitudes of residual currents in the Blaye channel and in the navigation channel are found to be the almost same, which is different from the results of the stair step boundary model. Between the islands of Philippe and Bouchaud, there is a small residual current flowing towards the head. In the same region, a clockwise residual eddy is observed in the case of stair step boundary model. These two results are comparable. At PK 52, residual currents are maximum in the navigation channel and feeble values are observed in median channel.

Between PK 55 to PK 60, the transversal variations in residual currents are not much marked. This is true in the case of stair step boundary model also for this region. Downstream, high intensities in residual currents are found in navigation channel. From Richard onwards upto nearly PK 85, small residual currents tend to flow towards the northern channel and at PK 90, maximum residual current is observed in the northern channel. Between Richard and Verdon, residual currents are extremely feeble at the south bank side.

This is a region of low depths due to the presence of sand banks. At Verdon, lateral differences are absent. At Grave, the intensity of residual currents occurs at the south bank side.

In general, the results obtained above are in agreement with the stair step boundary model results. An exception is observed in the Blaye channel in the upper estuary.

3) Lagrangian residual parameter

The residual displacements of a water particle during a tidal period are computed by the same method as that of trajectories of water particles, as described in page 50. The calculations are done using stair step boundary model.

The results are presented (figures 40 to 41) for low river flow rates(183 m^3/sec). Moreover, a few results can be seen in the diagrams of trajectories (figures 25 to 27) in Chapter III. It is to be noted that the lagrangian residual displacements depend on the instant of departure of a water particle. In figures 40 to 41, the instant of start is approximately middle of flood tide at Grave.

Fig. 40 shows that in general, the residual displacements are towards the mouth in the lower estuary. Between Richard and St.Christoly, the maximum displacements of water particles occur in the navigation channel. In the same region, the residual displacements are small along the south bank side and practically absent along the north bank side. From PK 80 onwards upto Grave, high displacements are found in the Saintonge channel. These are similar results to those obtained in the case of Eulerian residual parametres.

In the upper estuary, the pattern is more complicated. For a given instant of departure as in figure 41, the following aspects can be concluded. High residual displacements directed towards the mouth of the estuary are present in the navigation channel. Along the north bank side, the residual

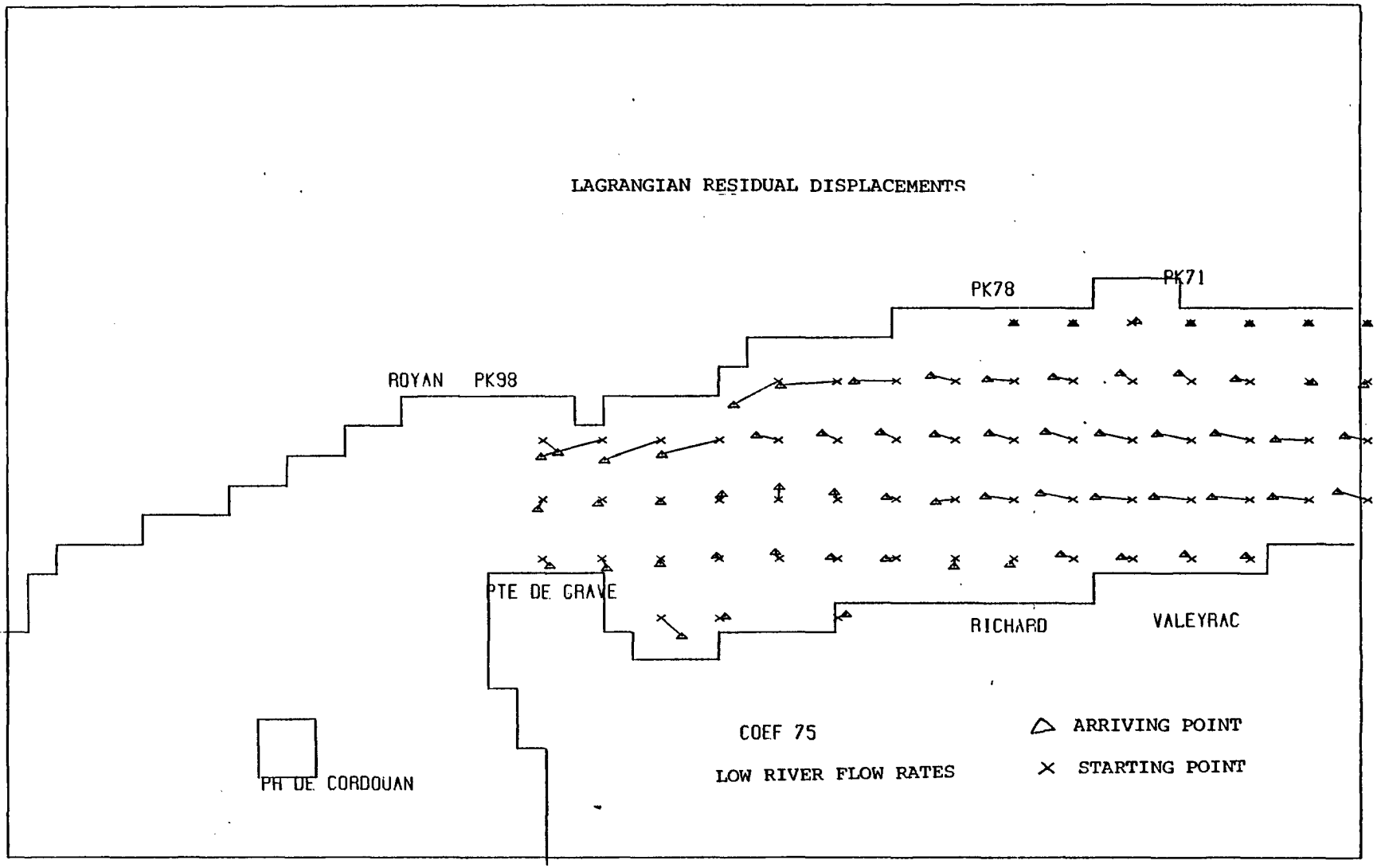

Figure 40 : Lagrangian residual displacements during low river flow rates

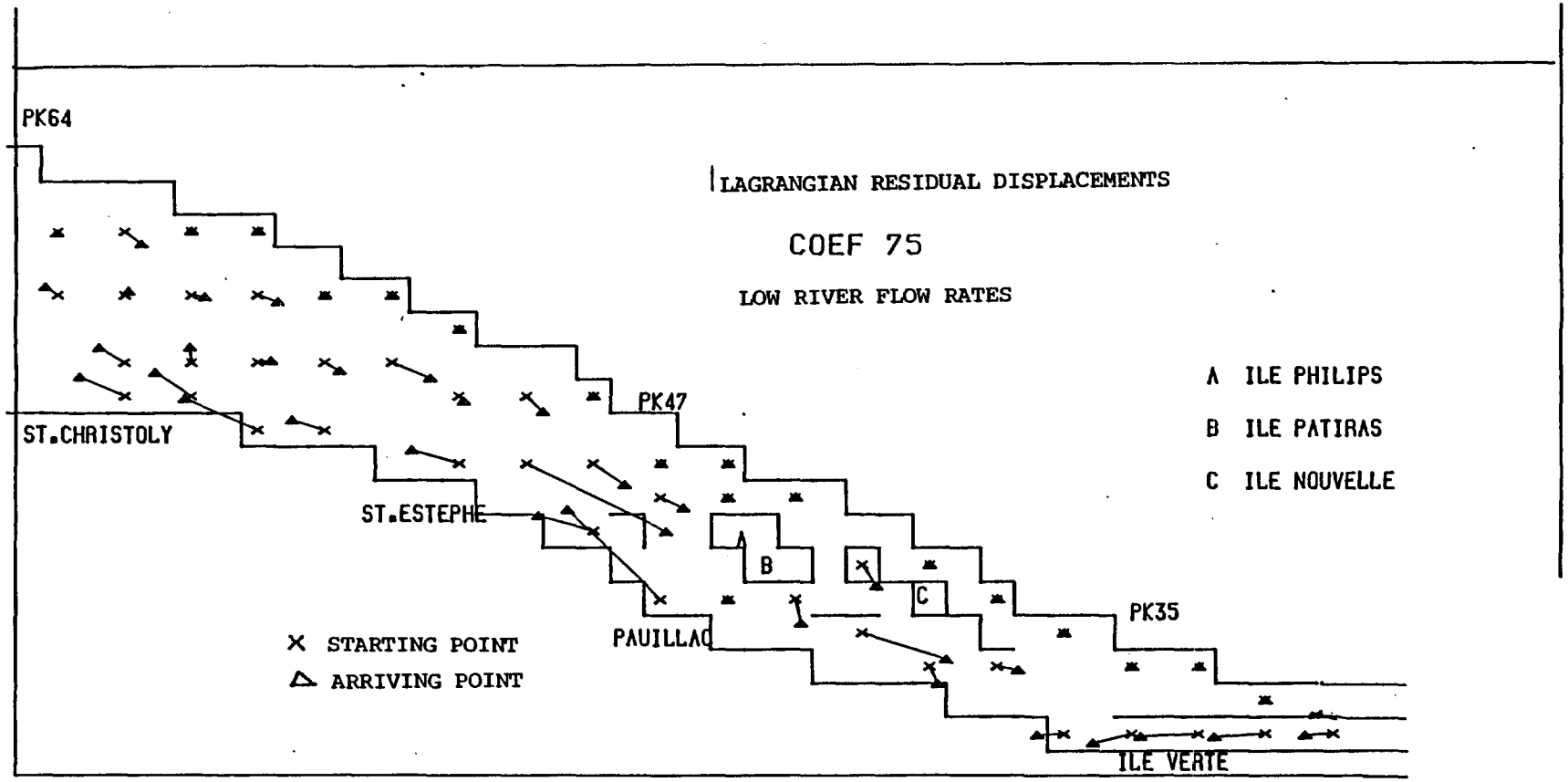

Figure 41 : Lagrangian residual displacements during low river flow rates

displacements are practically absent. In the central region between St. Estéphe and Ile Verte, the water particles have residual displacements towards the head. However, it can be seen in figure 27 that the particles starting at the beginning of flood at PK 52 have residual displacements towards the mouth of the estuary in the central region. During high river discharge rates (fig. 27), the residual displacements are towards the mouth of the estuary in the case of most of the trajectories.

The general picture of lagrangian residual circulation in the upper estuary is as follows. A predominance of residual displacements of high magnitudes towards the mouth in the navigation channel along the south bank side, residual displacements towards the head in the central region depending on the phase of the tide at the instant of departure and practical absence of displacements along the north bank side.

CONCLUSION

Figure 33 shows that the magnitudes of observed residual currents at the surface vary from 10-50 cm/sec. In the case of stair step boundary model simulations, the residual flux of water is concentred in the regions which canalise the ebb, i.e, the navigation channel in the upper and lower estuary and the Saintonge channel in the lower estuary between PK 80-90 approximately. This explains the higher magnitudes of depth averaged residual currents than the observed values at the surface (fig. 32 to 33) in certains regions.

In link node model simulations, the magnitudes of residual currents are of the order of 5 cm/sec^{-1} . These values are less than the computed values from the other two models as well as observed values at the surface. As indicated earlier in this chapter, the physical significance of residual currents obtained by this method is not clear. Moreover, in this model, there are not much lateral differences in residual current intensities in the upper estuary.

The computed lagrangian displacement field shows similar features to that of Eulerian residual current field. Some of the differences found in the former explain certain limitations of the latter parameters. The lagrangian residual displacement results give complimentary evidences to the phenomena observed by the Eulerian residual parameters.

CONCLUSION

CONCLUSION

We have made numerical modelling studies of the circulation in the Gironde estuary consisting of application of two models and developping a third one. Such a study becomes relevant in the case of the Gironde, in view of the complex topography of the upper estuary. Attempt is made to study the lateral variations of different physical parameters and circulation around the islands in relation to the observed data. The performance of different numerical methods are compared.

Stair step boundary model has been useful in describing the principal aspects of circulation and residual circulation in the estuary. The lateral variations are significant. The residual parameters have allowed to identify the ebb channels, namely the navigation channel in the upper estuary and Saintonge channel in the lower estuary. Influences of river discharges on circulation and residual circulation are studied.

However, in certain regions, the method of representing the coast by a stair step boundary has been poor. It is exposed that the computed currents and residual currents have given poor values in these regions.

Irregular grid finite difference model developed during the course of this work has overcome the above mentioned defect. Near the islands, the circulation is not well described and it may be improved by using smaller meshes than those choosen for the present application. In this model, lateral differences of different physical parameters are less significant. Using of extremly small values of smoothing factor is found to be necessary in order to guarantee numerical stability. However, when non linear terms (advection) are excluded this smoothing can be minimised further. The model is highly flexible which permits to use variable meshes. Adding or removal of a few grid points in the domain is simple. The model may be highly useful for littoral applications.

Link node model is an attempt to study two dimensional aspects of flow using a highly simplified model. Though lateral variations cannot be fully described, the model has reproduced well the longitudinal variations of currents. The model is found to be precise in the computation of water surface elevations. Flexibility of the model has allowed in describing the circulation around the islands relatively well.

Computation of lagrangian parameters has given supporting evidences for the determination of the circulation and residual circulation.

Attempt has been made to compare the simulation results with observed data as far as possible. Though each model has its own shortcomings, using different methods have helped in describing the circulation in a better way.

The following perspectives for future research are outlined. As far as modelling aspects are concerned, it is necessary to parameterise the lateral friction and introduce in the equations. In narrow estuaries such as the French estuaries, lateral friction plays an important role in balancing the variations of tidal propagation between two bank sides.

As far as observational aspects are concerned, it is desirable to have the tide gauge data at a few stations near the north bank side of the Gironde to study the variations of tidal propagation in different channels.

APPENDIX - IV

Performance of different models - in terms of computational aspects

The following table gives the computer time needed for the simulation of one period of tide (12 hours 25 minutes), the simulations being made in IRIS 80 and DPS 7 of CNEXO.

Model	Scheme	Time step in minutes	Computer timing in minutes
Stair step boundary model	Implicit in alternate direction	3	17 in IRIS 80
Link node	Explicit	1	4.8 in DPS 7
Irregular grid finite difference model	Leap frog	$1/2$	33 in DPS 7

(Note : DPS 7 is approximately 1.5 times faster than IRIS 80)

It is found that the irregular grid finite difference model needed almost double memory space than the stair step boundary model. It is due to two reasons. As discussed in page 26, a table of values of neigbouring grid points is stored for each grid point. So, to describe each grid point 6 memory locations are needed, except for the boundary points, which need 3, 4 or 5. Moreover, certain values necessary to evaluate the partial derivatives, according to the formulas (19-20) are computed in the beginning of the programme and stored. It is also possible to calculate those values at each time step to minimise the memory space, which may cause slight increase in computer time. It is true that these values are constant for interior points, when triangles of equal size are used. The smoothing procedure(equation 28) is expensive, as it is done every time step.

BIBLIOGRAPHY

BIBLIOGRAPHY

ALLEN, G.P., 1972. Etude des processus sédimentaires dans l'estuaire de la Gironde. Thèse Sc. Nat. Doctorat d'Etat, Université de Bordeaux I n° 353, 314 p.

ALLEN, G.P., CASTAING, P., 1973. Suspended sediment transport from the Gironde estuary (France) into the adjacent continental shelf. Marine Geology, Amsterdam, 14-M47-M53.

ALLEN, G.P., SALOMON, J.C., BASSOULET, P., DU PENHOAT, Y., DE GRANDPRE, C., 1980. Effects of tides on mixing and suspended sediment transport in macrotidal estuaries. Sedimentary Geology, Amsterdam, 26, 69-90.

BONNEFILLE, R., 1969 a. Etude de l'aménagement de l'estuaire de la Gironde. Rapport n° 4. Mesures de vitesse, salinité et concentration en Gironde en 1960 et 1961. Lab. National d'Hydraulique, Chatou, HCO 42 - R 411, T 649 - DHM, 85 p.

BONNEFILLE, R., 1969 b. Etude de l'aménagement de l'estuaire de la Gironde. Rapport n° 6. Mesures de vitesse, salinité et concentration en Gironde en 1967 et 1968. Lab. National d'Hydraulique. Chatou, HC 042 - R 411, T 658 - DHM, 175 p.

BONNEFILLE, R., GERMAIN, P., MARMOUGET, L., 1971. Etude de l'aménagement de l'estuaire de la Gironde. Modèle réduit de la région des îles. Etalonnage hydraulique. Rapport n° 17. Laboratoire National d'Hydraulique. Chatou. HCO 42/15., Mai 1971.

BONNEFILLE, R., 1977. Les phénomènes résiduels en estuaire de la Gironde. Application au cas de la Gironde. Lab. National d'Hydraulique, Chatou, n° E 30/77/01, 105 p.

CASTAING, P., 1981. Le transfert à l'océan des suspensions estuariennes - Cas de la Gironde. Thèse de Doctorat d'Etat ès Sciences, Université de Bordeaux I, n° 701, 530 p.

CAVANIE, A., HYACINTHE, J.L., 1976. Etudes des courants et de la marée à la limite du plateau continental d'après les mesures effectuées pendant la campagne "Golfe de Gascogne 1970". Rap. Scient. Techn. CNEXO, n° 23, 41 p.

CREMER, M., CASTAING, P., KLINGBIEL, A., 1976. L'évolution récente du banc de Sainte Estèphe dans l'estuaire de la Gironde. Bull. Inst. Géol. Bassin d'Aquitaine, Talence, n° 19, 187 - 196.

DE GRANDPRE, C., DU PENHOAT, Y., 1976. Calcul des hauteurs et vitesses en Gironde. Rapport de D.E.A. d'Océanographie physique, Université de Bretagne Occidentale, Brest, 91 p.

DE GRANDPRE, C., DU PENHOAT, Y., 1978. Contribution à l'étude dynamique de la marée dans l'estuaire de la Gironde. Thèse 3ème Cycle, Université de Bretagne Occidentale, Brest, 203 p.

FERAL, A., VILLEROT, M., 1982. Etude du débit fluvial. Rapport, Port Autonome de Bordeaux.

FICHOT, E., 1916. Reconnaissance hydrographique de l'embouchure de la Gironde exécutée en 1912. 19e Cah. de Rech. Hydro. sur le régime des côtes (1911 - 1914), Paris, Imp National, Rapport 431, 12 - 82.

GAUDETTE, M., 1980. Etude de la circulation dans la Gironde. Rapport intern. Université de Bretagne Occidentale, Brest.

KENNETH D., FEIGNER, et al., 1970. Documentation Report. FWQA Dynamic Estuary Model. PB 197 103, National Technical Information Service. U.S. Department Of Commerce, Washington D.C. 248 p.

LAI, CHINTU, 1966. Discussion - Computer simulation of estuarial networks. Journal of the Hydraulics Division, ASCE.

LANGLEY, R., MUIR, 1978. A one dimensional tidal model for estuarine networks. In : Hydrodynamics of estuaries and fjords. Elsvier Oceanographic series. 1978. 243.

LEENDERTSE, J.J., GRITTON, E.C., 1971. A water quality simulation model for well mixed estuaries. Vol II, computation procedures. R - 708 - NYC. The New-York City Rand Institude technical report. 53 p.

MOREAU, S., LEYMARIE, J.C., 1975. Etude de l'aménagement de l'estuaire. Modèle de St. Christoly. Deuxième étalonnage hydraulique du modèle. Rapport 32. Laboratoire Natioanal d'Hydraulique. Chatou. HCO 42/75. 40.

MOYES, J., 1975. Etude hydrobiologique de la Gironde. Rapport technique concernant la Campagne, les mesures hydrologiques in Situ, les turbidités et le carbone particulaire. Contrat n° 75/1239, I.G.B.A., Université de Bordeaux I.

PEARSON, C.E., WINTER, D.W., 1977. On the calculation of tidal currents in homogeneous estuaries. Journal of Physical Oceanography, Vol. 7, p 520 - 531.

PRITCHARD, D.W. 1956. The dynamic structure of a coastal plain estuary. Journal of Marine Research, New Haven, 15 (I), 33 - 42.

SALOMON, J.C., 1976. Modèle mathématique de la propagation de la marée en estuaire et des transports sableux associés. Application aux estuaires de la Loire et de la Seine. Thèse de Doctorat d'Etat ès Sciences, Université de Bretagne Occidentale. Brest. 257 p.

SALOMON, J.C., 1980. Etude de l'estuaire de la Seine. Modélisation numérique des phénomènes physiques. Rapport provisoire. Université de Bretagne Occidentale, Brest.

SALOMON, J.C., ALLEN, G.P., 1983. Rôle sédimentologique de la marée dans les estuaires à fort marnage. Notes et mémoires de la compagnie française des Pétroles, Paris, 18, 35 - 44.

SIMMON, B., 1979. Marée en Gironde. Observations, Analyse, Prédiction. Rapport de Service Hydrographique et Océanographique de la Marine. n° 273 EPSHOM/E/OC. p 69.

SUNDERMAN, J., 1966. Winderzeugter zwischen der analyteschen und der numerischen Berechnung Winderzengter strömungen und Wasserstände in einem Modellmeer mit Anwendungen auf die Nordsee, Universität Hamburg, Mitteillungen Inst. Mereskunde, NO IV.

TESSON GILET, M., 1981. Processus hydrodynamiques dans la région des îles de l'estuaire de la Gironde (Zone de Braud-et-Saint-Louis). Thèse de docteur ingénieur. Université de Bordeaux I, n° 310, 289 p.

THACKER, W.C., 1976. Irregular grid finite difference techniques : Simulation of Oscillations in shallow circular basins. Journal of Physical Oceanography. Vol. 7, p 284 - 292.

THACKER, W.C., 1979, Irregular grid finite difference technique for storm surge calculations for curving coastlines. In : Marine forescasting, ed. J.C.J. Nihoul, Elsvier Scientific Publishing Company, Amsterdam.

WANG, J.D., CONNOR, J.J., 1975. Mathematical modelling of near coastal circulation. MIT Sea Grant program Rep. NO. MITSG 75 - 13.